1,1′-Bis(*ortho*-carborane): Ruthenium Chelates, Phosphines and Tether Derivatives

Laura E. Riley

Submitted for the degree of Doctor of Philosophy at Heriot-Watt University, on completion of research in the School of Engineering and Physical Sciences.

February 2017

Abstract

Chapter one provides a brief exposition on the history and importance of boron and carboranes and introduces 1,1′-bis(*o*-carborane). It also provides literature examples of 1,1′-bis(*o*-carborane) chelates, 1,1′-bis(*o*-carboranyl)phosphines and tethered 1,1′-bis(*o*-carboranes).

Chapter two discusses the reaction between dilithiated 1,1′-bis(*o*-carborane) and di-halogenated ruthenium compounds to afford several new compounds of the formula [Ru($\kappa^{2/3}$-2,2′(3′)-{1-(1′-1′,2′-*closo*-$C_2B_{10}H_{10}$)-1,2-*closo*-$C_2B_{10}H_{10}$})(L)]. The first compound prepared, whereby L = *p*-cymene, reacts with either PPh_3 or dppe and shows unusual displacement of the *p*-cymene ligand and a change in the bonding mode of 1,1′-bis(*o*-carborane). The fully saturated (MeCN or CO) derivatives of these compounds are also synthesised and studied, some of which are excellent examples of illustrating the structural *trans* effect. The initial {Ru(*p*-cymene)} was tested as a catalyst and displayed good Lewis acid catalytic activity of a Diels-Alder cycloaddition.

Chapter three explores two carboranylphosphines [μ-2,2′-PR-{1-(1′-1′,2′-*closo*-$C_2B_{10}H_{10}$)-1,2-*closo*-$C_2B_{10}H_{10}$}], where R = Et or Ph. Two-dimensional NMR spectroscopy and DFT calculations are used to explain an unusual lack of observed $^2J_{PH}$ coupling in the ^{1}H NMR spectrum of the ethyl derivative. Their subsequent reactions with {AuCl} and {Se} are also discussed as they provide a route to identifying the steric bulk and electronic properties of these carboranylphosphines.

Chapter four discusses one new tethered 1,1′-bis(*o*-carborane) and its comparison with non-carborane analogues. A known tethered carborane is also synthesised and its single decapitation and metalation with {Ru(*p*-cymene)} explored producing the desired 12-vertex ruthenacarborane/12-vertex carborane but also an unusual 13-vertex diruthenacarborane/12-vertex carborane.

Chapter five gives all the synthetic and analytical details for the compounds discussed. Appendix one provides crystallographic tables and appendix two provides all the crystallographic information on a CD. Appendix three includes copies of all published work related to this thesis (to date).

Acknowledgements

Firstly, I would like to thank my supervisor Prof. Alan J. Welch. He has been a constant source of support and advice and is always ready with new ideas when old ones fail. All the guidance he has given over the last three and a half years has been incredibly beneficial. Of course, I must mention Dr Mark Fox, who supervised me during my MChem project at Durham University. His enthusiasm for carborane chemistry is contagious and without him, I would not have had the opportunity to do my PhD.

I would like to thank Dr Alasdair Robertson for always being on hand to help and to discuss both chemistry and more general life decisions. Special thanks has to go to Antony Chan who has endured three years of my terrible singing! Thank you to Amanda Benton who always brightens the lab with her laughter. Thanks also to Dr Sam Powley and Dr Dipendu Mandal who made me so welcome when I joined the group and have become good friends. Also to John Jones whose lab antics always make an excellent story to retell! Lastly to two MChem students Rebekah Jeans and Thomasine Curzon, who made the last year of my PhD less stressful and much more fun.

I have to also thank Dr Dave Ellis not only for his NMR expertise, but also for the countless discussions we have had regarding my work. Also to Dr Georgina Rosair for crystallography, Alan Taylor for mass spectrometry and Dr Koenraad Collart and Dr Brian Hutton for elemental analysis.

I would like to also acknowledge and thank several people for assisting with this work. Rebekah Jeans and Antony Chan for the catalysis work in Chapter 1 and Dr Tobias Kramer for all the DFT calculations in Chapter 3. I would also like to say how much I appreciate the discussions they have all had with me about these pieces of work.

Huge thanks go to my family for their continued support. In particular, I want to thank my parents, Graham Riley and Kim Mason, and my grandparents, Bill and Carole Barker, for always supporting my decisions and pushing me to be the best person possible.

Finally but most importantly, I would like to thank my fiancé and very soon to be husband Andy. Without him, I am not sure I would have seen this PhD through to the end and his support, guidance and constant reassurance has been invaluable.

I hereby declare that the work presented in this thesis was carried out by myself at Heriot-Watt University, Edinburgh, except where due acknowledgment is made, and has not been submitted for any other degree.

Laura E. Riley (Candidate)

Prof. Alan J. Welch

Date

Table of Contents

ACADEMIC REGISTRY

Research Thesis Submission

Name*:*			
School:			
Version: *(i.e. First, Resubmission, Final)*		Degree Sought:	

Declaration

In accordance with the appropriate regulations I hereby submit my thesis and I declare that:

1) the thesis embodies the results of my own work and has been composed by myself
2) where appropriate, I have made acknowledgement of the work of others and have made reference to work carried out in collaboration with other persons
3) the thesis is the correct version of the thesis for submission and is the same version as any electronic versions submitted*.
4) my thesis for the award referred to, deposited in the Heriot-Watt University Library, should be made available for loan or photocopying and be available via the Institutional Repository, subject to such conditions as the Librarian may require
5) I understand that as a student of the University I am required to abide by the Regulations of the University and to conform to its discipline.
6) I confirm that the thesis has been verified against plagiarism via an approved plagiarism detection application e.g. Turnitin.

* *Please note that it is the responsibility of the candidate to ensure that the correct version of the thesis is submitted.*

Signature of Candidate*:*		Date:	

Submission

Submitted By *(name in capitals):*	
Signature of Individual Submitting:	
Date Submitted:	

For Completion in the Student Service Centre (SSC)

Received in the SSC by *(name in capitals):*			
Method of Submission *(Handed in to SSC; posted through internal/external mail):*			
*E-thesis Submitted (**mandatory for final theses)***			
Signature:		Date:	

Please note this form should be bound into the submitted thesis.

Abbreviations

1,1′-bis(*o*-carborane)	[1-(1′-1′,2′-*closo*-$C_2B_{10}H_{11}$)-1,2-*closo*-$C_2B_{10}H_{11}$]
2c-2e	two-centre two-electron
κ	kappa
σ	sigma
δ	chemical shift
μ	bridging
Å	Angstrom
θ	Tolman cone angle (°)
br	broad
CO	carbon monoxide
d	doublet
DCM	dichloromethane
DFT	Density Functional Theory
dmpe	dimethylphosphinoethane
dppe	diphenylphosphinoethane
EIMS	Electron Ionisation Mass Spectrometry
HMBC	Heteronuclear Multiple Bond Coherence
Hz	Hertz (frequency)
IR	infrared
J	coupling constant (NMR)
KOH	potassium hydroxide
lp	lone pair
m	meta

m	multiplet
MeCN	acetonititrile
MW	molecular weight
m/z	mass to charge
NBO	Natural Bond Orbitals
[$HNMe_3$]Cl	trimethylammonium hydrochloride
NMR	nuclear magnetic resonance
o	ortho
p	para
PCy_3	tricyclohexylphosphine
PMe_3	trimethylphosphine
PPh_3	triphenylphosphine
ppm	parts per million
PSEPT	Polyhedral Skeletal Electron Pair Theory
QTAIM	Quantum Theory of Atoms in Molecules
rms	root-mean-square
s	singlet
THF	tetrahydrofuran
tht	tetrahydrothiophene
TLC	Thin Layer Chromatography

Abbreviations for Specific Compounds

1 [Ru(κ^3-2,2′,3′-{1′-(1′-1′,2′-*closo*-$C_2B_{10}H_{10}$)-1,2-*closo*-$C_2B_{10}H_{10}$})(*p*-cymene)]

2 [Ru(κ^2-2,2′-{1′-(1′-1′,2′-*closo*-$C_2B_{10}H_{10}$)-1,2-*closo*-$C_2B_{10}H_{10}$})(*p*-cymene)(CO)]

3 [Ru(κ^3-2,3′,3-{1′-(1′-1′,2′-*closo*-$C_2B_{10}H_{10}$)-1,2-*closo*-$C_2B_{10}H_{10}$})(PPh_3)$_2$]

4 [Ru(κ^3-2,3′,3-{1′-(1′-1′,2′-*closo*-$C_2B_{10}H_{10}$)-1,2-*closo*-$C_2B_{10}H_{10}$})(dppe)]

5 [Ru(κ^2-2,3′-{1′-(1′-1′,2′-*closo*-$C_2B_{10}H_{10}$)-1,2-*closo*-$C_2B_{10}H_{10}$})(PPh_3)$(CO)_3$]

6 [Ru(κ^2-2,3′-{1′-(1′-1′,2′-*closo*-$C_2B_{10}H_{10}$)-1,2-*closo*-$C_2B_{10}H_{10}$})(PPh_3)$(MeCN)_3$]

7 [Ru(κ^2-2,3′-{1′-(1′-1′,2′-*closo*-$C_2B_{10}H_{10}$)-1,2-*closo*-$C_2B_{10}H_{10}$})(dppe)$(CO)_2$]

8 [Ru(κ^2-2,3′-{1′-(1′-1′,2′-*closo*-$C_2B_{10}H_{10}$)-1,2-*closo*-$C_2B_{10}H_{10}$})(dppe)$(MeCN)_2$]

---

9 [μ-2,2′-PEt-{1-(1′-1′,2′-*closo*-$C_2B_{10}H_{10}$)-1,2-*closo*-$C_2B_{10}H_{10}$}]

10 [μ-2,2′-PPh-{1-(1′-1′,2′-*closo*-$C_2B_{10}H_{10}$)-1,2-*closo*-$C_2B_{10}H_{10}$}]

11 [μ-2,2′-P(Et)AuCl-{1-(1′-1′,2′-*closo*-$C_2B_{10}H_{10}$)-1,2-*closo*-$C_2B_{10}H_{10}$}]

12 [μ-2,2′-P(Ph)AuCl-{1-(1′-1′,2′-*closo*-$C_2B_{10}H_{10}$)-1,2-*closo*-$C_2B_{10}H_{10}$}]

13 [μ-2,2′-P(Et)Se-{1-(1′-1′,2′-*closo*-$C_2B_{10}H_{10}$)-1,2-*closo*-$C_2B_{10}H_{10}$}]

14 [μ-2,2′-P(Ph)Se-{1-(1′-1′,2′-*closo*-$C_2B_{10}H_{10}$)-1,2-*closo*-$C_2B_{10}H_{10}$}]

---

15 [μ-2,2′-C_6H_4-{1-(1′-1′,2′-*closo*-$C_2B_{10}H_{10}$)-1,2-*closo*-$C_2B_{10}H_{10}$}]

16 [μ-2,2′-CH_2CH_2-{7-(1′-1′,2′-*closo*-$C_2B_{10}H_{10}$)-7,8-*nido*-$C_2B_9H_9$}][$HNMe_3$]$_2$*

17 [2-(1′-1′,2′-*closo*-$C_2B_{10}H_{11}$)-4,5-(*p*-cymene)$_2$-7-Cl-4,5,2,3-*closo*-$Ru_2C_2B_9H_9$]

18 [μ-2,2′-CH_2CH_2-{1-(1′-1′,2′-*closo*-$C_2B_{10}H_{10}$)-3-(*p*-cymene)-3,1,2-*closo*-$RuC_2B_9H_9$}]

---

* No crystallographic information

Chapter 1: Introduction

1.1 Boron

Elemental boron was discovered by Humphry Davy (UK), and at the same time by Louis-Josef Gay-Lussac and Louis-Jaques Thénard (France), in 1808.[1] Boron has the atomic number five and is the first *p*-block element in the periodic table.

Boron is found naturally in borax [$Na_2B_4O_5(OH)_4 \cdot 8H_2O$], colemanite [$CaB_3O_4(OH)_3 \cdot H_2O$] and kernite [$Na_2B_4O_6(OH)_2 \cdot 3H_2O$]. Although elemental boron is not found naturally, it can be prepared by reducing boron trihalides with hydrogen, using electrically-heated filaments. Boron has the two isotopes ^{10}B and ^{11}B, which are found in 19.78% and 80.22% abundancies respectively.

Boron forms complexes with hydrogen that are known as boron hydrides, and further expansion produces boron-containing clusters that exhibit interesting bonding. Boron clusters have exciting properties that can be utilised in many reactions and applications. A very large area of study is the formation and uses of carboranes, whereby one or more $\{BH\}^-$ vertices have been substituted by an isolobal {CH} unit. Heteroboranes are also widely researched and in the many examples published the $\{BH\}^-$ unit has been substituted by another isolobal unit, with many elements of the periodic table possible.

1.2 Boranes

The simplest boron hydride is borane (BH_3) which is very reactive and dimerises to form diborane (B_2H_6). In 1933 Alfred Stock published the first report of the synthesis and structure of diborane,[2] the structure of which was later confirmed by Bauer, Figure 1.1.[3, 4] Diborane has four terminal hydrogen atoms and two bridging hydrogen atoms which give the 3c-2e (three-centre two-electron) bonding system.

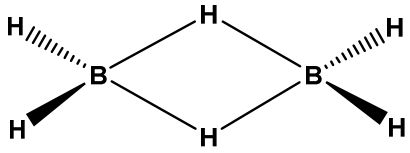

Figure 1.1 The structure of diborane (B_2H_6) as confirmed by Bauer to have two bridging H atoms.

Larger boranes can be described as boron clusters that have polyhedral structures with electron delocalisation. There are three common types of boron cluster: closo $[B_nH_n]^{2-}$ which is a closed polyhedron, nido (B_nH_{n+4}) which have one vertex removed compared to the parent closo structure and arachno (B_nH_{n+6}) which have two vertices missing compared to the parent closo structure. Two frequently used *nido*-boranes are pentaborane-[9] (B_5H_9) and decaborane-[14] ($B_{10}H_{14}$), Figure 1.2.

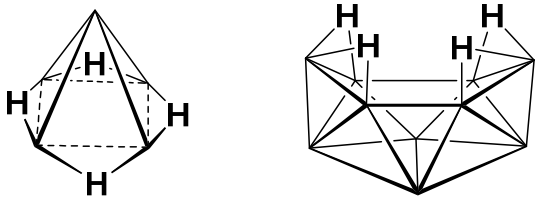

Figure 1.2 The structures of pentaborane-[9] (B_5H_9) and decaborane-[14] ($B_{10}H_{14}$). Unlabelled vertices are BH throughout this thesis.

In 1998 Schleyer et al. computationally researched the stability of the *closo*-borates $[B_nH_n]^{2-}$, with *n* ranging from 5 to 17 boron atoms.[5] A plot between the number of boron atoms and the cumulative BH addition energy (ΔH_{add}) shows clearly that the sequential stability of *closo*-borates generally increases upon addition of a {BH} unit, Figure 1.3. As the number of boron atoms increases from 5 to 11 each addition is exothermic and therefore favoured. Expansion from 11 to 12 boron atoms is considerably more exothermic, suggesting that the 12-vertex $[B_{12}H_{12}]^{2-}$ would be much more stable than the 11-vertex $[B_{11}H_{11}]^{2-}$. However, upon single BH addition to afford the 13-vertex *closo*-borate the calculated energy is endothermic. Further increase of cluster size from 13 to 17 boron atoms tends to be exothermic (except when *n* is 15).

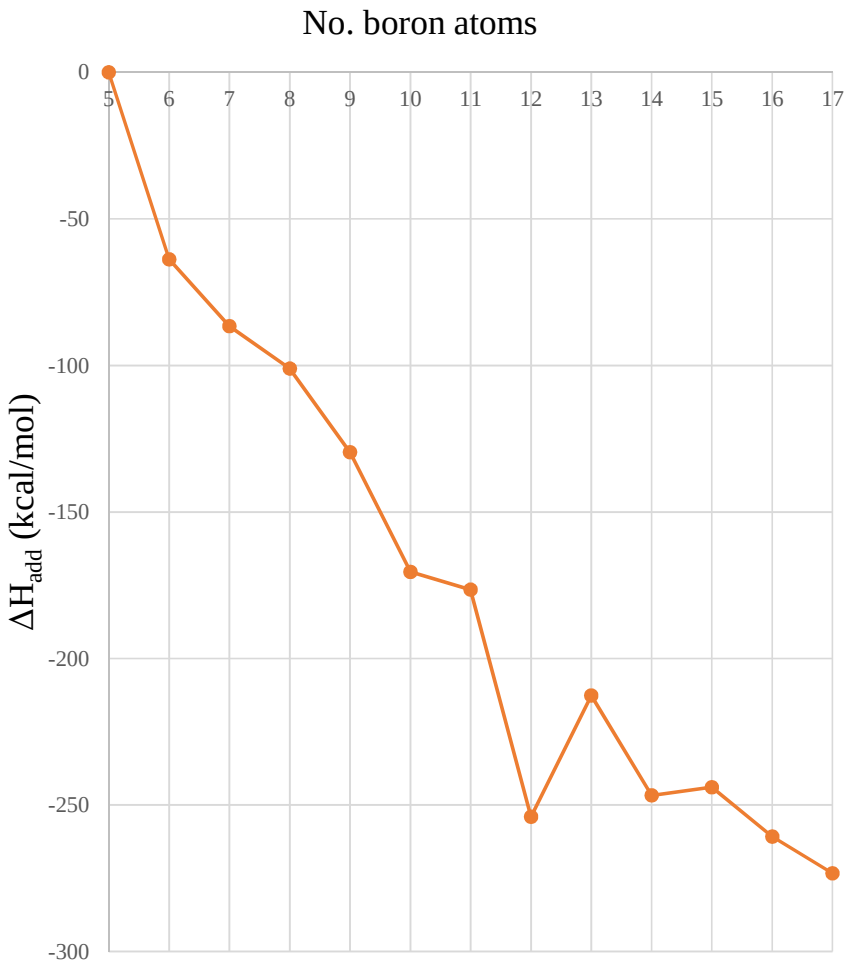

Figure 1.3 Graph showing the cumulative BH addition energy of *closo*-borates (ΔH_{add}, kcal mol^{-1}) for the range of 5 to 17 boron atoms.

1.3 Carboranes

Carboranes are classified as boron-carbon clusters, which have extensive "electron delocalised" covalent bonding in their skeletal atoms. The carbon atoms in the carborane cluster can have between three and six neighbours,[6] and each carbon atom within the molecule gives rise to stabilisation and neutralisation of the cluster as it adds electron density.[7]

Carboranes were first synthesised in the early 1960's by reaction of pentaborane (B_5H_9) with acetylene; this reaction yielded the first series of carborane compounds with the empirical formula $C_2B_nH_{n+2}$, where n = 3, 4 or 5.[8] In 1963 dicarba-*closo*-dodecaborane ($C_2B_{10}H_{12}$) was synthesised for the first time by reacting decaborane with acetylene in the presence of a Lewis base such as acetonitrile (MeCN), diethyl sulphide (SEt_2) or dimethyl sulphide (SMe_2), Scheme 1.1.[9, 10] The presence of a Lewis base increased yields from 0.2% to 74%, making this a viable route to carborane formation and is now the most prominent way of making dicarba-*closo*-dodecaborane.

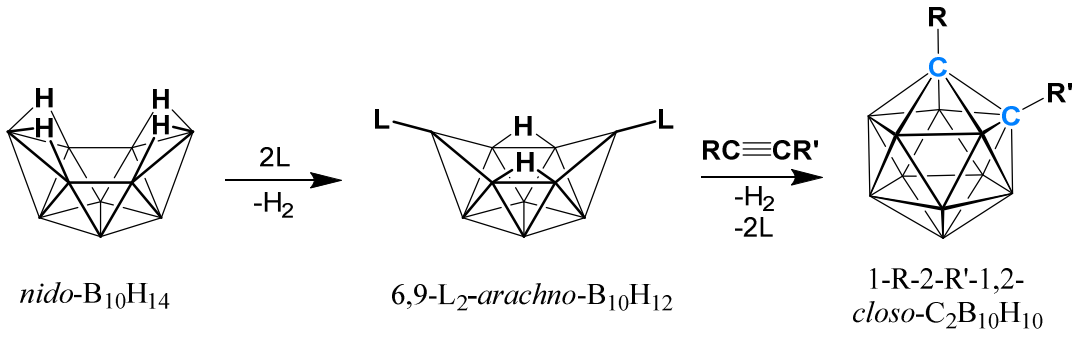

nido-$B_{10}H_{14}$ 6,9-L_2-*arachno*-$B_{10}H_{12}$ 1-R-2-R'-1,2-*closo*-$C_2B_{10}H_{10}$

Scheme 1.1 Reaction between decaborane and acetylene in the presence of a Lewis base for the synthesis of 1,2-$C_2B_{10}H_{12}$, L = MeCN, R_3N, R_2S and R, R′ = H, alkyl, haloalkyl, aryl, alkenyl, alkynyl.

The most widely researched carboranes are the dicarba-*closo*-dodecaboranes as they are commercially available, air-stable solids. They are also readily made *via* the aforementioned method and exhibit very interesting properties. There are three isomers of this carborane; ortho (1,2-), meta (1,7-) and para (1,12-) depending on where the two carbon atoms reside within the cluster, Scheme 1.2. *Ortho*-carborane can undergo

rearrangement to the meta and para isomers by heating to 400 °C and 700 °C respectively.[6]

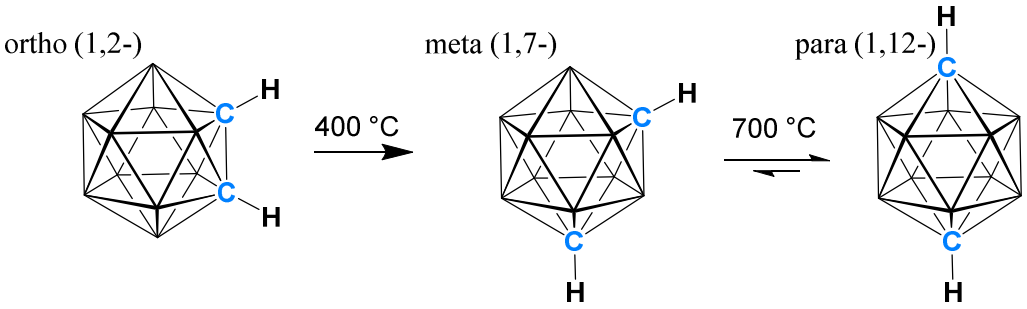

Scheme 1.2 The three isomers of dicarba-*closo*-dodecaborane ($C_2B_{10}H_{12}$).

The carborane $C_2B_{10}H_{12}$ has been described as *pseudo*-aromatic due to the delocalised bonding within the cage and the reactivity when substituents are introduced.[11] This is because introduction of a substituent onto a carbon or boron atom will affect the reactivity of the other atoms throughout the cage, normally seen with aromatic molecules.[12]

1.4 Applications

Carboranes have been studied for over 50 years and have many known applications such as polymers,[13-15] molecular scaffolding,[16], blue OLED's[17-20] and boron neutron capture therapy (BNCT).[21-23] BNCT (although not yet widely employed) is thought to be effective because it allows cancerous cells enriched with ^{10}B rich to be targeted. On neutron capture ^{10}B affords excited ^{11}B which then undergoes rapid nuclear fission to produce high energy α particles and ^{7}Li.

$$^{10}B + \text{irradiation} \rightarrow {}^{11}B^* \rightarrow \alpha + {}^{7}Li + \text{energy}$$

The high energy α particles have a path length of around 5 to 9 μm and as this is the approximate diameter of a target cell only those containing boron will be destroyed.

A feature of the ^{10}B delivery agents is that they need to be inert towards reactions with biological systems. In 2013 Núñez et al. reported several dendrimers that could be useful as BNCT agents due to their biological inertness but also their ability to be either neutral or charged (by decapitation using excess NaOH in EtOH).[24] One example is shown in Figure 1.4, synthesised from the reaction between 1,3,5-tris(4-(3-bromo-propoxy)phenyl)benzene and monolithiated 1-Me-1,2-$C_2B_{10}H_{11}$ or 1-Ph-1,2-$C_2B_{10}H_{11}$, under reflux conditions.

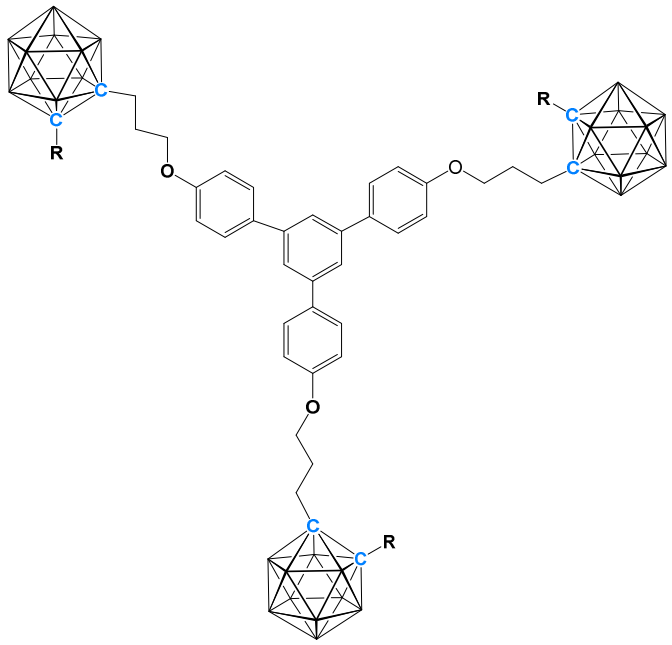

Figure 1.4 Carborane dendrimer, potentially useful for BNCT (R = Me or Ph).

In 2012 Viñas et al. reported carborane-stabilised gold nanoparticles which could be of significant interest for use in BNCT, Figure 1.5.[25] The gold nanoparticle is hydrophobic and insoluble in water, however it can transfer to the aqueous phase when electrons are available (i.e. from a reducing agent). Other properties include stabilisation of the gold core, movement of solvent to/from the gold surface and storage of exchangeable cations in the ligand shell.

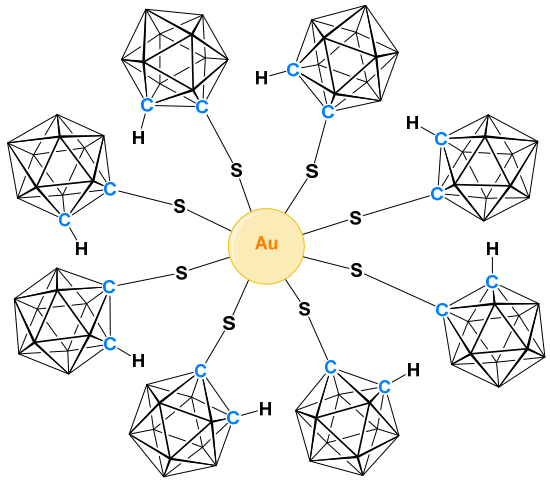

Figure 1.5 Carborane stabilised gold nanoparticle with a potential use for BNCT.

There are many other uses for carboranes and a review published by Grimes in 2015 detailed just a few of these.[26] These included catalysis, drug delivery, electronic devices, molecular machines, metal-organic frameworks, metal ion extraction, battery design and many more. The unique properties of (hetero)carboranes provide a foundation for a vast expanse of applications that is demonstrated by the many examples published in the literature.

1.5 Wade-Mingos Rules

The structure of boranes and carboranes has been an area of great interest since the introductory observations by Kasper in 1948 and by Lipscomb in 1963.[27, 28] The initial *X*-ray structures were interpreted in terms of the lower boranes being regarded as fragments of a parent 12-vertex icosahedron. Wade's rules, first proposed in 1971, showed however that there is a relationship between the number of skeletal electrons within a cage system and the geometric structure.[29, 30] Wade's rules were extended by Mingos in 1972[31] and therefore they are now commonly known as the Wade-Mingos rules, but can also be referred to as the Polyhedral Skeletal Electron Pair Theory (PSEPT). These rules allow the prediction of cluster geometry (closo, nido, arachno etc.) based on the number of vertices and skeletal electron pairs.

In general, each vertex within the cluster uses three orbitals when bonding to the surrounding neighbours in the skeleton, giving maximum bonding within the cage. A unit having less than three bonds to the cage can be described as an *exo*-polyhedral substituent; these are therefore not part of the cage skeleton. On this basis, the skeletal electron count can be calculated.

For dicarba-*closo*-dodecaborane ($C_2B_{10}H_{12}$):

2{CH}: 2 x $3e^-$ = $6e^-$
10{BH}: 10 x $2e^-$ = $20e^-$
Total skeletal electrons: $26e^-$
Skeletal electron pairs (SEP's): 13

As dicarba-*closo*-dodecaborane has 12 vertices (*n*) and 13 SEP's it can therefore be described as having (*n* + 1) SEP's.

PSEPT can be used to predict the geometry of clusters as they follow the general rule that closo clusters have (*n* + 1) SEP's, nido clusters have (*n* + 2) SEP's and arachno clusters have (*n* + 3) SEP's. Therefore as dicarba-*closo*-dodecaborane has (*n* + 1) SEP's it must have a closo geometry. This theory can be applied to polyhedral boranes, carboranes and heteroboranes, including metallacarboranes.

For pentaborane-[9] (B_5H_9):

5{BH}: 5 x $2e^-$ = $10e^-$

4(μ-H): 4 x $1e^-$ = $4e^-$

Total skeletal electrons: $14e^-$

Skeletal electron pairs (SEP's): 7

(*n* + 2) SEP's, **nido** geometry

For 3,1,2-cobaltacarborane ($CpCoC_2B_9H_{11}$):

{CpCo}: $2e^-$

2{CH}: 2 x $3e^-$ = $6e^-$

9{BH}: 10 x $2e^-$ = $18e^-$

Total skeletal electrons: $26e^-$

Skeletal electron pairs (SEP's): 13

(*n* + 1) SEP's, **closo** geometry

Carboranes normally exist in one of three forms, as a closed (closo) cage or two open (nido and arachno) forms. There exists a wide variety of carboranes ranging from small four vertex[32] carboranes with one carbon atom to larger (hetero)carboranes such as supraicosahedral 15 vertex metallacarboranes,[33, 34] and in the case of most closo architectures the cage is a closed polyhedron with triangular faces. A *nido*-carborane is formed by the removal of a boron vertex from a parent *closo*-carborane; in general, the boron atom removed is that which has the highest coordination number of all the skeletal atoms. The arachno form is derived from the removal of a boron vertex from the nido carborane, therefore overall two vertices are removed compared to the parent *closo*-carborane. The carbon atoms in these structures generally adopt the sites with the lowest coordination number in its parent *closo*-carborane.[35]

The structural relationship between closo, nido and arachno clusters is applicable to boranes and heteroboranes, and in the 1970's Rudolph showed succinctly these relationships, Figure 1.6.[36, 37] The left hand column shows the closo parent structures, upon removal of one or two vertices subsequently, the nido and arachno geometrical forms can be derived by following a diagonal progression.

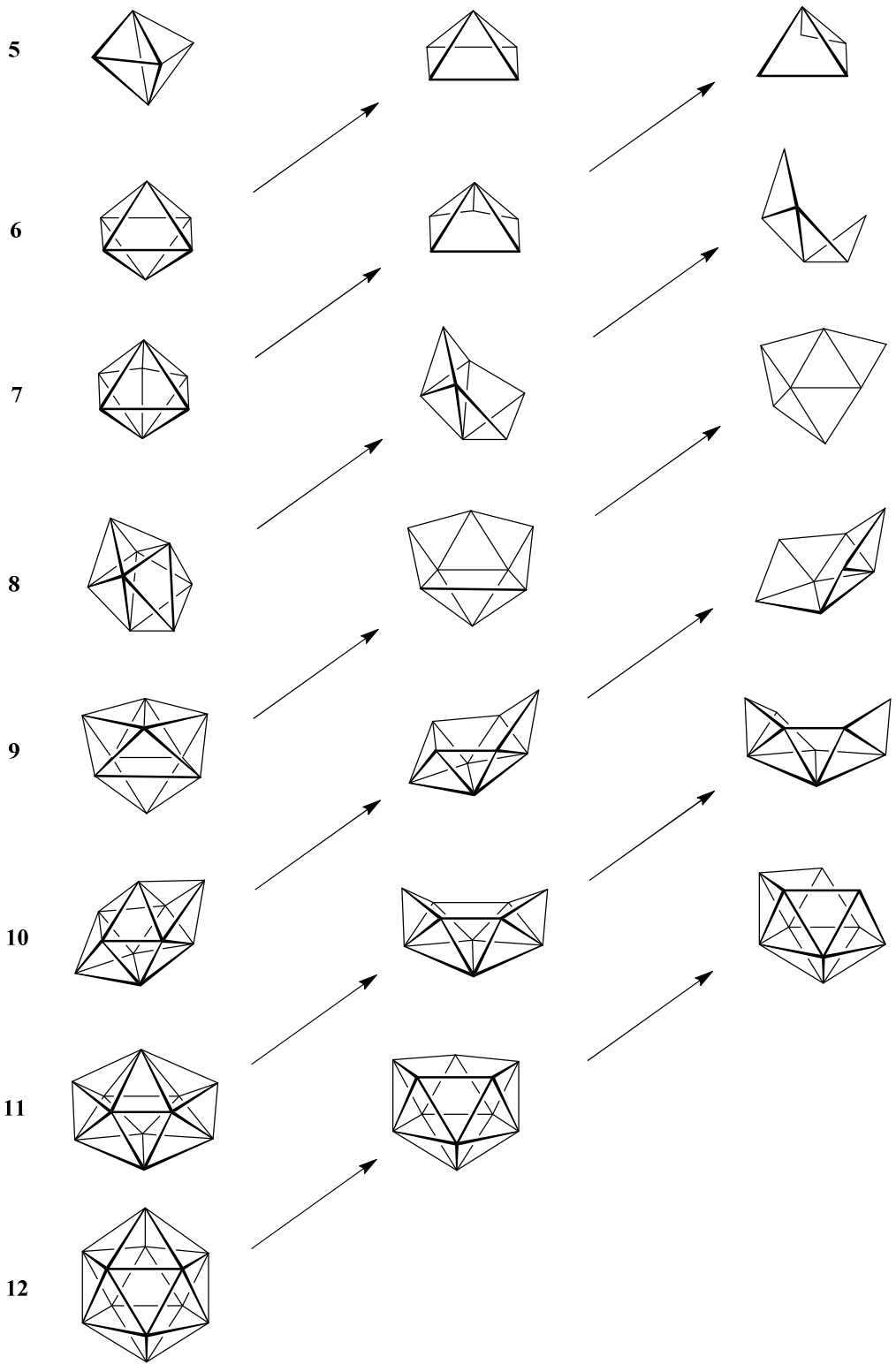

Figure 1.6 Representation of the relationship between closo (left), nido (central) and arachno (right) clusters, with the arrows depicting the parent polyhedra for the respective nido and arachno forms. Clusters with 5 to 12 vertices shown.

1.6 Distinguishing Between Boron and Carbon Atoms in Crystal Structures

When studying crystal structures of carboranes (and heteroboranes) it can be difficult to distinguish between carbon and boron atoms within the clusters when neither atom has non-hydrogen substituents. As boron and carbon are next to each other in the periodic table they have very similar *X*-ray scattering powers. In 2013 Welch and co-workers developed a method of differentiating between the two atoms by using the Vertex-to-Centroid Distance (VCD).[38] This method utilises the fact that the atomic radius of carbon is smaller than that of boron, and therefore should be distinguishable. VCD works by refining all the cage vertices as boron atoms (to get a pro-structure), defining a cluster centroid and measuring the distances from each vertex to the centroid. As the radius of carbon is smaller than that of boron, these vertices will be closer to the centroid compared to the rest of the VCD's. This method is applicable to most carboranes and carborane derivatives, including metallacarboranes and *nido*-carboranes.

VCD's of the *closo*-carborane $C_2B_{10}H_{12}$ can definitively assign the carbon and boron atoms to decipher which isomer is present: ortho, meta or para. As an illustrative example Welch and co-workers reviewed many carboranes in their original VCD paper, including one *closo*-$C_2B_{10}H_{12}$ carborane published by Wade et al. in 1996.[39] The values obtained when all vertices were refined as boron atoms are given in Table 1.1.

Table 1.1 VCD values for the *closo*-$C_2B_{10}H_{12}$ carborane published by Wade et al. in 1996.

Vertex	VCD (Å)
1	1.546
2	1.698
3	1.696
4	1.668
5	1.668
6	1.694
7	1.546
8	1.690
9	1.680
10	1.672
11	1.679
12	1.656

From the values in Table 1.1 it can be seen that there are two distinctly short VCD's, corresponding to vertex-1 and vertex-7. These values are shorter than the rest by 0.134 Å and these vertices can therefore be assigned as carbon atoms, with the remaining vertices all being boron atoms. As a result, the structure has been proved to be *meta*-$C_2B_{10}H_{12}$.

The boron-to-hydrogen distance (BHD) method, also developed by Welch et al. (2002, 2014), can also be used to distinguish C from B in crystal structures and is once again based on a carborane where all vertices are initially refined as boron atoms.[40, 41] If one or more of the vertices has been modelled with insufficient electron density (i.e. B instead of C) the bonded hydrogen atom will move closer to compensate. Therefore, carbon vertices are easily identified as they will have shortened vertex to hydrogen distances, compared to the rest. Both VCD and BHD can be used in combination to ensure the carbon atom locations are found correctly during analysis of single crystal *X*-ray structures.

1.7 Numbering of Carboranes

Numbering within the carborane cage is based on the highest order symmetry axis within the parent polyhedron and successive numbering follows belts (or rings) in a clockwise method, according to IUPAC rules, Figure 1.7. Heteroatoms in the polyhedron are allocated a number based upon their position in the periodic table; atoms of higher atomic number are given the higher precedence, the only exception being that carbon takes precedence over metals.

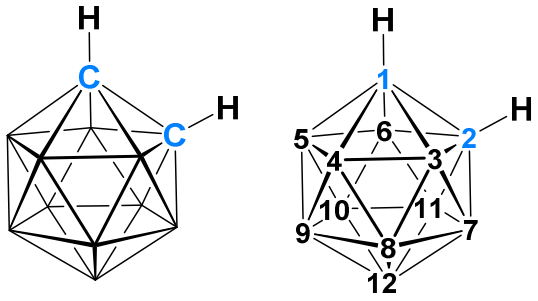

Figure 1.7 The numbering of 1,2-$C_2B_{10}H_{12}$ according to IUPAC rules.

1.8 Decapitation/Reduction and Metalation Reactions of *ortho*-Carborane

One of most common ways to synthesise a metallacarborane is to first decapitate *o*-carborane by heating to reflux with potassium hydroxide in ethanol, Scheme 1.3. Hawthorne et al. first reported this in 1964 whereby they isolated the carborane anion $[C_2B_9H_{12}]^-$ as its tetramethylammonium salt.[42] This *nido*-carborane has all the usual BH/CH units plus an additional hydrogen located on the open face. The location of this twelfth hydrogen is usually described as a BHB bridging proton located between boron atoms B9 and B10 or B10 and B11 (between two of the three boron atoms located on the open face). In 1990 Welch and co-workers determined by crystallographic methods that H12 is actually an *endo*-hydrogen located on B10 (central boron atom on the open face).[43]

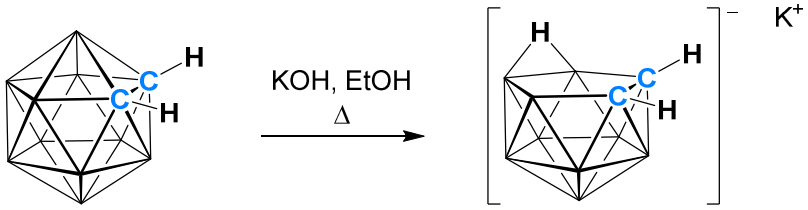

Scheme 1.3 Degradation of *o*-carborane to give $[7,8\text{-}C_2B_9H_{12}]^-$ as the potassium salt.

Hawthorne et al. reported the first example of a metallacarborane in 1965, with a subsequent full paper in 1968.[44, 45] In this work $[7,8\text{-}C_2B_9H_{11}]^{2-}$ was prepared for the first time by abstracting the *endo*-hydrogen using either sodium hydride or sodium metal. Reacting $FeCl_2$ with $[7,8\text{-}C_2B_9H_{11}]^{2-}$ afforded an iron-sandwich di-anion complex $[Fe(C_2B_9H_{11})_2]^{2-}$, Scheme 1.4, which could be converted to the mono-anion by aerial oxidation.

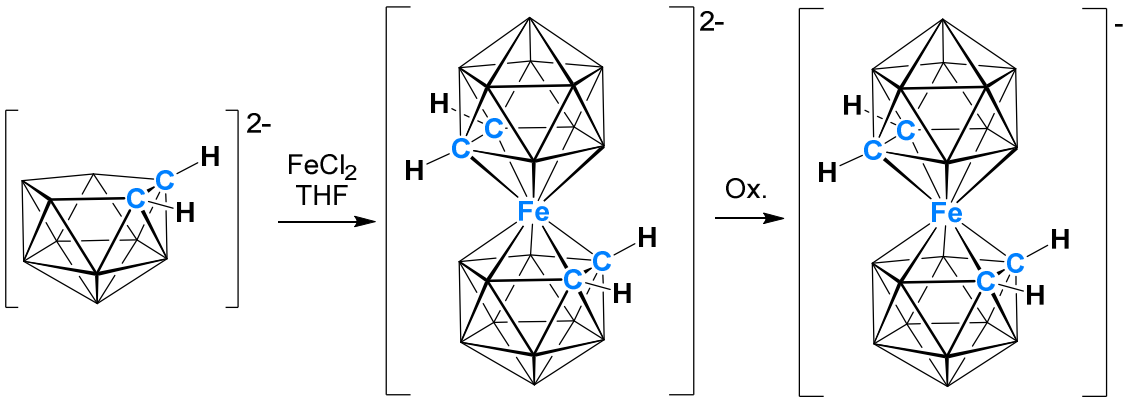

Scheme 1.4 Synthesis of the first metallacarborane $[Fe(C_2B_9H_{11})_2]^{2-}$.

Another method of producing metallacarboranes is *via* reduction of the parent carborane, which opens up the cage structure, allowing reaction with a suitable metal fragment.[46] The carborane is reduced by reaction with sodium metal (often in the presence of naphthalene) to give the dianion. By using reduction methods, the number of vertices in the cage can be increased as no {BH} units are lost (compared to decapitation). Following reduction to the dianion $[7,9\text{-}C_2B_{10}H_{12}]^{2-}$, a suitable reagent can be added to yield higher vertex structures. One of the first examples was reported by Hawthorne et al. in 1971, whereby reduced *o*-carborane was reacted with NaCp and $CoCl_2$ which *in situ* would form $\{CoCp\}^{2+}$.[47] This afforded the 13-vertex metallacarborane 4-Cp-4,1,6-*closo*-$CoC_2B_{10}H_{12}$, Scheme 1.5. This work was further expanded to include several other supraicosahedral metallacarboranes.[48] Depending on where the carbon atoms are placed within the cage, several isomers are possible, however the kinetically stable form is the 4-Cp-4,1,6-*closo*-$CoC_2B_{10}H_{12}$ isomer, produced from the initial reduction and metalation reaction.[40]

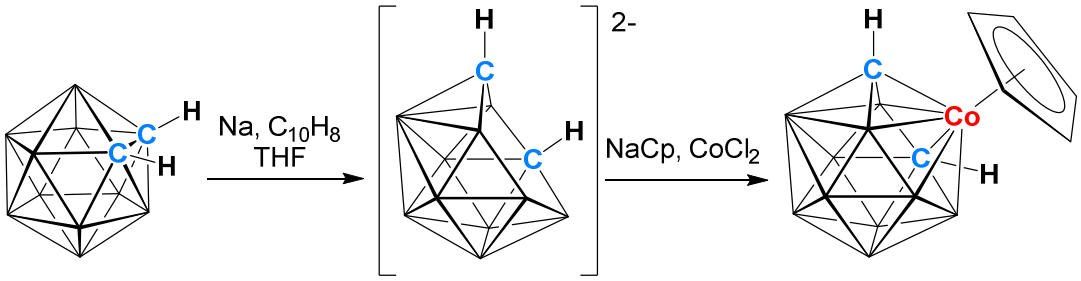

Scheme 1.5 The reduction of *o*-carborane using sodium naphthalenide to give 4-Cp-4,1,6-*closo*-$CoC_2B_{10}H_{12}$.

Although supraicosahedral metallacarboranes have been known for many years, it was only in 2003 that the first supraicosahedral carborane was synthesised, by Welch et al.[49] It was noted that upon reduction the carbon atoms are separated by a boron atom on the open face but become adjacent again upon oxidation back to the 12-vertex *closo*-cluster.[50] Therefore Welch and co-workers introduced a tether to *o*-carborane to prevent movement of the carbon atoms during reduction and metalation, which led to the synthesis of [1,2-μ-$C_6H_4(CH_2)_2$}-3-Ph-1,2-$C_2B_{11}H_{10}$], Figure 1.8.

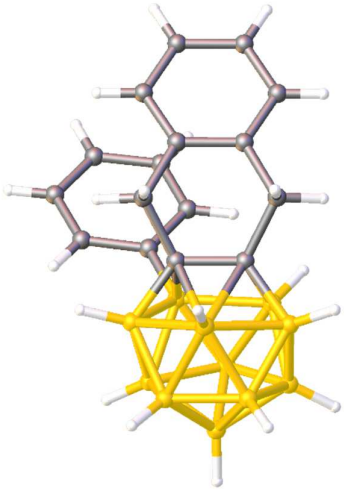

Figure 1.8 Perspective view of [1,2-μ-$C_6H_4(CH_2)_2$}-3-Ph-1,2-$C_2B_{11}H_{10}$].

1.9 1,1′-Bis(*o*-carborane)

In 1964 Hawthorne reported the first synthesis of 1,1′-bis(*o*-carborane) by the reaction between $B_{10}H_{12}(CH_3CN)_2$ and diacetylene in acetonitrile under reflux.[51] This produced 1,1′-bis(*o*-carborane) in low yields, 4%, and also ethynylcarborane, 35% yield. Heating to reflux for a longer period gave improved yields of 1,1′-bis(*o*-carborane), *ca*. 60%, Scheme 1.6.

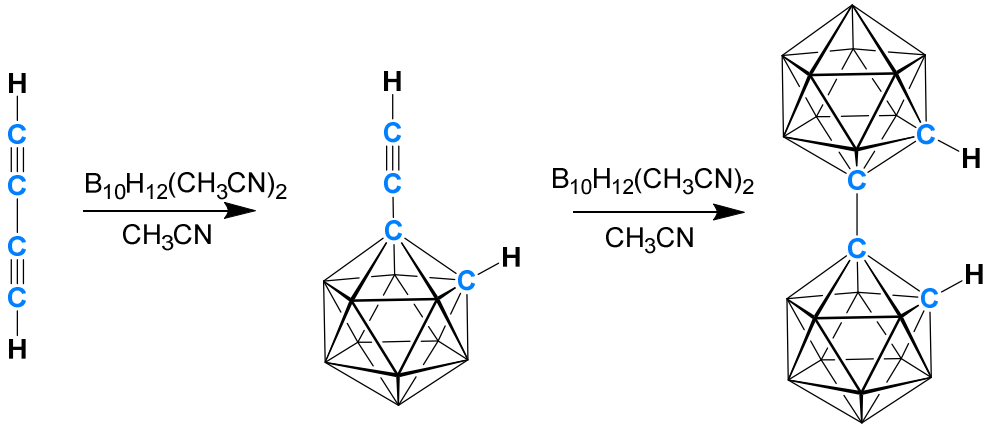

Scheme 1.6 First synthesis of 1,1′-bis(*o*-carborane) reported by Hawthorne in 1964.

In 1973 Hawthorne revisited the synthesis of the carborane dimer and substituted $B_{10}H_{12}[S(CH_2CH_3)_2]_2$ in place of $B_{10}H_{12}(CH_3CN)_2$, affording yields of 55-60%.[52] The reaction was carried out in toluene and the first stage was carried out at low temperature (-25 °C) to ensure the loss of diacetylene was minimised.

The γ-ray radiolysis of *o*-carborane by Klingen in 1976 yielded three gaseous products (hydrogen, methane and ethylene) and three solid products.[53] One of the observed solids was found to be an *o*-carborane dimer, showing a mass spectrometry envelope at *m/z* 278-290, and the report suggests linkage *via* a carbon-carbon bond. This indicates another method of synthesis although the reaction products were identified only by mass spectrometry and by the decreasing integral size of the cage CH peak in the ^{1}H NMR spectrum.

Hawthorne again explored the preparation of 1,1′-bis(*o*-carborane) in 1995 by reacting $Li_2[1,2\text{-}C_2B_{10}H_{10}]$ with copper (II) chloride in diethyl ether, which gave three products and a total yield of 30%.[54] The products were identified as 1,1′-bis(*o*-carborane), 1,3′-

bis(*o*-carborane) and 1,4′-bis(*o*-carborane) where the cages in the latter two products are linked by a carbon-boron bond, confirmed by the presence of unique cage CH peaks in their ^{1}H NMR spectra. The copper (II) chloride reaction with the monolithiated carborane salt also gave the three bis(*o*-carborane) products but in a reduced yield.

Both Zakharkin et al. (1973) and Hawthorne et al. (1992) explored the use of copper (I) or copper (II) chloride as a coupling agent.[55, 56] Subsequently, Xie reacted $Li_2[1,2\text{-}C_2B_{10}H_{10}]$ with 2.5 equivalents of copper (I) chloride in toluene at room temperature, hydrolysed with dil. HCl, and worked up to give the desired 1,1′-bis(*o*-carborane) in high yields, 83%.[57] The use of copper (I) salts minimises carbon-boron coupling between *o*-carborane cages. In this case using the monolithiated *o*-carborane as the starting material reduces the yield to 30% and it is also observed that the yield is significantly reduced when <2.5 equivalents of copper chloride are used. The synthetic route was shown, *via* a crystallographic study, to proceed *via* a copper-toluene carborane complex, Scheme 1.7.

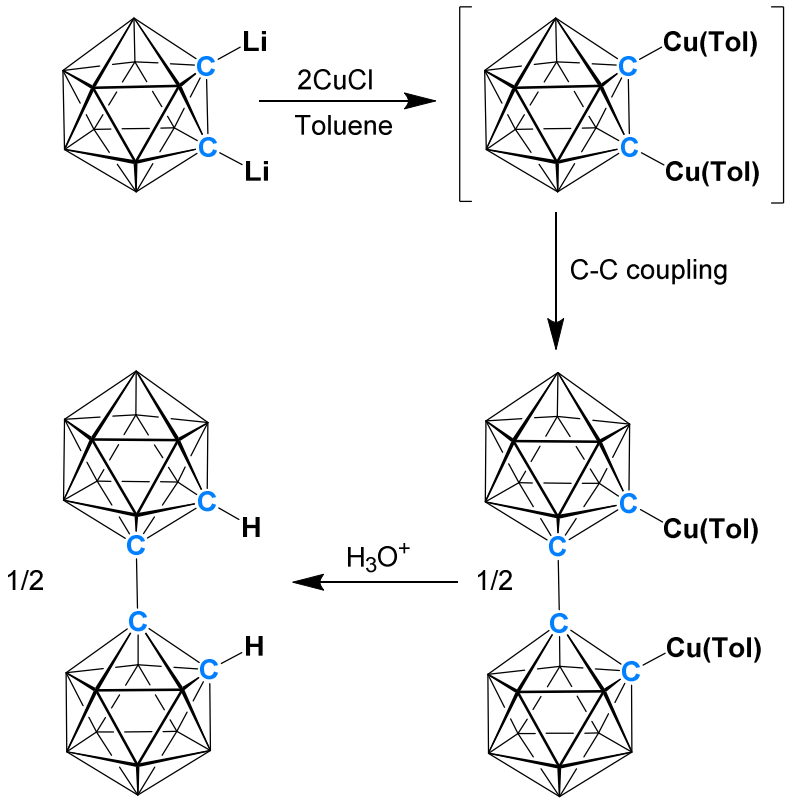

Scheme 1.7 Copper (I) coupling reaction of dilithiated *o*-carborane to give 1,1′-bis(*o*-carborane).

In 2014 Welch et al. determined that in the crystal structure of 1,1′-bis(*o*-carborane) there was disorder over two vertices which made distinguishing where C2 (the carbon atom not linking the cages together) was located quite difficult.[58] Welch and co-workers used the Vertex-to-Centroid distance (VCD) and the Boron-to-Hydrogen distance (BHD) methods to determine where C2 (and therefore also C2′) is located. Their work showed disorder between vertex-2 and vertex-3, with vertex-2 having 50% carbon and 50% boron character and vertex-3 also having 50% carbon and 50% boron character, Figure 1.9.

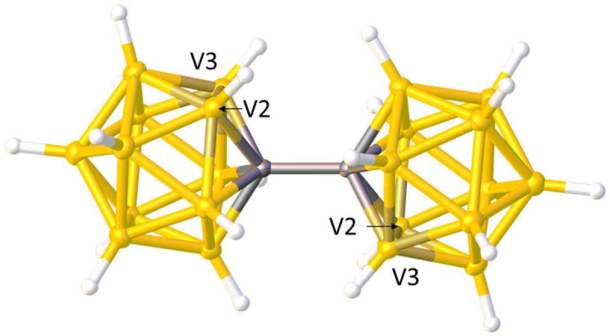

Figure 1.9 Perspective view of 1,1′-bis(*o*-carborane) which shows 50% occupancy of carbon and boron for both vertex-2 and vertex-3.

1.10 1,1′-Bis(*o*-carborane) as a Chelating Ligand to Metal Centres

Since its discovery in 1964, there has been a substantial amount of research into the reactivity and uses of 1,1′-bis(*o*-carborane).[59] Examples of transition metal monosubstituted *o*-carborane systems have been known since the 1960's,[60, 61] all exploiting a single metal-carbon σ-bond. In 1971 Hawthorne explored the potential of 1,1′-bis(*o*-carborane) as a σ-bonded chelating ligand.[62] 1,1′-Bis(*o*-carborane) has the ability to form two σ-bonds to a transition metal centre, producing a five membered ring, and consequently Hawthorne sought to utilise 1,1′-bis(*o*-carborane) as a bidentate ligand. Two equivalents of dilithiated 1,1′-bis(*o*-carborane) reacted at ambient temperature with transition metal dihalides to form a variety of derivatives all containing metal-carbon σ-bonds. The use of two equivalents of ligand provided the metal centre with the opportunity to form four σ-bonds to two bidentate 1,1′-bis(*o*-carborane) units, affording four-coordinate transition metal complexes, Figure 1.10.

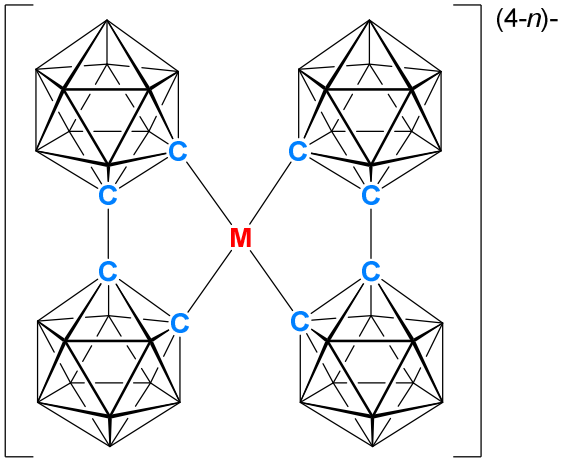

Figure 1.10 Use of 1,1′-bis(*o*-carborane) as a chelating bidentate ligand to transition metal centres to give $[M\{(C_2B_{10}H_{10})_2\}_2]^{(4-n)-}$. M = $Co^{II/III}$, $Ni^{II/III}$, $Cu^{II/III}$ or Zn^{II} and *n* is the metal oxidation state.

Using the ionic counting method each 1′-bis(*o*-carborane) would each donate four electrons to a metal centre; if two ligands are used this would give a total of eight bonding electrons. Given that there are no other ligands involved in these metal complexes, late

transition metals were used by Hawthorne to maximise the possibility of creating a stable 18-electron complex. The d^6 to d^{10} transition metals were used and the overall complexes synthesised were $[M\{(C_2B_{10}H_{10})_2\}_2]^{(4-n)-}$, with Cu^{II}, Ni^{II}, Co^{II} and Zn^{II} where n = 2 and Cu^{III}, Ni^{III} and Co^{III} where n = 1. These complexes were isolated as the tetraethylammonium salts *via* cation exchange and were thought to have square planar, tetragonal or *pseudo*-tetrahedral geometries depending on the metal cation.[63]

Another example whereby 1,1′-bis(*o*-carborane) acts as a chelating ligand to a metal centre was published by Welch et al. in 2015.[64] Dilithiated 1,1′-bis(*o*-carborane) was reacted with two nickel compounds, $NiCl_2$(dppe) and $NiCl_2$(dmpe), to produce [Ni(κ^2-2,2′-{1-(1′-1′,2′-*closo*-$C_2B_{10}H_{10}$)-1,2-*closo*-$C_2B_{10}H_{10}$})(dppe)] and [Ni(κ^2-2,2′-{1-(1′-1′,2′-*closo*-$C_2B_{10}H_{10}$)-1,2-*closo*-$C_2B_{10}H_{10}$})(dmpe)]. Two set of crystals were grown for the dppe derivative, both from THF/petroleum ether diffusion and from DCM/petroleum ether diffusion, with the latter shown in Figure 1.11 (left). Crystals of the dmpe derivative were also grown from a DCM/petroleum ether diffusion system, Figure 1.11 (right).

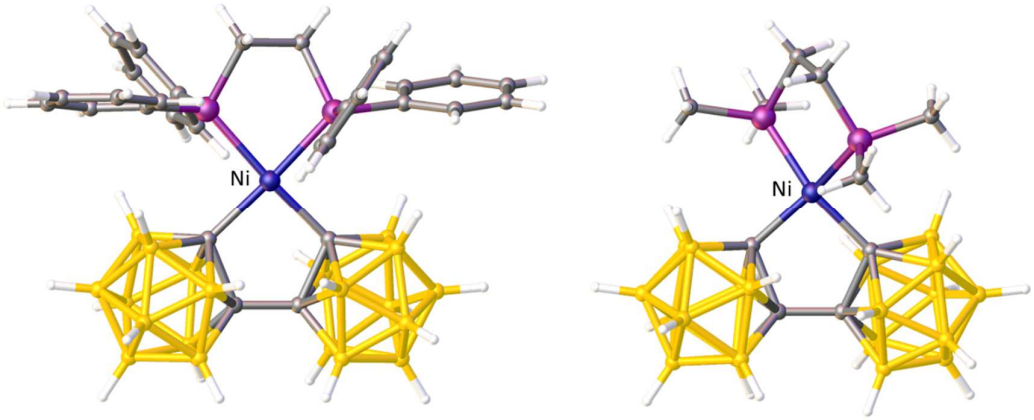

Figure 1.11 Perspective view of [Ni(κ^2-2,2′-{1-(1′-1′,2′-*closo*-$C_2B_{10}H_{10}$)-1,2-*closo*-$C_2B_{10}H_{10}$})(dppe)] (left) and [Ni(κ^2-2,2′-{1-(1′-1′,2′-*closo*-$C_2B_{10}H_{10}$)-1,2-*closo*-$C_2B_{10}H_{10}$})(dmpe)] (right).

Jin et al. published two compounds in 2015 whereby 1,1′-bis(*o*-carborane) acts as a ligand to {Ir(Cp*)} and {Rh(Cp*)}.[65] These were synthesised by reaction between dilithio-1,1′-bis(*o*-carborane) and $[Cp^*MCl_2]_2$ where M is iridium or rhodium. The products were

both identified by single crystal *X*-ray diffraction which confirmed bonding from 1,1′-bis(*o*-carborane) to the respective metal centres through two σ-bonds, Figure 1.12.

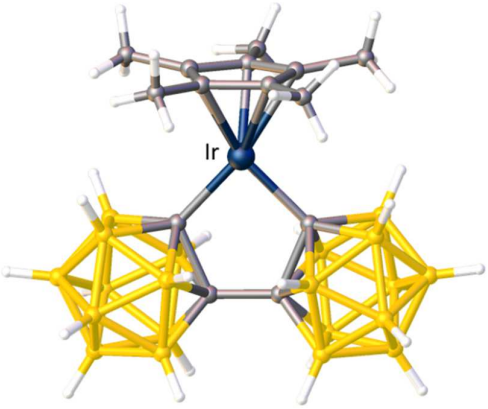

Figure 1.12 Perspective view of [Ir(κ^2-2,2′-{1-(1′-1′,2′-*closo*-$C_2B_{10}H_{10}$)-1,2-*closo*-$C_2B_{10}H_{10}$})(Cp*)].

Both [Ir(κ^2-2,2′-{1-(1′-1′,2′-*closo*-$C_2B_{10}H_{10}$)-1,2-*closo*-$C_2B_{10}H_{10}$})(Cp*)] and [Rh(κ^2-2,2′-{1-(1′-1′,2′-*closo*-$C_2B_{10}H_{10}$)-1,2-*closo*-$C_2B_{10}H_{10}$})(Cp*)] reported by Jin and co-workers are electronically unsaturated, *pseudo*-aromatic 16-electron compounds. Reaction between the iridium derivative and carbon monoxide yielded the corresponding 18-electron compound, Scheme 1.8.

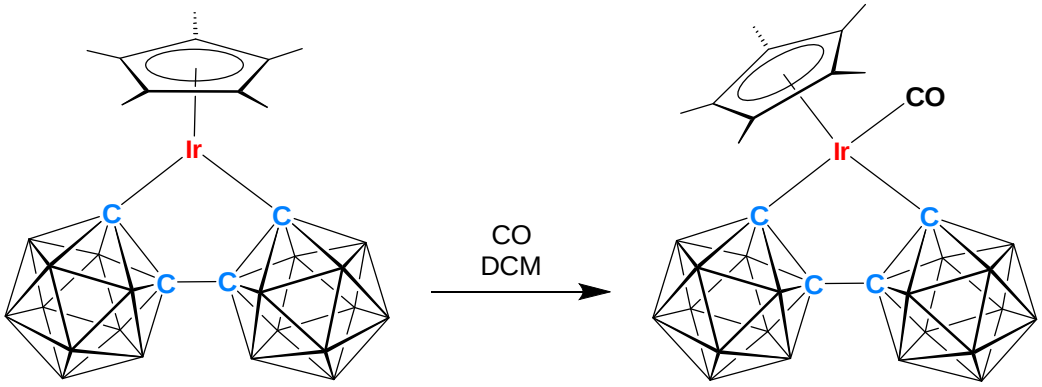

Scheme 1.8 Reaction to produce [Ir(κ^2-2,2′-{1-(1′-1′,2′-*closo*-$C_2B_{10}H_{10}$)-1,2-*closo*-$C_2B_{10}H_{10}$})(Cp*)(CO)], an electronically saturated compound.

In 2016 Spokoyny et al. reported two new compounds whereby a single 1,1′-bis(*o*-carborane) unit is chelated to either platinum or palladium dppe.[20] The first examples prepared by Spokoyny and co-workers were [Pd(κ^2-2,2′-{1-(1′-1′,2′-*closo*-$C_2B_{10}H_{10}$)-1,2-*closo*-$C_2B_{10}H_{10}$})(dppe)] and [Pt(κ^2-2,2′-{1-(1′-1′,2′-*closo*-$C_2B_{10}H_{10}$)-1,2-*closo*-$C_2B_{10}H_{10}$})(dppe)], which were synthesised in the hope of being used as a blue organic light emitting diode (OLED's), Figure 1.13. These were synthesised by reaction of dilithiated 1,1′-bis(*o*-carborane) with M(dppe)Cl_2 (M = Pd, Pt) in THF at -80 °C and then warming to room temperature and stirring overnight.

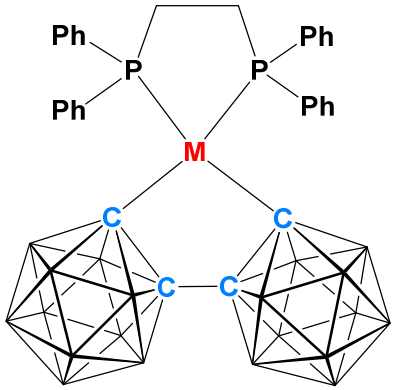

Figure 1.13 Representation of the compounds synthesised by Spokoyny et al., where M = Pd or Pt.

In an attempt to further improve the OLED efficiency of these carborane derivatives, Spokoyny and co-workers reacted dilithiated 1,1′-bis(*o*-carborane) with 4,4′-di-*tert*-2,2′-bipyridine (dtb-bpy) under the same conditions as previously used. This led to the formation of two products [Pt(κ^2-2,2′-{1-(1′-1′,2′-*closo*-$C_2B_{10}H_{10}$)-1,2-*closo*-$C_2B_{10}H_{10}$})(dtb-bpy)], Figure 1.14, and [Pt(κ^2-2,3′-{1-(1′-1′,2′-*closo*-$C_2B_{10}H_{10}$)-1,2-*closo*-$C_2B_{10}H_{10}$})(dtb-bpy)]. The two isomers were identified using ^{1}H NMR spectroscopy and the single crystal *X*-ray diffraction study of both compounds showed that in one isomer the 1,1′-bis(*o*-carborane) unit binds to the metal centre through two carbon σ-bonds [X_2(*C*,*C*′)], whereas the other binds through one carbon σ-bond and one boron σ-bond [X_2(*C*,*B*′)]. In an attempt to synthesise only the X_2(*C*,*B*′) derivative, ethyl groups were installed at B9, B12, B9′ and B12′ before reaction with {Pt(dtb-bpy)} and this successfully formed the desired product in over 80% yields.

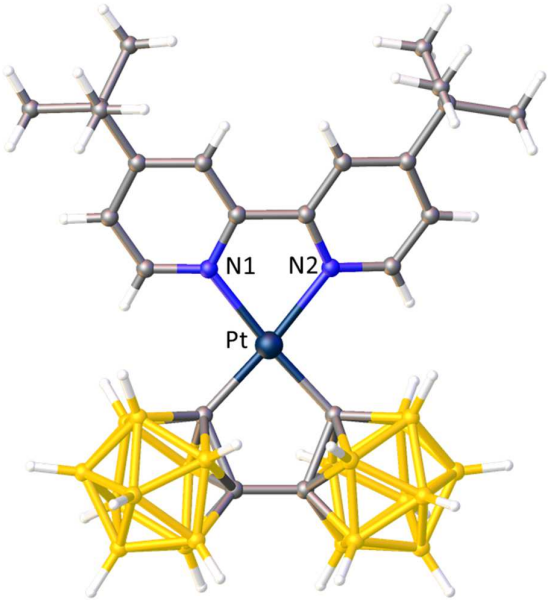

Figure 1.14 Perspective view of [Pt(κ^2-2,2′-{1-(1′-1′,2′-*closo*-$C_2B_{10}H_{10}$)-1,2-*closo*-$C_2B_{10}H_{10}$})(dtb-bpy)].

1.11 1,1′-Bis(*o*-carborane) as a Host for Incorporating Non-Transition Metal Units

There are few examples whereby 1,1′-bis(*o*-carborane) acts in a bridging manner to non-transition metal atoms. Two of the first examples were reported by Zakharkin et al. in 1978 and were synthesised by reaction of dilithio-1,1′-bis(*o*-carborane) with either $PPhCl_2$ or $AsMeCl_2$ to give [μ-2,2′-PPh-{1-(1′-1′,2′-*closo*-$C_2B_{10}H_{10}$)-1,2-*closo*-$C_2B_{10}H_{10}$}] and [μ-2,2′-AsMe-{1-(1′-1′,2′-*closo*-$C_2B_{10}H_{10}$)-1,2-*closo*-$C_2B_{10}H_{10}$}], Figure 1.15.[66] In both cases only the melting point and elemental analysis were reported and no further reactions were carried out on these compounds.

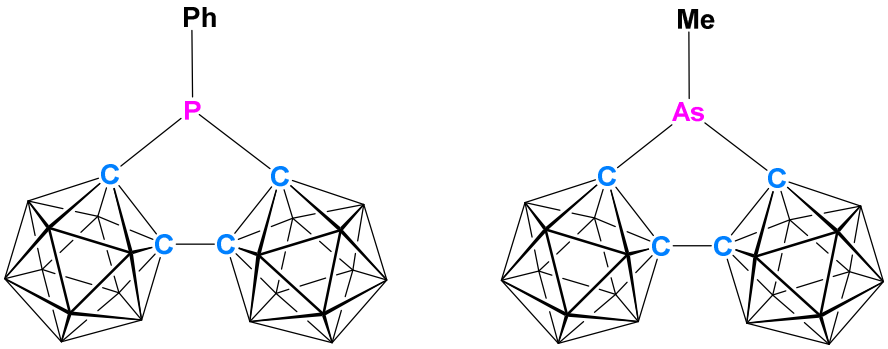

Figure 1.15 [μ-2,2′-PPh-{1-(1′-1′,2′-*closo*-$C_2B_{10}H_{10}$)-1,2-*closo*-$C_2B_{10}H_{10}$}] and [μ-2,2′-AsMe-{1-(1′-1′,2′-*closo*-$C_2B_{10}H_{10}$)-1,2-*closo*-$C_2B_{10}H_{10}$}].

Further discussion of [μ-2,2′-AsMe-{1-(1′-1′,2′-*closo*-$C_2B_{10}H_{10}$)-1,2-*closo*-$C_2B_{10}H_{10}$}] was given in a second paper by Zakharkin in 1979, including crystallographic information.[67] It was reported that the C-As-C angle was 89.9(2)°, much lower than in related compounds due to the rigidity of the bis(carborane) substituent. Another compound, [μ-1,1′-CH_2-μ-2,2′-PMe-{1-(1′-1′,2′-*closo*-$C_2B_{10}H_{10}$)-1,2-*closo*-$C_2B_{10}H_{10}$}], was also reported however as can be seen from Figure 1.16 this is not a direct 1,1′-bis(*o*-carborane) derivative.

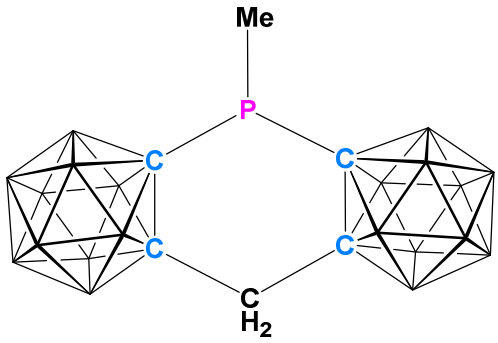

Figure 1.16 [μ-1,1′-CH_2-$μ^2$-2,2′-PMe-{1-(1′-1′,2′-*closo*-$C_2B_{10}H_{10}$)-1,2-*closo*-$C_2B_{10}H_{10}$}].

In 1996 Knobler and Johnson synthesised two carboranylhalophosphines by reacting dilithiated 1,1′-bis(*o*-carborane) with PCl_3 to give [μ-2,2′-PCl-{1-(1′-1′,2′-*closo*-$C_2B_{10}H_{10}$)-1,2-*closo*-$C_2B_{10}H_{10}$}]. This was converted to [μ-2,2′-PF-{1-(1′-1′,2′-*closo*-$C_2B_{10}H_{10}$)-1,2-*closo*-$C_2B_{10}H_{10}$}] by reaction with $AgSbF_6$, Scheme 1.9.[68]

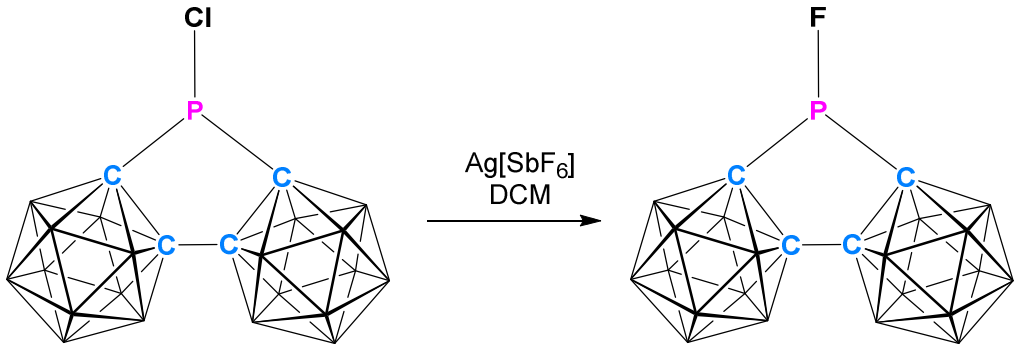

Scheme 1.9 Conversion of [μ-2,2′-PCl-{1-(1′-1′,2′-*closo*-$C_2B_{10}H_{10}$)-1,2-*closo*-$C_2B_{10}H_{10}$}] to [μ-2,2′-PF-{1-(1′-1′,2′-*closo*-$C_2B_{10}H_{10}$)-1,2-*closo*-$C_2B_{10}H_{10}$}] using Ag[SbF_6].

In 1996 Hawthorne et al. synthesised a gold phosphine compound that utilised one 1,1′-bis(*o*-carborane) unit.[69] Although gold is found in the transition metal group in the periodic table, by following IUPAC rules it can be considered a *pseudo* non-transition metal element as it has a full *d* sub-shell when in the gold(I) oxidation state. The compound [μ-2,2′-$(AuPPh_3)_2$-{1-(1′-1′,2′-*closo*-$C_2B_{10}H_{10}$)-1,2-*closo*-$C_2B_{10}H_{10}$}] was

afforded by reaction of dilithiated 1,1′-bis(*o*-carborane) with (triphenylphosphine)gold(I) chloride. An *X*-ray diffraction study of single crystals of this compound showed it to have an aurophilic Au-Au interaction with an Au(1)-Au(2) distance of 3.119(2) Å, Figure 1.17.

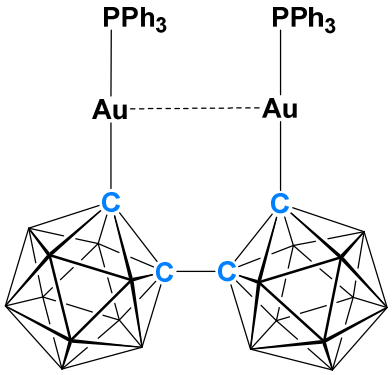

Figure 1.17 [μ-2,2′-(AuPPh$_3$)$_2$-{1-(1′-1′,2′-*closo*-$C_2B_{10}H_{10}$)-1,2-*closo*-$C_2B_{10}H_{10}$}].

The most recent publication regarding a 1,1′-bis(*o*-carborane) derivative was by Peryshkov et al. in 2016 and reported the first example of one cage remaining closo and the other being a 12-vertex nido cage, Figure 1.18.[70] This compound was synthesised by reaction of dilithiated 1,1′-bis(*o*-carborane) with 2.4 equivalents of methyl lithium and 2.4 equivalents of PR_2Cl_2 (where R is *i*Pr, N(*i*Pr)$_2$ or Ph) at room temperature. All three examples display 1,1′-bis(*o*-carborane) bonding to a phosphine through one carbon σ-bond (on the closo cage) and one boron σ-bond (on the nido cage). This is readily observed using $^{31}P\{^1H\}$ NMR whereby two phosphorus signals are observed, one sharp signal originating from the *exo*-phosphine coordinated only to the nido cage and one broad signal deriving from the phosphine coordinated to the boron atom of the nido cage and carbon atom of the closo cage.

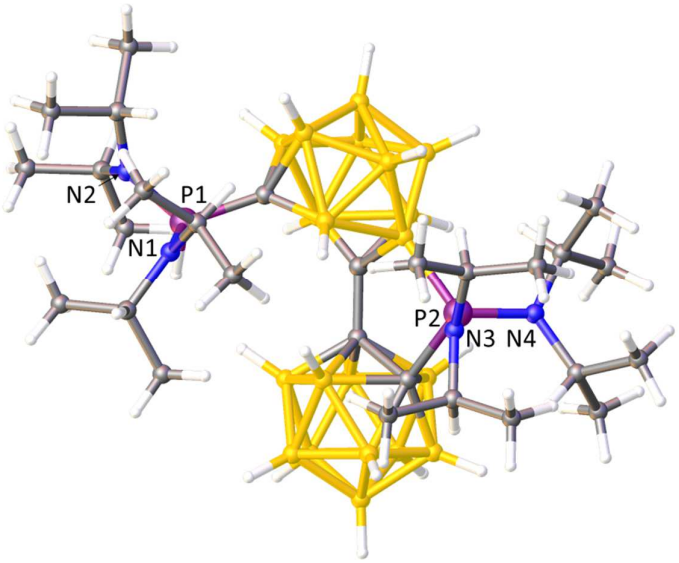

Figure 1.18 Perspective view of [μ-2,2′-P*i*Pr$_2$-{1-(1′-1′,2′-*closo*-$C_2B_{10}H_{10}$)-4-PH*i*Pr$_2$-1,2-*nido*-$C_2B_{10}H_{10}$}], one of the examples of a closo/nido 1,1′-bis(*o*-carborane) diphosphine synthesised by Peryshkov et al.

1.12 Decapitation and Metalation Reactions of 1,1′-Bis(*o*-carborane)

Decapitation and metalation reactions have been applied to *o*-carborane in many hundreds of examples and can also be applied to 1,1′-bis(*o*-carborane). In 1971 Hawthorne et al. reported the degradation (decapitation) of 1,1′-bis(*o*-carborane) using ethanolic potassium hydroxide at reflux temperatures.[71] After a 1.5 hour reflux a monoanion was synthesised and further reflux for 120 hours generated the dianion; these were isolated in high yields as the cesium or ammonium salts. Structures were proposed for the mono- and dianionic species, [7-(1′-1′,2′-*closo*-$C_2B_{10}H_{11}$)-7,8-*nido*-$C_2B_9H_{11}$]$^-$ and [7-(7′-7′,8′-*nido*-$C_2B_9H_{11}$)-7,8-*nido*-$C_2B_9H_{11}$]$^{2-}$, which were later confirmed by Welch et al., Figure 1.19.[72, 73]

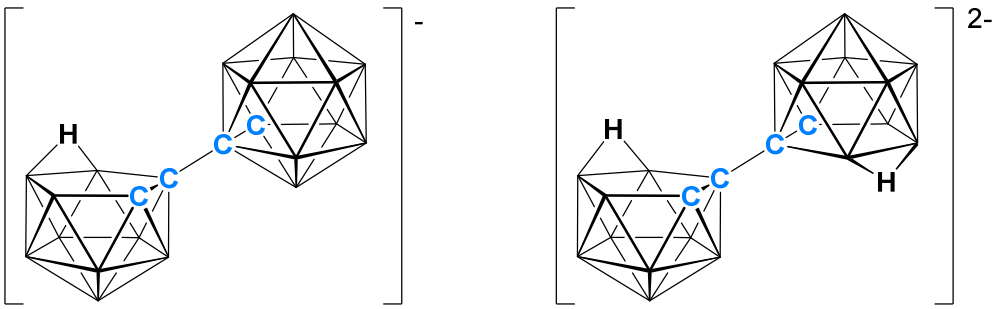

Figure 1.19 [7-(1′-1′,2′-*closo*-$C_2B_{10}H_{11}$)-7,8-*nido*-$C_2B_9H_{11}$]$^-$ and [7-(7′-7′,8′-*nido*-$C_2B_9H_{11}$)-7,8-*nido*-$C_2B_9H_{11}$]$^{2-}$. C2 and C2′ hydrogen atoms removed for clarity.

Another route to the monoanion [7-(1′-1′,2′-*closo*-$C_2B_{10}H_{11}$)-7,8-*nido*-$C_2B_9H_{11}$]$^-$ was reported in 2016 by Sivaev et al.[74] 1,1′-Bis(*o*-carborane) was decapitated using only water and acetonitrile at room temperature, affording the singly-deboronated product which was isolated as the trimethylammonium salt. This reaction was possible due to the strong electron withdrawing nature of the *o*-carboranyl group. Further decapitation was not possible, even at reflux temperatures, due to the loss of the electron withdrawing effect of the *o*-carboranyl group after the first deboranation.

Several metallabis(*o*-carboranes) have been published but one of the first was by Hawthorne et al. who reported the synthesis of a bimetallic 1,1′-bis(*o*-carborane),

whereby the two clusters were connected *via* four bonds, Figure 1.20.[75, 76] This was afforded by reaction between Cs_2[7-(7′-7′,8′-*nido*-$C_2B_9H_{11}$)-7,8-*nido*-$C_2B_9H_{11}$] and [RhCl(COD)(PEt_3)]. The original C-C connectivity between both 12-vertex cages remains, but there is also one Rh-Rh bond and two Rh-H-B 3c-2e bridging bonds joining the two clusters.

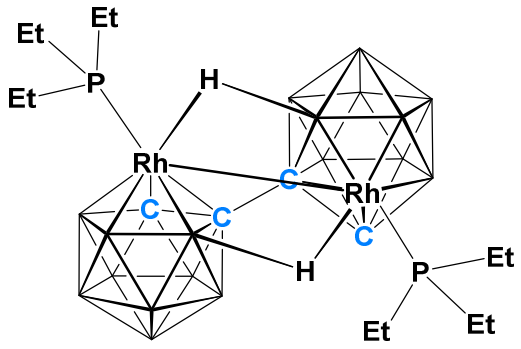

Figure 1.20 [Rh(PEt_3)$C_2B_9H_{10}$]$_2$ which contains one Rh-Rh bond and two Rh-H-B bridges. C2 and C2′ hydrogens removed for clarity.

In 1984, Hawthorne et al. reported the synthesis of a new species which was prepared by reacting Tl[7-(1′-1′,2′-*closo*-$C_2B_{10}H_{11}$)-7,8-*nido*-$C_2B_9H_{11}$] with [RhCl(PPh_3)$_3$].[77] The product was isolated in 91% yield and the structure proposed to be a salt, whereby the rhodium is not coordinated to the cage. Upon reaction with triethylphosphine the closo/nido salt [Rh(PPh_3)$_3$][7-(1′-1′,2′-*closo*-$C_2B_{10}H_{11}$)-7,8-*nido*-$C_2B_9H_{11}$] was transformed into a closo/closo metallacarborane, [2,2-(PEt_3)$_2$-2-H-8-(1′-1′,2′-*closo*$C_2B_{10}H_{11}$)-2,1,8-*closo*-Rh$C_2B_9H_{10}$], Scheme 1.10.

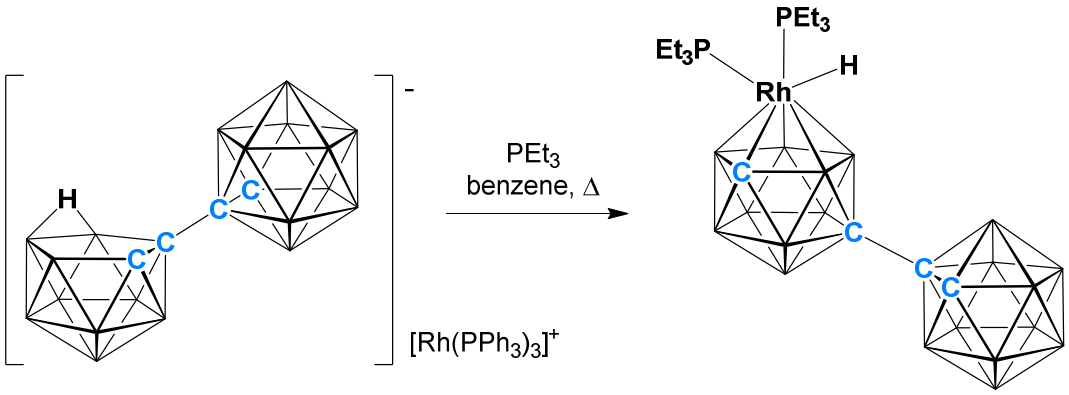

Scheme 1.10 Reaction of $[(PPh_3)_3Rh][7\text{-}(1'\text{-}1',2'\text{-}closo\text{-}C_2B_{10}H_{11})\text{-}7,8\text{-}nido\text{-}C_2B_9H_{11}]$ with PEt_3 to afford $[2,2\text{-}(PEt_3)_2\text{-}2\text{-}H\text{-}8\text{-}(1'\text{-}1',2'\text{-}closo C_2B_{10}H_{11})\text{-}2,1,8\text{-}closo\text{-}RhC_2B_9H_{10}]$. C2 and C2′ hydrogens removed for clarity.

In 2015 Welch et al. explored the reactivity of $[7\text{-}(1'\text{-}1',2'\text{-}closo\text{-}C_2B_{10}H_{11})\text{-}7,8\text{-}nido\text{-}C_2B_9H_{11}]^-$ with different metal fragments.[72] The synthesis involved reacting singly-decapitated bis(*o*-carborane) with *n*BuLi (to remove the bridging BHB proton) followed by reaction with $\{Ru(p\text{-cymene})\}^{2+}$. This produced two isomers, $[1\text{-}(1'\text{-}1',2'\text{-}closo\text{-}C_2B_{10}H_{11})\text{-}3\text{-}(p\text{-cymene})\text{-}3,1,2\text{-}closo\text{-}RuC_2B_9H_{10}]$ (**A**) and $[8\text{-}(1'\text{-}1',2'\text{-}closo\text{-}C_2B_{10}H_{11})\text{-}2\text{-}(p\text{-cymene})\text{-}2,1,8\text{-}closo\text{-}RuC_2B_9H_{10}]$ (**B**), in 8 and 19% yields respectively, Figure 1.21. It was observed that over time the 3,1,2-isomer transformed into the 2,1,8-isomer and a 2 hour reflux in THF resulted in full conversion.

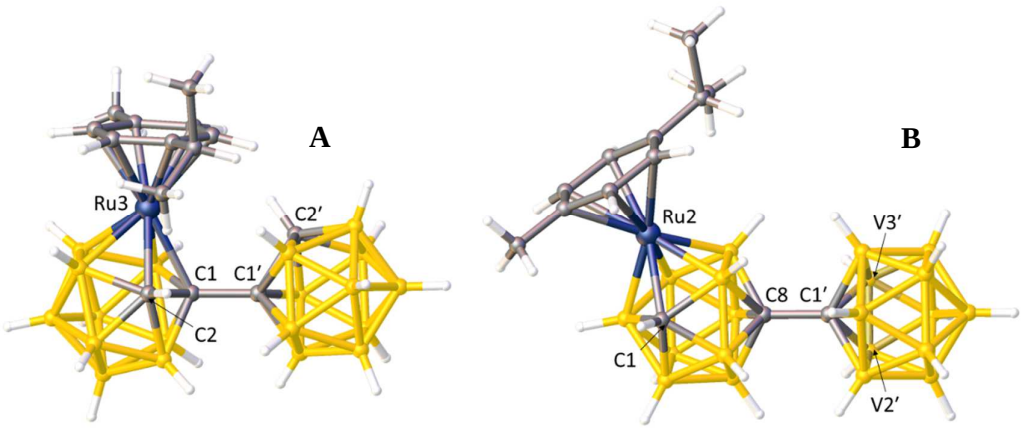

Figure 1.21 Perspective view of [1-(1′-1′,2′-*closo*-$C_2B_{10}H_{11}$)-3-(*p*-cymene)-3,1,2-*closo*-$RuC_2B_9H_{10}$] (**A**) and [8-(1′-1′,2′-*closo*-$C_2B_{10}H_{11}$)-2-(*p*-cymene)-2,1,8-*closo*-$RuC_2B_9H_{10}$] (**B**). Note that there is disorder in molecule **B** over vertices 2′ and 3′.

Further to this, Welch et al. carried out the reaction between [7-(1′-1′,2′-*closo*-$C_2B_{10}H_{11}$)-7,8-*nido*-$C_2B_9H_{10}]^{2-}$ and either [CoI_2(CO)Cp] to give [1-(1′-1′,2′-*closo*-$C_2B_{10}H_{11}$)-3-Cp-3,1,2-*closo*-$CoC_2B_9H_{10}$] (**C**) or $CoCl_2$/NaCp to give [8-(1′-1′,2′-*closo*-$C_2B_{10}H_{11}$)-2-Cp-2,1,8-*closo*-$CoC_2B_9H_{10}$] (**D**), Figure 1.22. Metallation using {CoCp} affords different isomers depending on whether the metal fragment is preformed, [CoI_2(CO)Cp], or made *in situ*, $CoCl_2$/NaCp. This is believed to be because the reactive fragment of the anion *in situ* reaction would be $\{Co^{II}Cp\}^+$, generating a 19-electron metallacarborane which isomerises before being oxidised to the 18-electron species **D**.

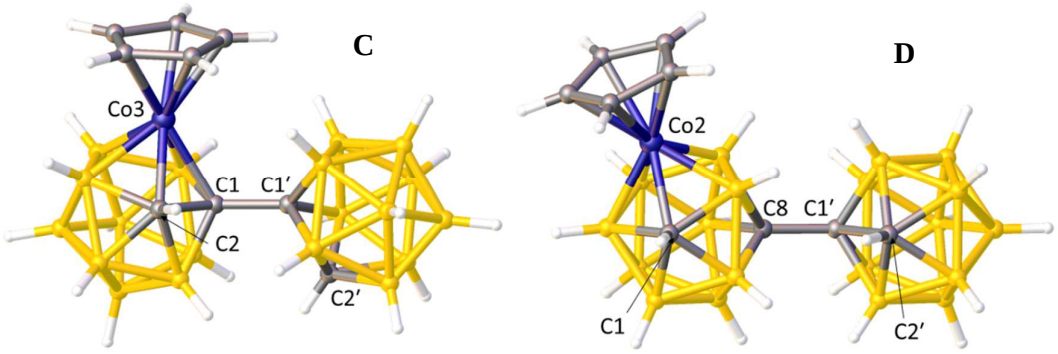

Figure 1.22 Perspective view of [1-(1′-1′,2′-*closo*-$C_2B_{10}H_{11}$)-3-Cp-3,1,2-*closo*-$CoC_2B_9H_{10}$] (**C**) and [8-(1′-1′,2′-*closo*-$C_2B_{10}H_{11}$)-2-Cp-2,1,8-*closo*-$CoC_2B_9H_{10}$] (**D**).

In 2016 Welch and co-workers further expanded the single metalation of 1,1′-bis(*o*-carborane) to produce eight new nickelacarboranes and several other derivatives.[78] The first to be synthesised was [1-(1′-1′,2′-*closo*-$C_2B_{10}H_{11}$)-3-dppe-3,1,2-*closo*-$NiC_2B_9H_{10}$] (**E**) which was isomerised to the 4,1,2-isomer under THF reflux conditions. The paper uses a range of {NiPR} fragments to show that the steric and electronic properties of the inserted metal unit have an effect on the isomer of metallacarborane formed. Another compound synthesised was [1-(1′-1′,2′-*closo*-$C_2B_{10}H_{11}$)-3-{$P(OMe)_3$}$_2$-3,1,2-*closo*-$NiC_2B_9H_{10}$] (**F**) which interestingly displayed a hydrogen bond between atoms O21 and H2′, of length 2.19(4) Å, Figure 1.23.

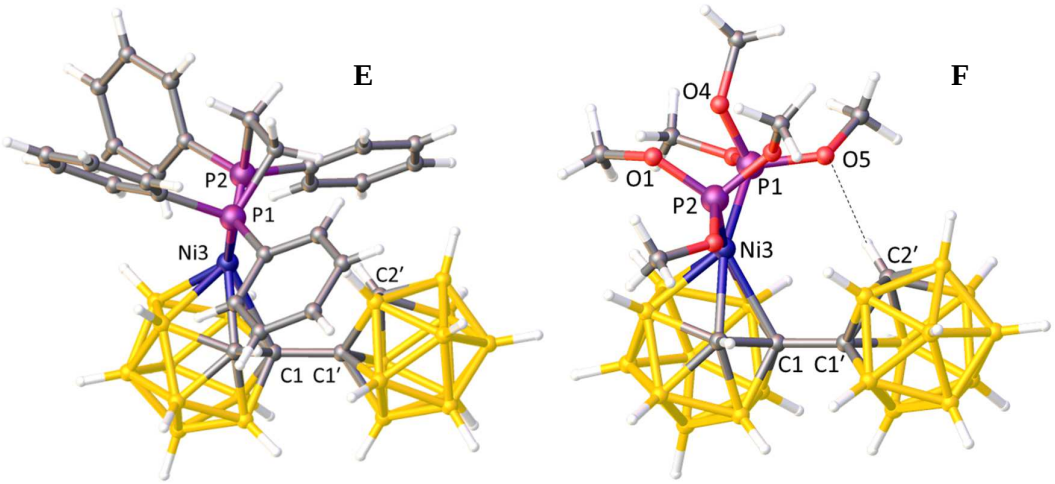

Figure 1.23 Perspective view of [1-(1′-1′,2′-*closo*-$C_2B_{10}H_{11}$)-3-dppe-3,1,2-*closo*-$NiC_2B_9H_{10}$] (**E**) and [1-(1′-1′,2′-*closo*-$C_2B_{10}H_{11}$)-3-{$P(OMe)_3$}$_2$-3,1,2-*closo*-$NiC_2B_9H_{10}$] (**F**), with hydrogen bond shown for **F**.

More recently Welch and co-workers reported an improved synthesis of [7-(7′-7′,8′-*nido*-$C_2B_9H_{11}$)-7,8-*nido*-$C_2B_9H_{11}$]$^{2-}$ by using a large excess of KOH (25 to 30 equivalents) in ethanol. They then went on to react salts (Tl, $HNMe_3$) of the doubly decapitated 1,1′-bis(*o*-carborane) with either {Ru(*p*-cymene)}$^{2+}$ or {CoCp}$^{2+}$.[73] Due to their being *rac* and *meso* forms of the doubly decapitated 1,1′-bis(*o*-carborane) the products were formed as diastereoisomers. Isomers of the 3,1,2-RuC_2B_9-2′,1′,8′-RuC_2B_9 species (**G**) were isolated upon reaction with {Ru(*p*-cymene)}$^{2+}$. Metalation with {CoCp}$^{2+}$ using [CpCo(CO)I_2] afforded the 3,1,2-CoC_2B_9-3′,1′,2′-CoC_2B_9 species (**H**) which produces the 2,1,8-CoC_2B_9-2′,1′,8′-CoC_2B_9 species (**Iα** & **Iβ**) upon redox and the 3,1,2-CoC_2B_9-2′,1′,8′-CoC_2B_9 species upon thermolysis. Selected single crystal *X*-ray structures are shown in Figure 1.24.

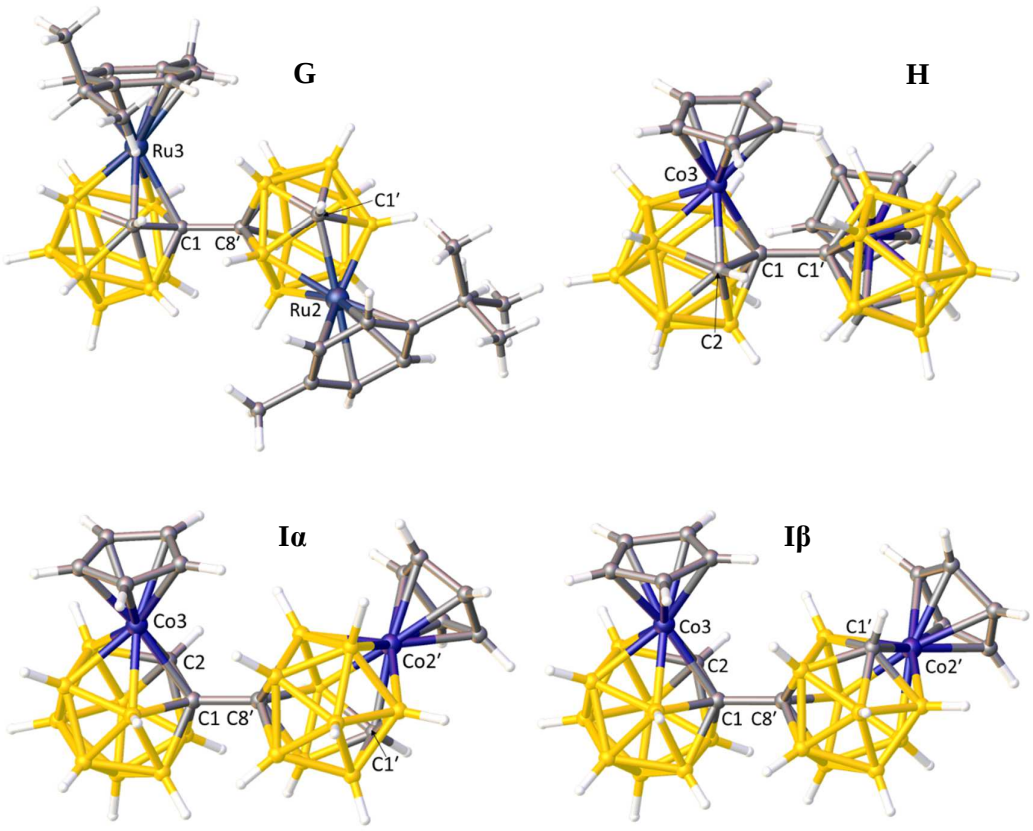

Figure 1.24 Perspective view of selected double metalation products: 3,1,2-RuC_2B_9-2′,1′,8′-RuC_2B_9 (**G**), 3,1,2-CoC_2B_9-3′,1′,2′-CoC_2B_9 (**H**) and 3,1,2-CoC_2B_9-2′,1′,8′-CoC_2B_9 (**Iα** & **Iβ**).

1.13 Reduction and Metalation Reactions of 1,1′-Bis(*o*-carborane)

As with *o*-carborane, 1,1′-bis(*o*-carborane) can be reduced by two electrons using two equivalents of sodium metal or a sodium naphthalenide solution, to give the sodium salt.[79, 80] The structure was revealed by Hawthorne and co-workers to have the two cages related by an inversion centre at the mid-point of the C-C bond and, as with *o*-carborane, the reduction has broken the C-C bonds within the cage. This structure is believed to be in equilibrium with a structure which has one nido 12-vertex cage and one closo 12-vertex cage, Scheme 1.11.[81] A four electron reduction is also viable, by using excess sodium metal or sodium naphthalenide solution which affords both cages of 1,1′-bis(*o*-carborane) as nido 12-vertex structures.

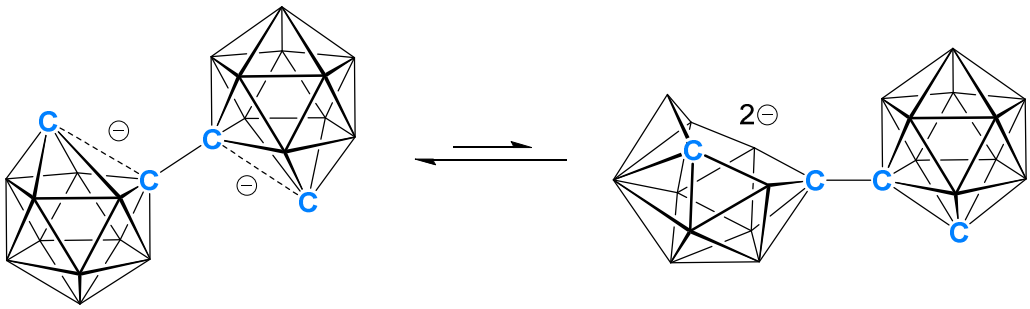

Scheme 1.11 The equilibrium of the two-electron reduction structures of 1,1′-bis(*o*-carborane). C2 and C2′ hydrogens removed for clarity.

In 2010 Welch et al. reported the synthesis of a 13-vertex/12-vertex 1,1′-bis(*o*-carborane) metal complex which was synthesised by a four electron reduction using lithium metal followed by reaction with $[RuCl_2(p\text{-cymene})]_2$.[82] The product was isolated as [1-(1′-1′,2′-*closo*-$C_2B_{10}H_{11}$)-4-{$C_{10}H_{14}$Ru(*p*-cymene)}-4,1,6-*closo*-$RuC_2B_{10}H_{11}$] in a 20% yield, Figure 1.25. The reaction was unprecedented as through addition of two equivalents of {Ru(*p*-cymene)} a flyover complex was formed, involving the cleavage of an aromatic C-C bond.

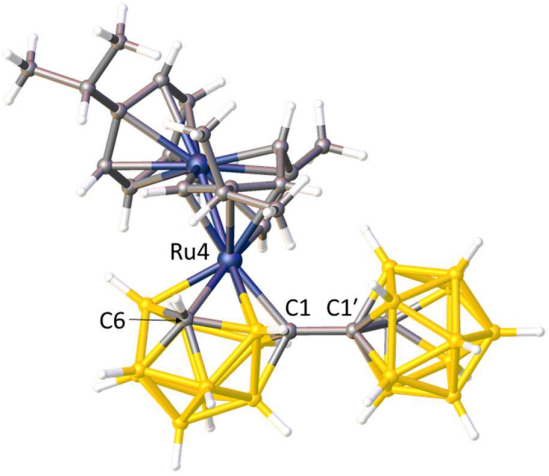

Figure 1.25 Perspective view of [1-(1′-1′,2′-*closo*-$C_2B_{10}H_{11}$)-4-{$C_{10}H_{14}$Ru(*p*-cymene)}-4,1,6-*closo*-$RuC_2B_{10}H_{11}$].

Metalation of both cages was achieved by Welch and co-workers in 2010 whereby the four-electron reduction of 1,1′-bis(*o*-carborane) *via* lithium naphthalenide followed by reaction with {CoCp} formed *in situ* using $CoCl_2$/NaCp, gave the *rac* and *meso* isomeric products of [1-(4′-Cp-4′,1′,6′-*closo*-$CoC_2B_{10}H_{11}$)-4-Cp-4,1,6-*closo*-$CoC_2B_{10}H_{11}$] (**J**), Figure 1.26.[83] In 2015 Welch et al. converted the 4,1,6-CoC_2B_{10}-4′,1′,6′-CoC_2B_{10} species to the *rac* and *meso* isomers of [1-(4′-Cp-4′,1′,12′-*closo*-$CoC_2B_{10}H_{11}$)-4-Cp-4,1,12-*closo*-$CoC_2B_{10}H_{11}$] (**K**) by heating to 180 °C.[84]

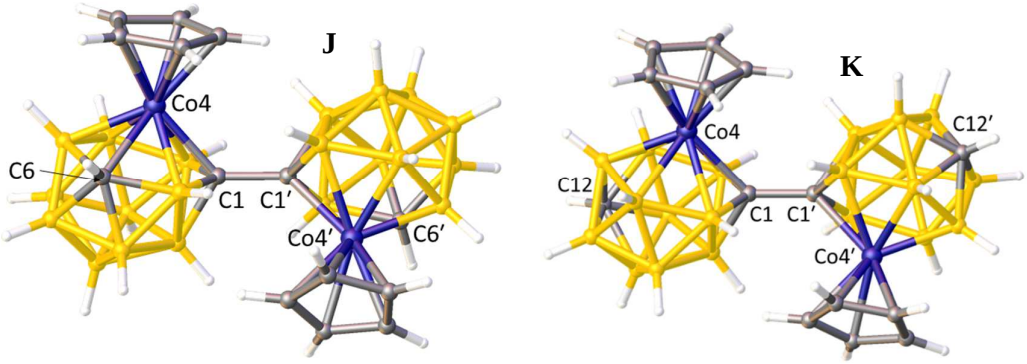

Figure 1.26 Perspective view of one of the diastereoisomers of both [1-(4′-Cp-4′,1′,6′-*closo*-$CoC_2B_{10}H_{11}$)-4-Cp-4,1,6-*closo*-$CoC_2B_{10}H_{11}$] (**J**) and [1-(4′-Cp-4′,1′,12′-*closo*-$CoC_2B_{10}H_{11}$)-4-Cp-4,1,12-*closo*-$CoC_2B_{10}H_{11}$] (**K**).

1.14 Tethered 1,1′-Bis(*o*-carborane)

There has been little research published whereby 1,1′-bis(*o*-carborane) has been used in organic frameworks or where a tether has been introduced into the unit. In 1976 Klingen and Mathur detected the presence of a trimer formed during the γ-ray radiolysis of *o*-carborane, identified by its envelope in the mass spectrum at *m/z* 416-425.[53] This was interpreted as the result of joining three *o*-carborane units, via carbon-carbon or carbon-boron bonds, to give a six membered ring, Figure 1.27, or alternatively, as a 1,1′-bis(*o*-carborane) unit with an *o*-carborane unit as a tether.

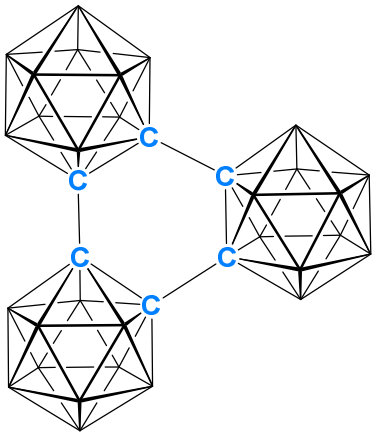

Figure 1.27 Proposed structure of an *o*-carborane trimer, with all C-C linkages, forming a central six membered ring.

Hawthorne, in 1995, went on to discuss the potential of synthesising such oligomers on a quantitative scale via a copper (II) coupling mechanism but with limited success, producing only the *o*-carborane dimers 1,1′-bis(*o*-carborane), 1,3′-bis(*o*-carborane) and 1,4′-bis(*o*-carborane).[54]

More recently in 2016 Xie et al. synthesised a CH_2CH_2 tethered 1,1′-bis(*o*-carborane) by reacting dilithiated 1,1′-bis(*o*-carborane) with dibromoethane.[85] The two carbon atoms from the tether, along with the carborane C2, C1, C1′ and C2′ atoms, produced a central six-membered ring. This compound was reduced using excess sodium metal and the *nido*-bis(*o*-carborane) tetraanion was isolated as the sodium salt and crystallised, Figure

1.28. It is interesting to note that both cages have been reduced by two electrons to give two nido cages, and although they are both dianions their structure differs slightly. One cage has an open face of six atoms, whereas the other cage only has five atoms on the open face.

Figure 1.28 Perspective view of the tethered *nido*-bis(*o*-carborane) tetranion.

Reaction of the reduced tetraanion with $\{Ru(p\text{-cymeme})\}^{2+}$ in THF gave four isolable products, with the starting material μ-2,2′-CH_2CH_2-1,1′-bis(*o*-carborane) as the major product in 70% yield. The second isolated compound (**L**) Figure 1.29, was a triple B-H insertion product isolated in 2% yield. A 12-vertex carborane/13-vertex ruthenacarborane (**M**) was synthesised in 10% yield and a 12-vertex ruthenacarborane/12-vertex ruthenacarborane (**N**) whereby the two cages are linked by CH_2CH_2 and CHCH was formed in 10% yield.

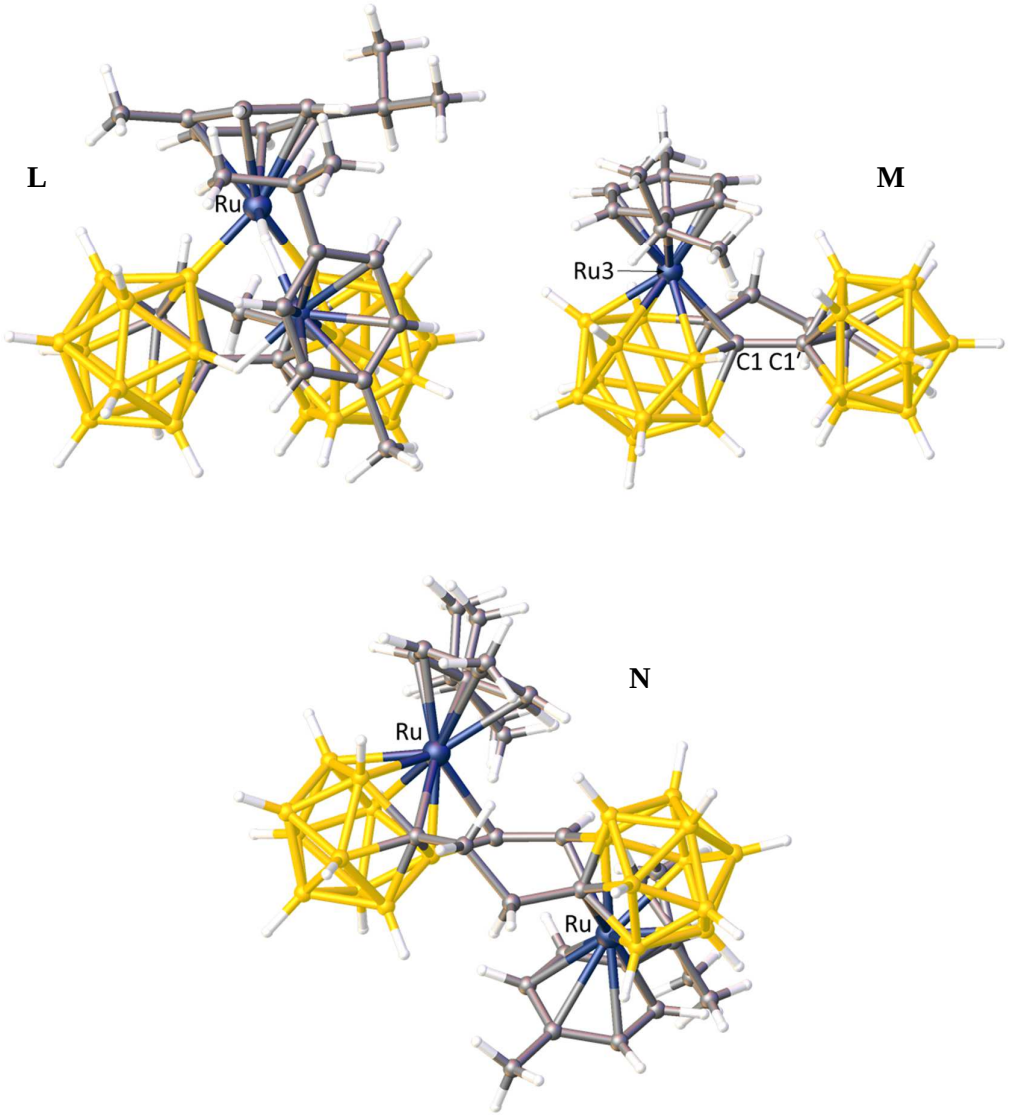

Figure 1.29 Perspective view of **L**: triple B-H insertion product, **M**: 12-vertex carborane/13-vertex ruthenacarborane and **N**: 12-vertex ruthenacarborane/12-vertex ruthenacarborane.

1.15 Scope of Thesis

Chapter 2 explores the reaction between dilithiated 1,1′-bis(*o*-carborane) and [$RuCl_2$(*p*-cymene)]$_2$, affording a new 16-electron 1,1′-bis(*o*-carborane) transition metal chelate. Its reaction with carbon monoxide to give the corresponding 18-electron species is discussed and catalysis results using the unsaturated 16-electron species are also described. Further to this, unusual displacement of the *p*-cymene unit is observed when reacting the 16-electron species with PPh_3 or dppe. The reactivities of these compounds are discussed in detail and three-channel NMR spectroscopy is used to explain the presence of two resonances in the agostic region of their $^1H\{^{11}B\}$ NMR spectra. Further reactions of these species with carbon monoxide and acetonitrile are discussed, with the results useful in demonstrating the structural *trans* effect. Throughout these reactions four bonding modes for 1,1′-bis(*o*-carborane) will be described, with two that are previously unreported.

Chapter 3 discusses the steric and electronic properties associated with two 1,1′-bis(*o*-carboranyl)phosphines. The synthesis of these phosphines is discussed, followed by their transformation to the gold chloride and selenide derivatives. NMR spectroscopy and DFT calculations are included which explain an unusual lack of observed coupling in the carboranylphosphine ^1H NMR spectrum. The Tolman cone angle and percent buried volumes are calculated to explore the steric bulk of these carboranylphosphines. The $^1J_{PSe}$ coupling constant is used as a guide to the basicities of these compounds.

Chapter 4 explores tethered 1,1′-bis(*o*-carboranes) and their subsequent reactions. Of significant interest was the decapitation and metalation reaction of CH_2CH_2 tethered 1,1′-bis(*o*-carborane). Single decapitation followed by reaction with {Ru(*p*-cymene)} gives the expected singly metallated carborane, but also an unusual 13-vertex/12-vertex species.

Chapter 5 contains all the experimental information including synthesis and analysis of all compounds discussed.

1.16 References

1. J. Daintith, *A Dictionary of Chemistry*, 6 edn., Oxford University Press, USA, 2008.
2. A. Stock, *Hydrides of Boron and Silicon*, Cornell University Press, Ithaca, New York, 1933.
3. S. H. Bauer, *J. Am. Chem. Soc.*, 1937, **59**, 1096.
4. S. H. Bauer, *Chem. Rev.*, 1942, **31**, 43.
5. P. v. R. Schleyer, K. Najafian and A. M. Mebel, *Inorg. Chem.*, 1998, **37**, 6765.
6. R. N. Grimes, in *Carboranes, 3rd Edition*, Elsevier Science Bv, Amsterdam, Editon edn., 2016.
7. J. N. Hohman, S. A. Claridge, M. Kim and P. S. Weiss, *Mater. Sci. Eng. R-Rep.*, 2010, **70**, 188.
8. I. Shapiro, R. E. Williams and C. D. Good, *J. Am. Chem. Soc.*, 1962, **84**, 3837.
9. M. M. Fein, M. S. Cohen, N. Mayes, N. Schwartz and J. Bobinski, *Inorg. Chem.*, 1963, **2**, 1111.
10. M. M. Fein, N. Mayes, M. S. Cohen, D. Grafstein, B. M. Lichstein, J. Bobinski, J. E. Paustian and N. N. Schwartz, *Inorg. Chem.*, 1963, **2**, 1115.
11. V. I. Bregadze, *Chem. Rev.*, 1992, **92**, 209.
12. M. L. McKee, *J. Am. Chem. Soc.*, 1997, **119**, 4220.
13. J. Green, N. Mayes and M. S. Cohen, *J. Polym. Sci. Part A*, 1965, **3**, 3275.
14. N. Mayes, J. Green and M. S. Cohen, *J. Polym. Sci. Part A*, 1967, **5**, 365.
15. M. Y. Tsang, S. Rodríguez-Hermida, K. C. Stylianou, F. Tan, D. Negi, F. Teixidor, C. Viñas, D. Choquesillo-Lazarte, C. Verdugo-Escamilla, M. Guerrero, J. Sort, J. Juanhuix, D. Maspoch and J. Giner Planas, *Cryst. Growth Des.*, 2017, **17**, 846.
16. R. N. Grimes, *Angew. Chem. Int. Ed.*, 1993, **32**, 1289.
17. B. P. Dash, R. Satapathy, E. R. Gaillard, J. A. Maguire and N. S. Hosmane, *J. Am. Chem. Soc.*, 2010, **132**, 6578.
18. K. Kokado and Y. Chujo, *Dalton Trans.*, 2011, **40**, 1919.
19. J. J. Peterson, Y. C. Simon, E. B. Coughlin and K. R. Carter, *Chem. Commun.*, 2009, 4950.
20. K. O. Kirlikovali, J. C. Axtell, A. Gonzalez, A. C. Phung, S. I. Khan and A. M. Spokoyny, *Chem. Sci.*, 2016, **7**, 5132.

21. C. L. Powell, M. Schulze, S. J. Black, A. S. Thompson and M. D. Threadgill, *Tet. Lett.*, 2007, **48**, 1251.
22. M. F. Hawthorne, *Angew. Chem. Int. Ed.*, 1993, **32**, 950.
23. H. Xiong, X. Wei, D. Zhou, Y. Qi, Z. Xie, X. Chen, X. Jing and Y. Huang, *Bioconjugate Chem.*, 2016, **27**, 2214.
24. A. González-Campo, A. Ferrer-Ugalde, C. Viñas, F. Teixidor, R. Sillanpää, J. Rodríguez-Romero, R. Santillan, N. Farfán and R. Núñez, *Chem. Eur. J.*, 2013, **19**, 6299.
25. A. M. Cioran, A. D. Musteti, F. Teixidor, Ž. Krpetić, I. A. Prior, Q. He, C. J. Kiely, M. Brust and C. Viñas, *J. Am. Chem. Soc.*, 2012, **134**, 212.
26. R. N. Grimes, *Dalton Trans.*, 2015, **44**, 5939.
27. J. S. Kasper, C. M. Lucht and D. Harker, *J. Am. Chem. Soc.*, 1948, **70**, 881.
28. W. N. Lipscomb, *Boron Hydrides*, Benjamin, New York, 1963.
29. K. Wade, *Adv. Inorg. Chem. Radiochem.*, 1976, **18**, 1.
30. K. Wade, *J. Chem. Soc. D*, 1971, 792.
31. D. M. P. Mingos, *Nat. Phys. Sci.*, 1972, **236**, 99.
32. P. Amseis, W. Mesbah, C. Prasang, M. Hofmann, G. Geiseler, W. Massa and A. Berndt, *Organometallics*, 2003, **22**, 1594.
33. R. D. McIntosh, D. Ellis, G. M. Rosair and A. J. Welch, *Angew. Chem. Int. Ed.*, 2006, **45**, 4313.
34. L. Deng, J. Zhang, H. S. Chan and Z. W. Xie, *Angew. Chem. Int. Ed.*, 2006, **45**, 4309.
35. R. E. Williams, *Inorg. Chem.*, 1971, **10**, 210.
36. R. W. Rudolph and W. R. Pretzer, *Inorg. Chem.*, 1972, **11**, 1974.
37. R. W. Rudolph, *Acc. Chem. Res.*, 1976, **9**, 446.
38. A. McAnaw, G. Scott, L. Elrick, G. M. Rosair and A. J. Welch, *Dalton Trans.*, 2013, **42**, 645.
39. M. G. Davidson, T. G. Hibbert, J. A. K. Howard, A. Mackinnon and K. Wade, *Chem. Commun.*, 1996, 2285.
40. A. Burke, R. McIntosh, D. Ellis, G. M. Rosair and A. J. Welch, *Collect. Czech. Chem. Commun.*, 2002, **67**, 991.
41. A. McAnaw, M. E. Lopez, D. Ellis, G. M. Rosair and A. J. Welch, *Dalton Trans.*, 2014, **43**, 5095.
42. R. A. Wiesboeck and M. F. Hawthorne, *J. Am. Chem. Soc.*, 1964, **86**, 1642.

43. J. Buchanan, E. J. M. Hamilton, D. Reed and A. J. Welch, *J. Chem. Soc. Dalton Trans.*, 1990, 677.
44. M. F. Hawthorne, D. C. Young and P. A. Wegner, *J. Am. Chem. Soc.*, 1965, **87**, 1818.
45. M. F. Hawthorne, D. C. Young, T. D. Andrews, D. V. Howe, R. L. Pilling, A. D. Pitts, M. Reintjes, L. F. Warren and P. A. Wegner, *J. Am. Chem. Soc.*, 1968, **90**, 879.
46. D. Grafstein and J. Dvorak, *Inorg. Chem.*, 1963, **2**, 1128.
47. G. B. Dunks, M. M. McKown and M. F. Hawthorne, *J. Am. Chem. Soc.*, 1971, **93**, 2541.
48. D. F. Dustin, G. B. Dunks and M. F. Hawthorne, *J. Am. Chem. Soc.*, 1973, **95**, 1109.
49. A. Burke, D. Ellis, B. T. Giles, B. E. Hodson, S. A. Macgregor, G. M. Rosair and A. J. Welch, *Angew. Chem. Int. Ed.*, 2003, **42**, 225.
50. T. D. Getman, C. B. Knobler and M. F. Hawthorne, *Inorg. Chem.*, 1990, **29**, 158.
51. J. A. Dupont and M. F. Hawthorne, *J. Am. Chem. Soc.*, 1964, **86**, 1643.
52. T. E. Paxson, K. P. Callahan and M. F. Hawthorne, *Inorg. Chem.*, 1973, **12**, 708.
53. M. A. Mathur and T. J. Klingen, *J. Inorg. Nucl. Chem.*, 1976, **38**, 1597.
54. X. Yang, W. Jiang, C. B. Knobler, M. D. Mortimer and M. F. Hawthorne, *Inorg. Chim. Acta*, 1995, **240**, 371.
55. X. Yang, W. Jiang, C. B. Knobler and M. F. Hawthorne, *J. Am. Chem. Soc.*, 1992, **114**, 9719.
56. L. I. Zakharkin and A. I. Kovredov, *Izv. Akad. Nauk SSSR, Ser. Khim*, 1973, 1428.
57. S. Ren and Z. Xie, *Organometallics*, 2008, **27**, 5167.
58. W. Y. Man, G. M. Rosair and A. J. Welch, *Acta Cryst., Sect. E*, 2014, **70**, 462.
59. I. B. Sivaev, *Commun. Inorg. Synth.*, 2016, **4**, 21.
60. S. Bresadola, P. Rigo and A. Turco, *Chem. Commun.*, 1968, 1205.
61. J. C. Smart, P. M. Garrett and M. F. Hawthorne, *J. Am. Chem. Soc.*, 1969, **91**, 1031.
62. D. A. Owen and M. F. Hawthorne, *J. Am. Chem. Soc.*, 1971, **93**, 873.
63. D. A. Owen and M. F. Hawthorne, *J. Am. Chem. Soc.*, 1970, **92**, 3194.
64. M. J. Martin, W. Y. Man, G. M. Rosair and A. J. Welch, *J. Organomet. Chem.*, 2015, **798**, 36.
65. Z.-J. Yao, Y.-Y. Zhang and G.-X. Jin, *J. Organomet. Chem.*, 2015, **798**, 274.

66. L. I. Zakharkin and N. F. Shemyakin, *Izv. Akad. Nauk SSSR, Ser. Khim*, 1978, 1450.
67. A. I. Yanovskii, N. G. Furmanova, Y. T. Struchkov, N. F. Shemyakin and L. I. Zakharkin, *Izv. Akad. Nauk SSSR, Ser. Khim*, 1979, 1523.
68. S. E. Johnson and C. B. Knobler, *Phosphorus, Sulfur Silicon Relat. Elem.*, 1996, **115**, 227.
69. D. E. Harwell, M. D. Mortimer, C. B. Knobler, F. A. L. Anet and M. F. Hawthorne, *J. Am. Chem. Soc.*, 1996, **118**, 2679.
70. Y. O. Wong, M. D. Smith and D. V. Peryshkov, *Chem. Eur. J.*, 2016, **22**, 6764.
71. M. F. Hawthorne, D. A. Owen and J. W. Wiggins, *Inorg. Chem.*, 1971, **10**, 1304.
72. G. Thiripuranathar, W. Y. Man, C. Palmero, A. P. Y. Chan, B. T. Leube, D. Ellis, D. McKay, S. A. Macgregor, L. Jourdan, G. M. Rosair and A. J. Welch, *Dalton Trans.*, 2015, **44**, 5628.
73. G. Thiripuranathar, A. Chan, D. Mandal, W. Man, M. Argentari, G. Rosair and A. J. Welch, *Dalton Trans.*, 2017, **46**, 1811.
74. G. S. Kazakov, I. B. Sivaev, K. Y. Suponitsky, A. D. Kirilin, V. I. Bregadze and A. J. Welch, *J. Organomet. Chem.*, 2016, **805**, 1.
75. P. E. Behnken, C. B. Knobler and M. F. Hawthorne, *Angew. Chem. Int. Ed.*, 1983, **22**, 722.
76. P. E. Behnken, T. B. Marder, R. T. Baker, C. B. Knobler, M. R. Thompson and M. F. Hawthorne, *J. Am. Chem. Soc.*, 1985, **107**, 932.
77. J. A. Long, T. B. Marder, P. E. Behnken and M. F. Hawthorne, *J. Am. Chem. Soc.*, 1984, **106**, 2979.
78. D. Mandal, W. Y. Man, G. M. Rosair and A. J. Welch, *Dalton Trans.*, 2016, **45**, 15013.
79. T. D. Getman, C. B. Knobler and M. F. Hawthorne, *J. Am. Chem. Soc.*, 1990, **112**, 4593.
80. T. D. Getman, C. B. Knobler and M. F. Hawthorne, *Inorg. Chem.*, 1992, **31**, 101.
81. W. Y. Man, D. Ellis, G. M. Rosair and A. J. Welch, *Angew. Chem. Int. Ed.*, 2016, **55**, 4596.
82. D. Ellis, D. McKay, S. A. Macgregor, G. M. Rosair and A. J. Welch, *Angew. Chem. Int. Ed.*, 2010, **49**, 4943.
83. D. Ellis, G. M. Rosair and A. J. Welch, *Chem. Comm.*, 2010, **46**, 7394.
84. D. Mandal, W. Y. Man, G. M. Rosair and A. J. Welch, *Acta Cryst., Sect. C*, 2015, **71**, 793.

85. D. Zhao, J. J. Zhang, Z. Y. Lin and Z. W. Xie, *Chem. Commun.*, 2016, **52**, 9992.

Chapter 2: Ruthenium 1,1′-Bis(*o*-carboranes)

2.1 Introduction

1,1′-bis(*o*-carborane) can act as a κ^2 (chelating) ligand by σ-bonding through two cluster vertices. A classical way to achieve this is to deprotonate the two available CH units on the carborane, allowing two σ-bonds from C2 and C2′ to a transition metal or main-group element. Deprotonation is carried out stoichiometrically using *n*-BuLi and the dilithio species can then go on to react with a suitable dihalogenated species, affording lithium halide through salt metathesis, Scheme 2.1.

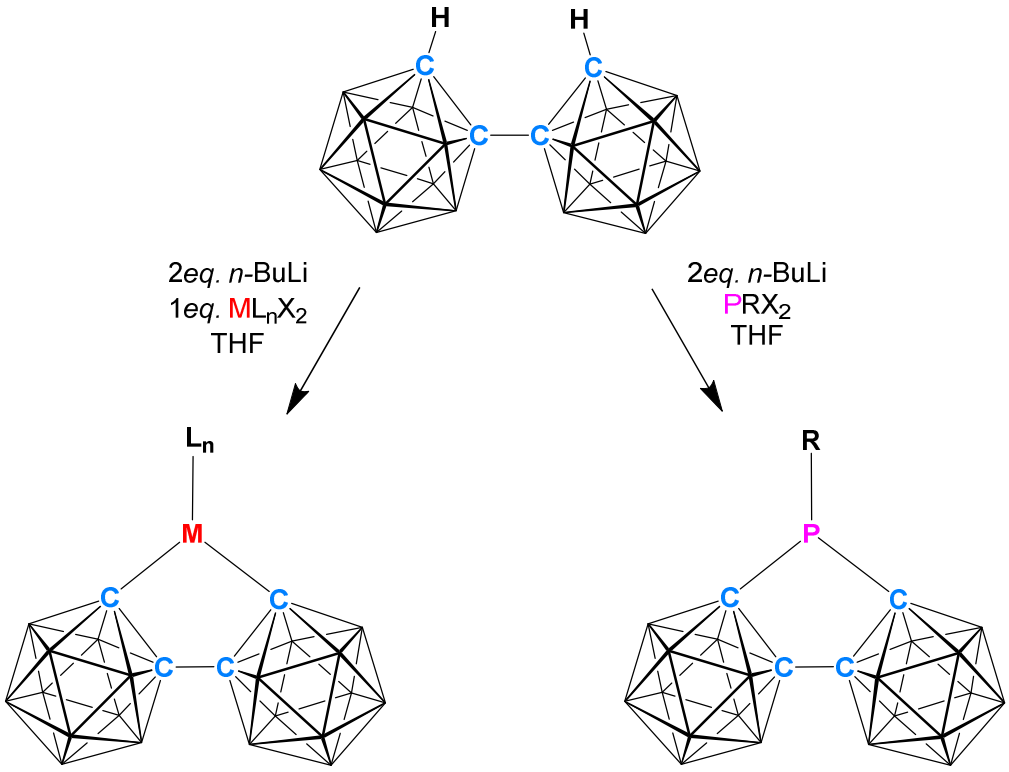

Scheme 2.1 Salt metathesis reaction achieved by deprotonating 1,1′-bis(*o*-carborane) then reacting with a dihalogenated species.

The first literature example of 1,1′-bis(*o*-carborane) being used as a κ^2 ligand was reported by Hawthorne et al. in 1971,[1] whereby the carborane unit bonds simply through two carbon σ-bonds as expected. Therefore the bonding mode of 1,1′-bis(*o*-carborane) can be described as $X_2(C,C')$. Four examples were initially prepared incorporating Co^{II}, Ni^{II}, Cu^{III} and Zn^{II}, and in each case the metal centre is bound to two 1,1′-bis(*o*-carborane) units, Figure 2.1. Three further examples were synthesised by reduction or oxidation of the initial products to give the Co^{III}, Ni^{III} and Cu^{II} compounds. The two proposed structures for these compounds were planar (Co^{III}, $Ni^{II/III}$, $Cu^{II/III}$) and pseudo-tetrahedral (Co^{II}, Zn^{II}). *X*-ray diffraction studies by Hawthorne et al. in 1997 confirmed square planar (Ni^{II}, Cu^{II}) and tetrahedral (Co^{II}) structures, but also found the Cu^{II} complex to be an intermediate between square planar and tetrahedral.[2]

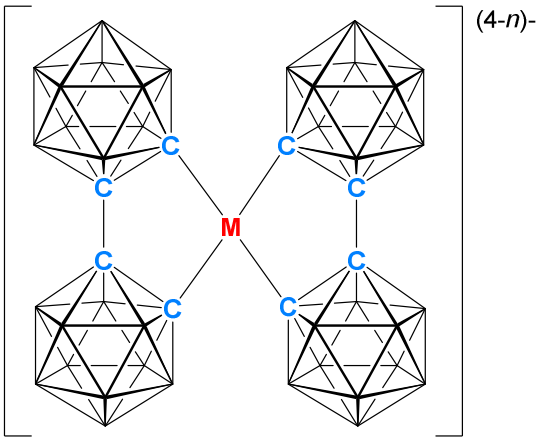

Figure 2.1 The first example of 1,1′-bis(*o*-carborane) as a chelating ligand, where M = $Co^{II/III}$, $Ni^{II/III}$, $Cu^{II/III}$ or Zn^{II} and n is the metal oxidation state.

Bau et al. carried out an *X*-ray diffraction study of the Co^{III} (d^6) complex in 1972, which identified the complex to have a distorted square pyramidal geometry.[3] This was due to the identification of a B-agostic B-H→Co bond in addition to the four carbon σ-bonds from the two 1,1′-bis(*o*-carborane) units. Therefore one of the 1,1′-bis(*o*-carborane) units was acting in a κ^3 fashion, with three bonds to the metal centre, and could be described as a $X_2(C,C')$L ligand (where L = B-agostic bond).

In 2015 Welch et al. reported two new compounds whereby only one κ^2 1,1′-bis(*o*-carborane) is bound to a d^8 nickel centre.[4] The nickel centre was electronically saturated

by also having either a dmpe or dppe ligand, Figure 2.2. Both [Ni(κ^2-2,2′-{1-(1′-1′,2′-*closo*-$C_2B_{10}H_{10}$)-1,2-*closo*-$C_2B_{10}H_{10}$})(dmpe)] and [Ni(κ^2-2,2′-{1-(1′-1′,2′-*closo*-$C_2B_{10}H_{10}$)-1,2-*closo*-$C_2B_{10}H_{10}$})(dppe)] are examples of 1,1′-bis(*o*-carborane) acting as a X_2(*C*,*C*′) ligand and in both structures the geometry is distorted square planar.

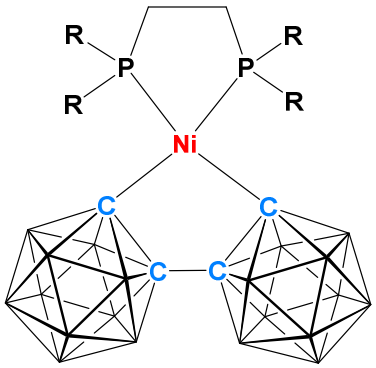

Figure 2.2 Representative drawing of [Ni(κ^2-2,2′-{1-(1′-1′,2′-*closo*-$C_2B_{10}H_{10}$)-1,2-*closo*-$C_2B_{10}H_{10}$})(R)] where R = Me (dmpe) or Ph (dppe).

Two further examples of where 1,1′-bis(*o*-carborane) acts as a κ^2 ligand to a metal centre were reported by Jin et al. in 2015, with both compounds [M(κ^2-2,2′-{1-(1′-1′,2′-*closo*-$C_2B_{10}H_{10}$)-1,2-*closo*-$C_2B_{10}H_{10}$})(Cp*)] (M = Ir or Rh) having a 1,1′-bis(*o*-carborane) X_2(*C*,*C*′) bonding mode, Figure 2.3.[5] Both compounds have 16-electron metal centres, with the iridium species being stable in air and the rhodium compound decomposing over a few minutes when both are in the solid state. Jin identified that the stability of the iridium complex was probably due to the size of 1,1′-bis(*o*-carborane) and Cp*.

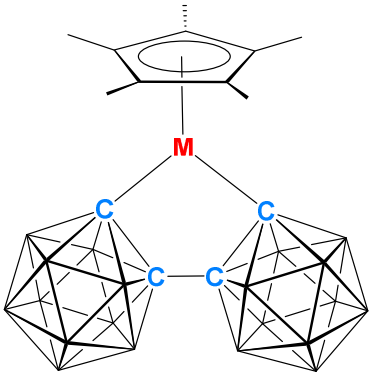

Figure 2.3 Representative drawing of [M(κ^2-2,2′-{1-(1′-1′,2′-*closo*-$C_2B_{10}H_{10}$)-1,2-*closo*-$C_2B_{10}H_{10}$})(Cp*)] (M = Ir or Rh).

In this chapter the use of 1,1′-bis(*o*-carborane) as a κ^2 or a κ^3 ligand in several ruthenium compounds will be discussed. This will include both coordinatively and electronically saturated and unsaturated compounds for direct comparison. It will also include examples of the previously shown X_2(*C*,*C*′) and X_2(*C*,*C*′)L bonding modes and also two new bonding modes X_2(*C*,*B*′) and X_2(*C*,*B*′)L.

2.2 [Ru(κ^3-2,2′,3′-{1-(1′-1′,2′-*closo*-$C_2B_{10}H_{10}$)-1,2-*closo*-$C_2B_{10}H_{10}$})(*p*-cymene)] (1)

Reaction between dilithiated 1,1′-bis(*o*-carborane) and [$RuCl_2$(*p*-cymene)] in THF, followed by purification by column chromatography afforded [Ru(κ^3-2,2′,3′-{1-(1′-1′,2′-*closo*-$C_2B_{10}H_{10}$)-1,2-*closo*-$C_2B_{10}H_{10}$})(*p*-cymene)] (**1**) as an orange solid in 34% yield, Scheme 2.2.

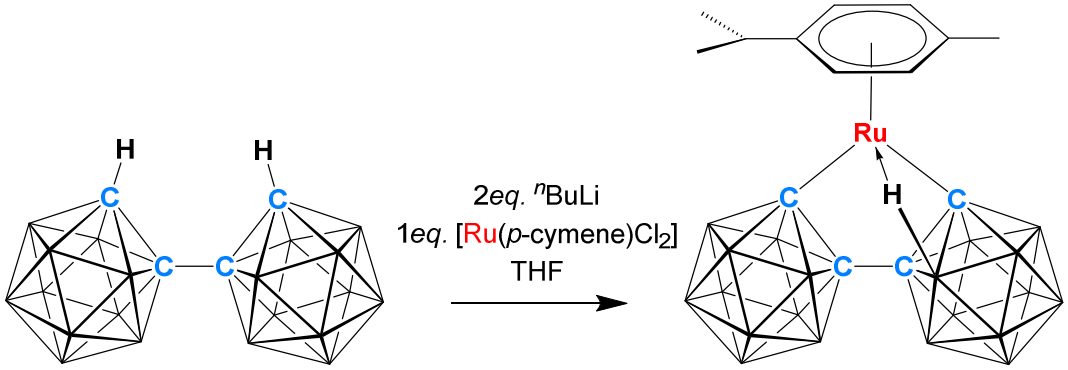

Scheme 2.2 Reaction of 1,1′-bis(*o*-carborane) with *n*-BuLi and [$RuCl_2$(*p*-cymene)] to afford [Ru(κ^3-2,2′,3′-{1-(1′-1′,2′-*closo*-$C_2B_{10}H_{10}$)-1,2-*closo*-$C_2B_{10}H_{10}$})(*p*-cymene)] (**1**).

Compound **1** was identified by electron ionisation mass spectrometry, elemental analysis, NMR spectroscopy and single crystal *X*-ray diffraction. Electron ionisation mass spectrometry of **1** gave a molecular ion peak at m/z 520.4 consistent with the molecular weight (520.57 g mol^{-1}).

Elemental analysis found carbon to be within 0.3% and hydrogen to be within 0.2% of the expected values for the empirical formula $C_{14}H_{34}B_{20}Ru$.

The room temperature ^{1}H NMR spectrum showed two integral-2 doublets at δ 5.48 and 5.30 ppm, an integral-1 septet at δ 2.81 ppm, an integral-3 singlet at δ 2.35 ppm and an integral-6 doublet at δ 1.39 ppm; these can all be assigned to the *p*-cymene unit. As the aromatic protons are observed as two doublets, compound **1** must have C_s symmetry in the solution phase.

The ^{11}B{^{1}H} NMR spectrum shows five resonances from δ -1.4 to -10.6 ppm with integrals of 2:2:4:8:4 from high to low frequency. As all the integrals are even, it would

indicate that the molecule contains a plane of symmetry in the solution state. The resonance of integral-8 is due to coincidental overlap of boron signals.

Single crystals of **1** were grown from slow evaporation of a saturated DCM solution at room temperature and crystallised in the $P\bar{1}$ space group. The *X*-ray diffraction study of compound **1** revealed that the 1,1′-bis(*o*-carborane) cage is bound to the ruthenium centre through a κ^3 interaction; two carbon σ-bonds and one agostic B-H→Ru interaction, Figure 2.4. The ability for the cage to have a further interaction with the ruthenium centre through {B3′H3′} means that in this case 1,1′-bis(*o*-carborane) bonds in an $X_2(C,C')L$ fashion.

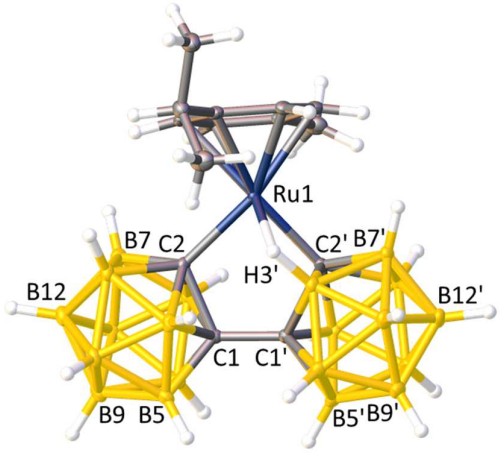

Figure 2.4 Perspective view of [Ru(κ^3-2,2′,3′-{1-(1′-1′,2′-*closo*-$C_2B_{10}H_{10}$)-1,2-*closo*-$C_2B_{10}H_{10}$})(*p*-cymene)] (**1**) and part of the atom numbering scheme. Some selected bond lengths are C1-C1′: 1.514(3) Å, Ru1-C2: 2.103(2) Å and Ru1-C2′: 2.124(3) Å.

The B-H→Ru agostic bond is a three-centre two-electron (3c-2e) bond that provides the ruthenium metal centre with enough electrons to make it electronically fully saturated and has been observed in many literature ruthenacarboranes.[6, 7] Evidence of this agostic B-H→Ru interaction was found by looking at the B-H bond lengths. In classical C-H→M agostic compounds the C-H bond distance involved in the agostic interaction is around 5-10% longer than the non-bridging C-H bonds.[8] The average length of non-bridging $B_{cage}H$ bonds in compound **1** is 1.07(3) Å, which can be compared to the B3-H3′ bond length involved in the agostic bond of 1.18(3) Å, Table 2.1. For compound **1** the agostic

B-H bond is 11% longer than normal cluster B-H bond distances and therefore is additional confirmation of the 3c-2e agostic bond.

Table 2.1 B-H bond lengths in [Ru(κ^3-2,2′,3′-{1-(1′-1′,2′-*closo*-$C_2B_{10}H_{10}$)-1,2-*closo*-$C_2B_{10}H_{10}$})(*p*-cymene)] (**1**), with the B-H→Ru bond length highlighted.

Atoms	**Bond Length (Å)**	**Atoms**	**Bond Length (Å)**
B3-H3	1.08(2)	B3′-H3′	1.18(3)
B4-H4	1.05(3)	B4′-H4′	1.05(2)
B5-H5	1.07(3)	B5′-H5′	1.09(3)
B6-H6	1.01(3)	B6′-H6′	1.07(3)
B7-H7	1.03(3)	B7′-H7′	1.06(3)
B8-H8	1.08(3)	B8′-H8′	1.02(3)
B9-H9	1.06(3)	B9′-H9′	1.07(3)
B10-H10	1.06(3)	B10′-H10′	1.12(3)
B11-H11	1.11(3)	B11′-H11′	1.05(3)
B12-H12	1.08(3)	B12′-H12′	1.08(3)

2.2.1 $^{1}H\{^{11}B\}$ Room Temperature and $^{1}H\{^{11}B\}$ Low Temperature NMR Spectroscopy of [Ru(κ^3-2,2′,3′-{1-(1′-1′,2′-*closo*-$C_2B_{10}H_{10}$)-1,2-*closo*-$C_2B_{10}H_{10}$})(*p*-cymene)] (1)

The $^{1}H\{^{11}B\}$ NMR spectrum of compound **1** displays all the expected *p*-cymene resonances, 16 $B_{cage}H$ resonances between δ 2.58 and 2.11 ppm and also a single integral-4 $B_{cage}H$ resonance at δ -0.02 ppm, Figure 2.5. Classical C-H⇀M compounds display agostic hydrogens at low frequency (δ 0 to -16 ppm),[8] and it can therefore be concluded that the signal at δ -0.02 ppm is resultant from B-*H*⇀Ru. The integral-4 suggests that there must be four hydrogens available to form the B-H⇀Ru agostic interaction with the units at B3, B3′, B6 and B6′ being most likely, Figure 2.7 (**C**) for cage numbering. As there was one integral-4 resonance observed it was assumed that there was a fluxional process between the four {BH} units, with only one acting in the agostic manner at any one time.

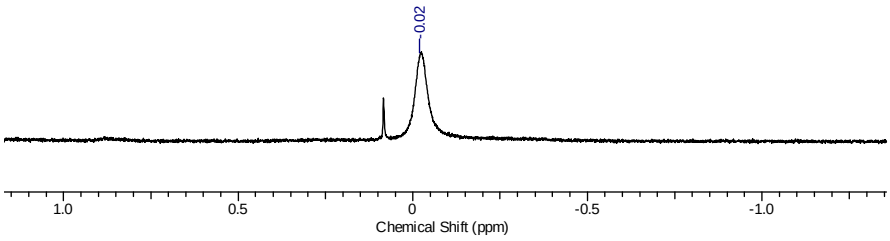

Figure 2.5 The $^{1}H\{^{11}B\}$ NMR spectrum of compound **1** at 298 K, displaying an integral-4 singlet at δ -0.02 ppm, consistent with B-*H*⇀Ru hydrogen shifts.

Cooling a sample of compound **1** to 233 K showed collapse of the peak into the baseline. Further cooling to 203 K saw two integral-2 singlets appear at δ 0.78 and -1.03 ppm, Figure 2.6. Therefore it seems plausible that at low temperatures the fluctionality of the agostic interaction was partially arrested because the higher frequency hydrogens are no longer in the agostic region of the $^{1}H\{^{11}B\}$ NMR spectrum. This would leave only two {BH} units that could be involved in the B-H⇀Ru bond.

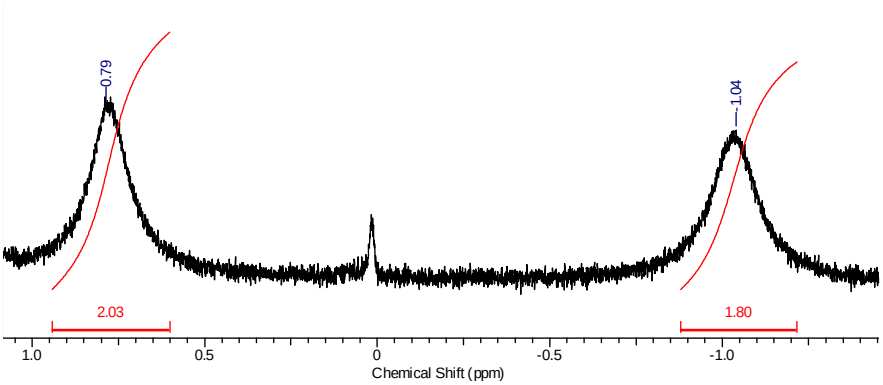

Figure 2.6 The $^{1}H\{^{11}B\}$ NMR spectrum of compound **1** at 203 K which displays two integral-2 singlets at δ 0.79 and -1.04 ppm, consistent with B-H⇀Ru hydrogen shifts.

The symmetry of the molecule can help explain which two BH units remain in the fluxional agostic process. Firstly, the ^{1}H NMR spectrum at 203 K shows two integral-2 doublets in the aromatic region corresponding to the four aromatic protons of the *p*-cymene ligand. As these signals remain two doublets, as opposed to four singlets, the C_s symmetry of the molecule remains intact.

Secondly, the integrals of the $B_{cage}H$ hydrogens in the 203 K $^{1}H\{^{11}B\}$ NMR spectrum are in the pattern 2:2:3:3:3:3, suggesting that the *p*-cymene unit is not rotating freely. The odd integrals also suggest that the *p*-cymene unit is now orientated in such a way that the 1,1′-bis(*o*-carborane) unit must have unique B-H vertices, Figure 2.7. If the *p*-cymene ligand lies parallel to 1,1′-bis(*o*-carborane) (**A**) then there are four unique boron vertices that could provide integral-1 resonances in the $^{11}B\{^{1}H\}$ NMR spectrum. When *p*-cymene lies perpendicular to 1,1′-bis(*o*-carborane) (**B**) the two cages would be equivalent and therefore there would be no unique, integral-1 resonances. Therefore, at 203 K molecule **A** must be the true orientation. If molecule **A** is the true structure of compound **1** then the two remaining {BH} units involved in the B-H⇀Ru bond must be in positions B3 and B6 (or B3′ and B6′) so that the C_s symmetry remains intact. However, spectroscopically it is impossible to say which pair of {BH} units are still involved in the fluctional B-H⇀Ru bond.

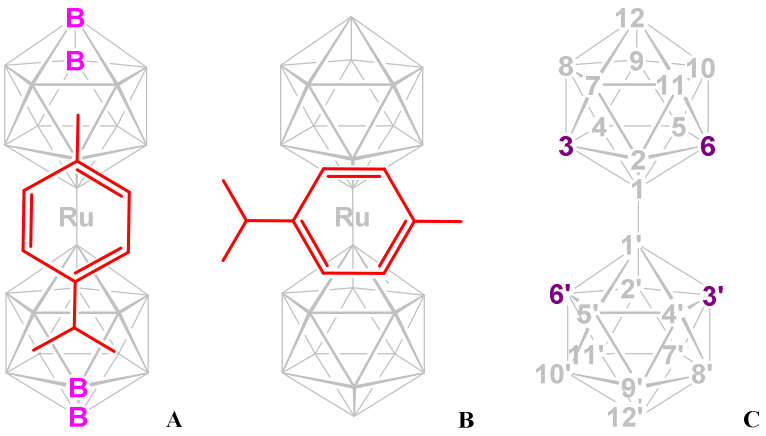

Figure 2.7 The two possible orientations of *p*-cymene when viewing the molecule from above the *p*-cymene ligand. Compound **A** shows the true structure where four unique {BH} units are observed and **B** shows the other possible orientation. **C** shows the numbering scheme with B3, B3′, B6 and B6′ highlighted as possible {BH} units involved in B-H→Ru.

2.3 [Ru(κ^2-2,2′-{1-(1′-1′,2′-*closo*-$C_2B_{10}H_{10}$)-1,2-*closo*-$C_2B_{10}H_{10}$})(*p*-cymene)(CO)] (2)

The lability of the agostic B-H⇀Ru bond was demonstrated by reaction of **1** with carbon monoxide. Vigorous stirring of a THF solution of **1** under a carbon monoxide atmosphere gave a colour change from orange to yellow-green when left overnight. Upon purification the yellow compound [Ru(κ^2-2,2′-{1-(1′-1′,2′-*closo*-$C_2B_{10}H_{10}$)-1,2-*closo*-$C_2B_{10}H_{10}$})(*p*-cymene)(CO)] (**2**) was afforded in 35% yield, Scheme 2.3.

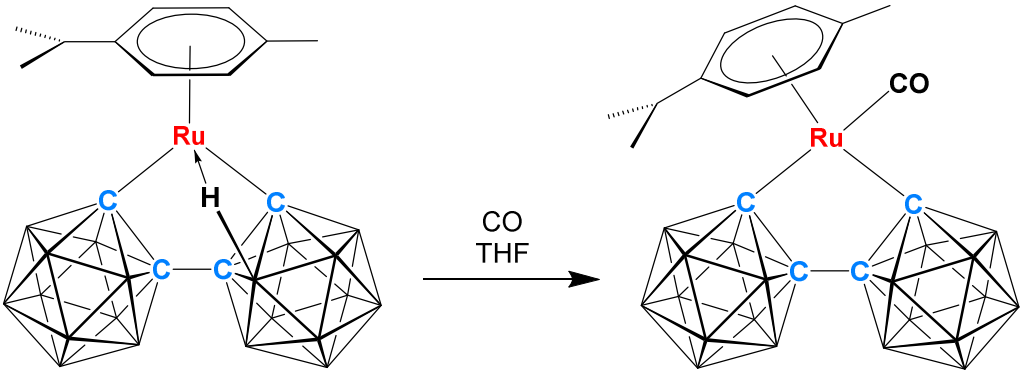

Scheme 2.3 Reaction of compound **1** with carbon monoxide to afford [Ru(κ^2-2,2′-{1-(1′-1′,2′-*closo*-$C_2B_{10}H_{10}$)-1,2-*closo*-$C_2B_{10}H_{10}$})(*p*-cymene)(CO)] (**2**).

Compound **2** was identified by electron ionisation mass spectrometry, elemental analysis, IR spectroscopy, NMR spectroscopy and *X*-Ray crystallography. The addition of one carbon monoxide ligand was initially confirmed by mass spectrometry with the centre of the distinctive cluster envelope at *m/z* 548.4 (MW = 547.73 g mol^{-1}) and a second envelope at *m/z* 520.4 (M^+ - CO).

Elemental analysis gave values of carbon within 0.5 % and hydrogen within 0.01 % for the empirical formula of $C_{15}H_{34}B_{20}ORu$.

IR spectroscopy showed one peak in the carbonyl region at υ_{CO} 2007 cm^{-1}.

The ^{1}H NMR spectrum of **2** shows two integral-2 doublets at δ 6.02 and 5.92 ppm, an integral-1 septet at δ 2.89 ppm, an integral-3 singlet at δ 2.40 ppm and an integral-6 doublet at δ 1.35 ppm; which are resonances from the *p*-cymene unit. The preservation of

the two doublets in the aromatic region, as with compound **1**, shows that the molecule has kept its C_s symmetry.

The $^{11}B\{^1H\}$ NMR spectrum displays an integral-4 peak at δ -2.60 ppm. There are three remaining overlapping peaks at δ -6.62, -7.79 and -8.62 ppm with a combined integration of 16 boron atoms.

The $^1H\{^{11}B\}$ NMR spectrum shows no peaks in the region between δ 0 and -10 ppm which confirms that the B-H⇀Ru bond has been displaced by the addition of a carbonyl ligand.

Single crystals of **2** were grown by slow diffusion of petrol and a saturated DCM solution of the compound at -18 °C. Compound **2** crystallised in the $Pna2_1$ space group and the *X*-ray crystallographic study confirmed the substitution of the B-agostic bond with a single carbon monoxide ligand, Figure 2.8.

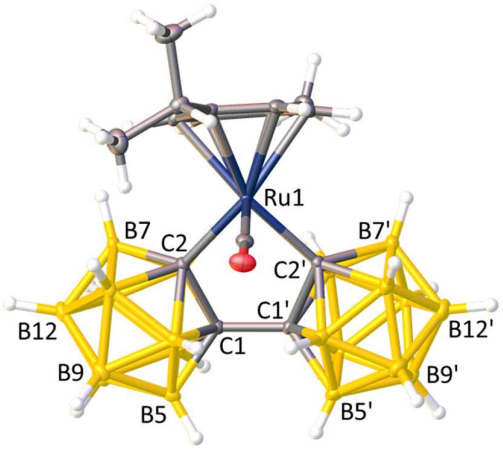

Figure 2.8 Perspective view of [Ru(κ^2-2,2′-{1-(1′-1′,2′-*closo*-$C_2B_{10}H_{10}$)-1,2-*closo*-$C_2B_{10}H_{10}$})(*p*-cymene)(CO)] (**2**) and part of the atom numbering scheme. Selected bond lengths are C1-C1′: 1.527(3) Å. Ru1-C2: 2.115(2) Å and Ru1-C2′: 2.133(3) Å.

Addition of carbon monoxide as a two-electron donor to compound **1** produced a fully saturated 18 electron compound that is stable in air for prolonged periods. The bonding of 1,1′-bis(*o*-carborane) has changed from $X_2(C,C')L$ (κ^3) to $X_2(C,C')$ (κ^2) due to loss of

the B-H⇀Ru agostic bond and the Ru-C bond lengths increased on average by 0.011 Å compared to **1**. Observing compound **2** as a space fill diagram shows the available space for two-electron donors, such as carbon monoxide, Figure 2.9. This indicates that reaction with other, potentially larger, two-electron donors may be possible.

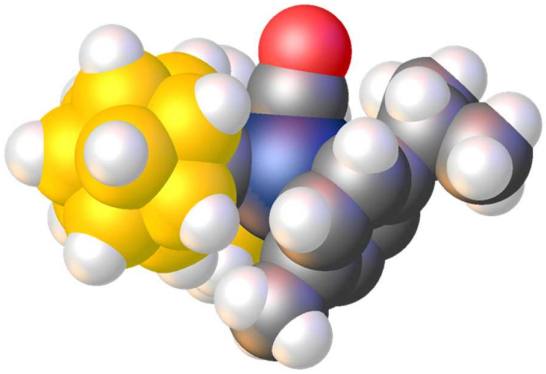

Figure 2.9 Space fill view of [Ru(κ^2-2,2′-{1-(1′-1′,2′-*closo*-$C_2B_{10}H_{10}$)-1,2-*closo*-$C_2B_{10}H_{10}$})(*p*-cymene)(CO)] (**2**), highlighting the available space for a two-electron donor such as carbon monoxide.

2.4 [Ru(κ^3-2,3′,3-{1-(1′-1′,2′-*closo*-$C_2B_{10}H_{10}$)-1,2-*closo*-$C_2B_{10}H_{10}$})(PPh_3)$_2$] (3)

Compound **1** was reacted with one equivalent of PPh_3 in the attempt to synthesise a fully saturated 18-electron compound similar to compound **2**, Scheme 2.4. A room temperature stir in THF exhibited a distinct colour change from orange to red. Upon purification of the product a small amount of yellow material was obtained which was subsequently identified as the unexpected product [Ru(κ^3-2,3′,3-{1-(1′-1′,2′-*closo*-$C_2B_{10}H_{10}$)-1,2-*closo*-$C_2B_{10}H_{10}$})(PPh_3)$_2$] (**3**).

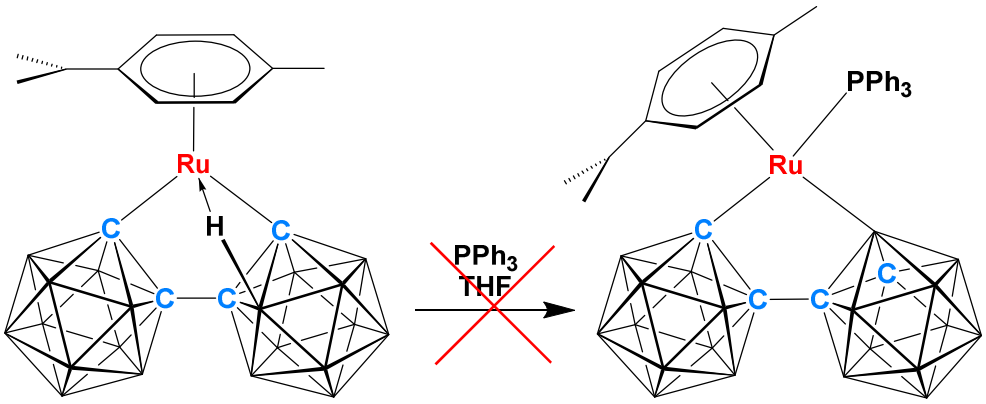

Scheme 2.4 Reaction of compound **1** with one equivalent of PPh_3 showing the predicted 18-electron product.

Compound **3** was identified by electron ionisation mass spectrometry, elemental analysis, NMR spectroscopy and *X*-ray crystallography. The results from the mass spectrum, showing the molecular ion peak at *m/z* 910.5, indicated that there had not been a simple addition of PPh_3 to compound **1**. The MW of a single addition of PPh_3 would be 782.86 g mol^{-1}, but if the *p*-cymene were to be displaced by two equivalents of PPh_3 the MW would be 910.01 g mol^{-1}, agreeing with the mass spectrometry results.

Elemental analysis of this compound confirmed this displacement product and the results agree within 0.3% for both carbon and hydrogen values when calculated for the empirical formula $C_{40}H_{50}B_{20}P_2Ru$.

What is most unusual about this reaction is the loss of the *p*-cymene unit, which was displaced at room temperature and within a very short timescale by PPh_3. Firstly, this

was unexpected as PPh_3 is a relatively weak base (its pK_b is 11.27 compared to the pK_b of PMe_3 which is 5.35).[9] Secondly, it is highly irregular for *p*-cymene to be displaced from a Ru-arene complex and only a few examples have been cited in the literature under ambient conditions,[10, 11] with most occurring through UV irradiation or heating.[12, 13] The Ru-arene unit has applications in both medicine[14, 15] and catalysis[16] and therefore it is surprising that displacement should occur under such mild conditions.

The displacement of the *p*-cymene ligand from compound **1** is thought to be facilitated by the presence of the B-H→Ru bond. Although compound **1** is an 18 electron species, due to the labile 3c-2e bond a Lewis base could approach the metal centre. Upon approach of PPh_3 the agostic bond would break, allowing the large PPh_3 to enter the coordination sphere of the ruthenium atom. This could start displacement of the *p*-cymene unit by pushing the ligand away from the ruthenium centre, subsequently reducing its bonding mode (usually η^6). Reduction of *p*-cymene's bonding mode would decrease the electron count at the ruthenium centre and another PPh_3 would then approach. The steric bulk of this second phosphine ligand would force the removal of *p*-cymene and to compensate for the electron deficiency at the metal centre a new B-H→Ru bond would be created.

After establishing that the product was formed by the displacement of *p*-cymene with two PPh_3 ligands, the reaction was altered to react <u>two</u> equivalents of PPh_3 with compound **1**, affording a 15% yield. Given that this yield was quite low, especially taking into account that synthesis of compound **1** is only 34%, a new synthetic method was devised. Reaction between dilithiated 1,1′-bis(*o*-carborane) and either $[RuCl_2(PPh_3)_3]$ or $[RuCl_2(PPh_3)_4]$ was carried out in THF affording 25% and 23% yields respectively, Scheme 2.5. Compound **3** is electronically unsaturated and has a 16-electron count at the ruthenium centre, even with the B-H→Ru bond, therefore it is not surprising that it is unstable and decomposes rapidly in the presence of air.

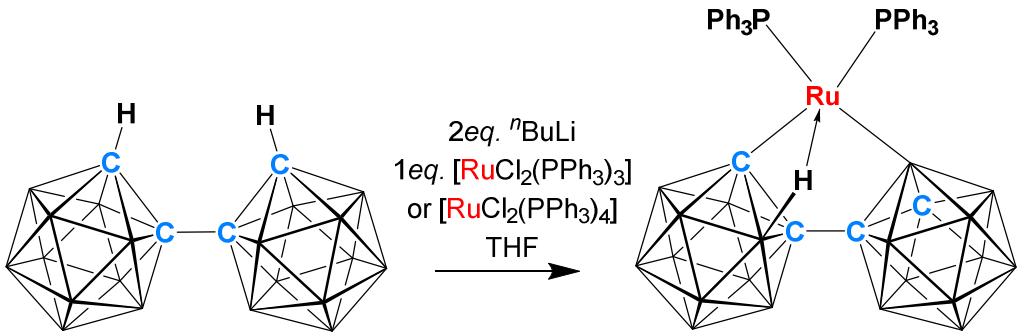

Scheme 2.5 Reaction of 1,1′-bis(*o*-carborane) with *n*-Buli then either $[RuCl_2(PPh_3)_3]$ or $[RuCl_2(PPh_3)_4]$ to afford $[Ru(\kappa^3\text{-}2,3',3\text{-}\{1\text{-}(1'\text{-}1',2'\text{-}closo\text{-}C_2B_{10}H_{10})\text{-}1,2\text{-}closo\text{-}C_2B_{10}H_{10}\})(PPh_3)_2]$ (**3**).

The ^1H NMR spectrum of **3** displays the aromatic protons of PPh_3 as a multiplet at δ 7.47 to 7.12 ppm. There is an unexpected integral-1 broad singlet at 1.94 ppm when the aromatic region is set to 30 protons (two PPh_3 units). This broad singlet is in the region classically observed for $C_{cage}H$ hydrogens which infers that the ruthenium centre is now bound to 1,1′-bis(*o*-carborane) through a carbon σ-bond and a boron σ-bond, hence leaving one carbon atom uncoordinated to either the ruthenium centre or the other carborane cage.

The $^1H\{^{11}B\}$ NMR spectrum of compound **3** again shows the aromatic PPh_3 protons as a multiplet from δ 7.47 to 7.12 ppm. When set as integral-30, the $C_{cage}H$ integral-1 broad singlet is at δ 1.94 ppm. There is also the appearance of 18 $B_{cage}H$ hydrogens seen as overlapping singlets from δ 2.56 to 1.47 ppm. The spectrum identifies one $B_{cage}H$ as a doublet at δ -4.23 ppm, with the coupling constant $^2J_{PH}$ = 32.0 Hz. This is in the agostic region, which would indicate that there is a B-H⇀Ru bond present.

The $^{11}B\{^1H\}$ NMR spectrum displays many overlapping peaks from δ 3 to -20 ppm with maxima at δ 0.1, -4.8, -7.9, -9.2, -10.1, -12.5, -14.6 and -17.4 ppm. However due to the overlapping resonances it is difficult to gain any chemical insight into compound **3** from this spectrum.

The $^{31}P\{^1H\}$ NMR spectrum of compound **3** displayed two integral-1 doublets, with a $^2J_{PP}$ coupling constant measured as 25.1 Hz. The doublet at δ 57.98 ppm appears to be slightly broader than that at the lower frequency of δ 40.25 ppm. This can be explained by the molecule having one PPh_3 group *trans* to C2 and one PPh_3 group *trans* to the

agostic hydrogen H3. It can be assumed that the PPh_3 ligand *trans* to H3 would be broadened due to the effects of the quadrupolar boron nucleus it is bound to. It is also likely that the stronger electronegativity of C2 would deshield its *trans* PPh_3, hence giving a higher frequency resonance.

Single crystals of **3** were afforded by slow diffusion of petrol and a concentrated DCM solution of the compound at -18 °C. Compound **3** crystallised in the $P\bar{1}$ space group and the structure confirmed the κ^3 bonding of 1,1′-bis(*o*-carborane), Figure 2.10. This is the first time that 1,1′-bis(*o*-carborane) has been observed in a κ^3 bonding manner through a B-H⇀Ru agostic bond, a carbon σ-bond and a boron σ-bond. Therefore the bonding mode can be written as $X_2(C,B')L$.

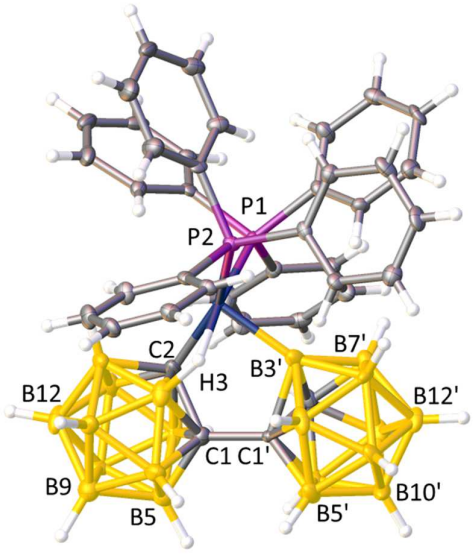

Figure 2.10 Perspective view of [Ru(κ^3-2,3′,3-{1-(1′-1′,2′-*closo*-$C_2B_{10}H_{10}$)-1,2-*closo*-$C_2B_{10}H_{10}$})$(PPh_3)_2$] (**3**) and part of the atom numbering scheme. Selected bond lengths are C1-C1′: 1.529(7) Å, Ru1-C2: 2.124(8) Å and Ru1-B3′: 2.423(7) Å.

Both NMR data and the vertex-to-centroid distance (VCD) method were used to determine where the carbon atoms were located in the carborane cages of compound **3**. The ^{1}H NMR spectrum established there was one $C_{cage}H$ resonance, implying that there is one boron σ-bond to the ruthenium centre. The VCD method was developed by Welch et al. to locate carbon and boron vertices in carboranes from *X*-ray diffraction data.[17] By

refining the whole cluster as boron atoms, the carbon atoms can be easily identified as they will have particularly short VCD′s.

The application of the VCD method to compound **3** gives the results listed in Table 2.2. The primed cage clearly shows two vertices, 1′ and 2′, which have significantly shorter VCD's and therefore these were assigned as C1′ and C2′. Atom C1′ is the carborane vertex bound to the second carborane cage. The location of the second carbon atom fits with NMR spectroscopy data; the $C_{cage}H$ resonance was assigned to C2′, leaving B3′ as the boron atom which is σ-bound to the ruthenium centre. As atom B3′ was involved in the B-H⇀Ru agostic bond in compound **1,** it could be deduced that upon displacement of the *p*-cymene unit in **1** by PPh_3 the agostic bond was broken. Subsequently a boron σ-bond from B3′ could be formed as it is already in close proximity to the ruthenium metal centre therefore changing the bonding mode to $X_2(C,B')L$. As **3** is a 16-electron species it would be favourable to have a boron σ-bond to ruthenium due to boron's larger orbital size, and therefore greater orbital overlap with the electron deficient ruthenium, compared to a carbon-ruthenium σ-bond.

Table 2.2 Vertex-to-centroid distances (VCD′s) for compound **3**, identifying the carbon atoms to be at C1, C2, C1′ and C2′.

Non-Primed Cage		**Primed Cage**	
Vertex	**VCD**	**Vertex**	**VCD**
1	1.594	1′	1.577
2	1.649	2′	1.554
3	1.656	3′	1.839
4	1.731	4′	1.669
5	1.708	5′	1.714
6	1.711	6′	1.747
7	1.703	7′	1.680
8	1.691	8′	1.675
9	1.694	9′	1.679
10	1.684	10′	1.711
11	1.710	11′	1.703
12	1.685	12′	1.687

The carbon atoms from the non-primed cage were also established by VCD methods with vertex-1 showing the shortest VCD, consistent with atom C1 being the carborane vertex bound to the primed cage. The second carbon atom was determined to be located at vertex-2 as this displayed a short VCD and therefore confirms that there is a carbon σ-bond to the ruthenium centre from the non-primed cage. Unfortunately, the crystallographic structure of **3** suffers from disorder whereby there are major and minor components of the ruthenium atom with site occupancy factors of 0.803(2) and 0.197(2). This gave rise to substitutional disorder in the non-primed cage with vertex-2 being 80(5)% C + 20(5)% B and vertex-3 being 80(5)% B + 20(5)% C. Although the major component has the carbon located at vertex-2, the disorder of the structure means that the VCD for vertex-3 is also short. However, recalling the spectroscopic data collected for compound **3** it is established that vertex-2 is C2 and vertex-3 is B3.

The geometry of compound **3** is square pyramidal with B3′ as the apex. The bond angles from the atoms involved in the square planar section of the square pyramid are P1-Ru1-

P2: 100.53(5)°, P2-Ru1-H3′: 90(2)°, C2′-Ru1-P1: 102.9(2)° and H3′-Ru1-C2′: 67(2)°. The latter angle is presumably smaller due to the constraints of the carborane cage.

2.5 [Ru(κ^3-2,3′,3-{1-(1′-1′,2′-*closo*-$C_2B_{10}H_{10}$)-1,2-*closo*-$C_2B_{10}H_{10}$})(dppe)] (4)

Reaction between compound **1** and one equivalent of dppe in THF gave [Ru(κ^3-2,3′,3-{1-(1′-1′,2′-*closo*-$C_2B_{10}H_{10}$)-1,2-*closo*-$C_2B_{10}H_{10}$})(dppe)] (**4**) as a yellow solid in a 28% yield once purified. The reaction mixture turned from orange to red within 10 minutes and was an indication once again of displacement of *p*-cymene under ambient conditions, Scheme 2.6.

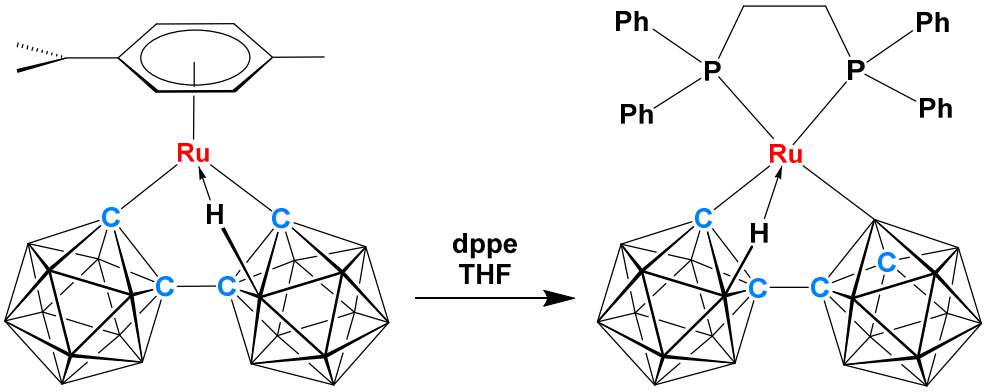

Scheme 2.6 Reaction of compound **1** with dppe to produce [Ru(κ^3-2,3′,3-{1-(1′-1′,2′-*closo*-$C_2B_{10}H_{10}$)-1,2-*closo*-$C_2B_{10}H_{10}$})(dppe)] (**4**).

Compound **4** was characterised by electron ionisation mass spectrometry, elemental analysis, NMR spectroscopy and *X*-ray crystallography. Mass spectrometry showed the molecular ion peak at *m/z* 783.3 which is in good agreement with that for the expected compound (MW = 784.76 g mol^{-1}). A second cluster envelope was observed at *m/z* 286.3, corresponding to the molecular ion minus {Ru(dppe)}.

Elemental analysis results were within 1.2% for carbon and 0.6% for hydrogen when compared to the expected values for the empirical formula $C_{30}H_{44}B_{20}P_2Ru$.

The ^{1}H NMR spectrum of **4** displays the phenyl aromatic protons as a multiplet between δ 7.92 and 7.01 ppm, with an integral of 20 protons. The integral-4 protons found on the carbon bridge of the dppe ligand are observed as a multiplet between δ 3.08 and 2.75 ppm. In the same manner as compound **3**, a broad integral-1 singlet assumed to be a $C_{cage}H$ was observed at 2.17 ppm. Once again, following the displacement of the *p*-

cymene ligand, 1,1′-bis(*o*-carborane) appears to bond to the ruthenium centre through one carbon σ-bond and one boron σ-bond, as opposed to two carbon σ-bonds as observed for compound **1**.

The $^{1}H\{^{11}B\}$ NMR spectrum showed the 20 aromatic phenyl protons as a multiplet between δ 7.90 and 7.01 ppm, the integral-4 carbon bridge protons as a multiplet between δ 3.07 and 2.75 ppm and the $C_{cage}H$ integral-1 singlet at 2.17 ppm. There were 18 $B_{cage}H$ hydrogens observed between δ 2.74 and 0.66 ppm. The final integral-1 $BH_{agostic}$ hydrogen was observed as a doublet at δ -2.25 ppm, with a $^{2}J_{PH}$ coupling constant of 28.0 Hz, Figure 2.11.

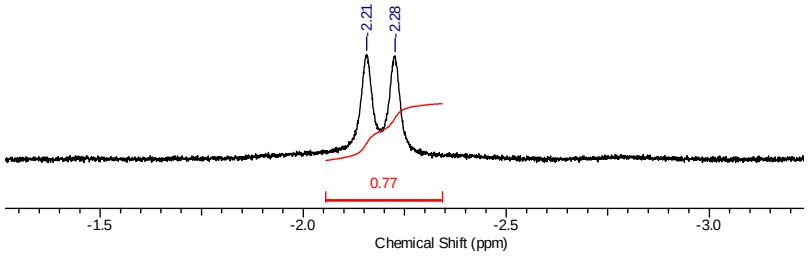

Figure 2.11 The $^{1}H\{^{11}B\}$ NMR spectrum displaying the $BH_{agostic}$ hydrogen doublet observed for compound **4**, with $^{2}J_{PH}$ = 28.0 Hz.

The $^{11}B\{^{1}H\}$ NMR spectrum shows overlapping peaks from δ 3 to -19 ppm with maxima at δ 0.5, -4.3, -7.0, -7.9, -9.2, -10.4, -14.5 and -16.1 ppm. Unfortunately, as with compound **3**, due to the coincidental boron peaks there was little information that could be gained from this spectrum.

The $^{31}P\{^{1}H\}$ NMR spectrum of **4** displays an unresolved doublet at δ 90.74 ppm and a doublet at δ 78.70 ppm with $^{3}J_{PP}$ being 11.3 Hz. Both resonances integrate as one phosphorus atom and correspond to the chelating dppe ligand. The broad resonance has been assigned to atom P2 *trans* to the B-H→Ru hydrogen atom and the resolved, sharp doublet is atom P1 *trans* to the carbon atom of 1,1′-bis(*o*-carborane). The resonance of the phosphorus atom *trans* to the B-H→Ru agostic bond is thought to be broad due to the effects of the quadrupolar boron atom.

Single crystals of **4** were grown from slow diffusion of petrol and a concentrated DCM solution of the compound at -18 °C. Compound **4** crystallised in the $P\bar{1}$ space group and the crystallographic study confirmed that there has been *p*-cymene displacement under ambient conditions by a chelating dppe ligand, Figure 2.12.

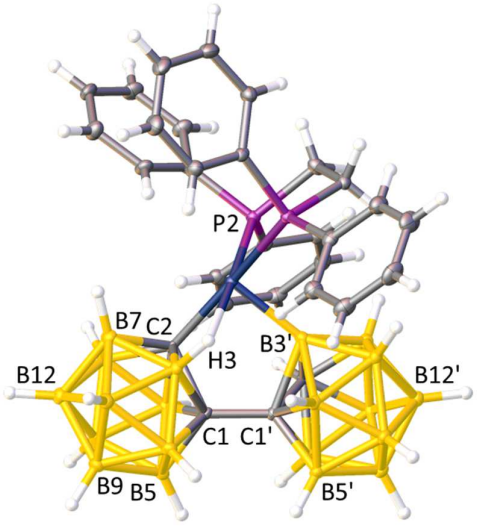

Figure 2.12 Perspective view of [Ru(κ^3-2,3′,3-{1-(1′-1′,2′-*closo*-$C_2B_{10}H_{10}$)-1,2-*closo*-$C_2B_{10}H_{10}$})(dppe)] (**4**) and part of the atom numbering scheme. Selected bond lengths are C1-C1′: 1.520(2) Å, Ru1-C2: 2.148(2) Å and Ru1-B3′: 2.034(2) Å.

It was established that the ruthenium centre is bound to the 1,1′-bis(*o*-carborane) unit in a κ^3 manner, through a carbon σ-bond, a boron σ-bond and through the agostic hydrogen from {B3H3}. The position of the carbon atom involved in the $C_{cage}H$ (as seen in the ^1H NMR spectrum) was identified by VCD methods, Table 2.3. The four carbon atoms of 1,1′-bis(*o*-carborane) were determined to be C1, C2, C1′ and C2′ as these showed significantly shorter VCD′s than all other cluster vertices when the molecule was refined with all cage atoms as boron.

Table 2.3 Vertex-to-centroid distances (VCD′s) for compound **4**, identifying the carbon atoms to be at C1, C2, C1′ and C2′.

Non-Primed Cage		**Primed Cage**	
Vertex	**VCD**	**Vertex**	**VCD**
1	1.586	1′	1.570
2	1.621	2′	1.538
3	1.672	3′	1.840
4	1.728	4′	1.676
5	1.716	5′	1.709
6	1.710	6′	1.735
7	1.697	7′	1.688
8	1.712	8′	1.697
9	1.681	9′	1.679
10	1.683	10′	1.717
11	1.703	11′	1.701
12	1.691	12′	1.675

The agostic B3-H3 bond length is 1.15(2) Å, which when compared to the rest of the B-H bond lengths in the carborane cage is 5% longer, Table 2.4. This falls in line with the expected bond length increase for an agostic interaction. Similarly to compound **3**, 1,1′-bis(*o*-carborane) is in a $X_2(C,B')L$ bonding mode and the metal centre has a maximum of 16 electrons even with the B-H⇀Ru agostic 3c-2e bond.

Table 2.4 B-H bond lengths in [Ru(κ^3-2,3′,3-{1-(1′-1′,2′-*closo*-$C_2B_{10}H_{10}$)-1,2-*closo*-$C_2B_{10}H_{10}$})(dppe)] (**4**), with the B-H⇀Ru bond length highlighted. The average B-H bond length (not including B3-H3) is 1.09(2) Å; therefore, B3-H3 is 5% longer.

Atoms	Bond Length (Å)	Atoms	Bond Length (Å)
B3-H3	1.15(3)	C2′-H2′	0.93(2)
B4-H4	1.09(2)	B4′-H4′	1.10(2)
B5-H5	1.11(2)	B5′-H5′	1.06(2)
B6-H6	1.10(2)	B6′-H6′	1.08(2)
B7-H7	1.08(3)	B7′-H7′	1.07(2)
B8-H8	1.09(2)	B8′-H8′	1.07(2)
B9-H9	1.09(2)	B9′-H9′	1.12(2)
B10-H10	1.07(2)	B10′-H10′	1.12(3)
B11-H11	1.10(2)	B11′-H11′	1.07(2)
B12-H12	1.12(2)	B12′-H12′	1.12(2)

The ruthenium centre and its surrounding ligands are in a square pyramidal arrangement with B3′ as the apex. The angles around the base of the square pyramid are P1-Ru1-P2: 82.70(2)°, P1-Ru1-H3: 101.5(6)° and P2-Ru1-C2: 104.67(5)°. However C2-Ru1-H3 has a smaller angle of 71.1(6)°, which is presumably due to the constraints of the 1,1′-bis(*o*-carborane) cage.

2.6 [Ru(κ^2-2,3′-{1-(1′-1′,2′-*closo*-$C_2B_{10}H_{10}$)-1,2-*closo*-$C_2B_{10}H_{10}$})(PPh_3)$(CO)_3$] (5)

Compound **5** was thought to be easily synthesised by reaction of [Ru(κ^3-2,3′,3-{1-(1′-1′,2′-*closo*-$C_2B_{10}H_{10}$)-1,2-*closo*-$C_2B_{10}H_{10}$})(PPh_3)$_2$] (**3**) with carbon monoxide. As synthesis of compound **3** is very low yielding, and due to its quick decomposition in air and during purification, the reaction with carbon monoxide was done with a freshly prepared, unpurified, sample of **3**. Vigorous stirring of a THF solution of **3** under a carbon monoxide atmosphere yielded the colour change from orange to yellow overnight. Upon purification [Ru(κ^2-2,3′-{1-(1′-1′,2′-*closo*-$C_2B_{10}H_{10}$)-1,2-*closo*-$C_2B_{10}H_{10}$})(PPh_3)$(CO)_3$] (**5**) was afforded in a 7% yield, Scheme 2.7.

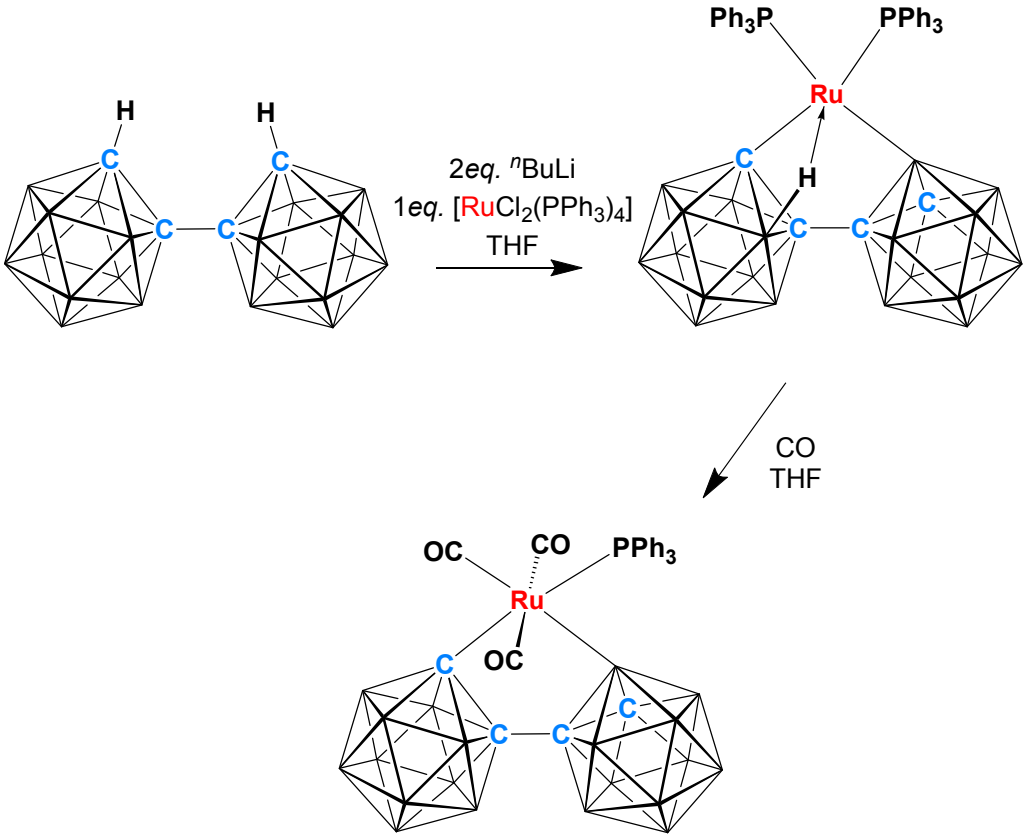

Scheme 2.7 Synthetic method of preparing [Ru(κ^2-2,3′-{1-(1′-1′,2′-*closo*-$C_2B_{10}H_{10}$)-1,2-*closo*-$C_2B_{10}H_{10}$})(PPh_3)$(CO)_3$] (**5**) from 1,1′-bis(*o*-carborane).

Compound **5** was identified by electron ionisation mass spectrometry, elemental analysis, infrared spectroscopy, NMR spectroscopy and *X*-ray crystallography. Mass spectrometry showed a cluster envelope at *m/z* 731.8 (M^+) consistent with the molecular weight (731.82 g mol^{-1}). Three further envelopes were observed with a difference of *m/z* 28 each, determined to be loss of subsequent carbonyl ligands, at *m/z* 703.1 (M^+ - CO), 675.1 (M^+ - 2 x CO) and 647.1 (M^+ - 3 x CO).

Elemental analysis of crystals of **5** (with one equivalent of solvated CH_2Cl_2) found values of carbon within 0.3% and hydrogen within 0.05%, agreeing with the empirical formula $C_{25}H_{35}B_{20}O_3PRu \cdot CH_2Cl_2$.

IR spectroscopy of compound **5** exhibited υ_{CO} bands at 2042, 2034 and 2028 cm^{-1}.

The ^1H NMR spectrum of compound **5** identified the phenyl protons as a multiplet between δ 7.58 and 7.30 ppm. When the phenyl protons were set as integral-15, two broad integral-0.5 singlets were identified in the classical $C_{cage}H$ region at δ 4.18 and 3.94 ppm. Due to the integral of the $C_{cage}H$ hydrogen atoms being 0.5 each, it suggested that two isomers were present. There are two possible orientations of the PPh_3 ligand if the carbonyl ligands are in a meridional arrangement. The PPh_3 could be *trans* to C2 or B3′, Figure 2.13.

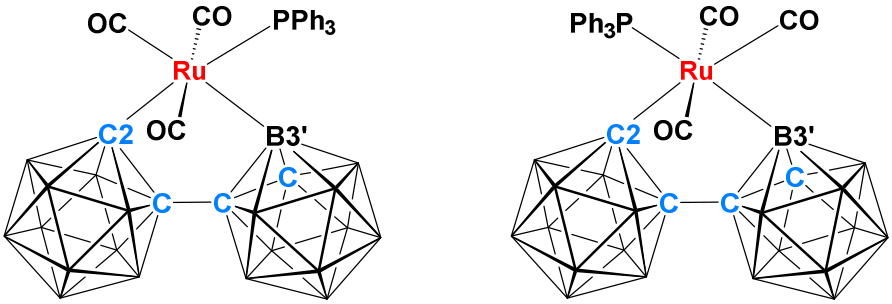

Figure 2.13 The two possible isomers of compound **5**, one with PPh_3 *trans* to C2 and the other with PPh_3 *trans* to B3′.

The $^{11}B\{^1H\}$ NMR spectrum has a resonance at δ 4.2 ppm integrating as two boron atoms. The remaining 38 boron atoms from the two isomers of **5** have resonances that overlap from δ 1 to -14 ppm and have maxima at δ -2.2, -6.8 and -8.9 ppm. The two boron atoms

at 4.2 ppm are at higher frequency and are therefore assumed to be B3′ from each isomer. This was confirmed by looking at the ^{11}B NMR spectrum as no splitting was observed in the proton-coupled experiment.

The $^{31}P\{^{1}H\}$ NMR spectrum of **5** displays two integral-1 resonances, a sharp singlet at δ 27.74 ppm and a very broad singlet at δ 17.12 ppm, Figure 2.14. This confirms the notion that there are two isomers present and that they are in a 1:1 ratio. The resonance at low frequency is thought to be when PPh_3 is *trans* to B3′ as the quadrupolar boron nuclei will have an effect on the width of the signal making it broader. The higher electronegativity of C2 will deshield the PPh_3 *trans* to it therefore giving it a higher frequency signal.

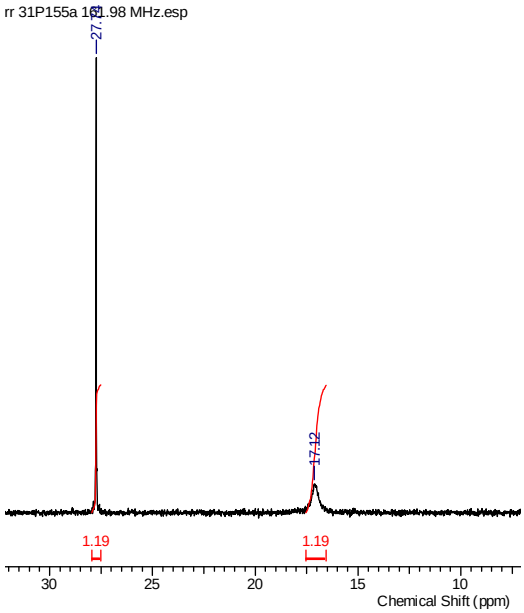

Figure 2.14 The $^{31}P\{^{1}H\}$ NMR spectrum of compound **5**.

Crystals of **5** were obtained by slow diffusion of petrol and a concentrated DCM solution of the compound at -18 °C. Compound **5** crystallised in the $P\bar{1}$ space group and it shows that atoms at cage vertices 2, 2′, 3 and 3′ have a site occupancy of 0.5C and 0.5B each, giving rise to two isomers. Figure 2.15 shows one of the possible isomers where cage vertex-2 has been set as carbon, therefore making vertices 3 and 3′ boron atoms and vertex-2′ a carbon atom. The site occupancy factors confirm that the ratio of the isomers is 1:1, with 50% having PPh_3 *trans* to C2 and 50% *trans* to B3′.

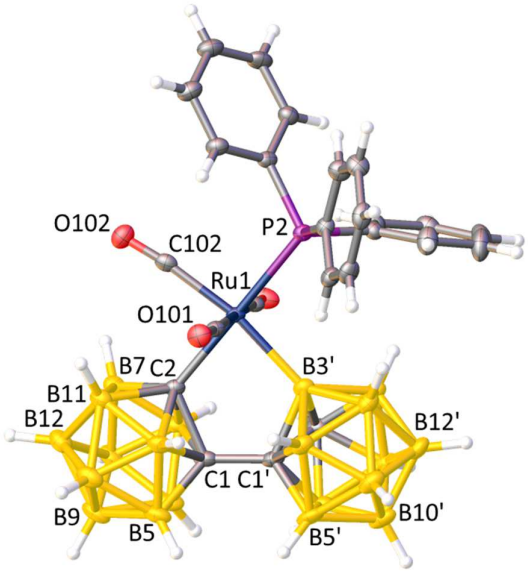

Figure 2.15 Perspective view of one isomer of [Ru(κ^2-2,3′-{1-(1′-1′,2′-*closo*-$C_2B_{10}H_{10}$)-1,2-*closo*-$C_2B_{10}H_{10}$})(PPh_3)$(CO)_3$] (**5**) and part of the atom numbering scheme. Selected bond lengths are C1-C1′: 1.534(3) Å, Ru1-C2: 2.187(3) Å, Ru1-B3′: 2.243(2) Å.

The *X*-ray structure confirms the loss of a PPh_3 ligand, which was replaced by three carbonyl ligands. The carbonyl ligands are in a meridional arrangement around the ruthenium centre, which has an octahedral geometry, and the angles around the ruthenium centre range from 82.89(9)° to 97.64(7)°.

Compound **5** shows 1,1′-bis(*o*-carborane) bonding as a κ^2 ligand to the ruthenium centre through a carbon σ-bond and a boron σ-bond, making its bonding mode X_2(*C*,*B*′). This is the first example of 1,1′-bis(*o*-carborane) bonding in this manner. Through the addition of three carbonyl ligands the B-agostic bond has been displaced in favour of a more stable, 18-electron compound and consequently **5** is stable for prolonged periods in air.

2.7 [Ru(κ^2-2,3′-{1-(1′-1′,2′-*closo*-$C_2B_{10}H_{10}$)-1,2-*closo*-$C_2B_{10}H_{10}$})(PPh_3)($MeCN)_3$] (6)

Compound **6** was synthesised by changing the work-up method of compound **3**. Dilithiated 1,1′-bis(*o*-carborane) was reacted with [$RuCl_2(PPh_3)_4$] in THF and the mixture was purified using preparative TLC plates. The yellow band of compound **3** was washed off the silica with excess MeCN. The yellow colour of compound **3** turned colourless on contact with MeCN and the washings were left to stir for two hours. Upon purification [Ru(κ^2-2,3′-{1-(1′-1′,2′-*closo*-$C_2B_{10}H_{10}$)-1,2-*closo*-$C_2B_{10}H_{10}$})(PPh_3)($MeCN)_3$] (**6**) was obtained in 7% yield, based on 1,1′-bis(*o*-carborane) as the starting material, Scheme 2.8.

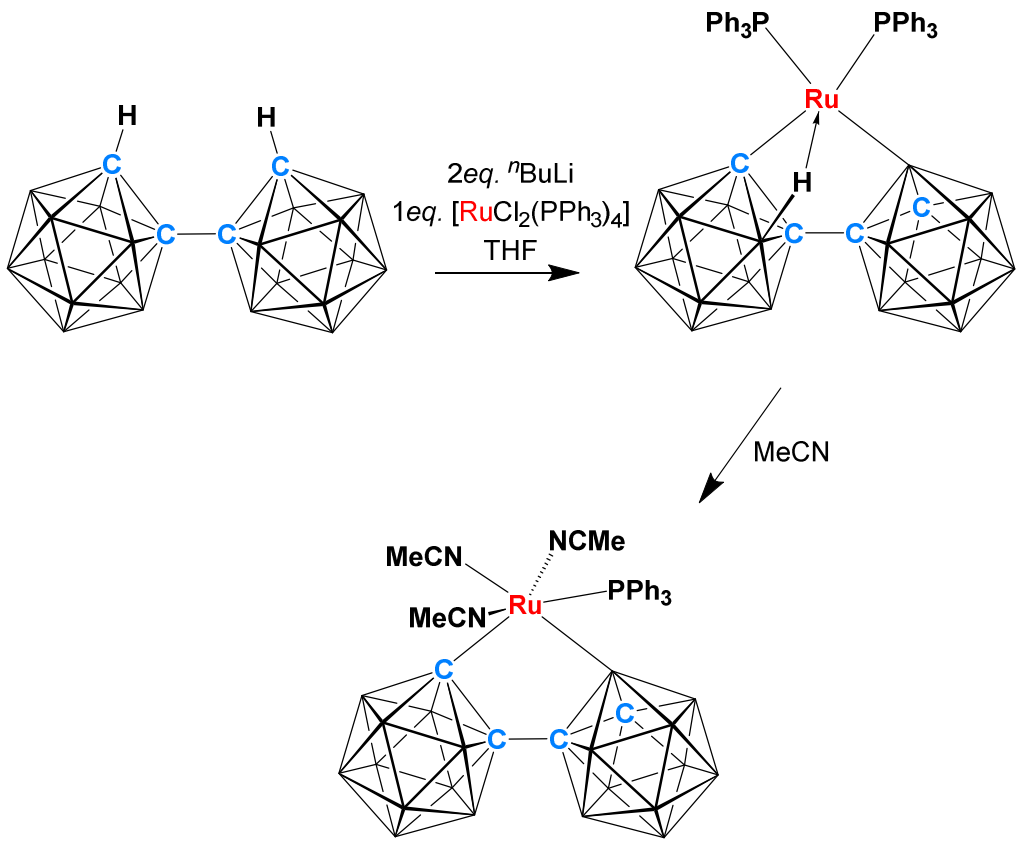

Scheme 2.8 Synthetic method of preparing [Ru(κ^2-2,3′-{1-(1′-1′,2′-*closo*-$C_2B_{10}H_{10}$)-1,2-*closo*-$C_2B_{10}H_{10}$})(PPh_3)($MeCN)_3$] (**6**) from 1,1′-bis(*o*-carborane).

Compound **6** was identified by electron ionisation mass spectrometry, elemental analysis, NMR spectroscopy and *X*-ray crystallography. Mass spectrometry of compound **6** gave good agreement with that of the expected product. The molecular ion envelopes were seen at *m/z* 647.2 (M^+ - 3 x MeCN) and 688.1 (M^+ - 2 x MeCN). No molecular ion peak (MW = 770.90 g mol^{-1}) was seen, presumably due to MeCN being such a weakly coordinating ligand.

The elemental analysis results agreed to within 0.7% for carbon and 0.4% for hydrogen for the theoretical empirical formula $C_{28}H_{44}B_{20}N_3PRu$.

The ^1H NMR spectrum of **6** showed the integral-15 aromatic phenyl protons as a multiplet between δ 7.48 and 7.38 ppm. A broad integral-1 singlet at δ 3.43 ppm was identified as a $C_{cage}H$ hydrogen. The three integral-3 MeCN resonances were observed as two sets of doublets at δ 2.11 ppm ($^5J_{PH}$ = 1.0 Hz) and at δ 2.04 ppm ($^5J_{PH}$ = 1.0 Hz) and a broad singlet at δ 2.00 ppm. As with compound **5** the three ligands are in a meridional arrangement around an octahedral ruthenium metal centre. Two MeCN ligands are *trans* to one another and give rise to the doublets at δ 2.11 and 2.04 ppm. The third MeCN ligand is *trans* to the cage vertex B3′ (as confirmed by *X*-ray crystallography). This will therefore be more shielded and also broadened by the quadrupolar boron nucleus giving rise to the broad signal observed at δ 2.00 ppm.

The $^{11}B\{^1H\}$ NMR spectrum displayed a single resonance at δ 12.8 ppm which integrates as one boron atom and is assumed to be B3′. This was confirmed by the lack of splitting in the proton-coupled boron spectrum. The remaining boron atoms were displayed as overlapping resonances from δ 0 to -17 ppm with maxima at δ -3.8, -8.4 and -13.9 ppm.

The $^{31}P\{^1H\}$ NMR spectrum exhibits a sharp singlet at δ 40.44 ppm and the sharpness of the signal indicates that PPh_3 is *trans* to the carbon atom (C2) as opposed to the boron atom (B3′).

Compound **6** was crystallised by slow evaporation of a saturated MeCN solution of the compound and it crystallised in the $P\bar{1}$ space group. The *X*-ray crystallographic study of compound **6** corroborates all the other information collected about this compound and it shows that a single PPh_3 ligand and the B-H→Ru agostic bond were replaced by three MeCN ligands, Figure 2.16. The position of the $C_{cage}H$ carbon atom was identified to be at C2′ by the VCD method.

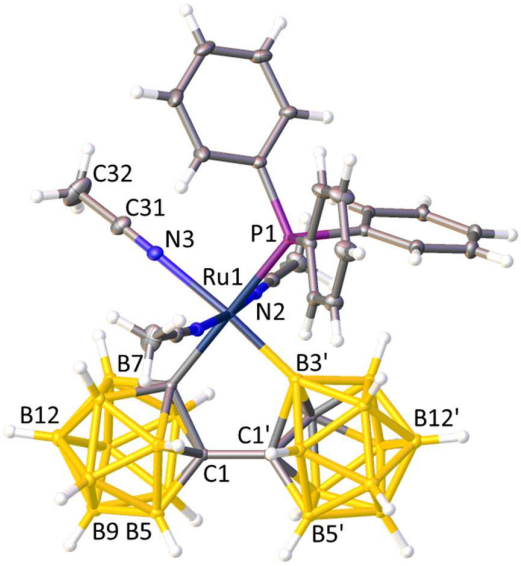

Figure 2.16 Perspective view of [Ru(κ^2-2,3′-{1-(1′-1′,2′-*closo*-$C_2B_{10}H_{10}$)-1,2-*closo*-$C_2B_{10}H_{10}$})(PPh_3)($MeCN)_3$] (**6**) and part of the atom numbering scheme. Selected bond lengths are C1-C1′: 1.535(2) Å, Ru1-C2: 2.164(2) Å and Ru1-B3′: 2.102(2) Å.

The three MeCN ligands are in a meridional arrangement around the octahedral ruthenium metal centre and the bond angles around the ruthenium centre range from 84.22(5)° to 98.18(6)°. The smallest angle is C2-Ru1-B3′ which is presumably due to the steric constraints of 1,1′-bis(*o*-carborane) and the largest angle is B3′-Ru1-P1 which is most likely to be due to having two sterically bulky ligands adjacent to one another. The PPh_3 ligand is *trans* to the carbon atom, C2, with one of the MeCN ligands *trans* to the boron atom, B3′. Compound **6** demonstrates that boron has a greater structural *trans* effect than carbon because the more labile ligand, MeCN, is *trans* to the stronger σ-donor B3′.

As with compound **5** the addition of three donor ligands to the metal centre has created a fully saturated 18-electron compound. The 1,1′-bis(*o*-carborane) ligand is now bonding as a κ^2 ligand through a carbon σ-bond and a boron σ-bond and therefore has a $X_2(C,B')$ bonding mode.

2.8 [Ru(κ^2-2,3′-{1-(1′-1′,2′-*closo*-$C_2B_{10}H_{10}$)-1,2-*closo*-$C_2B_{10}H_{10}$})(dppe)$(CO)_2$] (7)

A THF solution of [Ru(κ^3-2,3′,3-{1-(1′-1′,2′-*closo*-$C_2B_{10}H_{10}$)-1,2-*closo*-$C_2B_{10}H_{10}$})(dppe)] (**4**) stirred overnight with a carbon monoxide atmosphere afforded a yellow solid identified as [Ru(κ^2-2,3′-{1-(1′-1′,2′-*closo*-$C_2B_{10}H_{10}$)-1,2-*closo*-$C_2B_{10}H_{10}$})(dppe)$(CO)_2$] (**7**) in a 50% yield once purified, Scheme 2.9.

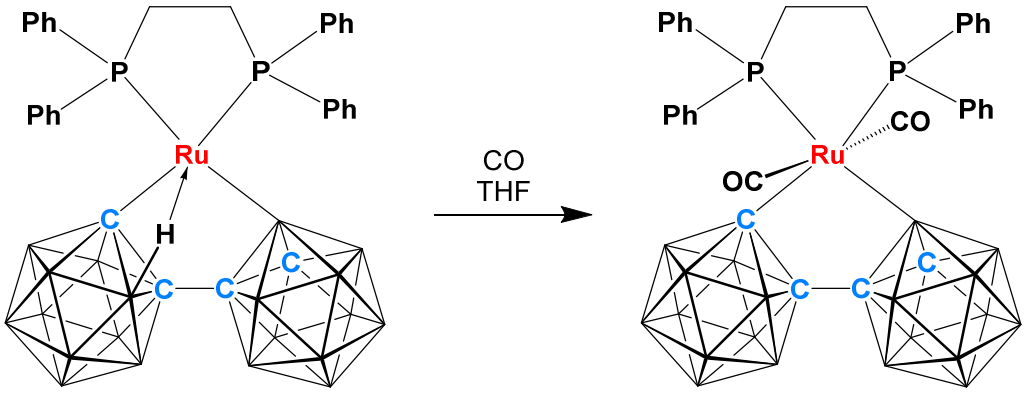

Scheme 2.9 Reaction of compound **4** with carbon monoxide to afford [Ru(κ^2-2,3′-{1-(1′-1′,2′-*closo*-$C_2B_{10}H_{10}$)-1,2-*closo*-$C_2B_{10}H_{10}$})(dppe)$(CO)_2$] (**7**).

Compound **7** was characterised by electron ionisation mass spectrometry, infrared spectroscopy, NMR spectroscopy and *X*-ray crystallography. Unfortunately mass spectrometry of compound **7** displayed two cluster envelopes that show decomposition of the product *via* loss of the carbonyl ligands with *m/z* 783.3 (M^+ - 2×CO) and 811.3 (M^+ - CO), where the molecular weight is 839.88 g mol^{-1}.

Elemental analysis of **7** was unavailable as the product decomposed very readily in air.

Infrared spectroscopy established the carbonyl stretch to be at ν_{CO} 1983 cm^{-1}.

The ^{1}H NMR spectrum of **7** displayed the integral-20 aromatic phenyl protons as a multiplet between δ 7.98 and 6.99 ppm and the integral-4 protons from the dppe bridge were found as a multiplet between δ 3.06 and 2.86 ppm. The $C_{cage}H$ hydrogen was observed as an integral-1 broad singlet at δ 3.90 ppm.

The $^{11}B\{^{1}H\}$ NMR spectrum had an integral-1 shift at high frequency, δ 8.52 ppm, believed to be atom B3′ as there was no splitting observed in the ^{11}B NMR spectrum (with proton coupling). The remaining 19 boron atoms were found as overlapping resonances between δ 0 and -15 ppm with maxima at δ -2.7, -7.1 and -9.8 ppm.

The $^{31}P\{^{1}H\}$ NMR spectrum had a sharp singlet at δ 49.15 ppm and a very broad singlet at δ 40.56 ppm with both integrating as one phosphorus atom, Figure 2.17. The low frequency signal at δ 40.56 ppm is presumed to be from PPh_3 which is *trans* to B3′ as the quadrupolar B3′ atom will have a broadening effect on the phosphorus signal it is *trans* to. Second to this, carbon is more electronegative than boron and therefore will pull electron density away from the phosphorus signal it is *trans* to. This in turn will decrease the shielding and therefore increase the frequency, so that the signal at δ 49.15 ppm is likely to be from the PPh_3 ligand *trans* to C2.

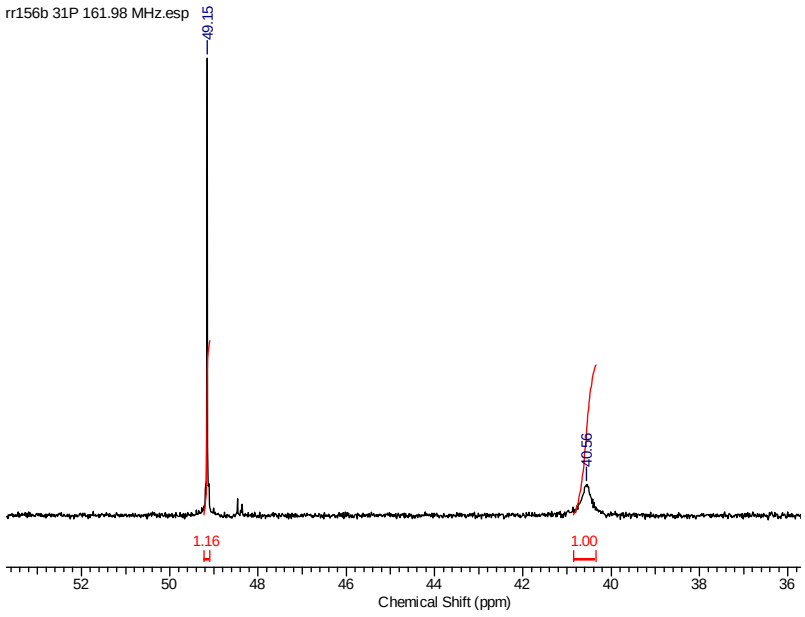

Figure 2.17 The $^{31}P\{^{1}H\}$ NMR spectrum of compound **7**.

Single crystals of **7** were grown from slow diffusion of petrol and a concentrated DCM solution of the compound at -18 °C. Compound **7** crystallised in the $P\bar{1}$ space group and shows the ruthenium centre is in a octahedral arrangement surrounded by 1,1′-bis(*o*-carborane), dppe and two carbonyl ligands, Figure 2.18. The angles around the

ruthenium centre range from 81.22(8)° to 98.56(8)° with the smallest angle being B3′-Ru1-C102 and the largest angle being B3′-Ru1-P1. Because of the chelating nature of both 1,1′-bis(*o*-carborane) and dppe the carbonyl ligands are in a *trans* arrangement to one another. The $C_{cage}H$ carbon atom was identified to be at C2′ using the VCD method. Compound **7** has an 18-electron, fully saturated ruthenium centre. 1,1′-Bis(*o*-carborane) is bound in a κ^2 manner to the ruthenium centre through one carbon σ-bond and one boron σ-bond and therefore it can be described as having a $X_2(C,B')$ bonding mode.

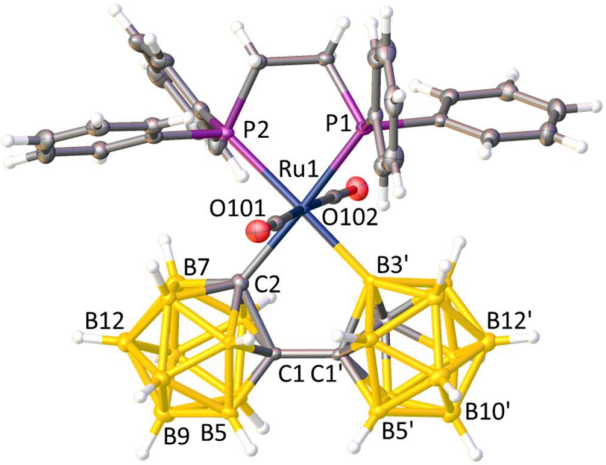

Figure 2.18 Perspective view of [Ru(κ^2-2,3′-{1-(1′-1′,2′-*closo*-$C_2B_{10}H_{10}$)-1,2-*closo*-$C_2B_{10}H_{10}$})(dppe)$(CO)_2$] (**7**) and part of the atom numbering scheme. Selected bond lengths are C1-C1′: 1.537(3) Å, Ru1-C2: 2.208(2) Å and Ru1-B3′: 2.242(2) Å.

The crystal structure proves to be an excellent example to demonstrate the structural *trans* effect of both carbon and boron. The Ru-P bond lengths, Figure 2.19, can be used to examine how strong the Ru1-C2 and Ru1-B3′ bonds are. The Ru1-P2 bond length (*trans* to B3′) is longer than Ru1-P1 (*trans* to C2) by 0.0365 Å. The lengthening of the Ru-P bond when opposite B3′ demonstrates that the boron σ-bond must be stronger than the carbon σ-bond, hence boron has a stronger structural *trans* effect.

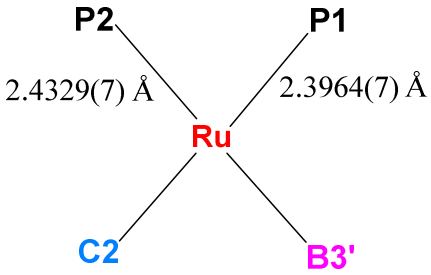

Figure 2.19 Partial view of compound **7** showing only the atoms bound to the ruthenium centre from dppe and 1,1′-bis(*o*-carborane), with selected bond lengths.

2.9 [Ru(κ^2-2,3′-{1-(1′-1′,2′-*closo*-$C_2B_{10}H_{10}$)-1,2-*closo*-$C_2B_{10}H_{10}$})(dppe)(MeCN)$_2$] (8)

Dissolving compound **4** in MeCN and stirring for two hours afforded [Ru(κ^2-2,3′-{1-(1′-1′,2′-*closo*-$C_2B_{10}H_{10}$)-1,2-*closo*-$C_2B_{10}H_{10}$})(dppe)(MeCN)$_2$] (**8**) as a pale yellow solid in 7% yield, Scheme 2.10.

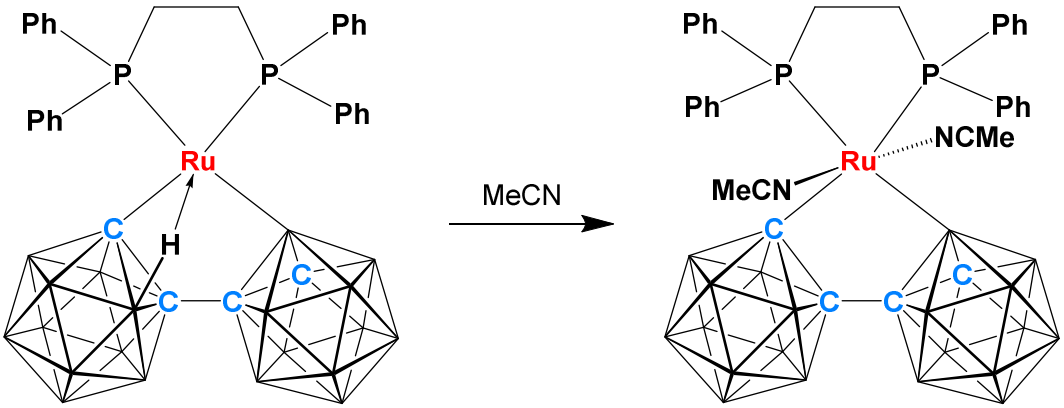

Scheme 2.10 Synthetic method for [Ru(κ^2-2,3′-{1-(1′-1′,2′-*closo*-$C_2B_{10}H_{10}$)-1,2-*closo*-$C_2B_{10}H_{10}$})(dppe)(MeCN)$_2$] (**8**).

Compound **8** was identified by electron ionisation mass spectrometry, elemental analysis, NMR spectroscopy and *X*-ray crystallography. Although mass spectrometry did not show the molecular ion (MW = 866.026 g mol^{-1}), an envelope was observed at *m/z* 783.3 which corresponds to loss of two MeCN ligands. This is not surprising as MeCN is very labile and is easily removed from the metal centre.

Elemental analysis confirmed the product to be **8** as the carbon value was within 1.1% and the hydrogen value was within 0.2% of those expected for the empirical formula $C_{34}H_{50}B_{20}N_2P_2Ru$.

The ^{1}H NMR spectrum displayed the 20 aromatic phenyl dppe protons as a multiplet between δ 7.97 and 6.91 ppm and the integral-4 bridging protons were seen as a multiplet between δ 3.00 and 2.75 ppm. The $C_{cage}H$ was seen as an integral-1 broad singlet at δ 3.47 ppm. One set of integral-3 MeCN protons appeared as a doublet of doublets at δ 2.07 ppm with the two values of $^5J_{PH}$ being 2.6 and 1.0 Hz. The second set of integral-3

MeCN protons appeared as a doublet of doublets (apparent triplet meaning the coupling constant could not be calculated) at δ 2.04 ppm.

The $^{11}B\{^{1}H\}$ NMR spectrum had one resonance at δ 19.4 ppm which integrated as one boron atom, and was assigned to B3′ due to the lack of splitting in the proton-coupled boron spectrum. The remaining 19 boron atoms were found as overlapping resonances from δ -1 to -15 ppm, with maxima at δ -2.9, -3.6, -6.0, -8.5 and -12.4 ppm.

The $^{31}P\{^{1}H\}$ NMR spectrum displays a sharp singlet at δ 55.89 ppm and a very broad singlet at δ 30.49 ppm with both integrating as one phosphorus. As with compound **7**, the low frequency broad signal can be associated with the phosphorus atom *trans* to B3′, which for compound **8** is P1.

Single crystals of **8** were grown from slow evaporation of a concentrated MeCN solution of the compound. It crystallises in the $C2/c$ space group and similar to compound **7** shows an octahedral ruthenium centre with two MeCN ligands, a dppe ligand and the κ^2 1,1′-bis(*o*-carborane) ligand, Figure 2.20. Due to the arrangement of both 1,1′-bis(*o*-carborane) and dppe the MeCN ligands are *trans* to one another. The bond angles around the ruthenium centre range from 83.05(2)° to 99.76(5)° and therefore are in agreement with an octahedral geometry. The carbon atom in the primed cage was identified to be at C2′ by the VCD method. The crystal structure of **8** once again demonstrates a fully saturated 18 electron compound. As the 1,1′-bis(*o*-carborane) unit is bonding to the ruthenium metal centre through a carbon σ-bond and boron σ-bond the bonding mode can be described as $X_2(C,B')$.

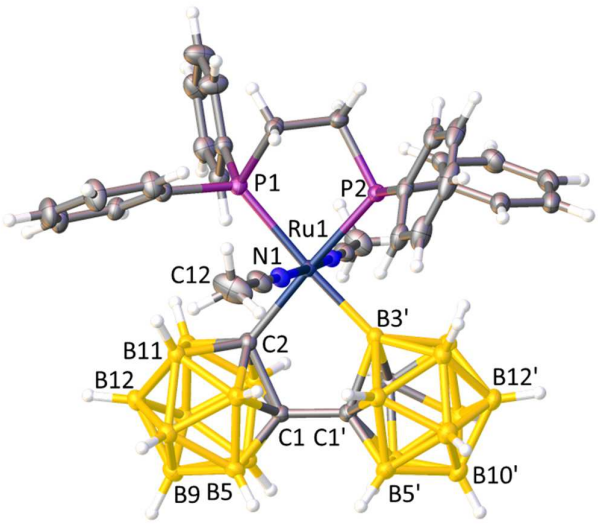

Figure 2.20 Perspective view of [Ru(κ^2-2,3′-{1-(1′-1′,2′-*closo*-$C_2B_{10}H_{10}$)-1,2-*closo*-$C_2B_{10}H_{10}$})(dppe)$(MeCN)_2$] (**8**) and part of the atom numbering scheme. Selected bond lengths are C1-C1′: 1.526(3) Å, Ru1-C2: 2.172(2) Å and Ru1-B3′: 2.144(2) Å.

As with compound **7**, the crystal structure of **8** demonstrates the structural *trans* effect of carbon and boron by the elongated Ru-P bond length when opposite B3′ (as opposed to C2), Figure 2.21. The longer bond length of Ru1-P1 of 2.4254(7) Å (trans to B3′), compared to Ru1-P2 at 2.3474(6) Å (trans to C2), establishes that B3′ must be a stronger σ-donor than C2.

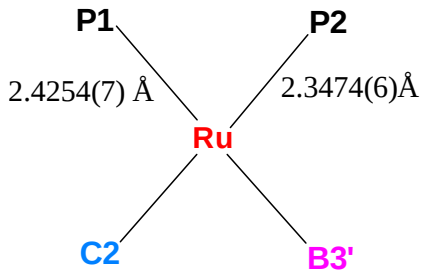

Figure 2.21 Partial view of compound **7** showing only the atoms bound to the ruthenium centre from dppe and 1,1′-bis(*o*-carborane) with selected bond lengths.

2.10 NMR Studies of Compounds 3 and 4

Both [Ru(κ^3-2,3′,3-{1-(1′-1′,2′-*closo*-$C_2B_{10}H_{10}$)-1,2-*closo*-$C_2B_{10}H_{10}$})(PPh_3)$_2$] (**3**) and [Ru(κ^3-2,3′,3-{1-(1′-1′,2′-*closo*-$C_2B_{10}H_{10}$)-1,2-*closo*-$C_2B_{10}H_{10}$})(dppe)] (**4**) exhibit two distinct resonances in the agostic region (δ 0 to -16 ppm)[8] of their $^1H\{^{11}B\}$ NMR spectra. In both cases the two peaks integrate in total as only one hydrogen when compared to the remaining 18 $B_{cage}H$ atoms of 1,1′-bis(*o*-carborane). Compound **3** (PPh_3 derivative) has two peaks at δ -4.19 and -4.27 ppm and compound **4** (dppe derivative) has two peaks at δ -2.21 and -2.28 ppm, Figure 2.22. Although both compounds have very similar NMR spectra, only compound **4** will be used for this discussion, as it tended to give better quality spectra.

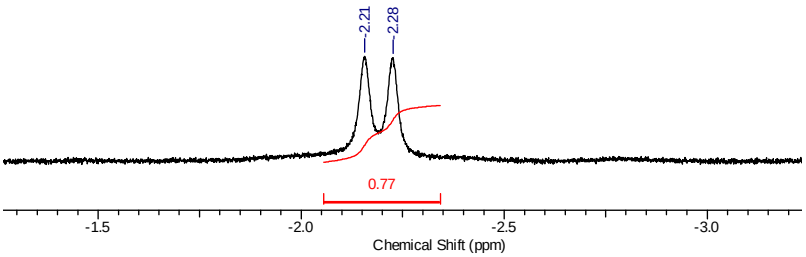

Figure 2.22 The agostic resonances observed in the $^1H\{^{11}B\}$ NMR spectrum of **4**.

In addition to this the $^{31}P\{^1H\}$ NMR spectrum was different to what was expected. At δ 90.77 ppm there was what looked to be either two peaks overlapping or an unresolved doublet. There were two peaks at δ 78.73 and 78.67 ppm which again could have also been interpreted as a doublet, Figure 2.23.

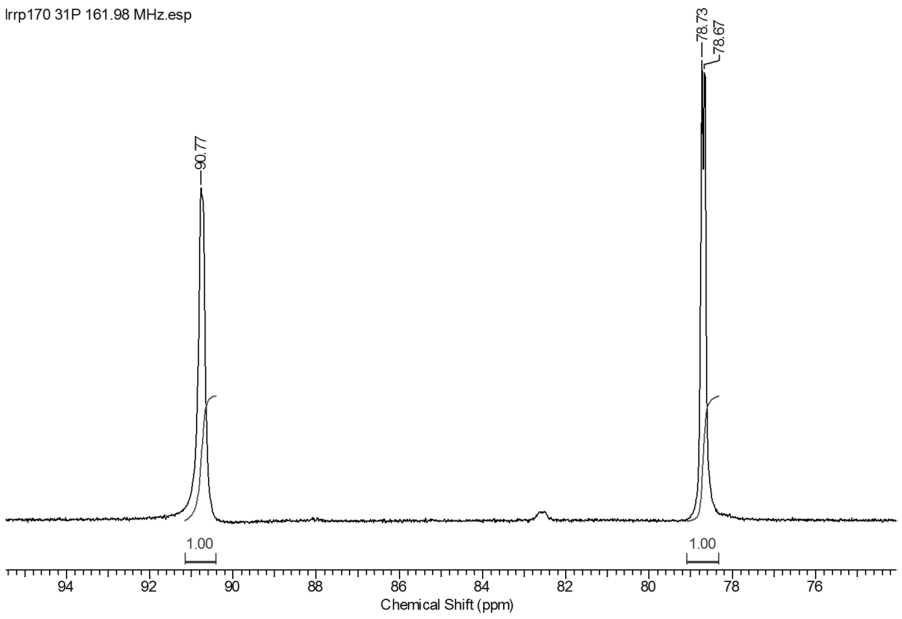

Figure 2.23 The $^{31}P\{^{1}H\}$ NMR spectrum of compound **4**.

Two explanations were initially proposed for the observations:

1. There were two isomers of compound **4** and each isomer had a marginally different shift for both the B*H*$_{agostic}$ hydrogen atoms and the phosphorus atoms. This would give rise to two singlets in the B-agostic region of the $^{1}H\{^{11}B\}$ NMR spectrum. It would also give four singlets in the $^{31}P\{^{1}H\}$ NMR spectrum, with each isomer having one broadened singlet corresponding to the phosphorus atom *trans* to BH$_{agostic}$ and one sharp singlet at lower frequency corresponding to the phosphorus atom *trans* to the carbon atom of 1,1′-bis(*o*-carborane). The isomers could arise from the C$_{cage}$H being located on the same side or the opposite side of the molecule to B-H→Ru, Figure 2.24.

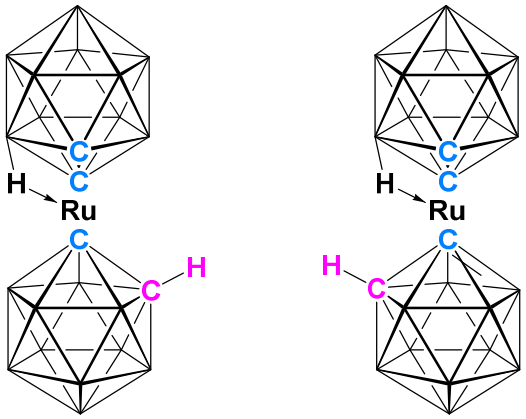

Figure 2.24 Representative drawings to show the two possible isomers of **4**. Some atoms and the dppe ligand have been removed for clarity.

2. Alternatively, the appearance of two peaks in the $^{1}H\{^{11}B\}$ NMR spectrum was due to splitting from a spin active nuclei (such as ^{31}P). Therefore a doublet was present, centred at δ -2.25 ppm and with a $^{2}J_{PH}$ coupling constant of 28.0 Hz. The two sets of peaks in the $^{31}P\{^{1}H\}$ NMR spectrum were again two doublets centred at δ 90.74 and 78.70 ppm with the latter (and most resolved doublet) having a $^{2}J_{PP}$ coupling constant of 11.3 Hz.

Explanation 1 was initially believed as the $^{1}H/^{31}P\{^{1}H\}$ HMBC and HMQC spectra of **4** did not show any coupling between the B-agostic hydrogen atom and either of the phosphorus atoms in dppe. Explanation 2 was eventually confirmed by using three-channel NMR spectroscopy. This enabled the $^{1}H\{^{11}B, ^{31}P\}$ NMR spectrum to be recorded, which displayed only a singlet, Figure 2.25. Therefore, the appearance of a doublet had to be due to splitting of the hydrogen by one of the phosphorus atoms from the dppe ligand.

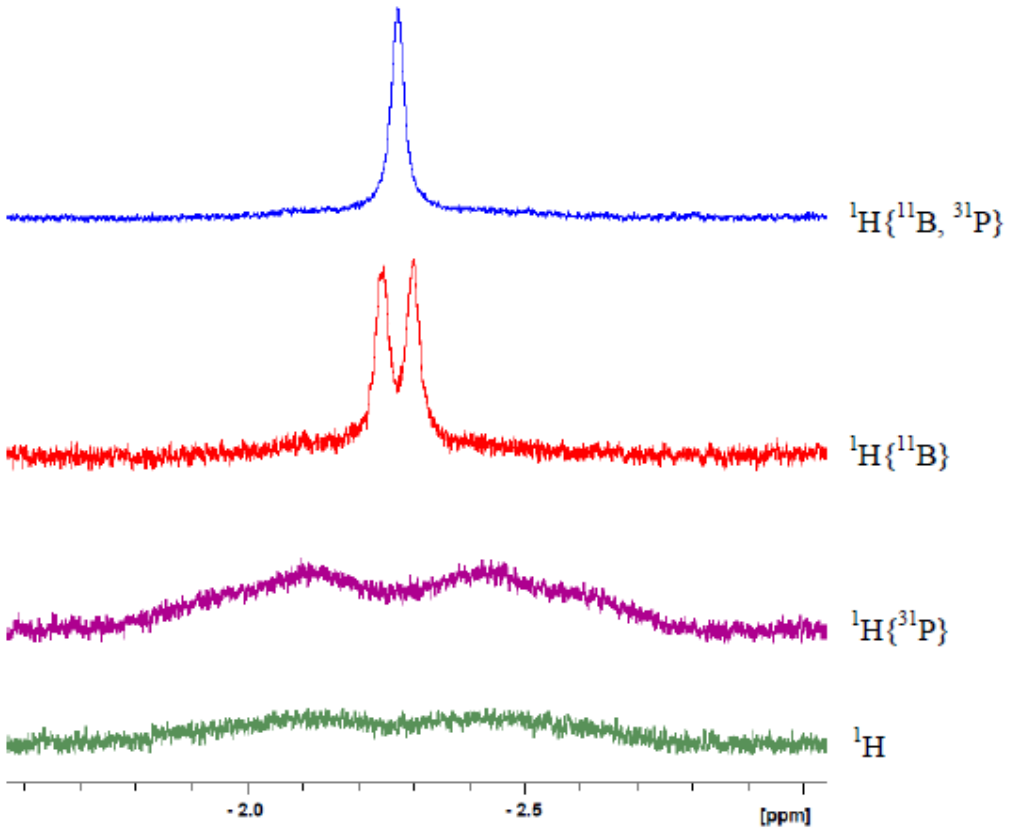

Figure 2.25 Three-channel NMR spectra of compound **4** confirming that the two resonances in the $^{1}H\{^{11}B\}$ NMR spectrum are in fact a doublet.

The three-channel NMR spectroscopy has shown that there is no possibility of two isomers being present, as the "doublet" would still have been seen in the $^{1}H\{^{11}B, ^{31}P\}$ NMR spectrum. It confirms explanation 2, whereby the doublet in the $^{1}H\{^{11}B\}$ NMR spectrum arises from ^{31}P splitting. The phosphorus decoupling removes this splitting and a singlet is observed.

2.11 Lewis Acid Catalysed Diels-Alder Cycloaddition

When a DCM solution of [Ru(κ^3-2,2′,3′-{1-(1′-1′,2′-*closo*-$C_2B_{10}H_{10}$)-1,2-*closo*-$C_2B_{10}H_{10}$})(*p*-cymene)] (**1**) was added to a solution of methacrolein and CpH catalytic activity was observed, Scheme 2.11. Samples of the reaction mixture were taken at regular intervals and were studied by ^{1}H NMR spectroscopy. The integrals of the *exo* and *endo* aldehyde proton resonances were used to calculate diastereomeric excess.

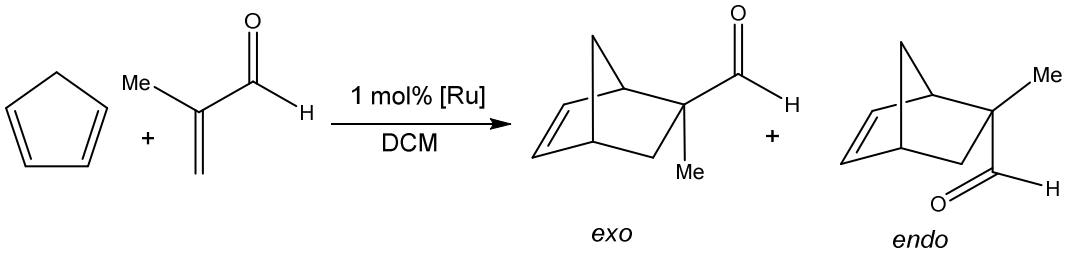

Scheme 2.11 The Lewis acid catalysed Diels-Alder cycloaddition between methacrolein and CpH, using compound **1** as the catalyst.

Full conversion was achieved after six hours at room temperature with a diastereomeric excess of 77% for the *exo* product when using a 1 mol% loading of compound **1**. A control reaction without catalyst was carried out and after 24 hours at room temperature, it gave only 55% conversion and 66% diastereomeric excess for the *exo* product.

Further catalytic tests were carried out, at room temperature using DCM as the solvent, between crotonaldehyde and CpH, using a 1 mol% loading of compound **1** as the catalyst, Scheme 2.12. Samples were again taken at regular intervals and the integrals of the *exo* and *endo* aldehyde proton resonances from the ^{1}H NMR spectra were used to calculate diastereomeric excess.

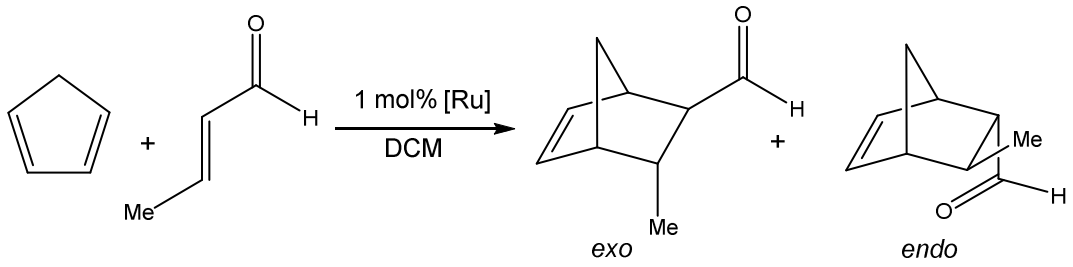

Scheme 2.12 The Lewis acid catalysed Diels-Alder cycloaddition between crotonaldehyde and CpH, using compound **1** as the catalyst.

After six hours, there was 89% conversion to the products at room temperature with a 1 mol% loading of compound **1**, Figure 2.26. There was a diastereomeric ratio of 30:70 *exo* to *endo*, which would give an *endo* diastereomeric excess of 40%. A control reaction using the same conditions produced 3% conversion after six hours with a diastereomeric ratio of 32:68 *exo* to *endo* (*endo* diastereomeric excess of 36%).

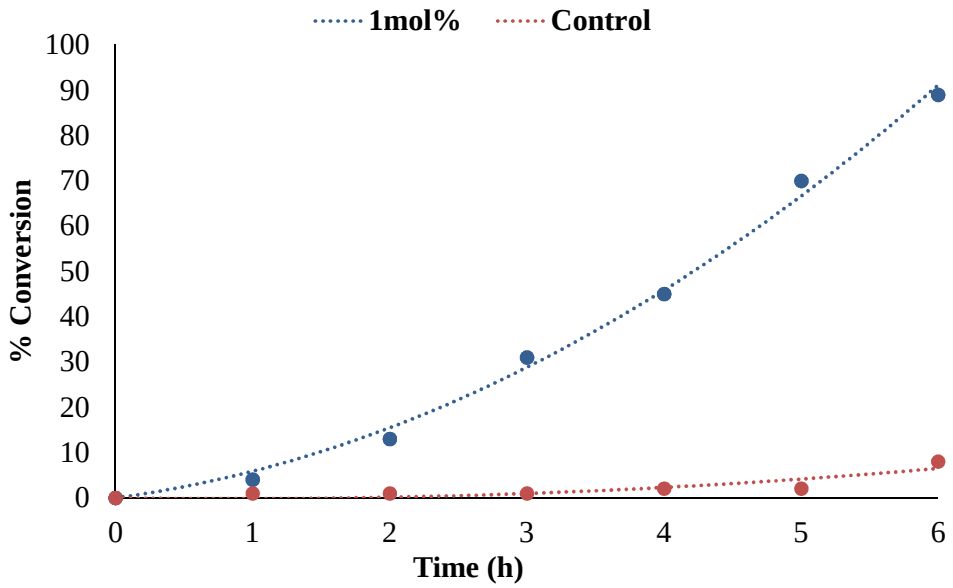

Figure 2.26 Graph showing Lewis acid catalysis of crotonaldehyde and CpH using a 1 mol% loading of compound **1** as the catalyst. After 6 hrs 89% conversion was observed with a diastereomeric excess of 40% for the *endo* product.

2.12 Conclusions

Eight new compounds have been synthesised and fully characterised. Of the eight compounds there were four bonding modes of 1,1′-bis(*o*-carborane). [Ru(κ^3-2,2′,3′-{1-(1′-1′,2′-*closo*-$C_2B_{10}H_{10}$)-1,2-*closo*-$C_2B_{10}H_{10}$})(*p*-cymene)] (**1**) and [Ru(κ^2-2,2′-{1-(1′-1′,2′-*closo*-$C_2B_{10}H_{10}$)-1,2-*closo*-$C_2B_{10}H_{10}$})(*p*-cymene)(CO)] (**2**) displayed the literature-known bonding modes of X_2(*C,C′*)L and X_2(*C,C′*) respectively. [Ru(κ^3-2,3′,3-{1-(1′-1′,2′-*closo*-$C_2B_{10}H_{10}$)-1,2-*closo*-$C_2B_{10}H_{10}$})(PPh_3)$_2$] (**3**) and [Ru(κ^3-2,3′,3-{1-(1′-1′,2′-*closo*-$C_2B_{10}H_{10}$)-1,2-*closo*-$C_2B_{10}H_{10}$})(dppe)] (**4**) both show 1,1′-bis(*o*-carborane) with the new bonding mode X_2(*C,B′*)L. [Ru(κ^2-2,3′-{1-(1′-1′,2′-*closo*-$C_2B_{10}H_{10}$)-1,2-*closo*-$C_2B_{10}H_{10}$})(PPh_3)$(CO)_3$] (**5**), [Ru(κ^2-2,3′-{1-(1′-1′,2′-*closo*-$C_2B_{10}H_{10}$)-1,2-*closo*-$C_2B_{10}H_{10}$})(PPh_3)$(MeCN)_3$] (**6**), [Ru(κ^2-2,3′-{1-(1′-1′,2′-*closo*-$C_2B_{10}H_{10}$)-1,2-*closo*-$C_2B_{10}H_{10}$})(dppe)$(CO)_2$] (**7**) and [Ru(κ^2-2,3′-{1-(1′-1′,2′-*closo*-$C_2B_{10}H_{10}$)-1,2-*closo*-$C_2B_{10}H_{10}$})(dppe)$(MeCN)_2$] (**8**) all have the same 1,1′-bis(*o*-carborane) bonding mode of X_2(*C,B′*) which is previously unseen.

Upon reaction with a suitable phosphine, the *p*-cymene is displaced from compound **1** at room temperature. This highly unusual reaction was observed from the reaction of **1** with both PPh_3 and dppe, affording **3** and **4** respectively.

Compounds **1**, **3** and **4** all have B-H⇀Ru agostic bonds which can be seen in both the $^1H\{^{11}B\}$ NMR spectra and in the crystal structures. These 3c-2e bonds stabilise the compounds by providing the ruthenium metal centre with extra electron density, taking compound **1** to 18 electrons and compounds **3** and **4** to 16 electrons. Due to the lability of the B-agostic bonds compounds **1**, **3** and **4** all react readily with two electron donors such as carbon monoxide and acetonititrile to give the fully saturated, 18-electron compounds **2** and **5**-**8**.

The $^1H\{^{11}B\}$ NMR spectra of compounds **1**, **3** and **4** all display peaks between δ 0.00 and -5.00 ppm corresponding to the B-H⇀Ru agostic bonds. Compound **1** has four fluctional available units that could be involved in this interaction; {B3H3}, {B6H6}, {B3′H3′} and {B6′H6′}. Cooling a sample of compound **1** to 203 K partially arrests the fluctionality of this agostic bond so that only two {BH} units could be involved in the B-H⇀Ru agostic bond, B3 and B6 or B3′ and B6′. Compounds **3** and **4** both display doublets in the agostic region of their $^1H\{^{11}B\}$ NMR spectra. After extensive NMR experiments the doublet was

found to arise from coupling to the spin active ^{31}P nucleus from either PPh_3 (**3**) or dppe (**4**), using $^{1}H\{^{11}B, ^{31}P\}$ NMR spectroscopy.

Due to the lability of the B-H⇀Ru agostic bond in compound **1**, Lewis acid catalysis was attempted and gave good results. When a 1 mol% loading of compound **1** was used, the Lewis acid catalysed Diels-Alder cycloaddition between methacrolein and CpH fully converted after six hours and gave a diastereomeric excess of 77% for the *exo* product. When a 1 mol% loading of compound **1** was used for the Lewis acid catalysed Diels-Alder cycloaddition between crotonaldehyde and CpH, there was 89% conversion after six hours and a diastereomeric excess of 40% for the *endo* product.

Compound **5**, an 18-electron compound with 1,1′-bis(*o*-carborane), a single PPh_3 and three carbonyl ligands had two isomers, in which PPh_3 was *trans* to either C2 or B3′. This gave rise to two resonances in the $^{31}P\{^{1}H\}$ NMR spectrum, one sharp peak from the isomer where PPh_3 was *trans* to C2 and one very broad peak from the isomer where PPh_3 was *trans* to B3′. Compound **6**, a similar compound whereby there were three MeCN ligands in place of the three carbonyl ligands, displayed only one isomer. This is due to the weaker bonding of MeCN and therefore a clear structural *trans* effect is observed. The only isomer shows one MeCN ligand *trans* to the strong boron σ-bond and the PPh_3 ligand *trans* to the weaker carbon σ-bond.

Compounds **7** and **8** were both 18-electron compounds with 1,1′-bis(*o*-carborane), dppe and either two carbonyl ligands or two MeCN ligands. The Ru-P bond lengths from both of these compounds demonstrated the structural *trans* effect and confirmed that boron has a stronger σ-bond than carbon when 1,1′-bis(*o*-carborane) is bound in a coordination complex.

2.13 References

1. D. A. Owen and M. F. Hawthorne, *J. Am. Chem. Soc.*, 1971, **93**, 873.
2. D. E. Harwell, J. McMillan, C. B. Knobler and M. F. Hawthorne, *Inorg. Chem.*, 1997, **36**, 5951.
3. R. A. Love and R. Bau, *J. Am. Chem. Soc.*, 1972, **94**, 8274.
4. M. J. Martin, W. Y. Man, G. M. Rosair and A. J. Welch, *J. Organomet. Chem.*, 2015, **798**, 36.
5. Z.-J. Yao, Y.-Y. Zhang and G.-X. Jin, *J. Organomet. Chem.*, 2015, **798**, 274.
6. C. Vinas, R. Nunez, M. A. Flores, F. Teixidor, R. Kivekas and R. Sillanpaea, *Organometallics*, 1995, **14**, 3952.
7. C. Viñas, R. Nuñez, F. Teixidor, R. Kivekäs and R. Sillanpää, *Organometallics*, 1996, **15**, 3850.
8. M. Brookhart, M. L. Green and L.-L. Wong, *Prog. Inorg. Chem.*, 1988, **36**, 1.
9. W. A. Henderson Jr and C. A. Streuli, *J. Am. Chem. Soc.*, 1960, **82**, 5791.
10. M. R. Crimmin, R. G. Bergman and F. D. Toste, *Angew. Chem. Int. Ed.*, 2011, **50**, 4484.
11. R. Castarlenas, C. Vovard, C. Fischmeister and P. H. Dixneuf, *J. Am. Chem. Soc.*, 2006, **128**, 4079.
12. M. A. Bennett and A. K. Smith, *J. Chem. Soc. Dalton Trans.*, 1974, 233.
13. C. Albrecht, S. Gauthier, J. Wolf, R. Scopelliti and K. Severin, *Eur. J. Inorg. Chem.*, 2009, 1003.
14. A. A. Nazarov, C. G. Hartinger and P. J. Dyson, *J. Organomet. Chem.*, 2014, **751**, 251.
15. G. Süss-Fink, *Dalton Trans.*, 2010, **39**, 1673.
16. P. Kumar, R. K. Gupta and D. S. Pandey, *Chem. Soc. Rev.*, 2014, **43**, 707.
17. A. McAnaw, G. Scott, L. Elrick, G. M. Rosair and A. J. Welch, *Dalton Trans.*, 2013, **42**, 645.

Chapter 3: 1,1′-Bis(*o*-carboranyl)phosphines

3.1 Introduction

Using 1,1′-bis(*o*-carborane) as a chelating ligand for non-transition metal elements is limited to only a handful of examples. The conventional method of producing these 1,1′-bis(*o*-carborane) derivatives is by a simple salt elimination reaction, Scheme 3.1. Reaction between dilithiated 1,1′-bis(*o*-carborane) and a suitable dihalogenated species, such as $PPhCl_2$, can be very high yielding.

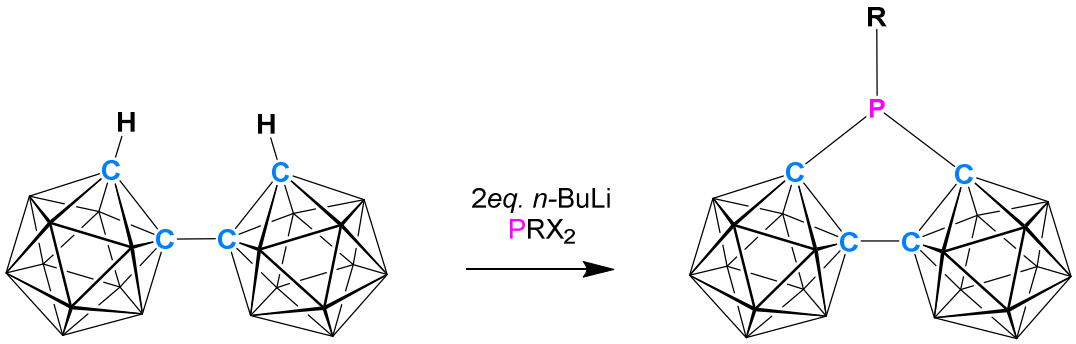

Scheme 3.1 Dilithiation of 1,1′-bis(*o*-carborane) using *n*-BuLi, followed by reaction with an appropriate di-halogenated phosphine.

The first examples noted in the literature were [μ-2,2′-PPh-{1-(1′-1′,2′-*closo*-$C_2B_{10}H_{10}$)-1,2-*closo*-$C_2B_{10}H_{10}$}] and [μ-2,2′-MeAs-{1-(1′-1′,2′-*closo*-$C_2B_{10}H_{10}$)-1,2-*closo*-$C_2B_{10}H_{10}$}], reported in 1978 by Zakharkin et al., Figure 3.1.[1] The reaction involved dilithiation of 1,1′-bis(*o*-carborane) using *n*-BuLi in Et_2O, followed by heating to reflux after addition of dichlorophenylphosphine or dichloromethylarsine. The {PPh} product was isolated in 40% yield, however this compound was only identified by elemental analysis and no further spectroscopic or experimental work was carried out. The {AsMe} compound was afforded in a 50% yield and was identified by elemental analysis and later by single crystal *X*-ray diffraction studies.[2]

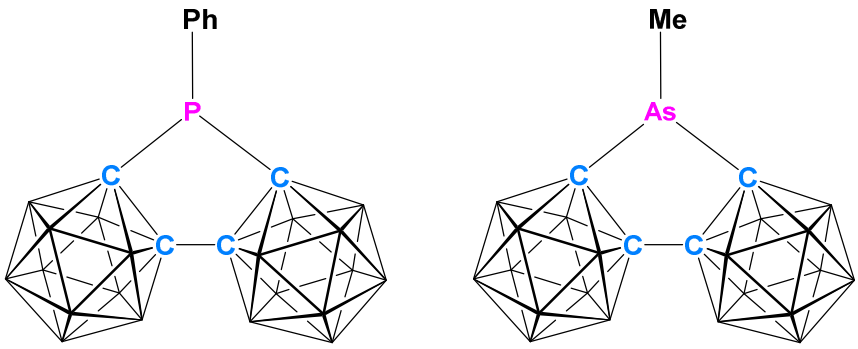

Figure 3.1 [μ-2,2′-PPh-{1-(1′-1′,2′-*closo*-$C_2B_{10}H_{10}$)-1,2-*closo*-$C_2B_{10}H_{10}$}] and [μ-2,2′-MeAs-{1-(1′-1′,2′-*closo*-$C_2B_{10}H_{10}$)-1,2-*closo*-$C_2B_{10}H_{10}$}].

In 1996 Knobler and Johnson reported the synthesis of two carboranylhalophosphines from the reaction of dilithiated 1,1′-bis(*o*-carborane) with PCl_3, which afforded [μ-2,2′-PCl-{1′-(1′,2′-*closo*-$C_2B_{10}H_{10}$)-1,2-*closo*-$C_2B_{10}H_{10}$}].[3] Subsequent reaction with $AgSbF_6$ afforded the fluorinated derivative [μ-2,2′-PF-{1′-(1′,2′-*closo*-$C_2B_{10}H_{10}$)-1,2-*closo*-$C_2B_{10}H_{10}$}], Scheme 3.2.

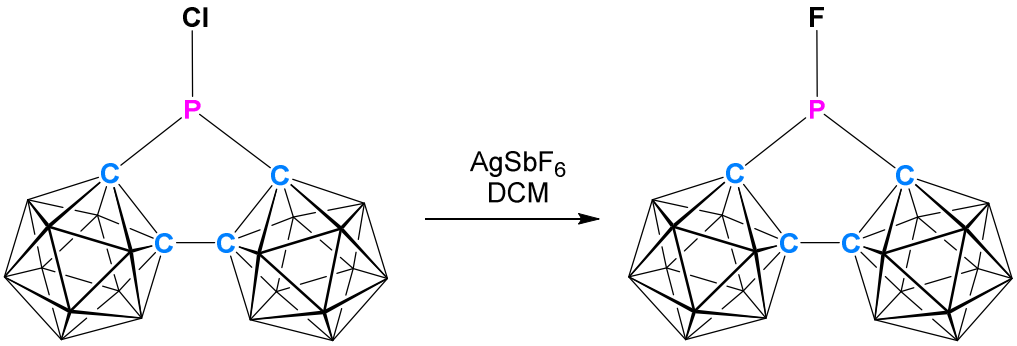

Scheme 3.2 Conversion of [μ-2,2′-PCl-{1′-(1′,2′-*closo*-$C_2B_{10}H_{10}$)-1,2-*closo*-$C_2B_{10}H_{10}$}] to [μ-2,2′-PF-{1′-(1′,2′-*closo*-$C_2B_{10}H_{10}$)-1,2-*closo*-$C_2B_{10}H_{10}$}] using $AgSbF_6$.

One of the last published examples in this series was 1,1′-bis(*o*-carborane) chelating to two gold atoms that display an aurophilic interaction, reported by Hawthorne et al. in 1996, Figure 3.2.[4] Although gold is found in the transition element block of the periodic table, according to IUPAC rules a transition element is an atom with an incomplete *d* sub-

shell. Therefore this example [gold(I)] can be thought of as a *pseudo* non-transition metal element. The compound [μ-2,2′-($AuPPh_3$)$_2$-{1-(1′-1′,2′-*closo*-$C_2B_{10}H_{10}$)-1,2-*closo*-$C_2B_{10}H_{10}$}] was synthesised by reacting one equivalent of 1,1′-bis(*o*-carborane) with two equivalents of *n*-BuLi followed by reaction with two equivalents of [$AuIPPh_3$], and was isolated in 59% yield.

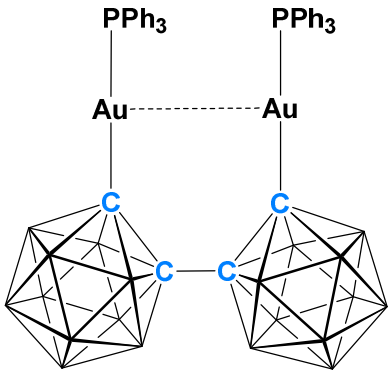

Figure 3.2 The auracarborane [μ-2,2′-($AuPPh_3$)$_2$-{1-(1′-1′,2′-*closo*-$C_2B_{10}H_{10}$)-1,2-*closo*-$C_2B_{10}H_{10}$}].

This chapter will expand on the compound [μ-2,2′-PPh-{1-(1′-1′,2′-*closo*-$C_2B_{10}H_{10}$)-1,2-*closo*-$C_2B_{10}H_{10}$}] initially prepared by Zakharkin et al. including full spectroscopic and crystallographic studies. In addition a second carboranylphosphine, [μ-2,2′-PEt-{1-(1′-1′,2′-*closo*-$C_2B_{10}H_{10}$)-1,2-*closo*-$C_2B_{10}H_{10}$}], is described. For both compounds their reactions with gold chloride will be described and subsequently the Tolman cone angles and percent buried volumes calculated of all four compounds, to quantify the steric bulk of these ligands. Their reactions with elemental selenium will also be described, and the $^2J_{PSe}$ coupling constants of the products will be used in comparison to literature analogues to estimate the basicities of the carboranylphosphines.

3.2 [μ-2,2′-PEt-{1-(1′-1′,2′-*closo*-$C_2B_{10}H_{10}$)-1,2-*closo*-$C_2B_{10}H_{10}$}] (9)

Compound **9** was produced by reacting dilithiated 1,1′-bis(*o*-carborane) with $PEtCl_2$ in THF. After purification by column chromatography and preparative TLC [μ-2,2′-PEt-{1-(1′-1′,2′-*closo*-$C_2B_{10}H_{10}$)-1,2-*closo*-$C_2B_{10}H_{10}$}] (**9**) was afforded as a white solid in 64% yield, Scheme 3.3.

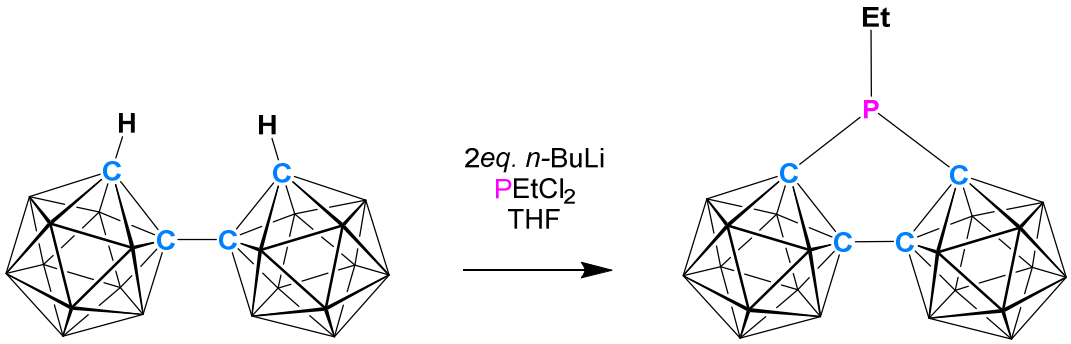

Scheme 3.3 Reaction between 1,1′-bis(*o*-carborane)and *n*-BuLi then $PEtCl_2$ to give [μ-2,2′-PEt-{1-(1′-1′,2′-*closo*-$C_2B_{10}H_{10}$)-1,2-*closo*-$C_2B_{10}H_{10}$}] (**9**).

Compound **9** was characterised by electron ionisation mass spectrometry, NMR spectroscopy and *X*-ray crystallography. Unfortunately, elemental analysis values for all compounds in this chapter gave significantly low results compared to the respective values from the empirical formulae, despite using multiple samples which were pure by NMR spectroscopy, mass spectroscopy and *X*-ray crystallography.

The mass spectrum of **9** showed an envelope characteristic of a carborane at *m/z* 344.3 which agrees with the molecular weight (MW = 344.43 g mol^{-1}).

The ^1H NMR spectrum of compound **9** displays an integral-2 quartet at δ 1.98 ppm corresponding to the methylene (PCH_2CH_3) protons of the ethyl substituent, with the $^3J_{HH}$ coupling being 7.9 Hz. There is a doublet of triplets at δ1.31 ppm integrating as the three methyl (PCH_2CH_3) protons of the ethyl substituent. The $^3J_{HH}$ coupling constant is 7.9 Hz and the $^3J_{PH}$ coupling constant, which gives rise to the triplet being split into a doublet of

triplets, is 23.0 Hz. The lack of an observed $^{2}J_{PH}$ coupling between the phosphorus atom and the CH_2 protons is discussed in detail in section **3.4** and also **3.12**.

The $^{11}B\{^{1}H\}$ NMR spectrum revealed six resonances with the integral pattern 2:2:6:2:2:6 at δ -0.3, -3.8, -6.6, -7.6, -8.5 and -10.6 ppm. The even integrals suggest there is C_s symmetry in compound **9** in solution.

The $^{31}P\{^{1}H\}$ NMR spectrum displays a singlet at δ 42.75 ppm.

Single crystals were grown by slow evaporation of a saturated petroleum ether solution and *X*-ray diffraction studies showed compound **9** crystallised in the $P2_1/n$ space group. The structure has two independent molecules in the asymmetric unit (molecules AB and CD) and molecule AB is shown in Figure 3.3. 1,1′-Bis(*o*-carborane) bonds through two carbon σ-bonds to the phosphorus atom, creating a five-membered central ring. The ethyl group sits in a position so that the P atom is trigonal pyramidal, allowing maximum space for the phosphorus lone pair. The ethyl group is also located in a conformation slightly stabilised by dihydrogen bonds between the ethyl hydrogen atoms (δ^+) and two cage boron hydrogen atoms (δ^-) in the solid state, Figure 3.3.[5] The bond lengths for the dihydrogen interactions for molecule AB are H11B-H12R: 2.51(5) Å, H6B-H11P: 2.28(5) Å, H3A-H11P: 2.45(4) Å and H7A-H11Q: 2.46(5) Å. For molecule CD the dihydrogen interactions are H11D-H12X: 2.40(5) Å, H6D-H11X: 2.29(5) Å, H3C-H11X: 2.39(4) Å and H7C-H11Y: 2.47(4) Å.

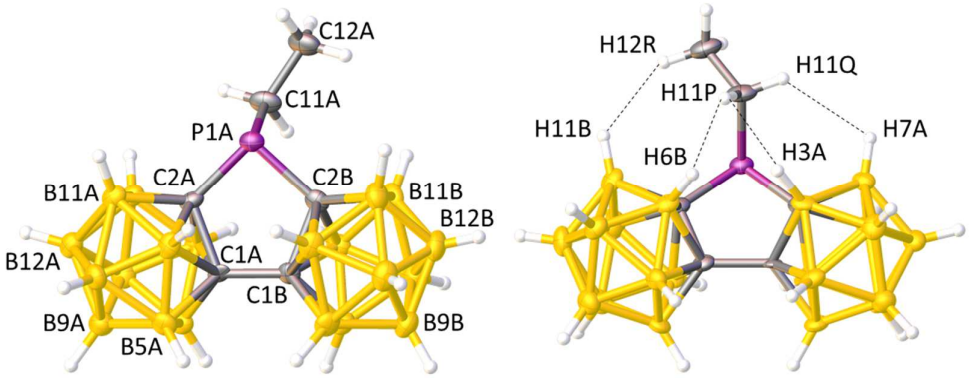

Figure 3.3 Two perspective views of molecule **9**AB [μ-2,2′-PEt-{1-(1′-1′,2′-*closo*-$C_2B_{10}H_{10}$)-1,2-*closo*-$C_2B_{10}H_{10}$}] and part of the atom numbering scheme. Some selected bond lengths are C1A-C1B: 1.533(7) Å, P1A-C2A: 1.870(5) Å, P1A-C2B: 1.890(5) Å, P1A–C11A 1.844(5) Å, C1C-C1D: 1.530(6) Å, P1C-C2C: 1.886(5) Å, P1C-C2D: 1.890(5) Å and P1C–C11C 1.818(5) Å.

3.3 [μ-2,2′-PPh-{1-(1′-1′,2′-*closo*-$C_2B_{10}H_{10}$)-1,2-*closo*-$C_2B_{10}H_{10}$}] (10)

Reaction between dilithiated 1,1′-bis(*o*-carborane) and $PPhCl_2$ in Et_2O, after heating to reflux for two hours, gave a pale yellow solution. Upon purification by column chromatography [μ-2,2′-PPh-{1-(1′-1′,2′-*closo*-$C_2B_{10}H_{10}$)-1,2-*closo*-$C_2B_{10}H_{10}$}] (**10**) was afforded as a white solid in 72% yield, Scheme 3.4. Although the synthesis is based on the original method by Zakharkin et al. the yield has been improved by over 30%.[1]

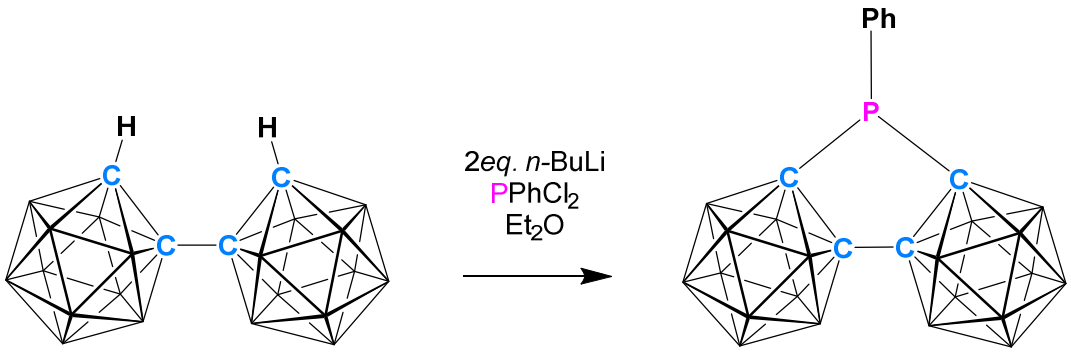

Scheme 3.4 Dilithiation of 1,1′-bis(*o*-carborane), followed by reaction with $PPhCl_2$ to afford [μ-2,2′-PPh-{1-(1′-1′,2′-*closo*-$C_2B_{10}H_{10}$)-1,2-*closo*-$C_2B_{10}H_{10}$}] (**10**).

Compound **10** was identified by electron ionisation mass spectrometry, NMR spectroscopy and *X*-ray crystallography. An envelope was seen in the mass spectrum at *m/z* 392.3 which agreed fully with the calculated molecular weight (MW = 392.47 g mol^{-1}).

The ^1H NMR spectrum displays an integral-2 multiplet between δ 7.77 and 7.73 ppm, an integral-1 multiplet between δ 7.65 and 7.62 ppm and an integral-2 multiplet between δ 7.59 and 7.54 ppm. All three sets of resonances account for the five proton signals of the phenyl substituent.

The $^{11}B\{^{1}H\}$ NMR spectrum shows one integral-2 resonance δ-0.1 ppm and overlapping peaks from δ-2.4 to -13.2 ppm with maxima at δ-3.9, -6.4, -8.7, -9.8 and -11.2 ppm, and a combined integral of 18 boron atoms.

The $^{31}P\{^{1}H\}$ NMR spectrum displays a singlet at δ40.35 ppm.

Single crystals of **10** were grown by slow evaporation of a concentrated petroleum ether solution and crystallised in the $P\bar{1}$ space group, Figure 3.4. Analysis of the structure reveals 1,1′-bis(*o*-carborane) as a chelating substituent to the {PPh} unit, wherein the P atom is trigonal pyramidal. The phenyl ring is tilted slightly due to a dihydrogen interaction between atoms H16 (on the ring) and H3/H6′ (on the carborane). Dihydrogen bonding would stabilise this conformation and occurs because of the δ^+ hydrogen atom on the phenyl ring and the δ^- hydrogen atoms on the cage boron atoms.[5] The dihydrogen bond distances are H6′-H16: 2.15(5) Å and H3-H16: 2.49(5) Å, Figure 3.4.

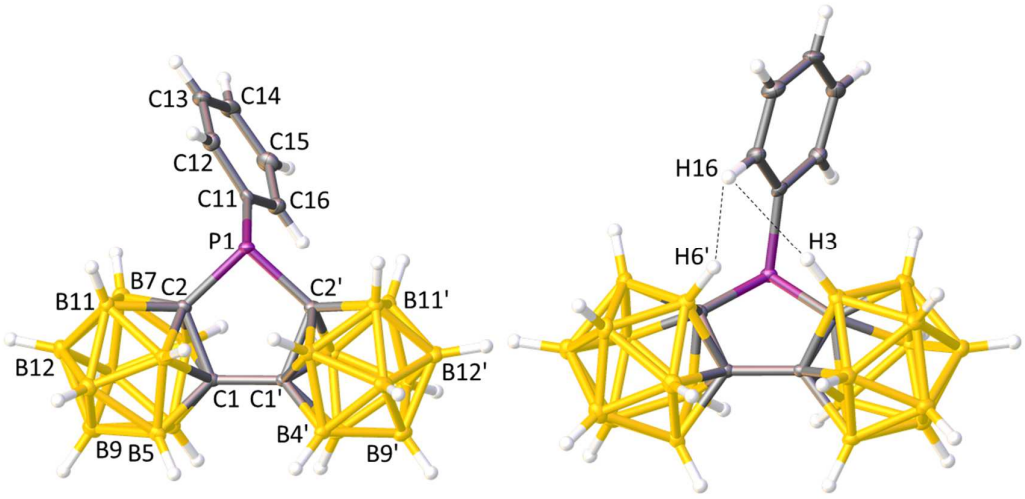

Figure 3.4 Perspective views of [μ-2,2′-PPh-{1-(1′-1′,2′-*closo*-$C_2B_{10}H_{10}$)-1,2-*closo*-$C_2B_{10}H_{10}$}] (**10**) and part of the atom numbering scheme. Some selected bond lengths are C1-C1′: 1.534(3) Å, P1-C2: 1.893(3) Å and P1-C2′: 1.887(3) Å.

3.4 Unusual NMR Spectroscopic Properties of [μ-2,2′-PEt-{1-(1′-1′,2′-*closo*-$C_2B_{10}H_{10}$)-1,2-*closo*-$C_2B_{10}H_{10}$}] (9)

The ^{1}H NMR spectrum of compound **9** is unusual because it does not display all the expected coupling, Figure 3.5. At δ 1.31 ppm an integral-3 doublet of triplets is observed, which corresponds to the methyl (CH_3) unit of the ethyl substituent. The triplet arises from coupling of the methyl protons with the methylene (CH_2) protons, giving a $^3J_{HH}$ coupling constant of 7.9 Hz. The doublet of triplets arises from the additional splitting of the methyl protons by the phosphorus nucleus, giving a $^3J_{PH}$ coupling constant of 23.0 Hz. In contrast to this, at δ 1.98 ppm the observed splitting pattern for the integral-2 methylene protons is a quartet, which is unusual because this infers that only proton-proton coupling from the methyl protons is observed ($^3J_{HH}$ = 7.9 Hz). What is significant about this is the lack of $^2J_{PH}$ coupling between the methylene protons and the phosphorus nucleus, especially as the methylene protons are closer to the phosphorus atom than are the methyl protons. It is unusual that $^3J_{PH}$ coupling, but not $^2J_{PH}$ coupling, would be observed in what seems to be a simple ethyl substituent on the carboranylphosphine.

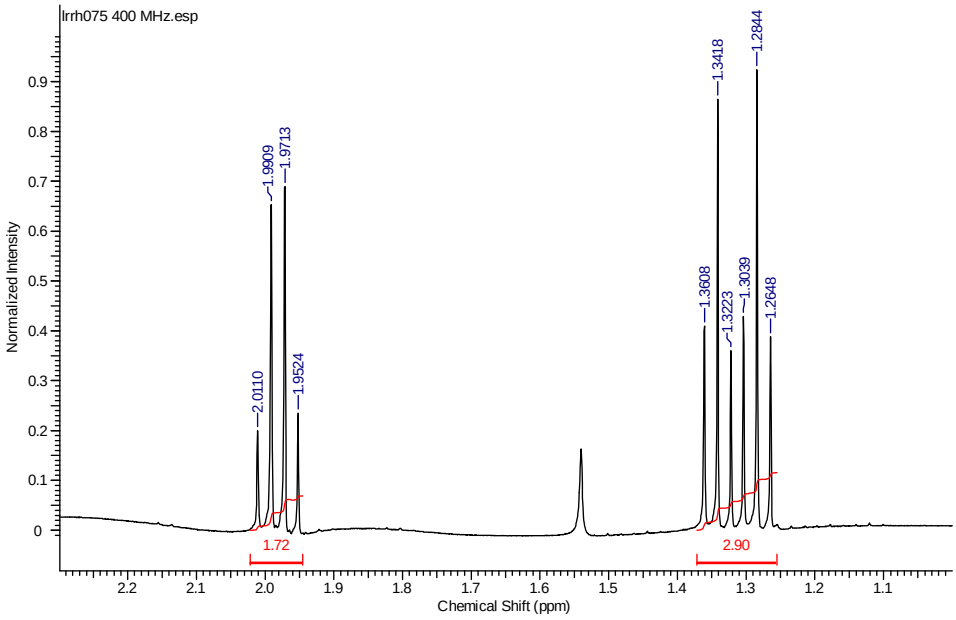

Figure 3.5 The ^{1}H NMR spectrum of compound **9**.

To confirm that the observed splitting pattern for the methyl protons was due to $^{3}J_{HH}$ and $^{3}J_{PH}$ coupling a $^{1}H\{^{31}P\}$ NMR spectrum was acquired, Figure 3.6. As can be seen from this spectrum only an integral-2 quartet and an integral-3 triplet are seen, confirming that the methyl protons displayed coupling to the phosphorus atom in the ^{1}H NMR spectrum.

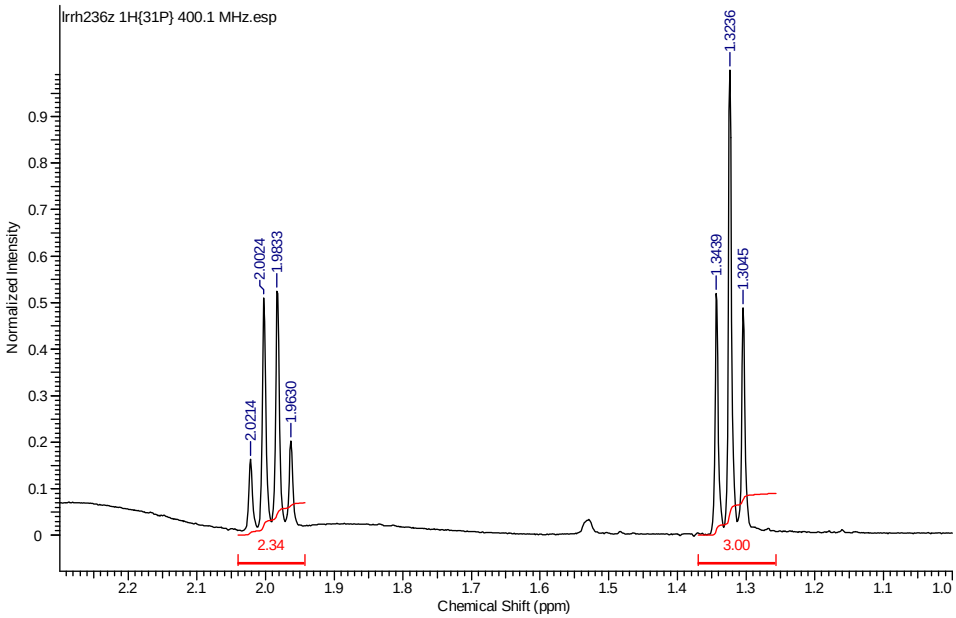

Figure 3.6 The $^{1}H\{^{31}P\}$ NMR spectrum of compound **9**.

In an effort to determine if there was any $^{2}J_{PH}$ coupling between the methylene protons and the phosphorus atom a two-dimensional NMR spectroscopy experiment was performed. The NMR experiment was ^{1}H-^{31}P Heteronuclear Multiple-Bond Correlation (HMBC) spectroscopy, Figure 3.7, which looks for any long-range communication between atoms, typically atoms separated by two to four bonds. The resultant NMR spectrum clearly shows a strong correlation between the methyl protons (doublet of triplets) and the phosphorus atom, already assigned as $^{3}J_{PH}$ = 23.0 Hz. There is also the presence of a small correlation between the methylene protons (quartet) and the phosphorus atom. As no splitting is observed in the ^{1}H NMR spectrum it can therefore be concluded that the two-bond phosphorus-proton coupling must be less than or equal to the half line-width of the methylene protons, i.e. $^{2}J_{PH} \leq \pm 1$ Hz.

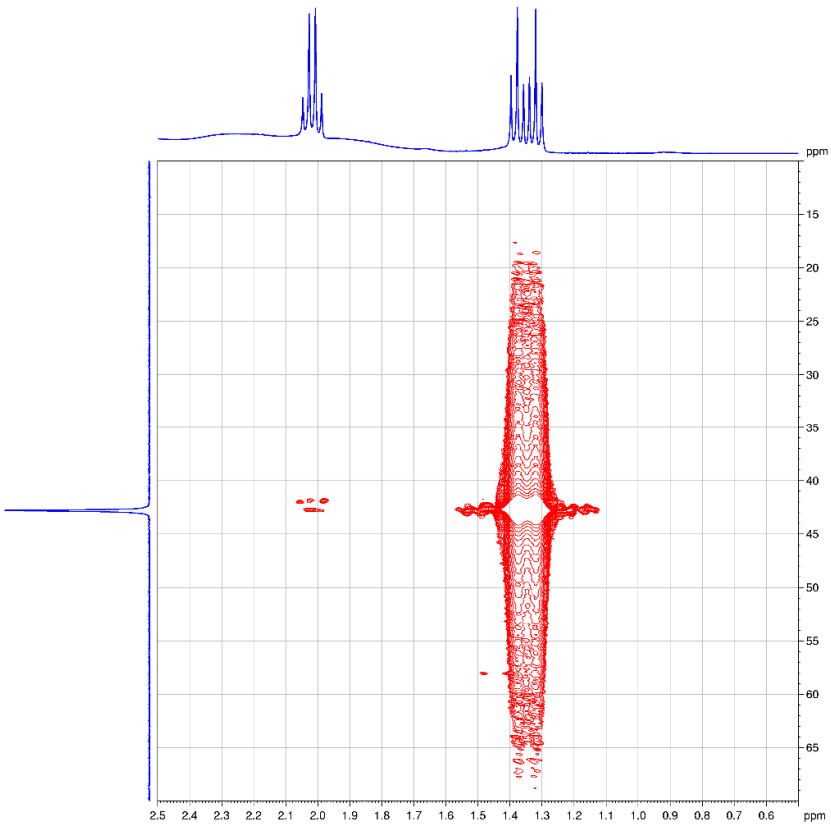

Figure 3.7 The ^{1}H-^{31}P NMR HMBC spectrum of compound **9**, displaying very weak $^{2}J_{PH}$ coupling and very strong $^{3}J_{PH}$ coupling.

3.4.1 Geminal Proton-Phosphorus Couplings, $^2J_{PH}$

The origin of the magnitude of the $^2J_{PH}$ coupling is likely to be a direct consequence of the structure of compound **9**. It has been noted in the literature that the torsion angle (α) relating the protons and the phosphorus lone pair (lp-P-C-H) is related to the geminal coupling constant.[6] Albrand et al. in 1968 considered the relationship between the torsion angles of several compounds and their $^2J_{PH}$ coupling constants, with the results shown in Figure 3.8.[7, 8] The graph showed, particularly with constrained or chelated phosphines, that with small α values (0° to 60°) the $^2J_{PH}$ coupling constant was likely to be both large and positive. However, as the value of α increased (60° to 180°) $^2J_{PH}$ would be much smaller and could be around zero or negative.

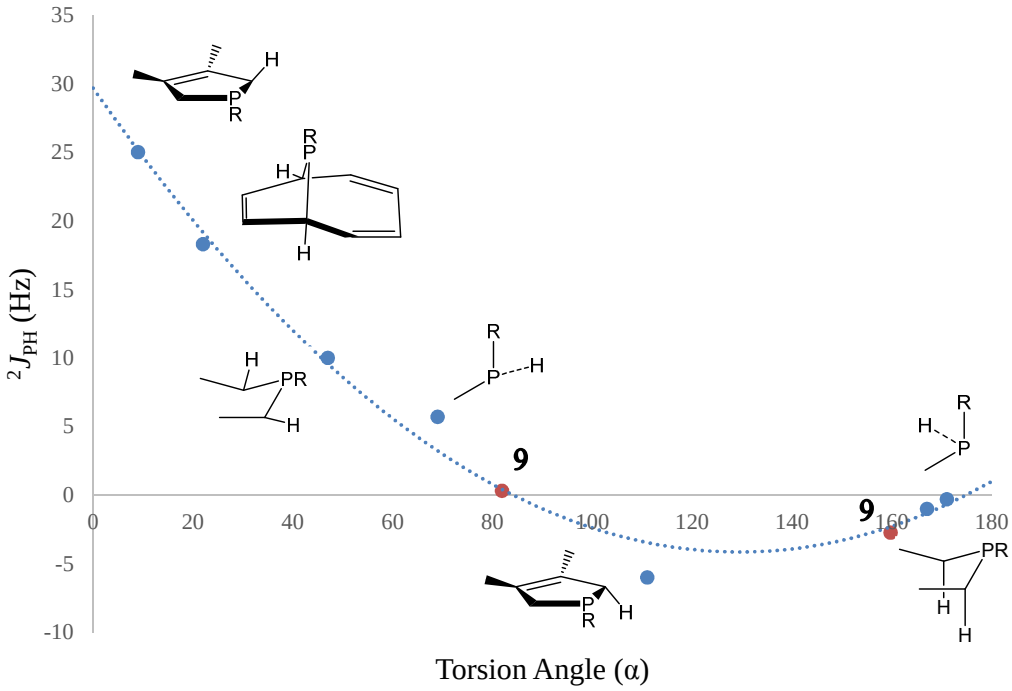

Figure 3.8 Graph showing the relationship between lp-P-C-H torsion angles and $^2J_{PH}$ coupling values, where R = Ph. Blue markers indicate values published by Albrand et al.[7, 8] Red markers show the two torsion angles of **9** when plotted on the curve.

For compound **9** the torsion angles of the two CH_2 protons (measured using the crystal structure AB) are 81.90° and 159.75°. When these values are plotted on the graph, the expected $^2J_{PH}$ would be 0.3 Hz and -2.8 Hz respectively. Therefore, the predicted average coupling using this relationship would be -1.23 Hz and, taking into consideration margins of error, the predicted value may well fit with the experimental value of $^2J_{PH} \leq \pm 1.0$ Hz. However, it has to be noted that the α values reported by Albrand et al. were calculated by drawing Newman projections based on observed P-C-P bond angles, thus they were not taken from crystallographic structures. Moreover, these values represent predicted static structures and do not take into account changes that might occur within the molecule in solution, such as rotation of the bonds. The results of this study are therefore used only as a possible explanation and further analysis was carried out to definitively assign the reason for $^2J_{PH}$ being so small, section **3.12**.

Solid-state NMR spectroscopy was considered for this work but the fine details of the spectrum would be lost which could make it impossible to see $^2J_{PH}$ coupling.

3.5 [μ-2,2′-P(Et)AuCl-{1-(1′-1′,2′-*closo*-$C_2B_{10}H_{10}$)-1,2-*closo*-$C_2B_{10}H_{10}$}] (11)

Two carboranylphosphines (**9** and **10**) have been synthesised in good yields, and have been fully characterised. To determine their steric bulk the {AuCl} derivatives of both were synthesised, allowing the Tolman cone angle and percent buried volume of both the carboranylphosphines and the {AuCl} carboranylphosphines to be calculated and compared. These values were also compared to literature examples to evaluate the size of the coordinated and uncoordinated 1,1′-bis(*o*-carboranyl)phosphines (**9** to **12**).

The carboranylphosphine [μ-2,2′-PEt-{1-(1′-1′,2′-*closo*-$C_2B_{10}H_{10}$)-1,2-*closo*-$C_2B_{10}H_{10}$}] (**9**) and [AuCl(tht)] were stirred in DCM for 30 mins at 0 °C, Scheme 3.5. Partial solvent evaporation followed by addition of petroleum ether precipitated a white powder which was subsequently identified as [μ-2,2′-P(Et)AuCl-{1-(1′-1′,2′-*closo*-$C_2B_{10}H_{10}$)-1,2-*closo*-$C_2B_{10}H_{10}$}] (**11**) in 32% yield.

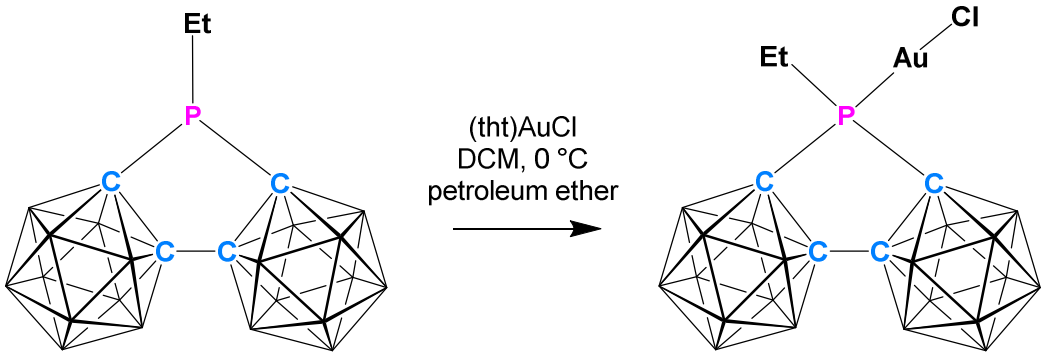

Scheme 3.5 Reaction between compound **9** and (tht)AuCl to afford [μ-2,2′-P(Et)AuCl-{1-(1′-1′,2′-*closo*-$C_2B_{10}H_{10}$)-1,2-*closo*-$C_2B_{10}H_{10}$}] (**11**).

Compound **11** was identified by electron ionisation mass spectrometry, NMR spectroscopy and *X*-ray crystallography. The mass spectrum exhibits an envelope at *m/z* 577.3 consistent with the molecular weight (MW = 576.88 g mol^{-1}).

The ^{1}H NMR spectrum of **11** displays an integral-2 doublet of quartets at δ 2.48 ppm corresponding to the methylene protons of the ethyl substituent. There is a $^{3}J_{HH}$ coupling of 7.7 Hz and now, upon coordination of the phosphorus lone pair, the $^{2}J_{PH}$ coupling constant can be observed as 10.9 Hz. There is also an integral-3 doublet of triplets at

δ 1.52 ppm assigned to the methyl protons of the ethyl substituent. The associated coupling constants are $^{3}J_{HH}$ = 7.7 Hz and $^{3}J_{PH}$ = 27.9 Hz.

The $^{11}B\{^{1}H\}$ NMR spectrum has five resonances in a 2:2:6:4:6 integral pattern with the shifts at δ 1.7, -3.3, -5.7, -7.6 and -10.4 ppm. The even integrals suggest a plane of symmetry through the molecule in solution.

The $^{31}P\{^{1}H\}$ NMR spectrum shows a singlet at δ 75.76 ppm, shifted 33 ppm to higher frequency compared to the uncoordinated phosphine **9**.

Single crystals of **11** were grown from slow evaporation of a concentrated DCM solution of the compound. It crystallised in the Pbca space group and showed the expected structure whereby the phosphorus lone pair has formed a bond with a gold atom, therefore forming a linear gold chloride adduct on the phosphorus centre, Figure 3.9, with the P-Au-Cl bond angle being 176.16(4)°.

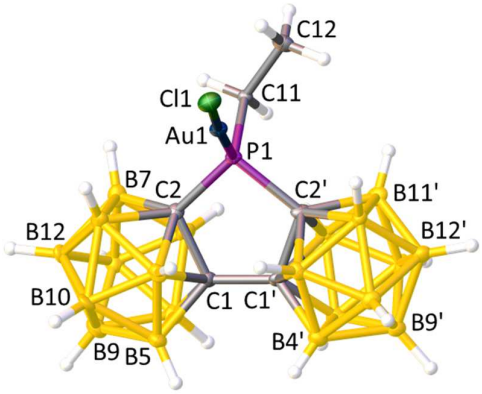

Figure 3.9 Perspective view of [μ-2,2′-P(Et)AuCl-{1-(1′-1′,2′-*closo*-$C_2B_{10}H_{10}$)-1,2-*closo*-$C_2B_{10}H_{10}$}] (**11**) and part of the atom numbering scheme. Some selected bond lengths are C1-C1′: 1.538(5) Å, P1-C2: 1.860(4) Å, P1-C2′: 1.883(4) Å, P1-Au1: 2.2181(11) Å and Au1-Cl1: 2.2910(11) Å.

The geometry around the phosphorus centre is *pseudo*-tetrahedral with four substituents: chelated 1,1′-bis(*o*-carborane), the ethyl group and the gold chloride. The bond angles around the phosphorus atom range from 95.74(18)° to 117.53(13)°. The smallest angle is C2-P-C2′ which is presumably due to the constrained conformation of 1,1′-bis(*o*-carborane) and the largest angle is C11-P-Au.

3.6 [μ-2,2′-P(Ph)AuCl-{1-(1′-1′,2′-*closo*-$C_2B_{10}H_{10}$)-1,2-*closo*-$C_2B_{10}H_{10}$}] (12)

[μ-2,2′-PPh-{1-(1′-1′,2′-*closo*-$C_2B_{10}H_{10}$)-1,2-*closo*-$C_2B_{10}H_{10}$}] (**10**) was stirred with [AuCl(tht)] as a DCM solution at 0 °C, then warmed to room temperature for 20 mins and the majority of the solvent removed *in vacuo*. Precipitation occurred by addition of petroleum ether and a white powder was collected which was subsequently identified as [μ-2,2′-P(Ph)AuCl-{1-(1′-1′,2′-*closo*-$C_2B_{10}H_{10}$)-1,2-*closo*-$C_2B_{10}H_{10}$}] (**12**), in 81% yield, Scheme 3.6.

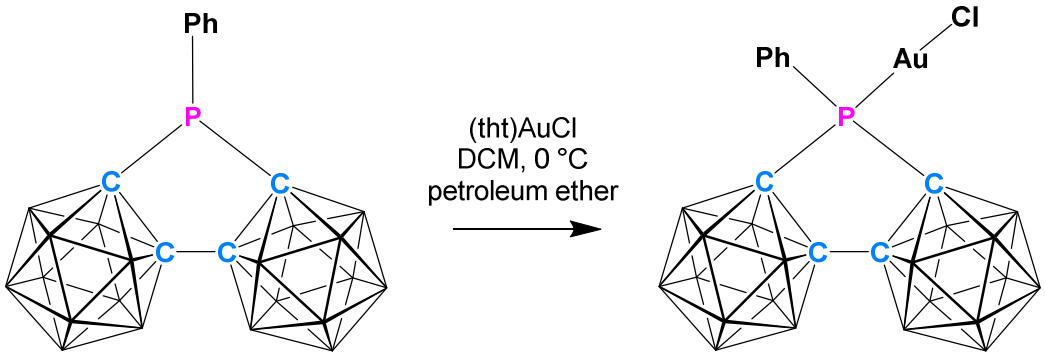

Scheme 3.6 Reaction between compound **10** and (tht)AuCl to afford [μ-2,2′-P(Ph)AuCl-{1-(1′-1′,2′-*closo*-$C_2B_{10}H_{10}$)-1,2-*closo*-$C_2B_{10}H_{10}$}] (**12**).

Compound **12** was characterised by electron ionisation mass spectrometry, NMR spectroscopy and *X*-ray crystallography. The mass spectrum of **12** displayed an envelope centred at *m/z* 624.1, consistent with it having a molecular weight of 624.93 g mol^{-1}.

The ^{1}H NMR spectrum shows an integral-2 multiplet from δ 8.15 to 8.09 ppm, an integral-1 multiplet from δ 7.86 to 7.81 ppm and an integral-2 multiplet from δ 7.75 to 7.70 ppm, with all the resonances corresponding to the five aromatic protons of the phenyl ring.

The $^{11}B\{^{1}H\}$ NMR spectrum exhibits an integral-2 peak at δ 1.9 ppm. The remaining boron atom signals are found as overlapping peaks from δ -0.7 to -10.9 ppm. The maxima appear at δ -3.6, -5.6, -7.6, -9.2 and -10.9 ppm and have an overall integral of 18 boron atoms.

The $^{31}P\{^{1}H\}$ NMR spectrum displays a singlet at δ 68.98 ppm, shifted 29 ppm to high frequency compared to the uncoordinated phosphine **10**.

Single crystals of **12** were grown from slow evaporation of a concentrated DCM solution and crystallised in the C2/c space group. Much like with compound **11**, the lone pair of the phosphorus atom has formed a bond with {AuCl} to form a linear adduct, Figure 3.10. The Au-Cl and P-Au bond lengths are 2.2699(8) Å and 2.2217(8) Å respectively and the P-Au-Cl bond angle is 178.83(3)°. The Au-Cl bond length is slightly shorter, and the P-Au bond length slightly longer, compared to compound **11**.

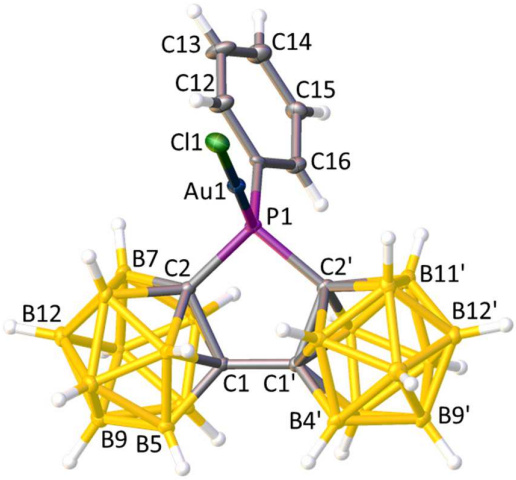

Figure 3.10 Perspective view of [μ-2,2′-P(Ph)AuCl-{1-(1′-1′,2′-*closo*-$C_2B_{10}H_{10}$)-1,2-*closo*-$C_2B_{10}H_{10}$}] (**12**) and part of the atom numbering scheme. Some selected bond lengths are C1-C1′: 1.523(4) Å, P1-C2: 1.879(3) Å, P1-C2′: 1.878(3) Å, P1-Au1: 2.2217(8) Å and Au1-Cl1: 2.2699(8) Å.

In this structure the phosphorus atom is in a *pseudo*-tetrahedral geometry with the chelating 1,1′-bis(*o*-carborane), the phenyl ring and the gold-chloride as the four substituents. The bond angles range from 95.07(13)° to 113.77(11)° with the smallest angle C2-P-C2′ due to the rigidity of 1,1′-bis(*o*-carborane), and the largest angle C11-P-Au.

3.7 Determining the Steric Bulk of 1,1′-Bis(*o*-carboranyl)phosphines (9 – 12)

An important feature of phosphines is their steric bulk and this can be measured by calculating their Tolman cone angles (θ) and percent buried volumes (%V_{bur}), Figure 3.11. The Tolman cone angle measures the angle of the cone created when a metal atom is at the apex and the hydrogens of the R groups are at the perimeter of the cone formed.[9, 10] The percent buried volume is described as the percentage of the first coordination sphere of a metal atom which is occupied by a phosphine, where the M-P distance is set at 2.28 Å.[11]

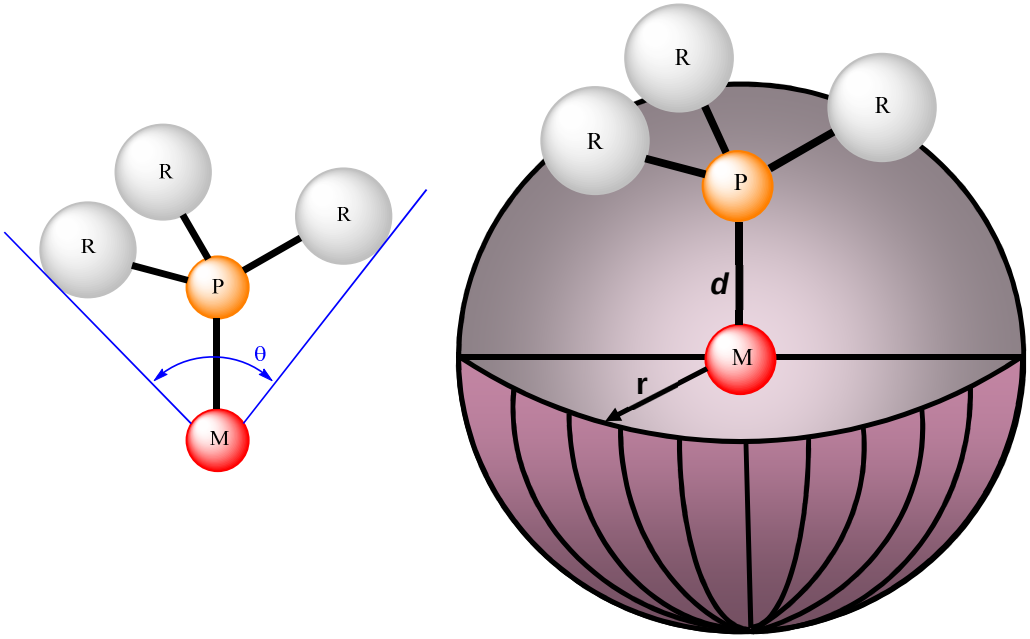

Figure 3.11 Pictorial representation of how the Tolman cone angle (θ, left) and percent buried volume (right, r = radius and *d* = M-P distance) are calculated. Grey spheres represent the van der Waals surface of the substituents R.

For the purpose of this work, the steric bulk was measured for both the free carboranylphosphine and the gold chloride carboranylphosphine. The gold chloride derivative was used as literature work by Clavier and Nolan in 2010 showed excellent correlations between the Tolman cone angles and percent buried volumes with these phosphine derivatives.[12] Both the Tolman cone angles and percent buried volumes were calculated with the Au-P bond length 2.28 Å for equal comparison. By calculating values

for both a free phosphine and its {AuCl} derivative there could be direct comparison between the two. The results showed that upon complexation the steric bulk slightly increased, Table 3.1.

Table 3.1 The Tolman cone angles (θ) and percent buried volumes (%V_{bur}) of compounds **9** to **12**.

Compound	**θ (°)**	**%V_{bur} (%)**
9 PEt	171.6/171.6	30.9/30.7
10 PPh	172.5	32.0
11 P(Et)AuCl	176.5	32.0
12 P(Ph)AuCl	176.2	33.2

The Tolman cone angles for compounds **9** (PEt) and **10** (PPh) were calculated to be 171.6/171.6° and 172.5° respectively, with **9** having one value for each of the independent molecules AB and CD. The percent buried volumes of **9** and **10** were calculated to be 30.9/30.7% and 32.0% respectively. The calculated θ and %V_{bur} values can be compared to literature values revealing that the carboranylphosphines **9** and **10** are larger than triphenylphosphine (145°, 29.6%), but comparable to tricyclohexylphosphine (170°, 31.8%).[12-14]

When the phosphines were coordinated to a gold chloride fragment the Tolman cone angle and the percent buried volume increased by an average of 4.3° and 1.2% respectively. This is because in compounds **9** and **10** the lone pair on the phosphorus will have a repulsive effect and push the substituents closer together. Upon complexation to {AuCl} the effects of the lone pair will be reduced, therefore allowing the substituents to sit further away from each other and increasing the steric bulk.

3.8 [μ-2,2′-P(Et)Se-{1-(1′-1′,2′-*closo*-$C_2B_{10}H_{10}$)-1,2-*closo*-$C_2B_{10}H_{10}$}] (13)

Coordination of **9** and **10** to {AuCl}, afforded **11** and **12** respectively, which allowed for estimation of the steric bulk of the bis(carboranyl)phosphines. The reaction between the **9** and **10** with elemental selenium are now described. The $^{1}J_{PSe}$ coupling constants of the products are determined and are used to estimate the basicities of the bis(carboranyl)phosphines **9** and **10**.

When a toluene solution of [μ-2,2′-PEt-{1-(1′-1′,2′-*closo*-$C_2B_{10}H_{10}$)-1,2-*closo*-$C_2B_{10}H_{10}$}] (**9**) was heated to reflux in the presence of elemental selenium a colour change was observed from colourless to pale pink. After filtration and removal of the solvent a pale pink solid was isolated which was subsequently identified as [μ-2,2′-P(Et)Se-{1-(1′-1′,2′-*closo*-$C_2B_{10}H_{10}$)-1,2-*closo*-$C_2B_{10}H_{10}$}] (**13**), Scheme 3.7. The yield was 71% by looking at the conversion of starting materials to products in the $^{31}P\{^{1}H\}$ NMR spectrum, but separation by preparative TLC gave **13** in 38% isolated yield.

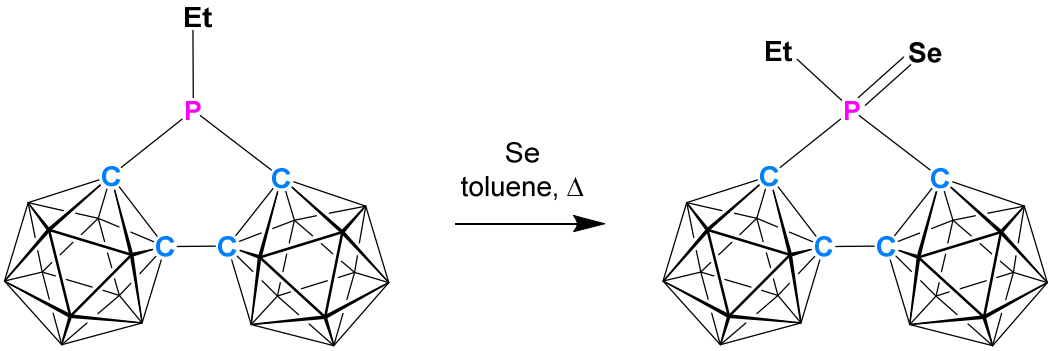

Scheme 3.7 Reaction between compound **9** and elemental selenium to afford [μ-2,2′-P(Et)Se-{1-(1′-1′,2′-*closo*-$C_2B_{10}H_{10}$)-1,2-*closo*-$C_2B_{10}H_{10}$}] (**13**).

Compound **13** was analysed using electron ionisation mass spectrometry, NMR spectroscopy and *X*-ray crystallography. The molecular ion peak in the mass spectrum was seen at *m/z* 423.4, consistent with the molecular weight (MW = 423.42 g mol^{-1}).

The ^{1}H NMR spectrum displays the methylene protons as an integral-2 doublet of quartets at δ 2.72 ppm, having $^{3}J_{HH}$ = 7.6 Hz and $^{2}J_{PH}$ = 11.6 Hz. The methyl protons are observed as an integral-3 doublet of triplets at δ 1.52 ppm, with $^{3}J_{HH}$ = 7.6 Hz and $^{3}J_{PH}$ = 25.9 Hz.

The ^{11}B{^{1}H} NMR spectrum showed an integral-2 peak at δ 0.9 ppm and and integral-2 peak at δ -3.7 ppm. Several overlapping resonances were observed between δ -4.8 and -12.3 ppm. The maxima were at δ -6.2, -7.6, -8.7, -9.2 and -10.6 ppm, having a total integration of 16 boron atoms.

The 162 MHz ^{31}P{^{1}H} NMR spectrum exhibits a singlet at δ 58.05 ppm, with selenium satellites at δ 60.80 and 55.28 ppm, Figure 3.12. Therefore, the one-bond phosphorus-selenium coupling constant ($^{1}J_{PSe}$) is 894.2 Hz.

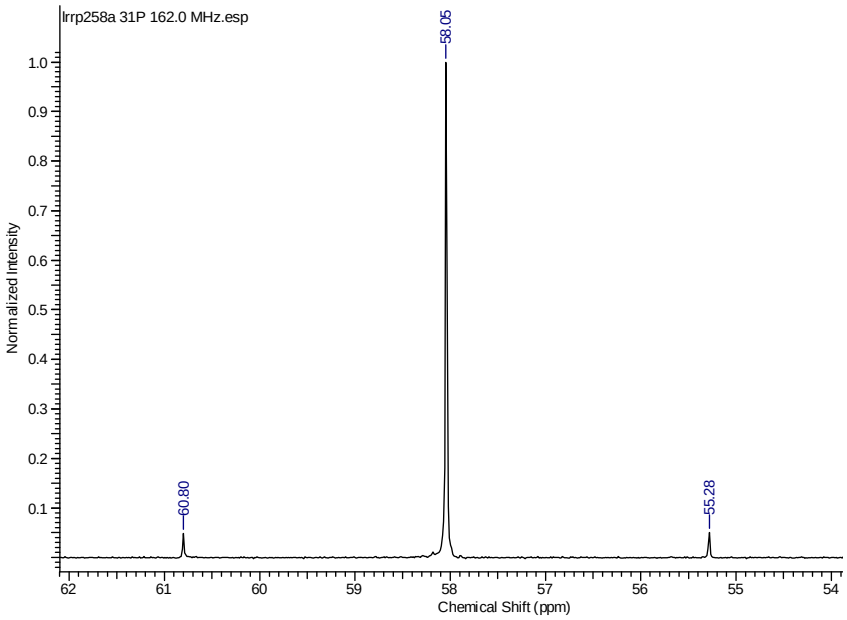

Figure 3.12 The ^{31}P{^{1}H} NMR spectrum of compound **13**, displaying the selenium satellites.

Single crystals were afforded by slow evaporation of a concentrated $CDCl_3$ solution. Compound **13** crystallised in the $P\bar{1}$ space group and the structure confirms the formation of a phosphorus-selenium bond [2.0801(7) Å], Figure 3.13. The geometry of the substituents around the phosphorus atom are tetrahedral with the bond angles ranging

from 95.28(10)° to 116.24(8)°. The smallest angle is C2-P-C2′, which is seemingly due to the rigid conformation of 1,1′-bis(*o*-carborane).

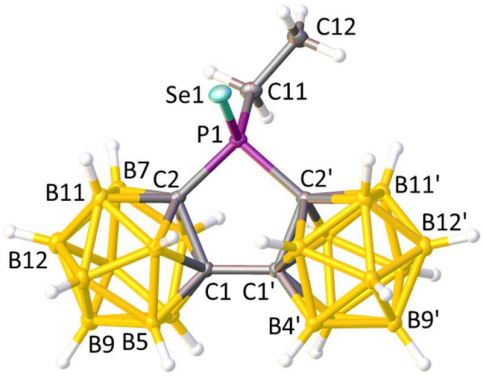

Figure 3.13 Perspective view of [μ-2,2′-P(Et)Se-{1-(1′-1′,2′-*closo*-$C_2B_{10}H_{10}$)-1,2-*closo*-$C_2B_{10}H_{10}$}] (**13**) and part of the atom numbering scheme. Some selected bond lengths are C1-C1′: 1.543(3) Å, P1-C2: 1.879(2) Å, P1-C2′: 1.893(2) Å and P1-Se1: 2.0801(7) Å.

3.9 [μ-2,2′-P(Ph)Se-{1-(1′-1′,2′-*closo*-$C_2B_{10}H_{10}$)-1,2-*closo*-$C_2B_{10}H_{10}$}] (14)

Reaction between [μ-2,2′-PPh-{1-(1′-1′,2′-*closo*-$C_2B_{10}H_{10}$)-1,2-*closo*-$C_2B_{10}H_{10}$}] (**10**) and elemental selenium in toluene when heated to reflux gave the pale pink compound [μ-2,2′-P(Ph)Se-{1-(1′-1′,2′-*closo*-$C_2B_{10}H_{10}$)-1,2-*closo*-$C_2B_{10}H_{10}$}] (**14**), Scheme 3.8. The yield was determined to be 74% from the conversion of starting material to product in the $^{31}P\{^1H\}$ NMR spectrum. After purification using preparative TLC the isolated yield was 47%.

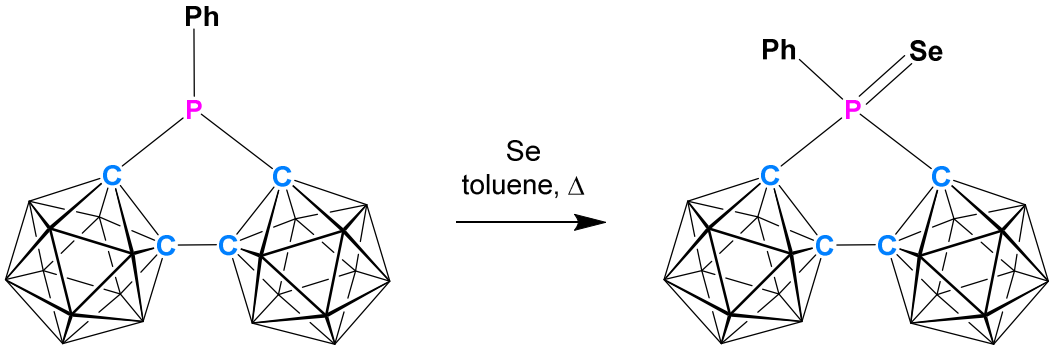

Scheme 3.8 Reaction between compound **10** and elemental selenium to afford [μ-2,2′-P(Ph)Se-{1-(1′-1′,2′-*closo*-$C_2B_{10}H_{10}$)-1,2-*closo*-$C_2B_{10}H_{10}$}] (**14**).

Compound **14** was identified by electron ionisation mass spectrometry, NMR spectroscopy and *X*-ray crystallography. The molecular ion was seen as part of a classical carborane envelope at *m/z* 471.3, consistent with the molecular weight of 471.46 g mol^{-1}.

The ^1H NMR spectrum displayed an integral-2 multiplet between δ 8.31 and 8.25 ppm, an integral-1 multiplet between δ 7.73 and 7.68 ppm and an integral-2 multiplet between δ 7.63 and 7.57 ppm, corresponding to the five phenyl protons.

The $^{11}B\{^1H\}$ NMR spectrum showed an integral-2 resonance at δ 1.2 ppm and further overlapping resonances between δ -2.6 and -13.2 ppm with maxima at δ -4.1, -6.0, -6.4, -8.5, -9.9 and -11.2 ppm, integrating for a total of 18 boron atoms.

The 162 MHz $^{31}P\{^{1}H\}$ NMR spectrum gives a singlet at δ 50.52 ppm with the two selenium satellites at δ 53.27 and 47.77 ppm, therefore giving a one-bond phosphorus selenium coupling constant of 891.0 Hz, Figure 3.14.

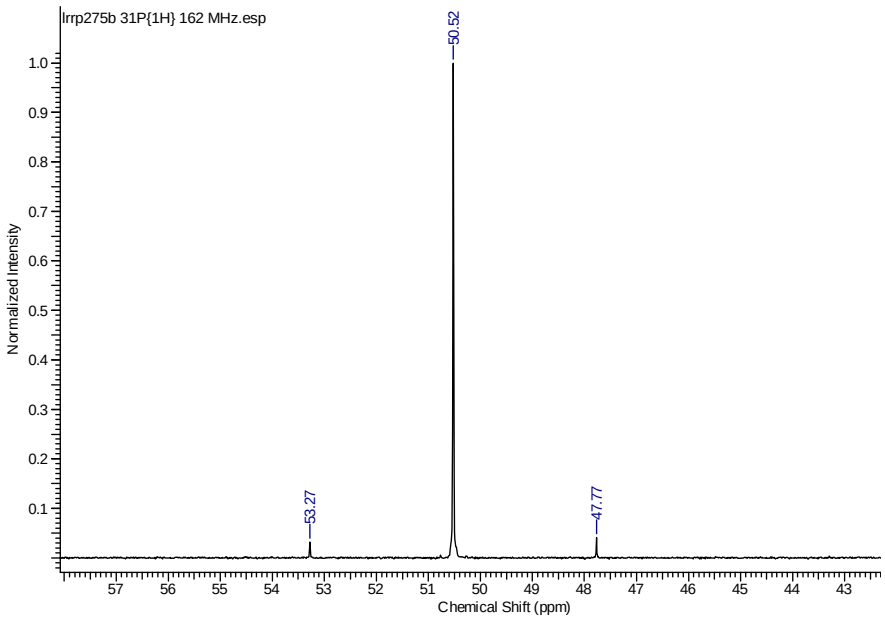

Figure 3.14 The $^{31}P\{^{1}H\}$ NMR spectrum of compound **14** showing the selenium satellites.

Compound **14** was crystallised by slow evaporation of a concentrated petroleum ether solution. The crystallographic study shows that it crystallises in the $P2_1/n$ space group. The structure of this compound confirms the formation of a phosphorus-selenium bond with a P-Se bond length of 2.0798(6) Å, Figure 3.15. The geometry around the phosphorus atom is tetrahedral with the bond angles ranging from 94.81(8)° to 114.38(7)° and the smallest angle being C2-P-C2′ due to the constraints of 1,1′-bis(*o*-carborane).

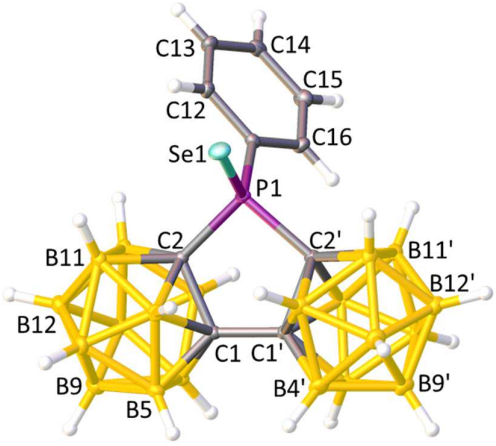

Figure 3.15 Perspective view of [μ-2,2′-P(Ph)Se-{1-(1′-1′,2′-*closo*-$C_2B_{10}H_{10}$)-1,2-*closo*-$C_2B_{10}H_{10}$}] (**14**) and part of the atom numbering scheme. Some selected bond lengths are C1-C1′: 1.536(3) Å, P1-C2: 1.886(2) Å, P1-C2′: 1.896(2) Å and P1-Se1: 2.0798(6) Å.

3.10 Comparison of $^1J_{PSe}$ Values of 1,1′-Bis(*o*-carboranyl)phosphine Selenides (13 & 14) with Literature Examples

Both compounds [μ-2,2′-P(Et)Se-{1-(1′-1′,2′-*closo*-$C_2B_{10}H_{10}$)-1,2-*closo*-$C_2B_{10}H_{10}$}] (**13**) and [μ-2,2′-P(Ph)Se-{1-(1′-1′,2′-*closo*-$C_2B_{10}H_{10}$)-1,2-*closo*-$C_2B_{10}H_{10}$}] (**14**) have large one bond phosphorus-selenium coupling constants, of 894 and 891 Hz respectively. These values can be directly compared to literature values of both standard phosphines and other carboranylphosphines. The value of $^1J_{PSe}$ depends on the electron-withdrawing or electron-donating substituents on phosphorus, giving either increased or reduced coupling constants respectively. As the amount of *s* character at the phosphorus centre increases, the magnitude of $^1J_{PSe}$ increases and therefore highly electron-withdrawing substituents will give large coupling constants, as seen with compounds **13** and **14**. The values of one-bond phosphorus-selenide coupling constants are always negative,[15] although they are most often written without the negative sign, a pattern which will be continued in this thesis.

Values of $^1J_{PSe}$ have been reported up to 1100 Hz, whereby the molecules are constrained phosphites.[16] For these examples, in addition to the constraints of the tridentate substituent on the phosphorus atom, the substituent would be very electron-withdrawing and therefore would increase the magnitude of $^1J_{PSe}$. Two other examples of carboranylphosphine selenides with high $^1J_{PSe}$ values are [1-P(Ph_2)Se-2-PPh_2-1,2-*closo*-$C_2B_{10}H_{10}$] (**A**) and [μ-1,1′-P(Ph)Se-3,3′-Co(1,2-$C_2B_9H_{10})_2$]$^-$ (**B**), Figure 3.16, which have $^1J_{PSe}$ values of 807 and 833 Hz respectively.[17, 18] The $^1J_{PSe}$ value of **B** is higher than that of **A** due to there being two carborane cages attached to the phosphorus atom (as opposed to one in compound **A**). The increase from one electron-withdrawing substituent to two would decrease the electron density on phosphorus giving it higher *s* character, in turn raising the magnitude of $^1J_{PSe}$.

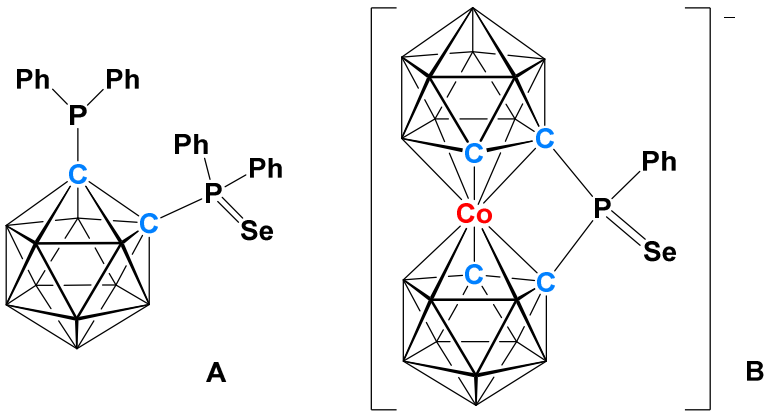

Figure 3.16 The carboranylphosphine selenides [1-P(Ph_2)Se-2-PPh_2-1,2-*closo*-$C_2B_{10}H_{10}$] (**A**) and [μ-1,1′-P(Ph)Se-3,3′-Co(1,2-$C_2B_9H_{10})_2]^-$ (**B**), which have $^1J_{PSe}$ values of 807 and 833 Hz respectively.

The $^1J_{PSe}$ magnitudes of molecules [μ-2,2′-P(Et)Se-{1-(1′-1′,2′-*closo*-$C_2B_{10}H_{10}$)-1,2-*closo*-$C_2B_{10}H_{10}$}] (**13**) and [μ-2,2′-P(Ph)Se-{1-(1′-1′,2′-*closo*-$C_2B_{10}H_{10}$)-1,2-*closo*-$C_2B_{10}H_{10}$}] (**14**) are higher still than those of **A** and **B**. This is believed to be because the carboranylphosphine selenides **13** and **14** have two highly electron withdrawing cages attached to the phosphorus centre, but also do not have an overall negative charge to restore electron density at the phosphorus atom (as with **B**).

The values for **A**, **B**, **13** and **14** can be compared to those of standard phosphine selenides, which are commonly found in the laboratory and used widely in both research and industry, Table 3.2. All the molecules discussed follow the trend that the stronger the electron-withdrawing substituents on the phosphorus atom, the greater the magnitude of $^1J_{PSe}$. It is interesting to note that the phosphine which has a similar steric bulk to **13** and **14**, PCy_3, has a much lower $^1J_{PSe}$ value, which can be attributed to its electron-donating substituents and consequently small amount of *s* character at the phosphorus atom. Therefore, although these three molecules may be of similar size they have very different electronic properties.

Table 3.2 Comparison of the $^{1}J_{PSe}$ values of standard phosphine selenides derived from phosphines commonly found in the laboratory against carboranylphosphine selenides (**A**, **B**, **13** and **14**).[14, 19-21]

Se=Phosphine	**$^{1}J_{PSe}$ (Hz)**
PCy_3	673
PMe_3	684
PEt_3	691
$PPhMe_2$	710
P(*p*-Tol)$_3$	715
PPh_2Me	725
PPh_3	732
A	807
B	833
14	891
13	894

As the $^{1}J_{PSe}$ values are determined by the nature of the electron-withdrawing substituents and therefore the amount of *s* character on the phosphorus atom, the $^{1}J_{PSe}$ values can be directly compared to the phosphorus-selenium bond length, Figure 3.17. This graph demonstrates a clear trend line between $^{1}J_{PSe}$ values and P=Se bond lengths for standard phosphine selenides, with only a few outliers. When the values for molecules **13** and **14** are added to the graph, they are consistent with the trend line.

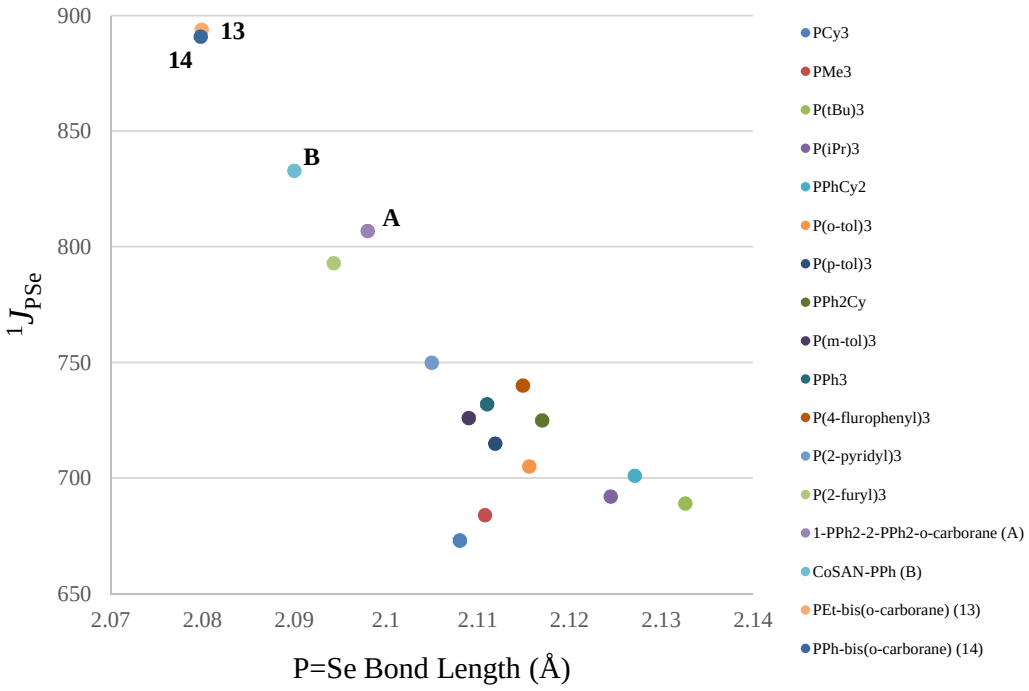

Figure 3.17 Graph showing the relationship between $^1J_{PSe}$ (Hz) and the P=Se bond length (Å) in phosphine selenides.[14, 17-20, 22-32] The values for **13** and **14** show good agreement with the trend.

As shown in the graph in Figure 3.17, the bond length of P=Se in phosphine selenides can be directly related to the phosphorus-selenium coupling constant. Large coupling constant values can be associated with a sizable amount of *s* character on the phosphorus atom and this is turn leads to short phosphorus-selenium bonds.

The P=Se bond lengths of **13**, 2.0801(7) Å, and **14**, 2.0798(6) Å, are very short when compared to known examples. A search on the Cambridge Structural Database[33] with fragments containing {$R^1R^2R^3P$=Se} revealed 378 reported structures, with only seven having P=Se bond distances shorter than 2.08 Å.[34-40]

3.11 Estimating the Basicity of 1,1′-Bis(*o*-carboranyl)phosphines (9 & 10) using the $^{1}J_{PSe}$ Values of 1,1′-Bis(*o*-carboranyl)phosphine Selenides (13 & 14)

The $^{1}J_{PSe}$ coupling constants can be used to explore the basicities of phosphines. As these coupling constants are related to the availability of electrons on the phosphorus centre, they can be used to predict the ability of phosphines to form their phosphonium ion complexes. In fact, it has been seen in the literature that there is a direct correlation between $^{1}J_{PSe}$ of phosphine selenides and the pK_b of phosphines. Figure 3.18 is a graph displaying experimental $^{1}J_{PSe}$ values of phosphine selenides and their experimental pK_b values of phosphines, determined by a protonation titration experiment.[41-44]

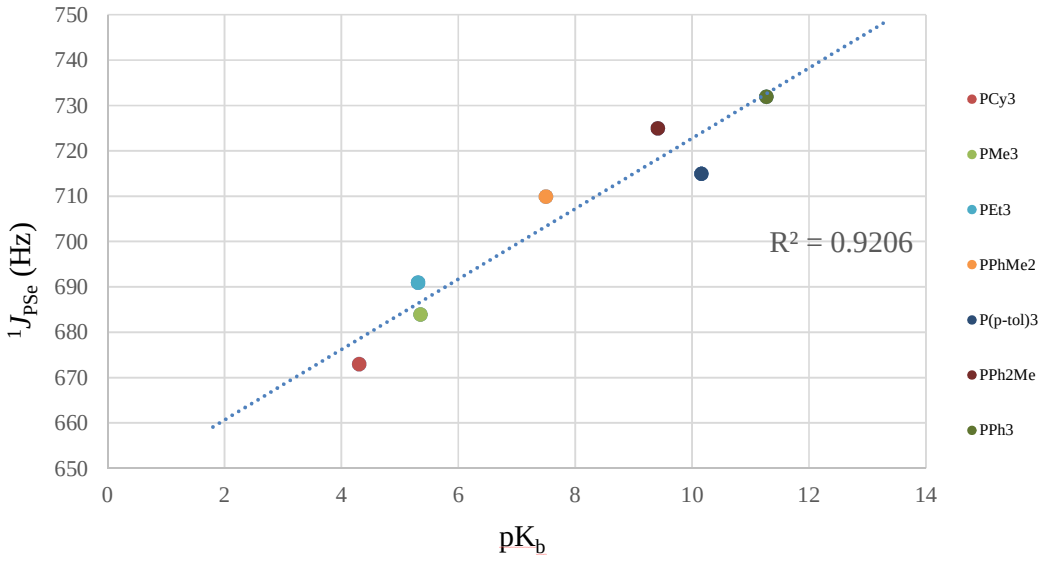

Figure 3.18 Graph showing the correlation between experimental $^{1}J_{PSe}$ (Hz) and basicity (pK_b) for common phosphines.[14, 19, 41-43]

As already determined in section **3.10**, the values of $^{1}J_{PSe}$ are related to the nature of the substituents on the phosphorus atom. Electron-withdrawing substituents, like those for compounds **9** to **14**, increase the $^{1}J_{PSe}$ value due to an increase in *s* character at the lone pair. This in turn means that the lone pair on phosphines with highly electron-withdrawing substituents will be less likely to become protonated and therefore will have larger pK_b's, and this trend can readily be seen in Figure 3.18. As highly basic phosphines, such as PCy_3 and PMe_3, have very small pK_b values it is favourable for them

to form phosphonium ions. For weakly-basic phosphines the opposite is true - it is unfavourable to form the phosphonium ions. This therefore means that protonation of very weakly-basic phosphines can be difficult.

From the graph in Figure 3.18, a trend line was calculated, the equation of which could be used to predict an estimate of the pK_b values of **9** and **10** by using the experimental $^1J_{PSe}$ values of [μ-2,2′-P(Et)Se-{1-(1′-1′,2′-*closo*-$C_2B_{10}H_{10}$)-1,2-*closo*-$C_2B_{10}H_{10}$}] (**13**) and [μ-2,2′-P(Ph)Se-{1-(1′-1′,2′-*closo*-$C_2B_{10}H_{10}$)-1,2-*closo*-$C_2B_{10}H_{10}$}] (**14**). The equation y = 7.7605x + 645.2 (where values of y are the experimental $^1J_{PSe}$ values 894 and 891 Hz) led to pK_b values of 32.1 and 31.7 for compounds **9** and **10** respectively. These pK_b values are much larger than any reported in the literature and this can be attributed to the highly electron-withdrawing bis(carborane) substituent on the phosphorus atom. Because 1,1′-bis(*o*-carborane) is an electron-withdrawing, chelating substituent it will reduce the *p* character of the lone pair on phosphorus limiting its ability to form a phosphonium ion. The large pK_b values calculated indicate that both compounds **9** and **10** are very weakly-basic and would be unlikely to be protonated under acidic conditions.

3.12 DFT Calculations

Density Functional Theory (DFT) calculations on compounds [μ-2,2′-PEt-{1-(1′-1′,2′-*closo*-$C_2B_{10}H_{10}$)-1,2-*closo*-$C_2B_{10}H_{10}$}] (**9**), [μ-2,2′-P(Et)AuCl-{1-(1′-1′,2′-*closo*-$C_2B_{10}H_{10}$)-1,2-*closo*-$C_2B_{10}H_{10}$}] (**11**) and [μ-2,2′-P(Et)Se-{1-(1′-1′,2′-*closo*-$C_2B_{10}H_{10}$)-1,2-*closo*-$C_2B_{10}H_{10}$}] (**13**) were performed (by Dr T. Krämer, Heriot-Watt University), with the aim of understanding their $^2J_{PH}$ coupling values. Upon bonding of the lone pair in compound **9** to either {AuCl} or {Se} the two compounds **11** or **13** respectively are afforded. In these compounds, the unobservable $^2J_{PH}$ coupling constant of **9** becomes large enough that it can now be observed in the ^{1}H NMR spectra.

Compound **9** has two independent molecules in the asymmetric fraction of the unit cell, which are almost superimposable. Using the *Structure Overlay* tool in Mercury[45] the independent molecules **9**AB and **9**CD can be compared to find out their rms (root-mean-square) misfit. When the {P{C_2B_{10})} units are overlaid the rms misfit is 0.024 Å with the largest individual misfit being 0.049 Å, associated with B4. When the two carbon atoms from the ethyl unit are also included the rms misfit increases to 0.029 Å with the biggest individual misfit being 0.073 Å, associated with C12. Having concluded that both **9**AB and **9**CD are almost geometrically equivalent, the computed model $\mathbf{9}_{DFT}$ (BP86-D3/def2-TZVP/def2-SVP), Figure 3.19, can be directly compared to ensure the optimised model is a good representation of **9**. When the {P{C_2B_{10})} units of $\mathbf{9_{DFT}}$ are overlaid with **9**AB the rms misfit is 0.019 Å with the greatest individual misfit being 0.031 Å, associated with P1. When the two carbon atoms of the ethyl unit are included the rms misfit increases to 0.029 Å with the biggest individual misfit being 0.081 Å (C12).

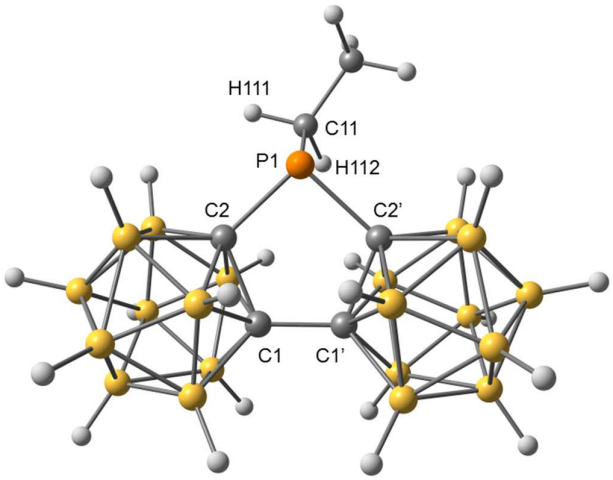

Figure 3.19 The optimised geometry of **9$_{DFT}$** (BP86-D3/def2-TZVP/def2-SVP). Some selected bond lengths are C1-C1′: 1.528, *1.533(7)*, **1.530(6)** Å, P1-C2: 1.889, *1.870(5)*, **1.886(5)** Å, P1-C2′: 1.892, *1.890(5)*, **1.890(5)** Å and P1-C11: 1.852, *1.844(5)*, **1.818(5)** Å. Bond lengths are written as DFT, *molecule AB*, **molecule CD**.

The optimised structures **11$_{DFT}$** and **13$_{DFT}$** were also determined (using BP86-D3/def2-TZVP/def2-SVP). The {P(C_2B_{10})$_2$} structures of **11** and **11$_{DFT}$** have good agreement with an rms misfit of 0.018 Å (greatest individual misfit 0.026 Å for B8′) when overlaying the structures. The rms misfit rises to 0.020 Å when the ethyl substituent is included (largest individual misfit 0.033 Å for C11) and further rises to 0.077 Å when the {AuCl} unit is included (largest individual misfit 0.345 Å for Cl). The {P(C_2B_{10})$_2$} structures of **13** and **13$_{DFT}$** also have good agreement with an rms misfit of 0.020 Å (largest individual misfit 0.034 Å for B11′). The rms misfit rises to 0.034 Å when the ethyl substituent is included (greatest individual misfit 0.100 Å for C11) and marginally rises to 0.036 Å when the {Se} is included (largest individual misfit 0.098 Å for C12). All three optimised models show excellent agreement with the crystallographic structures when comparing bond distances, Table 3.3.

Table 3.3 Comparison of selected bond distances (Å) between the crystallographic structures (**9**, **11** and **13**) and their optimised models (**9**$_{DFT}$, **11**$_{DFT}$ and **13**$_{DFT}$).

Compound	Bond	Bond Distance (Å)	
		Exp.	Calc.
9/**9**$_{DFT}$	**P1–C2**	1.870(5)	1.890
	P1–C2′	1.890(5)	1.892
	P1–C11	1.844(5)	1.852
	C1–C1′	1.533(7)	1.528
11/**11**$_{DFT}$	**P1–Au1**	2.2181(11)	2.211
	Au1–Cl1	2.2910(11)	2.269
	P1–C2	1.860(4)	1.869
	P1–C2′	1.883(4)	1.872
	P1–C11	1.816(4)	1.828
	C1–C1′	1.538(5)	1.530
13/**13**$_{DFT}$	**P1–Se1**	2.0801(7)	2.075
	P1–C2	1.879(2)	1.885
	P1–C2′	1.893(2)	1.890
	P1–C11	1.822(2)	1.831
	C1–C1′	1.543(3)	1.532

The optimised models were used to calculate the $^{2}J_{PH}$, $^{3}J_{PH}$ and $^{3}J_{HH}$ coupling constants, Table 3.4. The calculated values are in good agreement with experimental values for all compounds. It is important to note that for all compounds the major component of the coupling constants arises from the Fermi contact term, which is the through-bond communication between atoms, and is dependent upon the geometry of the atoms involved and the extent of *s* and *p* character in the relevant bonds.[46]

Table 3.4 Computationally calculated NMR coupling constants (Hz) of **9$_{DFT}$**, **11$_{DFT}$** and **13$_{DFT}$**. Experimental values given for comparison.

Compound	Method	$^{2}J_{PH}$ (Hz)	$^{3}J_{PH}$ (Hz)	$^{3}J_{HH}$ (Hz)
9$_{DFT}$	**Calculated**	–5.48 / +5.56 0.04 (avg.)	26.19 (avg.)	9.66 (avg.)
	Experimental	≤ ±1.0	23.0	7.9
11$_{DFT}$	**Calculated**	–19.87 / –6.65 − 13.26 (avg.)	31.18 (avg.)	9.57 (avg.)
	Experimental	10.9	27.9	7.7
13$_{DFT}$	**Calculated**	–14.91 / –13.29 − 14.10 (avg.)	29.76 (avg.)	9.52 (avg.)
	Experimental	11.6	25.9	7.6

3.12.1 DFT Calculations on 9, Dihydrogen Bonding and $^2J_{PH}$ Values

Using Quantum Theory of Atoms in Molecules (QTAIM) analysis the electron density of **9**$_{DFT}$ revealed bond critical points (BCP's) indicating the presence of dihydrogen bonds, Figure 3.20, as initially predicted from the crystal structure. The molecular graph shows BCP's (green) located in the middle of each dihydrogen interaction and the dihydrogen distances are H7-H11QY: 2.364 Å, H3-H11PX: 2.275 Å, H6′-H11PX: 2.101 Å and H11′-H12RX: 2.314 Å. As discussed by Crabtree et al., and later in more detail by Popelier, a dihydrogen bond is usually between 1.7 and 2.2 Å, with an average length of 1.96 Å and a standard deviation of 0.13 Å.[47, 48] Therefore H6′-H11PX (2.101 Å) falls within this range and H3-H11PX (2.275 Å) falls just outside it, indicating there is an interaction between these cage boron hydrides and the ethyl proton H11PX.

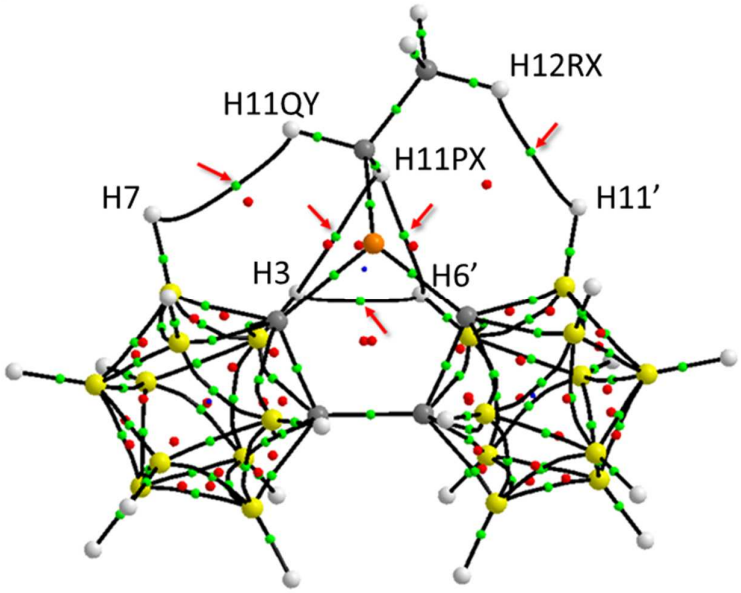

Figure 3.20 Partially labelled molecular graph of **9**$_{DFT}$ with stationary points and bond paths. Bond critical points (BCP's) shown in green with arrows highlighting the identified dihydrogen bonds. Ring critical points in red and cage critical points in blue.

The Laplacian [$\nabla^2\rho(r)$] of the electron density of the BCP has been observed to be positive for dihydrogen bonds and negative for covalent bonds,[48] with a range of 0.014 to 0.139

a.u. usual for dihydrogen interactions.[49] The calculated $\nabla^2\rho(r)$ values for the two identified dihydrogen bonds are H6′-H11PX: +0.038 a.u. and H3-H11PX: +0.031 a.u., hence providing further confirmation of the interactions.

The calculated Gibbs free energy profile for rotation of the ethyl group about the P-C bond in **9$_{DFT}$** is shown in Figure 3.21. This is useful to understand the possible orientations of the ethyl ligand in solution. The profile shows that there are three minimum energy orientations (**9$_{DFT}$**, **9′$_{DFT}$** and **9′′$_{DFT}$**) and three transition states [**TS(9$_{DFT}$-9′$_{DFT}$)**, **TS(9′$_{DFT}$-9′′$_{DFT}$)** and **TS(9′′$_{DFT}$-9′$_{DFT}$)**]. Whilst **9$_{DFT}$** and its isoenergetic conformer **9′$_{DFT}$** lie at 0.0 kcal mol^{-1} and are therefore the most stable conformations, the conformer **9′′$_{DFT}$** is higher in energy, lying at 3.6 kcal mol^{-1}, and will be unpopulated. According to the Boltzmann distribution, the populations of each conformer would be **9$_{DFT}$**: 50%, **9′$_{DFT}$**: 50% and **9′′$_{DFT}$**: 0%. Due to the low transition state barrier between **9$_{DFT}$** and **9′$_{DFT}$** there will be rapid exchange between the two conformers in solution. Conformers **9$_{DFT}$** and **9′$_{DFT}$** are symmetrically related with dihydrogen bonds stabilising the structures, this therefore makes them more favourable compared to conformer **9′′$_{DFT}$**.

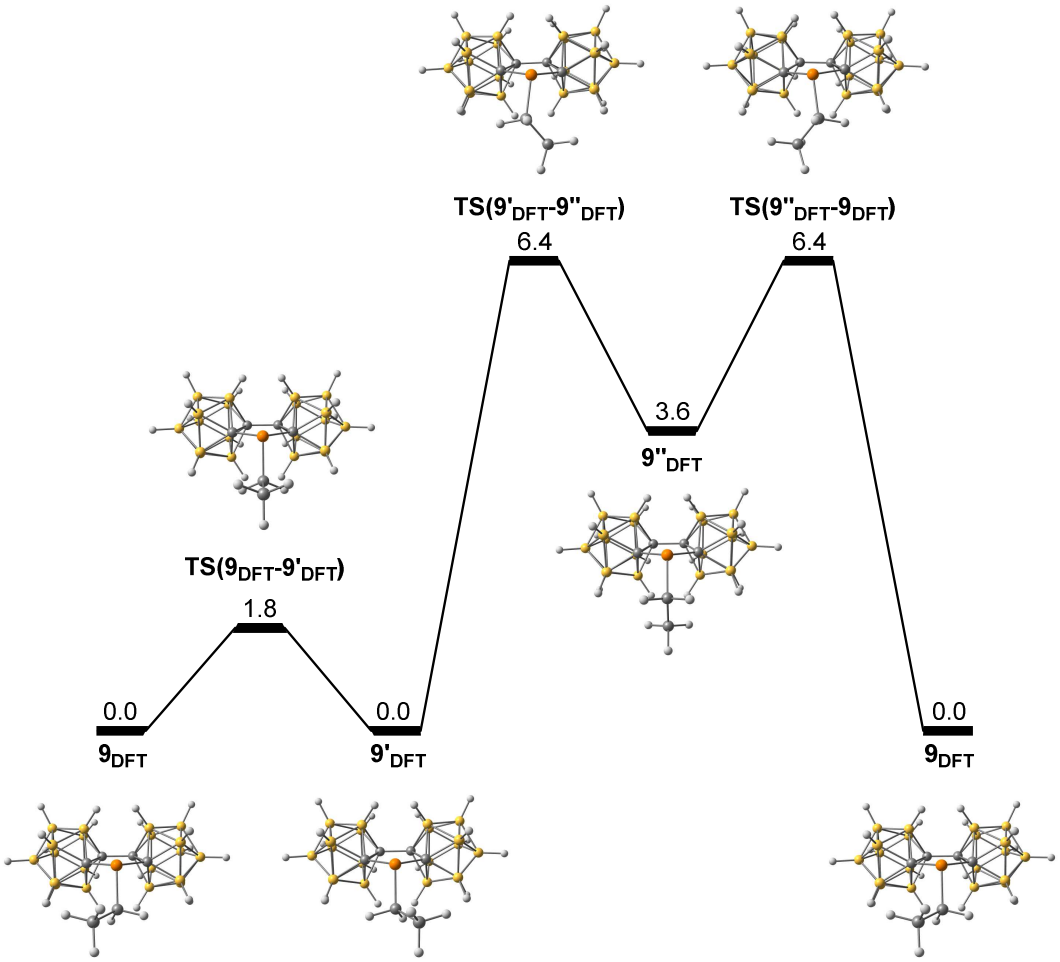

Figure 3.21 Gibbs free energy profile (kcal mol^{-1}) for rotation of the ethyl substituent of **9$_{DFT}$**. Calculated using BP86-D3/def2-TZVP/def2-SVP.

The $^{2}J_{PH}$ coupling constants in **9$_{DFT}$** are calculated to be $^{2}J_{P\text{-}H11PX}$ = -5.48 Hz and $^{2}J_{P\text{-}H11QY}$ = +5.56 Hz. Due to the fast exchange between **9$_{DFT}$** and **9′$_{DFT}$** in solution the methylene protons will be rapidly exchanging and therefore the coupling constants will average out, giving $^{2}J_{PH}$ (average) = 0.04 Hz. This means that in solution the observed coupling falls within the half line-width of the resonances observed (*ca.* 1.0 Hz).

3.12.2 DFT Calculations on 9, $^3J_{PH}$ Values

The computed model $\mathbf{9_{DFT}}$ was used to calculate the individual vicinal $^3J_{PH}$ coupling constants of the methyl protons affording H12PY: 9.2 Hz, H12QZ: 61.0 Hz and H12RX: 8.3 Hz, which gives an average of 26.2 Hz (*cf.* experimental $^3J_{PH}$ = 23.0 Hz). In 2012 Panagiotakis et al. stated that large coupling constants (i.e. with H12QZ) are observed for hydrogen atoms that have a P-C-C-H torsion angle (ω) of ~180°, and only when the phosphorus lone pair is in a gauche conformation with the corresponding carbon atom.[50] From aligning C11 directly over P1 in the molecule, diagrammatically it can be observed that the phosphorus lone pair is indeed in a gauche conformation with C12 (lp-P-C11-C12 torsion angle 38.36°), Figure 3.22. Therefore, this vicinal coupling relationship applies to compound **9**.

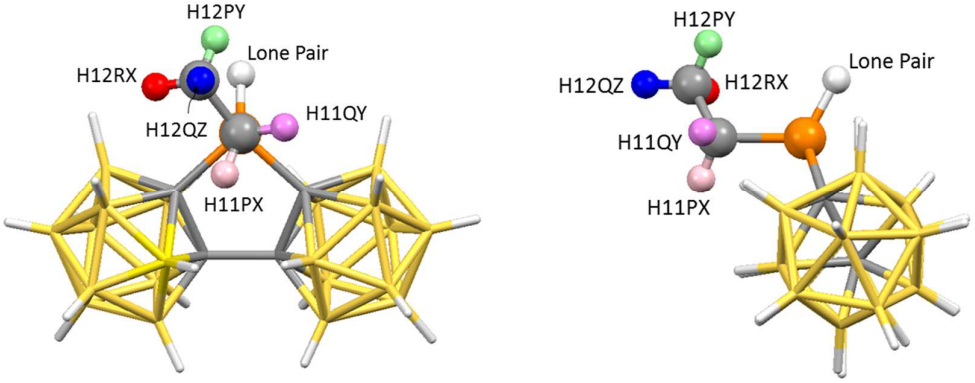

Figure 3.22 Two perspective views of [μ-2,2′-PEt-{1-(1′-1′,2′-*closo*-$C_2B_{10}H_{10}$)-1,2-*closo*-$C_2B_{10}H_{10}$}] (**9**) which highlight the five protons involved in the $^2J_{PH}$ and $^3J_{PH}$ coupling constants. The lone pair has also been modelled for calculation of torsion angles.

The ω torsion angles were calculated for all three methyl protons, Table 3.5, and it can be seen that the proton H12QZ has ω equal to -177.67°, very close to the 180° requirement for a large vicinal coupling constant. The ω torsion angles for H12PY and H12RX are significantly lower (and importantly not near 180°), at -57.74° and 62.89° respectively,

and hence these protons have coupling constants of a smaller magnitude, 9.2 Hz and 8.3 Hz respectively.

Table 3.5 The calculated $^{3}J_{PH}$ coupling constants (Hz) and torsion angles (°) for the methyl protons of **9$_{DFT}$**.

	H12PY	**H12QZ**	**H12RX**
Colour	Green	Blue	Red
$^{3}J_{PH}$ (Hz)	9.2	61.0	8.3
Torsion Angle (ω/°)	-57.74	-177.67	62.89

3.13 Conclusions

In conclusion two new large, weakly-basic phosphines [μ-2,2′-PEt-{1-(1′-1′,2′-*closo*-$C_2B_{10}H_{10}$)-1,2-*closo*-$C_2B_{10}H_{10}$}] (**9**) and [μ-2,2′-PPh-{1-(1′-1′,2′-*closo*-$C_2B_{10}H_{10}$)-1,2-*closo*-$C_2B_{10}H_{10}$}] (**10**) have been synthesised. What initially looked like an unusual lack of $^2J_{PH}$ coupling in the ^{1}H NMR spectrum of **9** (and less noticeably in **10**) was shown by a ^{1}H-^{31}P HMBC NMR spectroscopy experiment to be a very small observed coupling, whereby $^2J_{PH}$ had to be within the line-width ($\leq \pm 1.0$ Hz).

Compounds **9** and **10** were reacted with (tht)AuCl to give the gold chloride derivatives [μ-2,2′-P(Et)AuCl-{1-(1′-1′,2′-*closo*-$C_2B_{10}H_{10}$)-1,2-*closo*-$C_2B_{10}H_{10}$}] (**11**) and [μ-2,2′-P(Ph)AuCl-{1-(1′-1′,2′-*closo*-$C_2B_{10}H_{10}$)-1,2-*closo*-$C_2B_{10}H_{10}$}] (**12**). Upon coordination of the gold chloride through the phosphorus lone pair, $^2J_{PH}$ could be observed and was 10.9 Hz for compound **11**. The crystal structures of the gold chloride derivatives were used to calculate the Tolman cone angles and percent buried volumes, giving 176.5° and 32% respectively for **11** and 176.2° and 33.2% respectively for **12**. When compared to the Tolman cone angles and percent buried volumes for **9** and **10** there was an average increase of 4.3° and 1.2% upon coordination. This increase in steric bulk was associated with the coordination of the lone pair in the gold chloride compounds, as this led to less steric repulsion between the lone pair and the substituents. The steric bulk of these compounds is comparable to other large phosphines, and in particular PCy_3.

Reaction between **9** or **10** and elemental selenium gave the compounds [μ-2,2′-P(Et)Se-{1-(1′-1′,2′-*closo*-$C_2B_{10}H_{10}$)-1,2-*closo*-$C_2B_{10}H_{10}$}] (**13**) and [μ-2,2′-P(Ph)Se-{1-(1′-1′,2′-*closo*-$C_2B_{10}H_{10}$)-1,2-*closo*-$C_2B_{10}H_{10}$}] (**14**). The $^1J_{PSe}$ values were calculated using the selenium satellites in the ^{31}P NMR spectra, giving 894 and 891 Hz for **13** and **14** respectively. The values for these carboranylphosphine selenides appeared to follow the trend between the $^1J_{PSe}$ coupling constant and P=Se bond length when compared to values from the literature. The $^1J_{PSe}$ values were also used to estimate the pK_b (basicities) of **9** and **10** and these were found to be 32.1 and 31.7 respectively. Therefore, it can be stated that compounds **9** and **10** are large, weakly-basic phosphines derived from 1,1′-bis(*o*-carborane).

DFT optimised structures on $\mathbf{9_{DFT}}$, $\mathbf{11_{DFT}}$ and $\mathbf{13_{DFT}}$ show good correlation with the crystallographic structures using *Structure Overlay* and by comparing computational and

experimental bond lengths. The calculated $^{2}J_{PH}$, $^{3}J_{PH}$ and $^{3}J_{HH}$ couplings constants are in good agreement with those observed in the ^{1}H NMR spectra of **9**, **11** and **13**.

The calculated $^{2}J_{PH}$ coupling constant for each geminal proton of $\mathbf{9_{DFT}}$ gave values of -5.48 and +5.56 Hz. From the Gibbs free energy profile of $\mathbf{9_{DFT}}$ it was recognised that there would be fast interconversion between the two favourable isoenergetic conformers $\mathbf{9_{DFT}}$ and $\mathbf{9'_{DFT}}$ in solution. This implies that there would be fast exchange between the methylene protons and therefore the observed $^{2}J_{PH}$ coupling would average to 0.04 Hz, which is within the predicted value of $^{2}J_{PH} \leq \pm 1.0$ Hz.

The calculated $^{3}J_{PH}$ coupling constant for the methyl protons of $\mathbf{9_{DFT}}$ are in good agreement with the experimental values [26.19 Hz (calc.), 23.0 Hz (exp.)]. When looking at the three-bond coupling to the individual methyl protons one proton (H12QZ) has a large coupling constant compared to the others (61.0 Hz, compared to 9.2 and 8.3 Hz). This was explained by the H12QZ-C12-C11-P1 torsion angle being ~180°.

3.14 References

1. L. I. Zakharkin and N. F. Shemyakin, *Izv. Akad. Nauk SSSR, Ser. Khim*, 1978, 1450.
2. A. I. Yanovskii, N. G. Furmanova, Y. T. Struchkov, N. F. Shemyakin and L. I. Zakharkin, *Izv. Akad. Nauk SSSR, Ser. Khim*, 1979, 1412.
3. S. E. Johnson and C. B. Knobler, *Phosphorus, Sulfur Silicon Relat. Elem.*, 1996, **115**, 227.
4. D. E. Harwell, M. D. Mortimer, C. B. Knobler, F. A. L. Anet and M. F. Hawthorne, *J. Am. Chem. Soc.*, 1996, **118**, 2679.
5. C. F. Matta, J. Hernandez-Trujillo, T. H. Tang and R. F. W. Bader, *Chem. Eur. J.*, 2003, **9**, 1940.
6. R. H. Contreras and J. E. Peralta, *Prog. Nucl. Magn. Reson. Spectrosc.*, 2000, **37**, 321.
7. J. P. Albrand, D. Gagnaire, J. Martin and J. B. Robert, *Bull. Soc. Chim. Fr.*, 1969, 40.
8. J. P. Albrand, D. Gagnaire and J. B. Robert, *Chem. Commun.*, 1968, 1469.
9. C. A. Tolman, *J. Am. Chem. Soc.*, 1970, **92**, 2956.
10. T. E. Muller and D. M. P. Mingos, *Trans. Met. Chem.*, 1995, **20**, 533.
11. A. Poater, B. Cosenza, A. Correa, S. Giudice, F. Ragone, V. Scarano and L. Cavallo, *Eur. J. Inorg. Chem.*, 2009, 1759.
12. H. Clavier and S. P. Nolan, *Chem. Commun.*, 2010, **46**, 841.
13. J. J. Daly, *J. Chem. Soc.*, 1964, 3799.
14. J. A. Davies, S. Dutremez and A. A. Pinkerton, *Inorg. Chem.*, 1991, **30**, 2380.
15. J. G. Verkade and J. A. Mosbo, *Phosphorus-31 NMR Spectroscopy in Stereochemical Analysis: Organic Compounds and Metal Complexes*, VCH Publishers, USA, 1987.
16. R. D. Kroshefsky, R. Weiss and J. G. Verkade, *Inorg. Chem.*, 1979, **18**, 469.
17. A.-R. Popescu, A. Laromaine, F. Teixidor, R. Sillanpää, R. Kivekäs, J. Ignasi Llambias and C. Viñas, *Chem. Eur. J.*, 2011, **17**, 4429.
18. P. Farràs, F. Teixidor, I. Rojo, R. Kivekäs, R. Sillanpää, P. González-Cardoso and C. Viñas, *J. Am. Chem. Soc.*, 2011, **133**, 16537.
19. A. Cogne, A. Grand, J. Laugier, J. B. Robert and L. Wiesenfeld, *J. Am. Chem. Soc.*, 1980, **102**, 2238.

20. A. Muller, S. Otto and A. Roodt, *Dalton Trans.*, 2008, 650.
21. U. Beckmann, D. Süslüyan and P. C. Kunz, *Phosphorus, Sulfur Silicon Relat. Elem.*, 2011, **186**, 2061.
22. H. U. Steinberger, B. Ziemer and M. Meisel, *Acta Crystallogr., Sect. C*, 2001, **57**, 323.
23. C. G. Hrib, F. Ruthe, E. Seppälä, M. Bätcher, C. Druckenbrodt, C. Wismach, P. G. Jones, W. W. du Mont, V. Lippolis, F. A. Devillanova and M. Bühl, *Eur. J. Inorg. Chem.*, 2006, 88.
24. T. S. Cameron and B. Dahlen, *J. Chem. Soc., Perkin Trans. 2*, 1975, 1737.
25. A. Muller, *Acta Cryst., Sect. E*, 2011, **67**, O45.
26. T. S. Cameron, K. D. Howlett and K. Miller, *Acta Crystallogr., Sect. B*, 1978, **34**, 1639.
27. R. P. Pinnell, C. A. Megerle, S. L. Manatt and P. A. Kroon, *J. Am. Chem. Soc.*, 1973, **95**, 977.
28. P. G. Jones, C. Kienitz and C. Thone, *Z. Kristallogr.*, 1994, **209**, 80.
29. D. W. Allen and B. F. Taylor, *J. Chem. Soc., Dalton Trans.*, 1982, 51.
30. A. Muller and R. Meijboom, *Acta Cryst., Sect. E*, 2007, **63**, O4055.
31. A. N. Kharat, A. Bakhoda, T. Hajiashrafi and A. Abbasi, *Phosphorus, Sulfur Silicon Relat. Elem.*, 2010, **185**, 2341.
32. D. W. Allen, I. W. Nowell and B. F. Taylor, *J. Chem. Soc., Dalton Trans.*, 1985, 2505.
33. C. R. Groom and F. H. Allen, *Angew. Chem. Int. Ed.*, 2014, **53**, 662.
34. A. Sun, M.-Q. Yan, Y. Liu, Z.-Y. Lian, T. Meng, S.-H. Liu, J. Chen and Y. G.-A., *RSC Advances*, 2015, **5**, 71437.
35. K. D. Reichl, C. L. Mandell, O. D. Henn, W. G. Dougherty, W. S. Kassel and C. Nataro, *J. Organomet. Chem.*, 2011, **696**, 3882.
36. R. Kabe, V. M. Lynch and P. Anzenbacher, *Cryst. Eng. Comm.*, 2011, **13**, 5423.
37. T. Stampfl, R. Gutmann, G. Czermak, C. Langes, A. Dumfort, H. Kopacka, K.-H. Ongania and P. Brüggellar, *Dalton Trans.*, 2003, 3425.
38. Q. Zhang, M. Hong and H. Liu, *Trans. Met. Chem.*, 1997, **22**, 156.
39. M. Birkel, L. Schulz, U. Bergsträsser and M. Regitz, *Angew. Chem. Int. Ed.*, 1992, **31**, 879.
40. O. Orama, K. Nieminen, M. Karhu and R. Uggla, *Cryst. Struct. Commun.*, 1979, **8**, 909.
41. W. A. Henderson Jr and C. A. Streuli, *J. Am. Chem. Soc.*, 1960, **82**, 5791.

42. C. A. Streuli, *Anal. Chem.*, 1960, **32**, 985.
43. R. C. Bush and R. J. Angelici, *Inorg. Chem.*, 1988, **27**, 681.
44. T. Allman and R. G. Goel, *Can. J. Chem.*, 1982, **60**, 716.
45. C. F. Macrae, P. R. Edgington, P. McCabe, E. Pidcock, G. P. Shields, R. Taylor, M. Towler and J. van de Streek, *J. Appl. Crystallogr.*, 2006, **39**, 453.
46. C. J. Jameson, *J. Am. Chem. Soc.*, 1969, **91**, 6232.
47. T. Richardson, S. de Gala, R. H. Crabtree and P. E. M. Siegbahn, *J. Am. Chem. Soc.*, 1995, **117**, 12875.
48. P. L. A. Popelier, *J. Phys. Chem. A*, 1998, **102**, 1873.
49. U. Koch and P. L. A. Popelier, *J. Phys. Chem.*, 1995, **99**, 9747.
50. W. H. Hersh, S. T. Lam, D. J. Moskovic and A. J. Panagiotakis, *J. Org. Chem.*, 2012, **77**, 4968.

Chapter 4: Decapitation and Metalation of Tethered 1,1′-Bis(*o*-carborane)

4.1 Introduction

Although the chemistry of 1,1′-bis(*o*-carborane) has been widely explored there has been little research into the effects of tethering the two cages, which would give the molecule rigidity by preventing rotation around the C1-C1′ bond. In 2016 Xie et al. reported the first tethered 1,1′-bis(*o*-carborane), using a CH_2CH_2 linker between atoms C2 and C2′, Figure 4.1.[1]

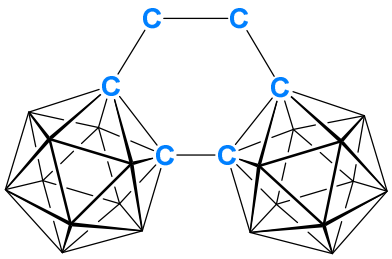

Figure 4.1 [μ-2,2′-CH_2CH_2-{1-(1′-1′,2′-*closo*-$C_2B_{10}H_{10}$)-1,2-*closo*-$C_2B_{10}H_{10}$}] (**I**).

Xie also reported the four-electron reduction of this carborane using excess sodium metal, affording a nido tetraanion. This was isolated and crystallised showing that both cages have an open face, however one has six atoms on the open face and the other has only five. Further reaction with {Ru(*p*-cymene)} yielded several products including the starting material μ-2,2′-CH_2CH_2-1,1′-bis(*o*-carborane) (**I**) (70%), a triple B-H insertion product (2%), a 12-vertex carborane/13-vertex ruthenacarborane (10%) and a 12-vertex ruthenacarborane/12-vertex ruthenacarborane (10%), Figure 4.2. The variety of products formed suggest that the reduction and metalation reactions of tethered 1,1′-bis(*o*-carborane) are complicated and hard to predict.

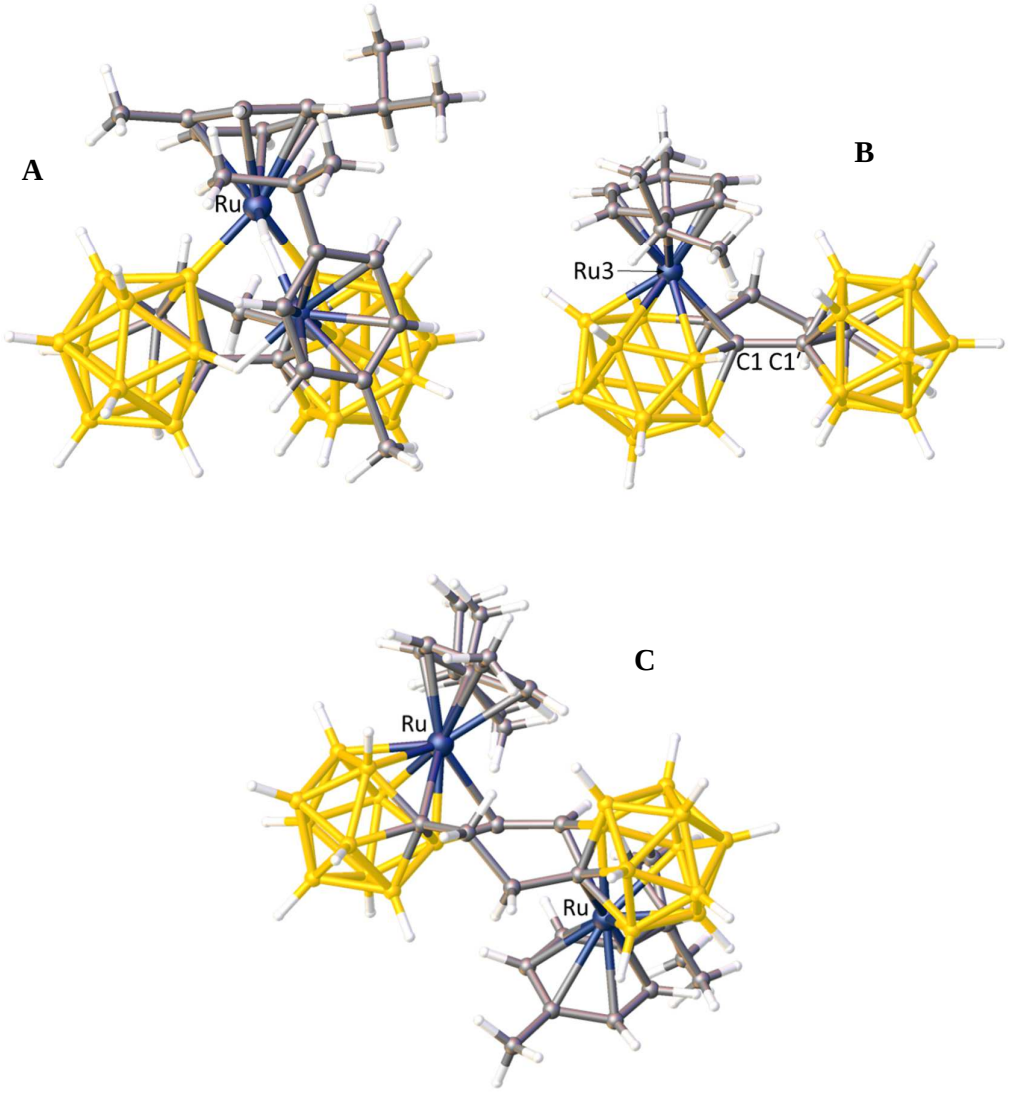

Figure 4.2 The three products from the reduction and metalation of 1,1′-bis(*o*-carborane). A triple B-H insertion product (**A**), a 12-vertex carborane/13-vertex ruthenacarborane (**B**) and a 12-vertex ruthenacarborane/12-vertex ruthenacarborane (**C**).

This chapter discusses the synthesis of another example of a tethered 1,1′-bis(*o*-carborane) and its comparison to non-carborane containing analogues. The compound initially prepared by Xie at al., [μ-2,2′-CH_2CH_2-{1-(1′-1′,2′-*closo*-$C_2B_{10}H_{10}$)-1,2-*closo*-$C_2B_{10}H_{10}$}] (**I**), is synthesised and its single decapitation and metalation reaction with {Ru(*p*-cymene)} explored.

This work has been carried out as the first step on a potential pathway to making a di-metalated bis(*o*-carborane) catalyst. Successful single decapitation and metalation of a tethered 1,1′-bis(*o*-carborane) would imply that double decapitation and metalation would be possible. Although having {Ru(*p*-cymene)} as the transition metal unit does not yield an active catalyst, its successful synthesis infers that other transition metal derivatives could be synthesised. Having a doubly-metalated tethered 1,1′-bis(*o*-carborane) would plausibly allow targeted catalysis across a molecule, by using two catalytically active sites that are locked in place by the tether.

These molecules also allow us to investigate the changes in reactivity when the two available carbon atoms (C2 and C2′) on 1,1′-bis(*o*-carborane) are tethered together.

4.2 [μ-2,2′-C_6H_4-{1-(1′-1′,2′-*closo*-$C_2B_{10}H_{10}$)-1,2-*closo*-$C_2B_{10}H_{10}$}] (15)

Dilithiated 1,1′-bis(*o*-carborane) was stirred with copper(I) chloride and pyridine for 15 mins giving an orange-brown solution. Following this 1,2-diiodobenzene was added and the solution heated to reflux for 60 hours to give a red-brown solution. After cooling the copper-pyridine complex was removed and the crude mixture was subjected to column chromatography and preparative TLC to afford [μ-2,2′-C_6H_4-{1-(1′-1′,2′-*closo*-$C_2B_{10}H_{10}$)-1,2-*closo*-$C_2B_{10}H_{10}$}] (**15**) as a white solid in 10% yield, Scheme 4.1.

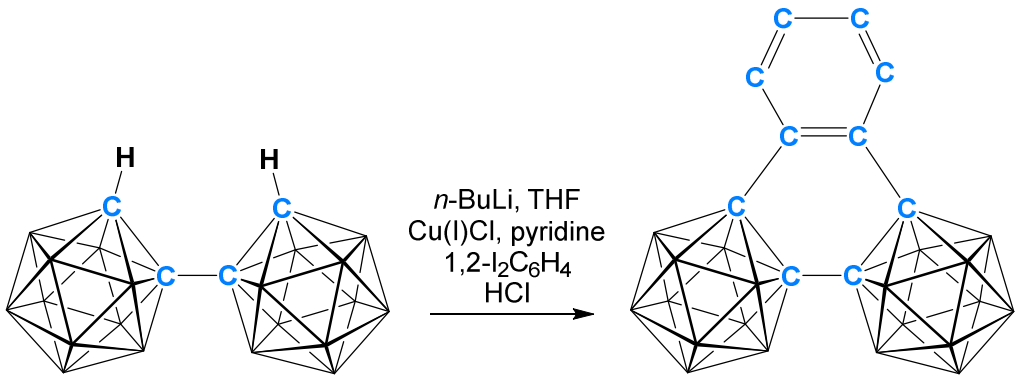

Scheme 4.1 Dilithiation of 1,1′-bis(*o*-carborane) followed by reaction with 1,2-diiodobenzene using copper(I) chloride to afford [μ-2,2′-C_6H_4-{1-(1′-1′,2′-*closo*-$C_2B_{10}H_{10}$)-1,2-*closo*-$C_2B_{10}H_{10}$}] (**15**).

Compound **15** was characterised by electron ionisation mass spectrometry, NMR spectroscopy and *X*-ray crystallography. The mass spectrum shows a classic carborane envelope at *m/z* 360.4, consistent with the molecular weight (360.52 g mol^{-1}).

The ^{1}H NMR spectrum of **15** displays an integral-2 multiplet between δ 7.90 and 7.89 ppm and an integral-2 multiplet between δ 7.06 and 7.02 ppm. Both sets of signals correspond to the aromatic protons of the *o*-phenylene group.

The $^{11}B\{^{1}H\}$ NMR spectrum has an integral-4 resonance at δ -2.5 ppm and the remaining 16 boron atoms are found as overlapping resonances between δ -5.1 and -11.8 ppm, with maxima at δ -7.0, -8.2 and -9.0 ppm.

Single crystals of **15** were afforded by the slow diffusion of a concentrated DCM solution with petroleum ether. It crystallises in the Pbcn space group and has crystallographically-required C_2 but effective C_{2v} symmetry with the C_2 axis running through the centre of the C1-C1′ bond, Figure 4.3. The crystal structure confirms that an *o*-phenylene unit has been inserted into 1,1′-bis(*o*-carborane) and now acts as a tether between C2 and C2′.

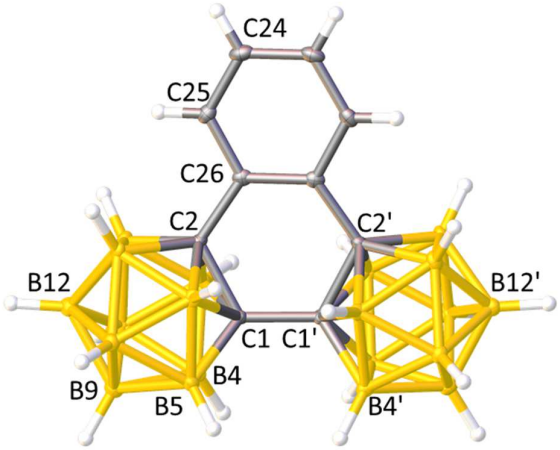

Figure 4.3 Perspective view of [μ-2,2′-C_6H_4-{1-(1′-1′,2′-*closo*-$C_2B_{10}H_{10}$)-1,2-*closo*-$C_2B_{10}H_{10}$}] (**15**) and part of the atom numbering scheme. Selected bond lengths are C1-C1′: 1.541(6) Å, C1-C2 1.650(4) Å: and C2-C26: 1.505(4) Å.

4.3 Comparison of 1,1′-Bis(*o*-carborane) and Compound 15 with their Non-Carborane Analogues, Biphenyl and Triphenylene

Carboranes can be described as having *pseudo*-aromaticity within the cage and can therefore be thought of as an analogue of benzene. 1,1′-Bis(*o*-carborane) contains two carborane cages linked by a C-C bond and can therefore be thought of as an analogue of biphenyl. In a similar fashion [μ-2,2′-C_6H_4-{1-(1′-1′,2′-*closo*-$C_2B_{10}H_{10}$)-1,2-*closo*-$C_2B_{10}H_{10}$}] (**15**) can be viewed as an analogue of triphenylene as it is the result of insertion of an *o*-phenylene unit into 1,1′-bis(*o*-carborane), creating three linked aromatic units, Figure 4.4.

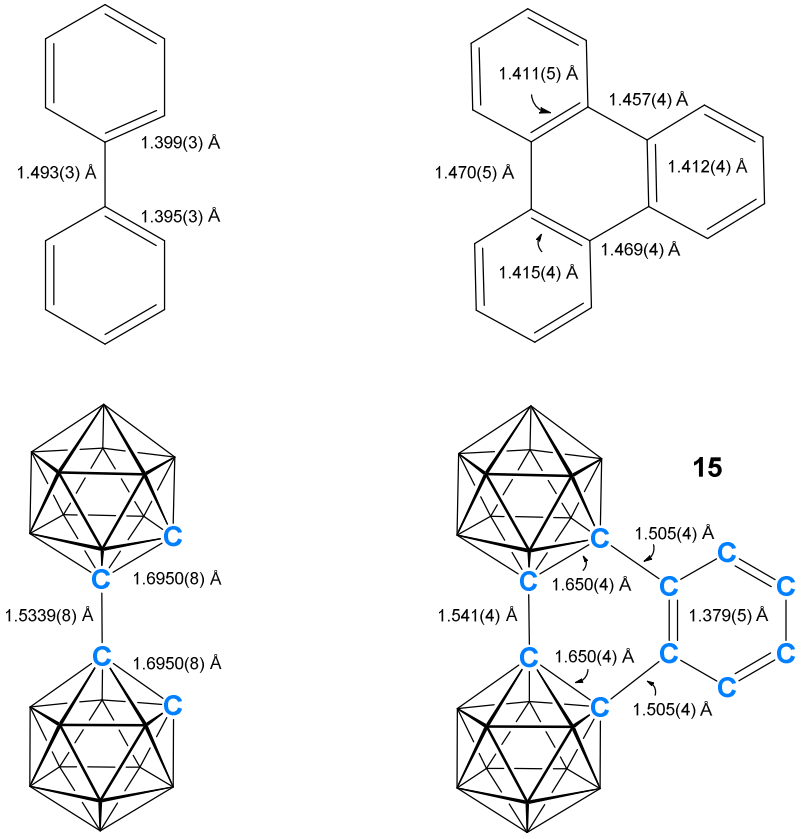

Figure 4.4 Selected bond lengths in biphenyl,[2] triphenylene,[3] 1,1′-bis(o-carborane)[4] and [μ-2,2′-C_6H_4-{1-(1′-1′,2′-*closo*-$C_2B_{10}H_{10}$)-1,2-*closo*-$C_2B_{10}H_{10}$}] (**15**). Note: there is disorder between vertex-2 and vertex-3 in 1,1′-bis(o-carborane) which means the true C1-C2 bond length may be shorter than given.

When an *o*-phenylene unit is added to biphenyl, the carbon-carbon bond lengths noted in Figure 4.4 become closer together giving smaller differences in triphenylene. The difference between the C-C bond lengths in biphenyl are 0.1 Å and for triphenylene are *ca.* 0.06 Å. This implies that there is a degree of aromaticity in the central six-membered ring. Polycyclic aromatic hydrocarbons can have different degrees of aromaticity for each ring segment, but according to Clar's rule,[5] the resonance structure with most disjoint aromatic π-sextets will best represent the molecule. When looking at triphenylene, Figure 4.5, of the two possible resonance structures the left would be the better representation as it has three separated π-sextets, opposed to the right structure, which would have only one π-sextet. Taking into consideration the bond lengths noted in Figure 4.4 there may be a small amount of aromaticity within the central ring, even though the majority of the aromaticity would be in the external three rings.

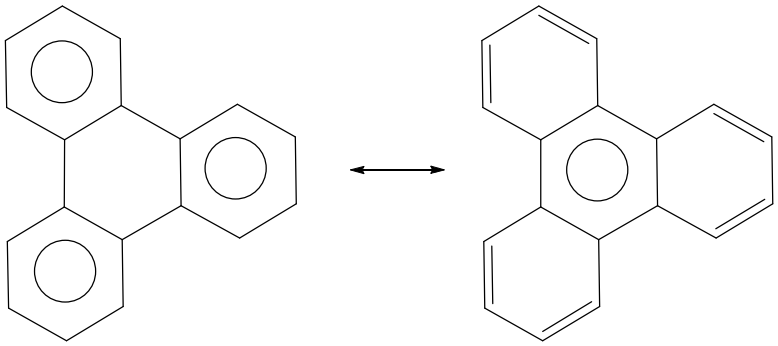

Figure 4.5 The two resonance structures of triphenylene with the left having three π-sextets and the right having only one π-sextet.

Compound **15** can be viewed as having one aromatic *o*-phenylene unit and two *pseudo*-aromatic carborane cages around a central six-membered ring. Following Clar's rule the majority of the aromaticity will be expected to be found within the three aromatic and *pseudo*-aromatic groups. There may also be a small amount of aromaticity within the central six-membered ring, much like in triphenylene. However due to the disorder over vertex-2 and vertex-3 in 1,1′-bis(o-carborane), the change in C-C bond lengths upon insertion of *o*-phenylene are not known exactly and therefore the amount of aromaticity will be difficult to estimate.

4.4 [HNMe$_3$][μ-2,2′-CH$_2$CH$_2$-{7-(1′-1′,2′-*closo*-C$_2$B$_{10}$H$_{10}$)-7,8-*nido*-C$_2$B$_9$H$_{10}$}] (16)

Due to the low yield of [μ-2,2′-C$_6$H$_4$-{1-(1′-1′,2′-*closo*-C$_2$B$_{10}$H$_{10}$)-1,2-*closo*-C$_2$B$_{10}$H$_{10}$}] (**15**) it was decided that a better alternative for the decapitation and metalation reactions of a tethered 1,1′-bis(*o*-carborane) would be [μ-2,2′-CH$_2$CH$_2$-{1-(1′-1′,2′-*closo*-C$_2$B$_{10}$H$_{10}$)-1,2-*closo*-C$_2$B$_{10}$H$_{10}$}] (**I**). This was reported by Xie et al. in 2016 as being high yielding (87%) and easily synthesised.[1] Unfortunately in our hands this synthesis did not go to 100% completion and some 1,1′-bis(*o*-carborane) remained in the crude mixture. Several methods were used in an attempt to separate these compounds (column chromatography, preparative TLC, cold column chromatography, recrystallisation, sublimation) but all were unsuccessful presumably due to the close molecular weight and R_f values of both. Subsequently, both compounds were decapitated during the reaction to form [HNMe$_3$][μ-2,2′-CH$_2$CH$_2$-{7-(1′-1′,2′-*closo*-C$_2$B$_{10}$H$_{10}$)-7,8-*nido*-C$_2$B$_9$H$_{10}$}] (**16**).

[μ-2,2′-CH$_2$CH$_2$-{1-(1′-1′,2′-*closo*-C$_2$B$_{10}$H$_{10}$)-1,2-*closo*-C$_2$B$_{10}$H$_{10}$}] (**I**) and potassium hydroxide were heated to reflux in ethanol overnight, yielding a colourless solution. After removal of the solvent, the white solids were dissolved in water, filtered and an aqueous solution of trimethylammonium hydrochloride added. This afforded as a precipitate a mixture of [HNMe$_3$][7-(1′-1′,2′-*closo*-C$_2$B$_{10}$H$_{10}$)-7,8-*nido*-C$_2$B$_9$H$_{11}$] (**II**) and [HNMe$_3$][μ-2,2′-CH$_2$CH$_2$-{7-(1′-1′,2′-*closo*-C$_2$B$_{10}$H$_{10}$)-7,8-*nido*-C$_2$B$_9$H$_{10}$}] (**16**), with a combined yield of around 42%, Scheme 4.2.

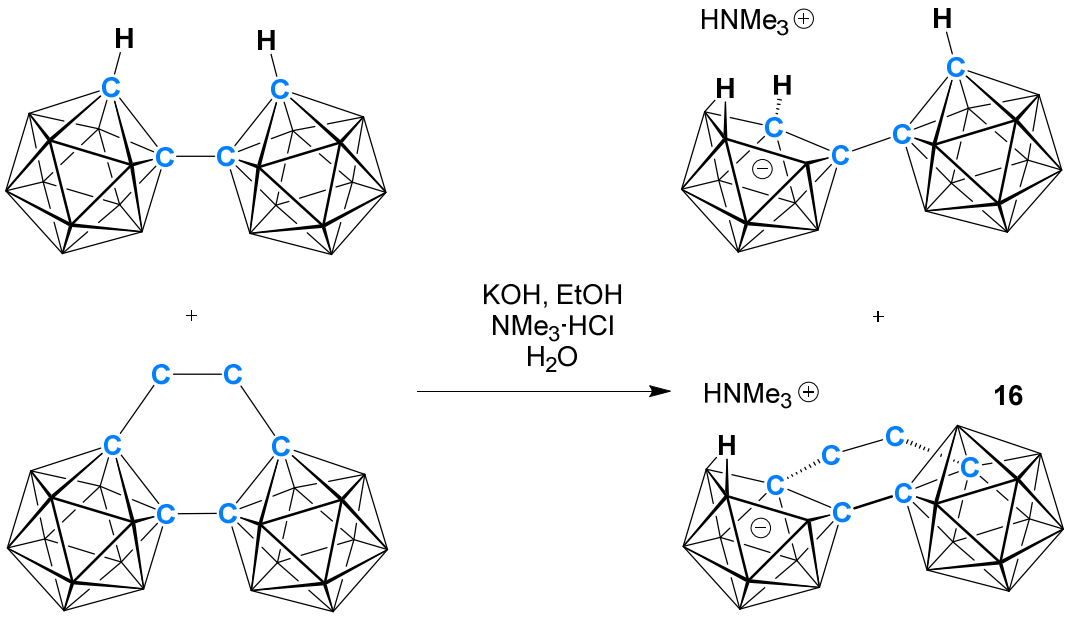

Scheme 4.2 Decapitation of a mixture of 1,1′-bis(*o*-carborane) and [μ-2,2′-CH_2CH_2-{1-(1′-1′,2′-*closo*-$C_2B_{10}H_{10}$)-1,2-*closo*-$C_2B_{10}H_{10}$}] (**I**), affording [$HNMe_3$][7-(1′-1′,2′-*closo*-$C_2B_{10}H_{10}$)-7,8-*nido*-$C_2B_9H_{11}$] (**II**) and [$HNMe_3$][μ-2,2′-CH_2CH_2-{7-(1′-1′,2′-*closo*-$C_2B_{10}H_{10}$)-7,8-*nido*-$C_2B_9H_{10}$}] (**16**).

As the products included a mixture of [$HNMe_3$][7-(1′-1′,2′-*closo*-$C_2B_{10}H_{10}$)-7,8-*nido*-$C_2B_9H_{11}$] (**II**) and [$HNMe_3$][μ-2,2′-CH_2CH_2-{7-(1′-1′,2′-*closo*-$C_2B_{10}H_{10}$)-7,8-*nido*-$C_2B_9H_{10}$}] (**16**) the most successful method of characterisation was NMR spectroscopy.

The ^{1}H NMR spectrum displayed an integral-1 broad singlet at δ 8.47 ppm, corresponding the lone trimethylammonium [*H*NMe_3]$^+$ proton; the remaining methyl protons were displayed as an integral-9 singlet at δ 3.25 ppm. A broad integral-0.6 singlet at δ 4.38 ppm was assigned to the C_{cage}*H* of the decapitated residual 1,1′-bis(*o*-carborane). The tether protons of **16** were displayed as two integral-2 multiplets from δ 2.49 to 2.38 ppm and from δ 2.21 to 2.15 ppm.

The ^{11}B{^{1}H} NMR spectrum was relatively uninformative as it showed a combination of signals from the [$HNMe_3$]$^+$ salt of both decapitated 1,1′-bis(*o*-carborane) and **16**. There were however two integral-2 peaks at δ -32.9 and -35.2 ppm, which are distinctive of

nido-7,8-C_2B_9 species. The remaining resonances were displayed in a pattern 1:1:2:3:2:7:7:3:1:2:1:1:1:1:1, from δ -3.8 to -22.3 ppm.

4.5 [2-(1′-1′,2′-*closo*-$C_2B_{10}H_{11}$)-4,5-(*p*-cymene)$_2$-7-Cl-4,5,2,3-*closo*-$Ru_2C_2B_9H_9$] (**17**) and [μ-2,2′-CH_2CH_2-{1-(1′-1′,2′-*closo*-$C_2B_{10}H_{10}$)-3-(*p*-cymene)-3,1,2-*closo*-$RuC_2B_9H_9$}] (**18**)

A mixture of [$HNMe_3$][7-(1′-1′,2′-*closo*-$C_2B_{10}H_{10}$)-7,8-*nido*-$C_2B_9H_{11}$] (**II**) and [$HNMe_3$][μ-2,2′-CH_2CH_2-{7-(1′-1′,2′-*closo*-$C_2B_{10}H_{10}$)-7,8-*nido*-$C_2B_9H_{10}$}] (**16**) were lithiated with two equivalents of *n*-BuLi to deprotonate the B-H-B bridging proton on the decapitated cage and also the unique proton of $HNMe_3$. The amount of *n*-BuLi (and subsequently the amount of [$RuCl_2$(*p*-cymene)]$_2$) was calculated by using the ratio of decapitated 1,1′-bis(*o*-carborane) to **16** taken from the ^{1}H NMR spectrum. Lithiation yielded a yellow solution that was frozen to -196 °C. {Ru(*p*-cymene)} was added and the reagents stirred overnight to give a brown solution. The products were purified using column chromatography and preparative TLC to afford:

R_f = 0.48, colourless, [1-(1′-1′,2′-*closo*-$C_2B_{10}H_{11}$)-2-(*p*-cymene)-2,1,8-*closo*-$RuC_2B_9H_{10}$] (0.048 g, 0.094 mmol, 22%),

R_f = 0.37, pale yellow, [1-(1′-1′,2′-*closo*-$C_2B_{10}H_{11}$)-3-(*p*-cymene)-3,1,2-*closo*-$RuC_2B_9H_{10}$] (0.014 g, 0.028 mmol, 7%),

R_f = 0.30, bright yellow, [μ-2,2′-CH_2CH_2-{1-(1′-1′,2′-*closo*-$C_2B_{10}H_{10}$)-3-(*p*-cymene)-3,1,2-*closo*-$RuC_2B_9H_9$}] (**18**) (0.036 g, 0.067 mmol, 16%),

Baseline, red, [2-(1′-1′,2′-*closo*-$C_2B_{10}H_{11}$)-4,5-(*p*-cymene)$_2$-7-Cl-4,5,2,3-*closo*-$Ru_2C_2B_9H_9$] (**17**) (0.010 g, 0.013 mmol, 3%).

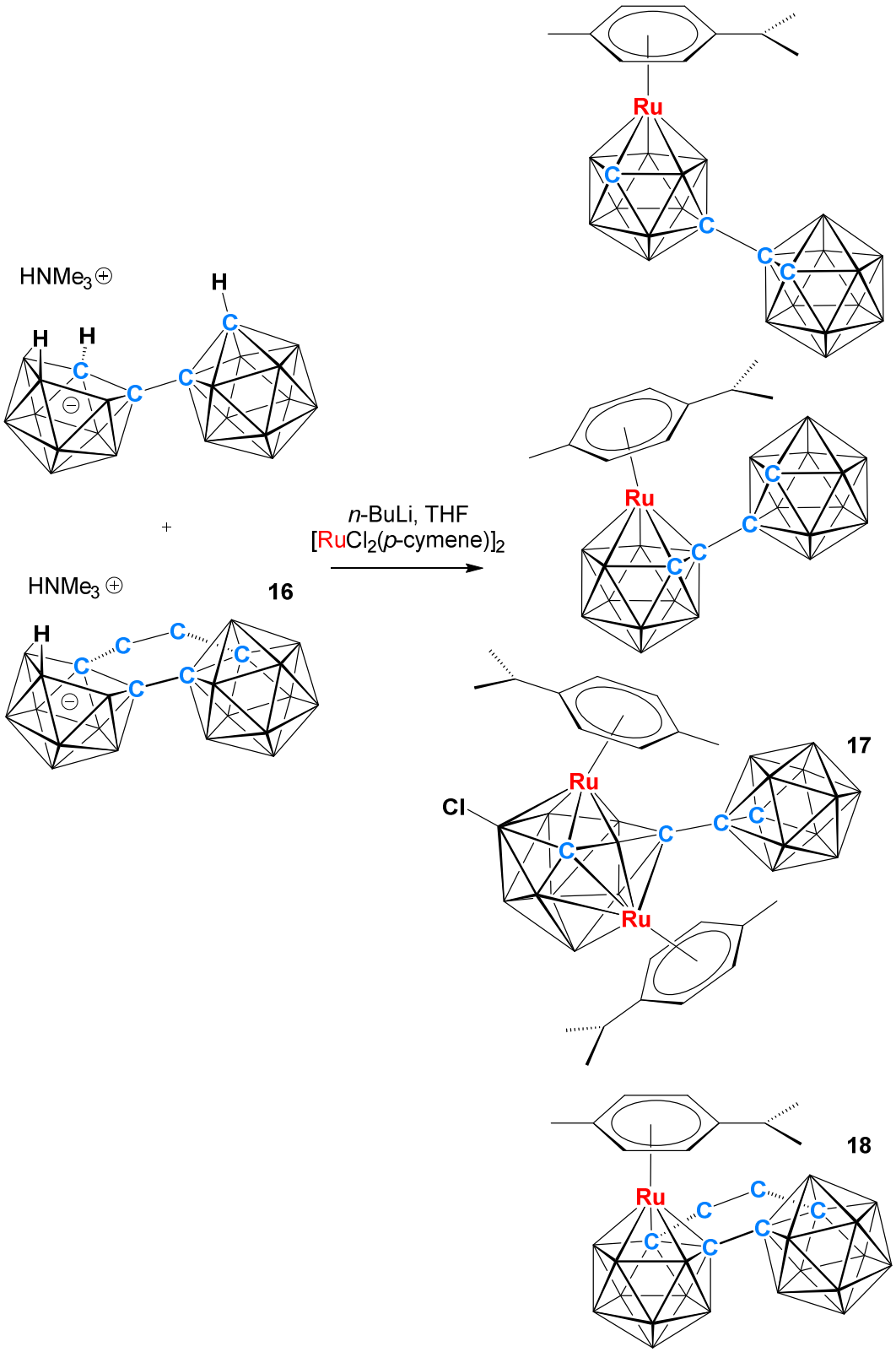

Scheme 4.3 Metalation of the $[HNMe_3]^+$ salts of decapitated 1,1′-bis(*o*-carborane) and **16**, affording a mixture of four products. Some C2 and C2′ hydrogen atoms removed for clarity.

This reaction gave a variety of products with two of these being direct metalation products of decapitated 1,1′-bis(*o*-carborane). [1-(1′-1′,2′-*closo*-$C_2B_{10}H_{11}$)-2-(*p*-cymene)-2,1,8-*closo*-$RuC_2B_9H_{10}$] and [1-(1′-1′,2′-*closo*-$C_2B_{10}H_{11}$)-3-(*p*-cymene)-3,1,2-*closo*-$RuC_2B_9H_{10}$] were afforded in 22% and 7% yields respectively. Both products have been reported from the decapitation and metalation of 1,1′-bis(*o*-carborane), whereby in a subsequent reaction the 3,1,2-isomer was converted to the 2,1,8-isomer by heating to 66 °C, Scheme 4.4.[6]

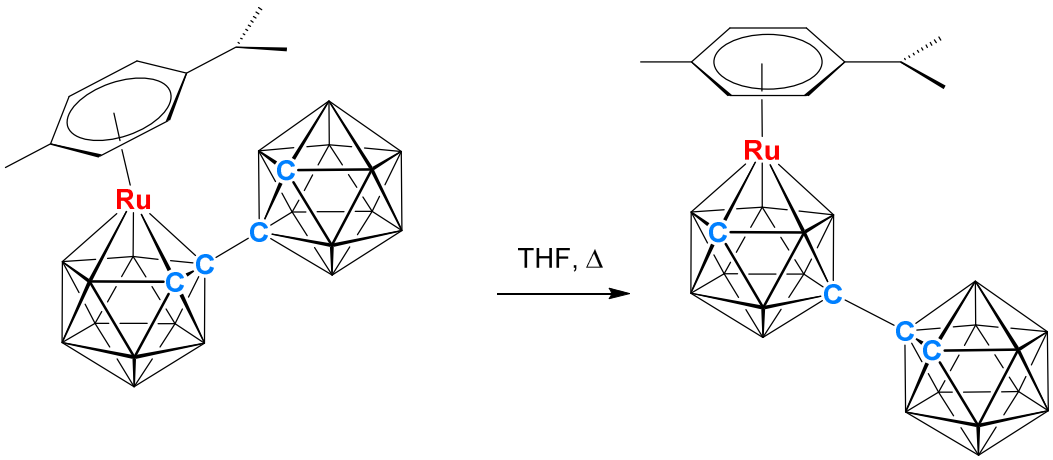

Scheme 4.4 Thermal isomerisation of [1-(1′-1′,2′-*closo*-$C_2B_{10}H_{11}$)-3-(*p*-cymene)-3,1,2-*closo*-$RuC_2B_9H_{10}$] to [1-(1′-1′,2′-*closo*-$C_2B_{10}H_{11}$)-2-(*p*-cymene)-2,1,8-*closo*-$RuC_2B_9H_{10}$]. C2 and C2′ hydrogen atoms removed for clarity.

4.5.1 [2-(1′-1′,2′-*closo*-$C_2B_{10}H_{11}$)-4,5-(*p*-cymene)$_2$-7-Cl-4,5,2,3-*closo*-$Ru_2C_2B_9H_9$] (**17**)

A red band in 3% yield found on the baseline (removed from the preperative TLC plates using 100% DCM) was subsequently identified as [2-(1′-1′,2′-*closo*-$C_2B_{10}H_{11}$)-4,5-(*p*-cymene)$_2$-7-Cl-4,5,2,3-*closo*-$Ru_2C_2B_9H_9$] (**17**), Figure 4.6. Compound **17** was characterised by electron ionisation mass spectrometry, NMR spectroscopy and *X*-ray crystallography. The mass spectrum displayed an envelope at *m/z* 780.4 which is in agreement with the molecular weight (779.65 g mol^{-1}).

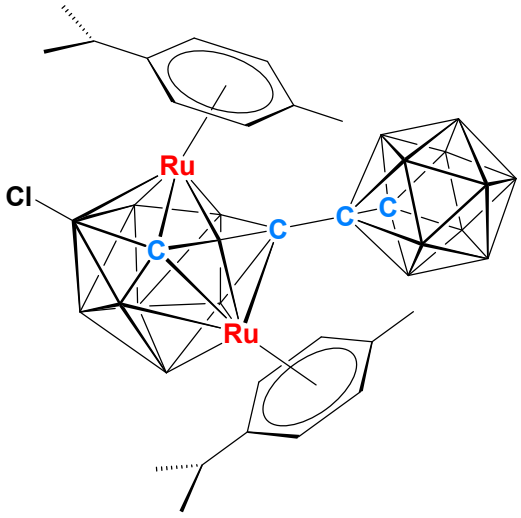

Figure 4.6 [2-(1′-1′,2′-*closo*-$C_2B_{10}H_{11}$)-4,5-(*p*-cymene)$_2$-7-Cl-4,5,2,3-*closo*-$Ru_2C_2B_9H_9$] (**17**).

The elemental analysis results are in good agreement with the calculated formula with the analysis performed using single crystals, containing one THF solvent molecule per molecule of **17**. The value for carbon is within 0.7% and for hydrogen is within 0.2% when calculated using the empirical formula $C_{24}H_{48}B_{19}ClRu_2 \cdot C_4H_8O$.

The ^{1}H NMR spectrum of **17** displayed the aromatic protons from the *p*-cymene units as an integral-8 multiplet between δ 6.28 and 5.73 ppm. The unique isopropyl protons from both *p*-cymene units are observed as two integral-1 multiplets at δ 2.92 to 2.85 ppm and δ 2.82 to 2.75 ppm. The *para*-methyl protons are displayed as two integral-3 singlets at

δ 2.28 and 2.24 ppm. The methyl protons from the *p*-cymene isopropyl unit are seen as two integral-6 multiplets from δ 1.36 to 1.31 ppm and δ 1.25 to 1.23 ppm. There are two broad integral-1 singlets associated with the cage hydrogen atoms at δ 3.75 and 3.47 ppm. The signal at higher frequency is tentatively assigned to the $C_{cage}H$ from the 12-vertex carborane cage with the signal at lower frequency arising from the 13-vertex metallacarborane cage.

The $^{11}B\{^{1}H\}$ NMR spectrum is relatively uninformative as there are many overlapping peaks. There is an integral-2 resonance at δ 20.81 ppm and two integral-1 resonances at δ 13.7 and 10.6 ppm. The remaining 15 boron atoms are found between δ 6.8 and -17.2 ppm with maxima at δ 3.9, 2.4, -2.9, -5.6, -9.0, -10.4 and -13.2 ppm. Atom B7 (with the chlorine substituent) can be assigned as the resonance at δ 10.6 ppm as there is no splitting in the proton-coupled boron NMR spectrum.

Single crystals of **17** were grown from slow diffusion of a concentrated THF solution and petroleum ether. Compound **17** crystallises in the $P\bar{1}$ space group and the structure is unexpected, where there has been metalation of one cage by two ruthenium *p*-cymene units giving a 13-vertex/12-vertex product, Figure 4.7.

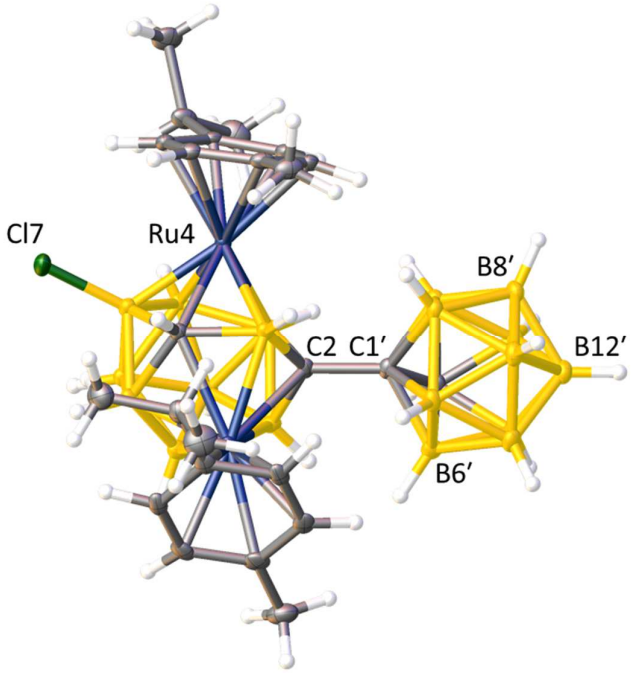

Figure 4.7 Perspective view of [2-(1′-1′,2′-*closo*-$C_2B_{10}H_{11}$)-4,5-(*p*-cymene)$_2$-7-Cl-4,5,2,3-*closo*-$Ru_2C_2B_9H_9$] (**17**) and part of the atom numbering scheme. Selected bond lengths are C1-C1′: 1.541(3) Å, C1′-C2′: 1.671(4) Å Ru4-C3: 2.218(2) Å, Ru5-C3: 2.328(2) Å and Ru5-C2: 2.298(2) Å.

Close inspection of the structure reveals that the 13-vertex cage is a docosahedron, but with one connectivity missing between Ru4 and C2 [2.836(2) Å], Figure 4.8. There is the possibility that there could be a fluxional equilibrium in solution, with one of two connectivities missing at any one time (Ru4-C2 or Ru5-C2). Docosahedral geometries are overall C_{2v}-symmetric but, as illustrated by the crystal structure, there is a chlorine atom bound to vertex seven of the cage (presumably formed during the reaction with [$RuCl_2$(*p*-cymene)]$_2$) that disrupts this symmetry. This is demonstrated by considering the ^{1}H NMR spectrum which indicates that the *p*-cymene units are inequivalent and display unique signals.

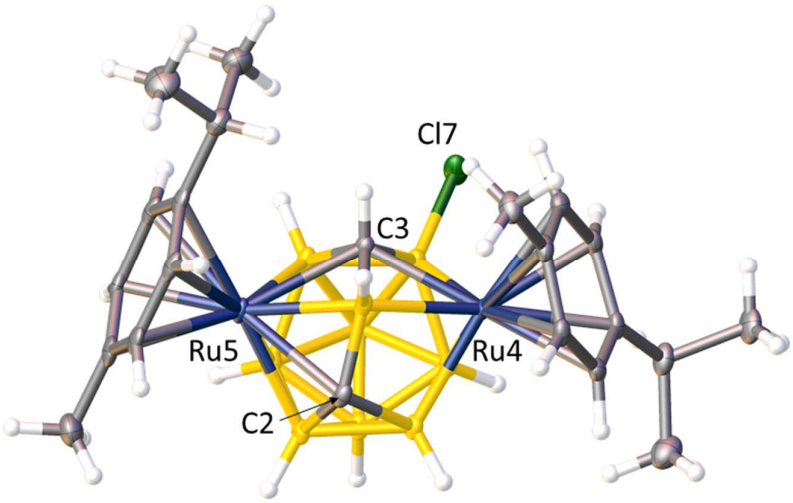

Figure 4.8 Alternative view of [2-(1′-1′,2′-*closo*-$C_2B_{10}H_{11}$)-4,5-(*p*-cymene)$_2$-7-Cl-4,5,2,3-*closo*-$Ru_2C_2B_9H_9$] (**17**) and part of the atom numbering scheme. The primed cage (attached to C2) has been removed for clarity.

As there is no tether present in compound **17** it is likely that it is formed from the reaction between [$HNMe_3$][7-(1′-1′,2′-*closo*-$C_2B_{10}H_{11}$)-7,8-*nido*-$C_2B_9H_{11}$] (**II**) and [$RuCl_2$(*p*-cymene)]$_2$, as opposed to reaction with the $[HNMe_3]^+$ salt of decapitated **16**.

4.5.2 [μ-2,2′-CH_2CH_2-{1-(1′-1′,2′-*closo*-$C_2B_{10}H_{10}$)-3-(*p*-cymene)-3,1,2-*closo*-$RuC_2B_9H_9$}] (18)

A bright yellow band in 16% yield was observed at R_f = 0.30 which was subsequently identified as the desired product [μ-2,2′-CH_2CH_2-{1-(1′-1′,2′-*closo*-$C_2B_{10}H_{10}$)-3-(*p*-cymene)-3,1,2-*closo*-$RuC_2B_9H_9$}] (**18**), Figure 4.9. Compound **18** was characterised by electron ionisation mass spectrometry, NMR spectroscopy and *X*-ray crystallography. The mass spectrum displayed an envelope at *m/z* 535.4, which is in agreement with the molecular weight (535.95 g mol^{-1}).

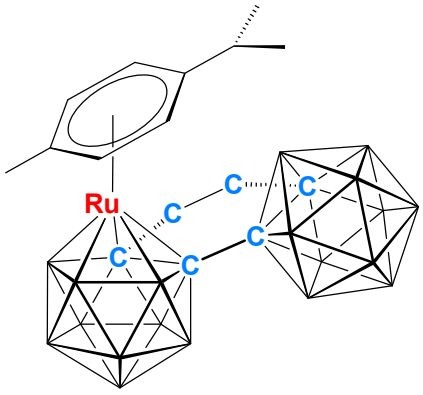

Figure 4.9 [μ-2,2′-CH_2CH_2-{1-(1′-1′,2′-*closo*-$C_2B_{10}H_{10}$)-3-(*p*-cymene)-3,1,2-*closo*-$RuC_2B_9H_9$}] (**18**).

The elemental analysis was in good agreement for the expected carbon and hydrogen values compared to the empirical formula, $C_{16}H_{37}B_{19}Ru$, within 0.1% for both.

The ^1H NMR spectrum of **18** displays the aromatic *p*-cymene protons as four integral-1 doublet of doublets at δ 6.05, 6.01, 5.93 and 5.87 ppm. The remaining signals appear as an integral-1 multiplet between δ 2.52 and 2.47 ppm (unique isopropyl proton), an integral-3 singlet at δ 2.49 ppm (*para*-methyl protons) and an integral-6 apparent triplet (two overlapping doublets) at δ 1.40 ppm (isopropyl methyl protons). The tether protons appear as a two sets of integral-2 multiplets between δ 3.24 and 3.11 ppm and δ 2.86 and 2.75 ppm.

The $^{11}B\{^{1}H\}$ NMR spectrum has nine resonances in the pattern 1:1:2:2:3:3:3:3:1, from high to low frequency, with 19 boron atoms in total. The signals are displayed at δ 3.0, -0.6, -3.5, -4.8, -6.3, -8.1, -9.3, -11.2 and -13.9 ppm.

Single crystals of **18** were grown from the slow diffusion of a concentrated DCM solution and petroleum ether and the *X*-ray diffraction study showed that it crystallises in the $P2_1$ space group and is the desired product, Figure 4.10. The product is the 3,1,2-isomer, as expected due to the tether holding the carbon atoms adjacent to one another. The tethering prevents movement of the carbon atoms and therefore prevents isomerisation of the metallacarborane cage. Isomerisation usually occurs due to steric crowding as observed in the facile isomerisation of the 3,1,2-isomer to the 2,1,8-isomer of singly metalated bis(*o*-carborane).[6] In this structure the fact that the *p*-cymene ring is titled away from the second cage shows that the molecule suffers from steric crowding, but the presence of the tether means that isomerisation is not possible.

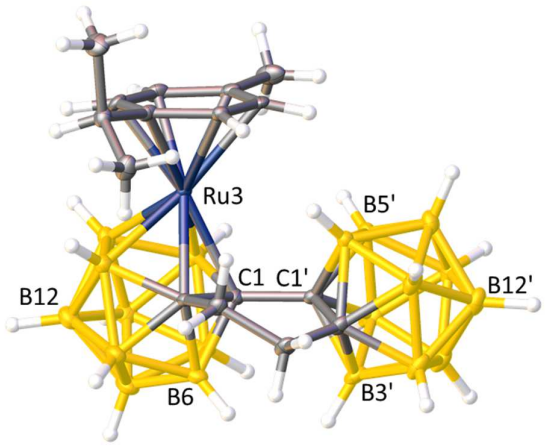

Figure 4.10 Perspective view of [μ-2,2′-CH_2CH_2-{1-(1′-1′,2′-*closo*-$C_2B_{10}H_{10}$)-3-(*p*-cymene)-3,1,2-*closo*-$RuC_2B_9H_9$}] (**18**) and part of the atom numbering scheme. Selected bond lengths are C1-C1′: 1.543(5) Å, C1-C2: 1.632(4) Å and C1′-C2′: 1.657(4) Å.

4.6 Conclusions

The work in this chapter illustrates that tethering the C2 and C2′ carbon atoms of 1,1′-bis(*o*-carborane) is possible, with either {C_6H_4} or {CH_2CH_2}. The compound [μ-2,2′-C_6H_4-{1-(1′-1′,2′-*closo*-$C_2B_{10}H_{10}$)-1,2-*closo*-$C_2B_{10}H_{10}$}] (**15**), has been synthesised in 10% yield and structurally characterised. According the Clar's rule compound **15** would most likely have aromaticity within the *o*-phenylene unit and the two *pseudo*-aromatic carborane cages.

The {CH_2CH_2} tethered carborane, [μ-2,2′-CH_2CH_2-{1-(1′-1′,2′-*closo*-$C_2B_{10}H_{10}$)-1,2-*closo*-$C_2B_{10}H_{10}$}] (**I**), was synthesised following literature methods, although unfortunately purification from residual 1,1′-bis(*o*-carborane) was not possible. Subsequent decapitation using ethanolic potassium hydroxide resulted in a mixture of [$HNMe_3$][7-(1′-1′,2′-*closo*-$C_2B_{10}H_{11}$)-7,8-*nido*-$C_2B_9H_{11}$] (**II**) and [$HNMe_3$][μ-2,2′-CH_2CH_2-{7-(1′-1′,2′-*closo*-$C_2B_{10}H_{10}$)-7,8-*nido*-$C_2B_9H_{10}$}] (**16**). When the decapitated salts were lithiated and reacted with {Ru(*p*-cymene)} four products were formed. [1-(1′-1′,2′-*closo*-$C_2B_{10}H_{11}$)-3-(*p*-cymene)-3,1,2-*closo*-$RuC_2B_9H_{10}$] and [1-(1′-1′,2′-*closo*-$C_2B_{10}H_{11}$)-2-(*p*-cymene)-2,1,8-*closo*-$RuC_2B_9H_{10}$] are singly-metalated isomers of 1,1′-bis(*o*-carborane) and a literature reference demonstrates that thermal isomerisation of the 3,1,2-isomer to the 2,1,8-isomer is possible. An unexpected product [2-(1′-1′,2′-*closo*-$C_2B_{10}H_{11}$)-4,5-(*p*-cymene)$_2$-7-Cl-4,5,2,3-*closo*-$Ru_2C_2B_9H_9$] (**17**) was isolated, a 13-vertex/12-vertex structure that unusually displayed a missing Ru-C connectivity from the docosahedral geometry in the single crystal *X*-ray diffraction study. The desired product [μ-2,2′-CH_2CH_2-{1-(1′-1′,2′-*closo*-$C_2B_{10}H_{10}$)-3-(*p*-cymene)-3,1,2-*closo*-$RuC_2B_9H_9$}] (**18**) was afforded in 16% yield and structural analysis confirmed the synthesis of a tethered 12-vertex ruthenacarborane/12-vertex carborane.

4.7 References

1. D. Zhao, J. J. Zhang, Z. Y. Lin and Z. W. Xie, *Chem. Commun.*, 2016, **52**, 9992.
2. G. P. Charbonneau and Y. Delugeard, *Acta Cryst., Sect. B*, 1977, **33**, 1586.
3. J. C. Collings, K. P. Roscoe, R. L. Thomas, A. S. Batsanov, L. M. Stimson, J. A. K. Howard and T. B. Marder, *New J. Chem.*, 2001, **25**, 1410.
4. W. Y. Man, G. M. Rosair and A. J. Welch, *Acta Cryst., Sect. E*, 2014, **70**, 462.
5. E. Clar, *Polycyclic Hydrocarbons*, Academic Press, London, New York, 1964.
6. G. Thiripuranathar, W. Y. Man, C. Palmero, A. P. Y. Chan, B. T. Leube, D. Ellis, D. McKay, S. A. Macgregor, L. Jourdan, G. M. Rosair and A. J. Welch, *Dalton Trans.*, 2015, **44**, 5628.

Chapter 5: Experimental

5.0 General Experimental

Synthesis

Experiments were performed under dry, oxygen free N_2, using standard Schlenk techniques, although subsequent manipulations were sometimes performed in the open laboratory. Solvents were freshly distilled under nitrogen from the appropriate drying agent immediately before use [THF, Et_2O and 40-60 petroleum ether (sodium wire); DCM and MeCN (CaH)] or were stored over 4 Å molecular sieves ($CDCl_3$, CD_2Cl_2) and were degassed (3×freeze-pump-thaw cycles) before use.

Chromatography

Preparative TLC employed 20×20 cm Kieselgel F_{254} glass plates and for column chromatography 60 Å silica was used as the stationary phase.

Spectroscopy

IR spectra were obtained from DCM solutions using a PerkinElmer Spectrum 100 FT-IR spectrometer. NMR spectra at 400.1 MHz (^{1}H), 128.4 MHz (^{11}B) or 162.0 MHz (^{31}P) were recorded on a Bruker DPX-400 spectrometer from $CDCl_3$ solutions and at 298 K unless otherwise stated. Electron impact mass spectrometry (EIMS) was carried out using a Finnigan (Thermo) LCQ Classic ion trap mass spectrometer (at the University of Edinburgh). Elemental analyses were conducted using an Exeter CE-440 elemental analyser.

X-ray Crystallography

Single crystals suitable for *X*-ray diffraction were grown by using solvent evaporation from DCM (**1**, **11**, **12**), MeCN (**6** and **8**), petroleum ether (**9**, **10**, **14**), $CDCl_3$ (**13**) or by solvent diffusion using either a DCM/petroleum ether system (**2**-**5**, **7**, **15**, **18**) or a THF/petroleum ether system (**17**) at -18 °C. The crystals were mounted using paraffin oil on a cryoloop and were cooled to 100 K by an Oxford Cryosystems Cryostream. Diffraction data were collected using a Bruker X8 APEX2 diffractometer with graphite-monochromated Mo-K_α *X*-radiation. The APEXII suite of programs was used for indexing, data collection and absorption correction.[1] The structures were solved using SHELXS-97 (direct methods) and refined using SHELXL-97 (full-matrix least-squares methods).[2] Vertex-to-centroid values were measured using Olex2 software.[3] All other geometric measurements were made using Mercury software.[4]

Standard Preparations

The starting materials 1,1ˈ-bis(*o*-carborane),[5] $[RuCl_2(p\text{-cymene})]_2$,[6] $[RuCl_2(PPh_3)_3]$[7], $[RuCl_2(PPh_3)_4]$[7], (tht)AuCl[8] and μ-2,2′-CH_2CH_2-1,1′-bis(*o*-carborane)[9] (**I**) were prepared by literature methods or slight variations thereof. All other reagents were supplied commercially.

5.2 Synthesis of [Ru(κ^3-2,2′,3′-{1-(1′-1′,2′-*closo*-$C_2B_{10}H_{10}$)-1,2-*closo*-$C_2B_{10}H_{10}$})(*p*-cymene)] (1)

n-BuLi (2.80 mL of 2.5M solution, 6.982 mmol) was added dropwise to a cooled (0°C) solution of 1,1'-bis(*o*-carborane) (1.000 g, 3.491 mmol) in THF (20 mL) and the products stirred for 1 hr. The pale yellow solution was frozen at -196 °C then $[RuCl_2(p\text{-cymene})]_2$ (1.069 g, 1.746 mmol) was added and the reaction mixture stirred overnight at room temperature to give a green solution. The THF was removed *in vacuo* and the crude mixture dissolved in DCM and filtered. Following spot TLC (DCM:petroleum ether, 50:50, R_f = 0.71) purification by column chromatography using the same eluent gave, on removal of solvent, an orange solid (0.678 g, 37%), subsequently identified as [Ru(κ^3-2,2′,3′-{1-(1′-1′,2′-*closo*-$C_2B_{10}H_{10}$)-1,2-*closo*-$C_2B_{10}H_{10}$})(*p*-cymene)] (**1**).

CHN: $C_{14}H_{34}B_{20}Ru$ requires C 32.3, H 6.59. Found for **1**: C 32.6, H 6.76%.

EIMS: *m/z* 520.4 (M^+).

NMR: **^{1}H NMR (CD_2Cl_2),** δ 5.48 [d, $^3J_{HH}$ = 6.0 Hz, 2H, $CH_3C_6H_4CH(CH_3)_2$], 5.30 [d, $^3J_{HH}$ = 6.0 Hz, 2H, $CH_3C_6H_4CH(CH_3)_2$], 2.81 [sept, $^3J_{HH}$ = 6.8 Hz, 1H, $CH_3C_6H_4CH(CH_3)_2$], 2.35 [s, 3H, $CH_3C_6H_4CH(CH_3)_2$], 1.39 [d, $^3J_{HH}$ = 6.8 Hz, 6H, $CH_3C_6H_4CH(CH_3)_2$].

^{1}H{^{11}B} NMR (CD_2Cl_2), δ 5.48 [d, $^3J_{HH}$ = 6.0 Hz, 2H, $CH_3C_6H_4CH(CH_3)_2$], 5.31[d, $^3J_{HH}$ = 6.0 Hz, 2H, $CH_3C_6H_4CH(CH_3)_2$], 2.81 [sept, $^3J_{HH}$ = 6.8 Hz, 1H, $CH_3C_6H_4CH(CH_3)_2$], 2.58 (s, 4B*H*), 2.36 (s, 3H, $CH_3C_6H_4CH(CH_3)_2$], 2.25 (s, 4B*H*), 2.21 (s, 2B*H*), 2.15 (s, 4B*H*), 2.11 (s, 2B*H*), 1.40 [d, *J* = 6.8 Hz, 6H, $CH_3C_6H_4CH(CH_3)_2$], -0.02 (s, 4H, $BH_{agostic}$).

^{1}H{^{11}B} NMR (CD_2Cl_2, 203 K), δ 5.44 [d, $^3J_{HH}$ = 6.0 Hz, 2H, $CH_3C_6H_4CH(CH_3)_2$], 5.24 [d, $^3J_{HH}$ = 6.0 Hz, 2H, $CH_3C_6H_4CH(CH_3)_2$], 2.74 [sept, $^3J_{HH}$ = 6.8 Hz, 1H, $CH_3C_6H_4CH(CH_3)_2$], 2.52 (s, 2B*H*), 2.47 (s, 2 B*H*), 2.29 [s, 3H, $CH_3C_6H_4CH(CH_3)_2$], 2.12 (s, 3B*H*), 2.06 (s, 3B*H*), 2.02 (s, 3B*H*), 1.96 (s, 3B*H*), 1.30 [d, $^3J_{HH}$ = 6.8 Hz, 6H, $CH_3C_6H_4CH(CH_3)_2$], 0.78 (s, 2B*H*), -1.03 (s, 2H, 2$BH_{agostic}$).

^{11}B{^{1}H} NMR (CD_2Cl_2), δ -1.4 (2B), -4.8 (2B), -7.1 (4B), -9.5 plus shoulder (8B), -10.6 (4B).

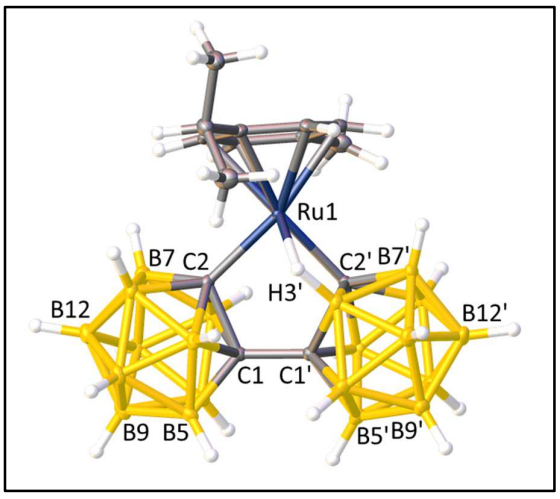

5.3 Synthesis of [Ru(κ^2-2,2′-{1-(1′-1′,2′-*closo*-$C_2B_{10}H_{10}$)-1,2-*closo*-$C_2B_{10}H_{10}$})(*p*-cymene)(CO)] (2)

Compound **1** (0.100 g, 0.192 mmol) was dissolved in THF (10 mL), frozen at -196 °C and the Schlenk tube was then charged with carbon monoxide (0.3 bar). The orange solution was left to warm to room temperature and stirred vigorously overnight to yield a yellow-green solution. The THF was removed *in vacuo* and the product isolated by preparative TLC (DCM:petroleum ether, 50:50), affording a yellow band (R_f = 0.34), subsequently identified as [Ru(κ^2-2,2′-{1-(1′-1′,2′-*closo*-$C_2B_{10}H_{10}$)-1,2-*closo*-$C_2B_{10}H_{10}$})(*p*-cymene)(CO)] (**2**) (0.037 g, 35%).

CHN: $C_{15}H_{34}B_{20}ORu$ requires C 32.9, H 6.26. Found for **2**: C 32.4, H 6.27%.

EIMS: *m/z* 520.4 (M^+-CO), 548.4 (M^+).

IR: υ_{max} 2570 (BH), 2007 (CO) cm^{-1}.

NMR: **^{1}H NMR,** δ 6.02 [d, $^{3}J_{HH}$ = 6.6 Hz, 2H, $CH_3C_6H_4CH(CH_3)_2$], 5.92 [d, $^{3}J_{HH}$ = 6.6 Hz, 2H, $CH_3C_6H_4CH(CH_3)_2$], 2.89 [sept, $^{3}J_{HH}$ = 6.8 Hz, 1H, $CH_3C_6H_4CH(CH_3)_2$], 2.40 [s, 3H, $CH_3C_6H_4CH(CH_3)_2$], 1.35 [d, $^{3}J_{HH}$ = 6.8 Hz, 6H, $CH_3C_6H_4CH(CH_3)_2$].

^{1}H{^{11}B} NMR, δ 6.03 [d, $^{3}J_{HH}$ = 6.6 Hz, 2H, $CH_3C_6H_4CH(CH_3)_2$], 5.94 [d, $^{3}J_{HH}$ = 6.6 Hz, 2H, $CH_3C_6H_4CH(CH_3)_2$], 2.88 (s, 2B*H*), 2.87 [sept, $^{3}J_{HH}$ = 6.8 Hz, 1H, $CH_3C_6H_4CH(CH_3)_2$], 2.72 (s, 2B*H*), 2.41-2.12 (m, 16B*H*), 2.36 [s, 3H, $CH_3C_6H_4CH(CH_3)_2$], 1.31 [d, $^{3}J_{HH}$ = 6.8 Hz, 6H, $CH_3C_6H_4CH(CH_3)_2$].

^{11}B{^{1}H} NMR, δ -2.6 (4B), -5 to -11 (overlapping resonances with maxima at -6.6, -7.8, -8.5, 16B).

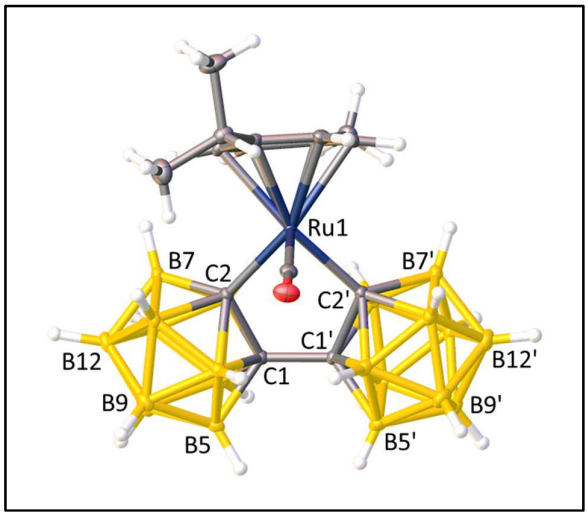

5.4 Synthesis of [Ru(κ^3-2,3′,3-{1-(1′-1′,2′-*closo*-$C_2B_{10}H_{10}$)-1,2-*closo*-$C_2B_{10}H_{10}$})(PPh_3)$_2$] (3)

Method A: Displacement of (p-cymene). Compound **1** (0.100 g, 0.192 mmol) was dissolved in THF (10 mL), frozen at -196 °C then triphenylphosphine (0.111 g, 0.423 mmol) was added. The orange solution was allowed to warm to room temperature and stirred for 2 hrs to yield a dark red solution. The THF was removed *in vacuo* and the product purified by preparative TLC (DCM:petroleum ether, 20:80) affording a yellow-orange band (R_f = 0.19), subsequently identified as [Ru(κ^3-2,3′,3-{1-(1′-1′,2′-*closo*-$C_2B_{10}H_{10}$)-1,2-*closo*-$C_2B_{10}H_{10}$})(PPh_3)$_2$] (**3**) (0.027 g, 15%).

Method B1: Reaction between [$RuCl_2(PPh_3)_4$] and dilithiated 1,1′-bis(o-carborane). *n*-BuLi (0.30 mL of 2.3M solution, 0.698 mmol) was added dropwise to a cooled (0°C) solution of 1,1′-bis(*o*-carborane) (0.100 g, 0.349 mmol) in THF (10 mL) and the products stirred for 1 hr. The pale yellow solution was frozen at -196 °C then [$RuCl_2(PPh_3)_4$] (0.426 g, 0.349 mmol) was added and the reaction mixture was stirred for 4 hrs at room temperature to give a dark red solution. The THF was removed *in vacuo* and the crude mixture dissolved in DCM and filtered. The product was purified using preparative TLC (DCM:petroleum ether, 30:70) affording an orange band (R_f = 0.24, trace) and a yellow band (R_f = 0.42), subsequently identified as [Ru(κ^3-2,3′,3-{1-(1′-1′,2′-*closo*-$C_2B_{10}H_{10}$)-1,2-*closo*-$C_2B_{10}H_{10}$})(PPh_3)$_2$] (**3**) (0.073 g, 23%).

Method B2: Reaction between [$RuCl_2(PPh_3)_3$] and dilithiated 1,1′-bis(o-carborane). *n*-BuLi (0.30 mL of 2.3M solution, 0.698 mmol) was added dropwise to a cooled (0°C) solution of 1,1′-bis(*o*-carborane) (0.100 g, 0.349 mmol) in THF (10 mL) and the products stirred for 1 hr. The pale yellow solution was frozen at -196 °C, [$RuCl_2(PPh_3)_3$] (0.335 g, 0.349 mmol) was added and the reaction mixture was stirred for 4 hrs at room temperature to give a dark red solution. THF was removed *in vacuo* and the crude mixture dissolved in DCM. Purification by preparative TLC (DCM:petroleum ether, 30:70) yielded a yellow-orange band (R_f = 0.51), subsequently identified as [Ru(κ^3-2,3′,3-{1-(1′-1′,2′-*closo*-$C_2B_{10}H_{10}$)-1,2-*closo*-$C_2B_{10}H_{10}$})(PPh_3)$_2$] (**3**) (0.078 g, 25%).

CHN: $C_{40}H_{50}B_{20}P_2Ru$ requires C 52.8, H 5.54. Found for **3**: C 52.5, H 5.53%.

EIMS: *m/z* 910.5 (M^+).

NMR: **^{1}H NMR,** δ 7.47-7.12 (m, 30 H, C_6H_5), 1.94 (br. s, 1H, $C_{cage}H$).

^{1}H{^{11}B} NMR, δ 7.47-7.12 (m, 30H, C_6H_5), 1.94 (br. s, 1H, $C_{cage}H$), [2.56, 2.47, 2.34, 2.30, 2.24, 2.19, 2.14, 2.10, 2.04, 1.87, 1.79, 1.58, 1.47 (total 19H, B*H*)], -4.23 (d, 32.0 Hz, 1H, $BH_{agostic}$).

^{11}B{^{1}H} NMR, δ 3 to -20 (overlapping resonances with maxima at 0.1, -4.8, -7.9, -9.2, -10.1, -12.5, -14.6, -17.4 , assume 20 B).

^{31}P{^{1}H} NMR, δ 57.98 (br. d, 25.1 Hz, 1P), 40.17 (d, 25.1 Hz, 1P).

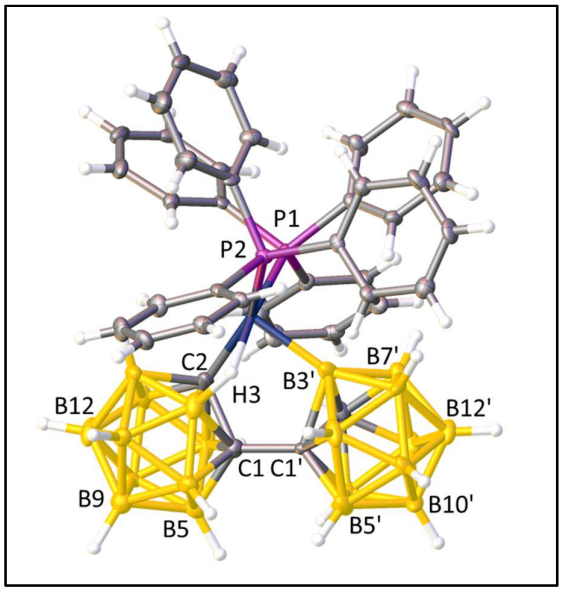

5.5 Synthesis of [Ru(κ^3-2,3′,3-{1-(1′-1′,2′-*closo*-$C_2B_{10}H_{10}$)-1,2-*closo*-$C_2B_{10}H_{10}$})(dppe)] (4)

Compound **1** (0.140 g, 0.269 mmol) was dissolved in THF (10 mL), frozen at -196 °C then 1,2-bis(diphenylphosphino)ethane (0.107 g, 0.269 mmol) was added. The orange solution was allowed to warm to room temperature and stirred for 2 hrs to yield a dark red solution. The THF was removed *in vacuo* and the product was purified by preparative TLC (DCM:petroleum ether, 50:50) affording a yellow band (R_f = 0.69), subsequently identified as [Ru(κ^3-2,3′,3-{1-(1′-1′,2′-*closo*-$C_2B_{10}H_{10}$)-1,2-*closo*-$C_2B_{10}H_{10}$})(dppe)] (**4**) (0.085 g, 28%).

CHN: $C_{30}H_{44}B_{20}P_2Ru$ requires C 46.0, H 5.66. Found for **4**: C 44.8, H 6.25%.

EIMS: *m/z* 286.3 [M^+-Ru(dppe)], 783.3 (M^+).

NMR: **^{1}H NMR,** δ 7.92-7.01 (m, 20H, C_6H_5), 3.08-2.75 (m, 4H, CH_2), 2.17 (br. s, 1H, $C_{cage}H$).

^{1}H{^{11}B} NMR, δ 7.90-7.01 (m, 20H, C_6H_5), 3.07-2.75 (m, 4H, CH_2), 2.17 (br. s, 2H, $C_{cage}H$), [2.74, 2.63, 2.57, 2.42, 2.23, 2.13, 2.09, 1.78, 1.75, 1.70, 1.30, 0.66 (total 19H, B*H*)], -2.25 (d, 28.0 Hz, 1H, $B_{agostic}H$).

^{11}B{^{1}H} NMR, δ 3 to -19 (overlapping resonances with maxima at 0.5, -4.3, -7.0, -7.9, -9.2, -10.4, -14.5, -16.1, assume 20 B).

^{31}P{^{1}H} NMR, δ 90.77 (br. unresolved d, 1P), 78.70 (d, 11.3 Hz, 1P).

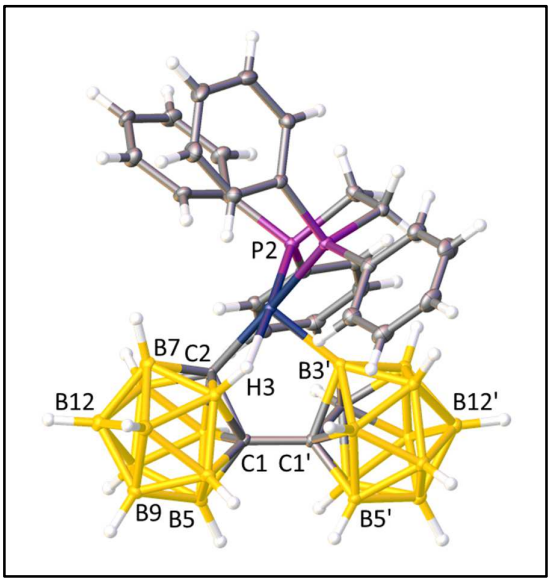

5.6 Synthesis of [Ru(κ^2-2,3′-{1-(1′-1′,2′-*closo*-$C_2B_{10}H_{10}$)-1,2-*closo*-$C_2B_{10}H_{10}$})(PPh_3)$(CO)_3$] (5)

Compound **3** was synthesised using Method **B1** (0.20 g, 0.70 mmol of 1,1′-bis(*o*-carborane)) and the compound was removed from the silica using THF (30 mL). The THF solution was reduced in volume to 10 mL, frozen at -196 °C and the Schlenk tube was then charged with carbon monoxide (0.3 bar). The orange solution was left to warm to room temperature and stirred vigorously overnight to yield a pale yellow solution. The THF was removed *in vacuo* and the product was purified by preparative TLC (DCM:petroleum ether, 50:50) affording a colourless band (R_f = 0.76), subsequently identified as [Ru(κ^2-2,3′-{1-(1′-1′,2′-*closo*-$C_2B_{10}H_{10}$)-1,2-*closo*-$C_2B_{10}H_{10}$})(PPh_3)$(CO)_3$] (**5**) (0.036 g, 7% based on 1,1′-bis(*o*-carborane)).

CHN: $C_{25}H_{35}B_{20}O_3PRu{\cdot}CH_2Cl_2$ requires C 38.2, H 4.57. Found for **5**$\cdot CH_2Cl_2$ (crystals submitted): C 38.5, H 4.62%.

EIMS: *m/z* 647.1 (100%, M^+-3×CO), 675.1 (57%, M^+-2×CO), 703.1 (<1%, M^+-CO), 731.8 (<1%, M^+).

IR: υ_{max} 2570 (BH), 2042 (CO), 2034 (CO), 2028 (CO) cm^{-1}.

NMR: NMR spectra consistent with a 1:1 mixture of two isomers.

^{1}H NMR, δ 7.58-7.47 (m, 30H, C_6H_5), 4.18 (br. s, 1H, $C_{cage}H$), 3.94 (br. s, 1H, $C_{cage}H$).

^{11}B{^{1}H} NMR, δ 4.2 (br. 2B, B3′), 1 to -14 (overlapping resonances with maxima at -2.2, -6.8, -8.9, 38B).

^{31}P{^{1}H} NMR, δ 27.74 (s, 1P), 17.12 (v. br s, 1P).

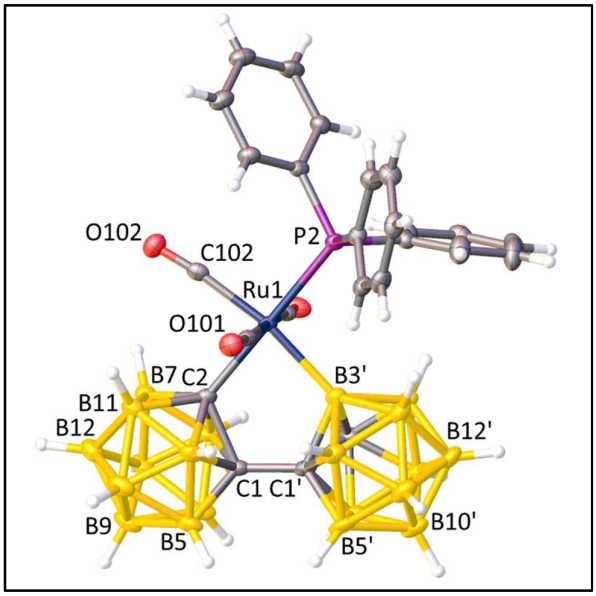

5.7 Synthesis of [Ru(κ^2-2,3′-{1-(1′-1′,2′-*closo*-$C_2B_{10}H_{10}$)-1,2-*closo*-$C_2B_{10}H_{10}$})(PPh_3)($MeCN)_3$] (6)

Compound **3** was synthesised using Method **B1** (0.20 g, 0.70 mmol of 1,1′-bis(*o*-carborane)) and the compound was removed from the silica using MeCN (30 mL). The orange compound instantly became colourless on contact with MeCN. The solution was left to stir for 2 hrs then the MeCN was removed *in vacuo*. The compound was separated by preparative TLC (DCM:petroleum ether, 50:50) affording an unidentified yellow band (R_f = 0.60, trace) and a colourless band (R_f = 0.14), which was subsequently identified as [Ru(κ^2-2,3′-{1-(1′-1′,2′-*closo*-$C_2B_{10}H_{10}$)-1,2-*closo*-$C_2B_{10}H_{10}$})(PPh_3)($MeCN)_3$] (**6**) (0.035 g, 7% based on 1,1′-bis(*o*-carborane)).

CHN: $C_{28}H_{44}B_{20}N_3PRu$ requires C 43.6, H 5.75, N 5.45. Found for **6**: C 44.3, H 5.81, N 4.32%.

EIMS: *m/z* 647.2 (M^+ - 3 x MeCN), 688.1 (M^+ - 2 x MeCN).

NMR: **^{1}H NMR,** δ 7.48-7.38 (m, 15H, C_6H_5), 3.43 (br. s, 1H, $C_{cage}H$), 2.11 (d, $^{5}J_{PH}$ = 1.0 Hz, 3H, CH_3CN), 2.04 (d, $^{5}J_{PH}$ = 1.0 Hz, 3H, CH_3CN), 2.00 (br. s, 3H, CH_3CN).

^{11}B{^{1}H} NMR, δ 12.8 (1B, B3′), 0 to -17 (overlapping resonances with maxima at -3.8, -8.4, -13.9, 19B).

^{31}P{^{1}H} NMR, δ 40.44 (s, 1P).

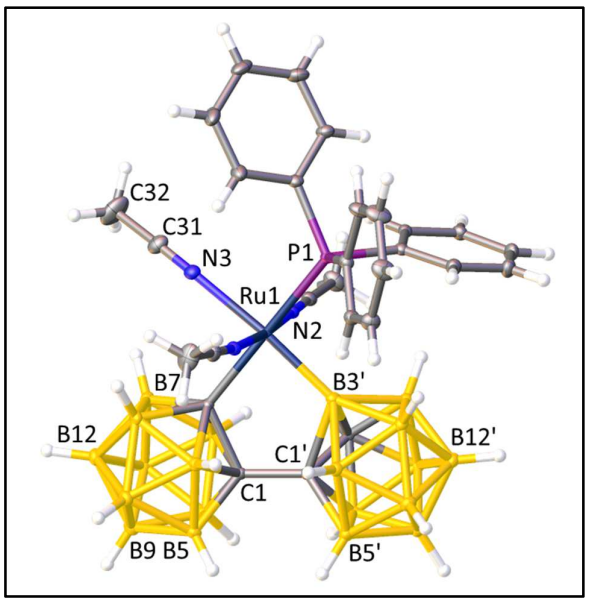

5.8 Synthesis of [Ru(κ^2-2,3′-{1-(1′-1′,2′-*closo*-$C_2B_{10}H_{10}$)-1,2-*closo*-$C_2B_{10}H_{10}$})(dppe)$(CO)_2$] (7)

Compound **4** (0.037 g, 0.05 mmol) was dissolved in THF (10 mL), frozen at -196 °C and the Schlenk tube was then charged with carbon monoxide (0.3 bar)**.** The yellow solution was left to warm to room temperature and stirred vigorously overnight to yield a pale yellow solution. The THF was removed *in vacuo* and the product was purified by preparative TLC (DCM:petroleum ether, 50:50) affording a yellow band (R_f = 0.50), subsequently identified as [Ru(κ^2-2,3′-{1-(1′-1′,2′-*closo*-$C_2B_{10}H_{10}$)-1,2-*closo*-$C_2B_{10}H_{10}$})(dppe)$(CO)_2$] (**7**) (0.020 g, 50%).

CHN: Microanalysis unavailable due to air-instability of compound.

EIMS: *m/z* 510.3 (100%), 783.3 (42%, M^+-2×CO), 811.3 (<1%, M^+-CO).

IR: υ_{max} 2566 (BH), 1983 (CO) cm^{-1}.

NMR: **^{1}H NMR,** δ 7.98-6.99 (m, 20H, C_6H_5), 3.90 (br. s, 1H, $C_{cage}H$), 3.06-2.86 (m, 4H, CH_2).

^{11}B{^{1}H} NMR, δ 8.5 (1B, B3′), 0 to -15 (overlapping resonances with maxima at -2.7, -7.1, -9.8, 19B).

^{31}P{^{1}H} NMR, δ 49.15 (s, 1P), 40.56 (v. br. s, 1P) .

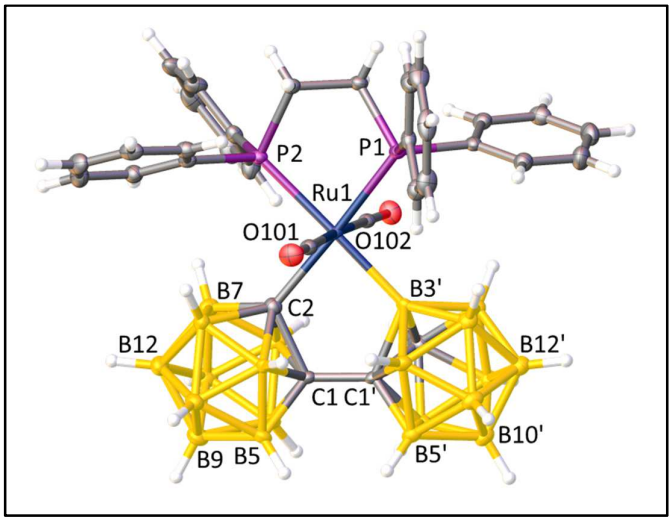

5.9 Synthesis of [Ru(κ^2-2,3′-{1-(1′-1′,2′-*closo*-$C_2B_{10}H_{10}$)-1,2-*closo*-$C_2B_{10}H_{10}$})(dppe)(MeCN)$_2$] (8)

Compound **4** (0.052 g, 0.06 mmol) was dissolved in MeCN (10 mL) and stirred for 2 hrs to give a pale yellow solution. The solvent was removed *in vacuo* and the product was purified by preparative TLC (DCM:petroleum ether, 50:50) affording a pale yellow band (R_f = 0.32), subsequently identified as [Ru(κ^2-2,3′-{1-(1′-1′,2′-*closo*-$C_2B_{10}H_{10}$)-1,2-*closo*-$C_2B_{10}H_{10}$})(dppe)(MeCN)$_2$] (**8**) (0.004 g, 7%).

CHN: $C_{34}H_{50}B_{20}P_2N_2P_2Ru$ requires C 47.2, H 5.82, N 3.23. Found for **8**: C 46.1, H 5.97, N 3.47%.

EIMS: *m/z* 783.3 (100%, M^+-2×MeCN).

NMR: **^{1}H NMR (CD_2Cl_2),** δ 7.97-6.91 (m, 20H, C_6H_5), 3.47 (br. s, 1H, $C_{cage}H$), 3.00-2.75 (m, 4H, CH_2), 2.07 (dd, $^{5}J_{PH}$ = 2.6 and 1.0 Hz, 3H, CH_3CN), 2.04 [dd (app. t), 3H, CH_3CN].

^{11}B{^{1}H} NMR (CD_2Cl_2), δ 19.4 (1B, B3′), -1 to -15 (overlapping resonances with maxima at -2.9, -3.6, -6.0, -8.5, -12.4, 19B).

^{31}P{^{1}H} NMR (CD_2Cl_2), δ 55.89 (s, 1P), 30.49 (v. br. s, 1P).

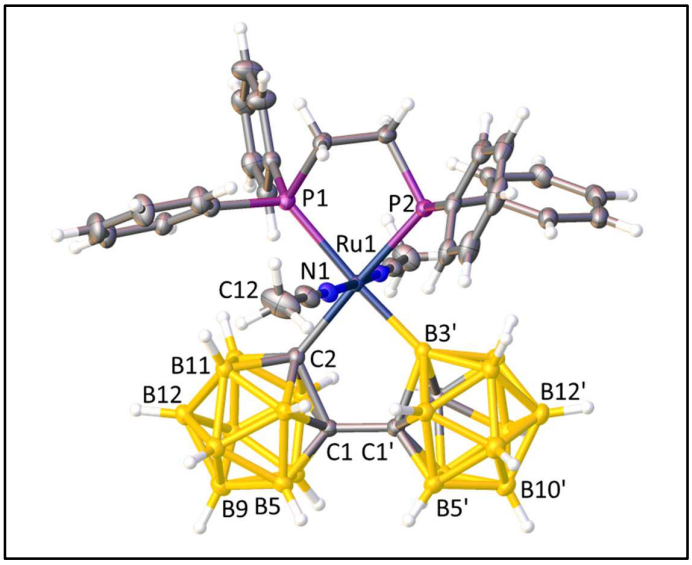

5.10 Lewis Acid Catalysed Diels-Alder Cycloaddition of Methacrolein or Crotonaldehyde and CpH.[10]

A solution of **1** (1 mol%) in DCM (1.5 mL) was added to a solution of crotonaldehyde (1 eq.) in DCM (1 mL) to produce a yellow solution. An aliquot of freshly cracked CpH (10 eq.) was added to the reaction mixture and the resultant yellow solution stirred under N_2. Samples of the reaction mixture (0.1 mL) were taken at regular intervals for solution NMR study to determine conversion. Integration of the *exo* and *endo* aldehyde ^{1}H NMR resonances [($CDCl_3$, 298 K) Bicyclo[2,2,1]hept-5-ene-2methyl-2-carboxaldehyde: δ 9.69 *exo*-C*H*O (s, 1H), 9.39 *endo*-C*H*O (s, 1H); Methylbicyclo[2,2,1]hept-5-ene-2-carboxaldehyde: δ 9.81 *exo*-C*H*O (d, *J* = 2.93 Hz, 1H), 9.42 *endo*-C*H*O (d, *J* = 2.57 Hz, 1H)][11] were used to calculate diastereomeric excess.

5.11 Synthesis of [μ-2,2′-PEt-{1-(1′-1′,2′-*closo*-$C_2B_{10}H_{10}$)-1,2-*closo*-$C_2B_{10}H_{10}$}] (9)

n-BuLi (0.56 mL of 2.5M solution, 1.396 mmol) was added dropwise to a cooled (0°C) solution of 1,1'-bis(*o*-carborane) (0.200 g, 0.698 mmol) in THF (10 mL) and the products stirred for 1 hr. The pale yellow solution was frozen at -196 °C then $PEtCl_2$ (0.70 mL of 1.0M solution, 0.698 mmol) was added and the reaction mixture stirred overnight at room temperature to give a colourless solution. The THF was removed *in vacuo* and the crude mixture dissolved in DCM and filtered. Purification by flash chromatography (petroleum ether) followed by preparative TLC (DCM:petroleum ether, 5:95) yielded a colourless band (R_f = 0.97) subsequently identified as [μ-2,2′-PEt-{1-(1′-1′,2′-*closo*-$C_2B_{10}H_{10}$)-1,2-*closo*-$C_2B_{10}H_{10}$}] (**9**) (0.154 g, 64%).

EIMS: *m/z* 344.3 (M^+).

NMR: **^{1}H NMR,** δ 1.98 (q, 2H, CH_2CH$_3$, $^{3}J_{HH}$ = 7.9 Hz), 1.31 (dt, 3H, CH$_2$CH_3, $^{3}J_{HH}$ = 7.9 Hz, $^{3}J_{PH}$ = 23.0 Hz).

^{1}H{^{31}P} NMR, δ 1.99 (q, 2H, CH_2CH$_3$, $^{3}J_{HH}$ = 7.9 Hz), 1.32 (t, 3H, CH$_2$CH_3, $^{3}J_{HH}$ = 7.9 Hz).

^{11}B{^{1}H} NMR, δ -0.3 (2B), -3.8 (2B), -6.6 (6B), -7.6 (2B), -8.5 (2B), -10.6 (6B).

^{31}P{^{1}H} NMR, δ 42.75 (s, 1P).

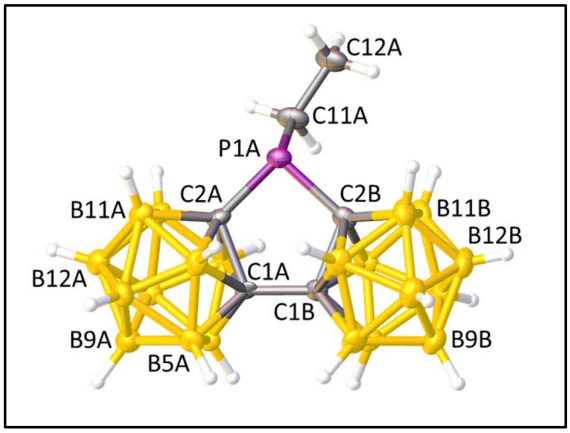

5.12 Synthesis of [μ-2,2′-PPh-{1-(1′-1′,2′-*closo*-$C_2B_{10}H_{10}$)-1,2-*closo*-$C_2B_{10}H_{10}$}] (10)

n-BuLi (2.79 mL of 2.5M solution, 6.982 mmol) was added dropwise to a cooled (0°C) solution of 1,1'-bis(*o*-carborane) (1.000 g, 3.491 mmol) in Et_2O (20 mL) and the products were stirred for 1 hr at room temperature. The pale yellow solution was cooled to 0 °C then $PPhCl_2$ (0.47 mL, 3.491 mmol) in Et_2O (10 mL) was added over 30 mins to give a green-yellow solution. This was heated to reflux for 2 hrs producing a pale yellow solution. Once cooled it was filtered and the solvent removed *in vacuo*. Purification by chromatography (petroleum ether) yielded a white solid subsequently identified as [μ-2,2′-PPh-{1-(1′-1′,2′-*closo*-$C_2B_{10}H_{10}$)-1,2-*closo*-$C_2B_{10}H_{10}$}] (**10**) (0.981 g, 72%).

EIMS: *m/z* 392.3 (M^+).

NMR: **^{1}H NMR,** δ 7.77-7.73 (m, 2H, C_6H_5), 7.65-7.62 (m, 1H, C_6H_5), 7.59-7.54 (m, 2H, C_6H_5).

^{1}H{^{31}P} NMR, δ 7.76 (d, 2H, C_6H_5), 7.64 (t, 1H, C_6H_5), 7.57 (t, 2H, C_6H_5).

^{11}B{^{1}H} NMR, δ -0.1 (2B), -2.4 to -13.2 (overlapping resonances with maxima at -3.9, -6.4, -8.7, -9.8, -11.2, 18B).

^{31}P{^{1}H} NMR, δ 40.35 (s, 1P).

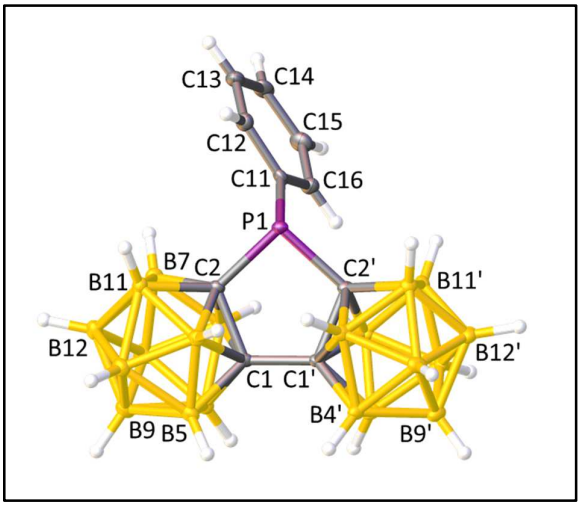

5.13 Synthesis of [μ-2,2′-P(Et)AuCl-{1-(1′-1′,2′-*closo*-$C_2B_{10}H_{10}$)-1,2-*closo*-$C_2B_{10}H_{10}$}] (11)

A DCM (5 mL) solution of [μ-2,2′-PEt-{1-(1′-1′,2′-*closo*-$C_2B_{10}H_{10}$)-1,2-*closo*-$C_2B_{10}H_{10}$}] (**1**) (0.100 g, 0.291 mmol) was transferred *via* cannula to a DCM (10 mL) solution of (tht)AuCl (0.093 g, 0.291 mmol) at 0 °C. The colourless solution was stirred at 0 °C for 30 mins, then reduced to ~3 mL *in vacuo.* Petroleum ether (10 mL) was added which caused precipitation of a white powder. This was collected by filtration and washed with petroleum ether (10 mL) to give a white solid subsequently identified as [μ-2,2′-P(Et)AuCl-{1-(1′-1′,2′-*closo*-$C_2B_{10}H_{10}$)-1,2-*closo*-$C_2B_{10}H_{10}$}] (**11**) (0.053 g, 32%).

EIMS: *m/z* 577.3 (M^+).

NMR: **^{1}H NMR,** δ 2.48 (dq, 2H, CH_2CH$_3$, $^{3}J_{HH}$ = 7.7 Hz, $^{2}J_{PH}$ = 10.9 Hz), 1.52 (dt, 3H, CH$_2$CH_3, $^{3}J_{HH}$ = 7.7 Hz, $^{3}J_{PH}$ = 27.9 Hz).

^{11}B{^{1}H} NMR, δ 1.7 (2B), -3.3 (2B), -5.7 (6B), -7.6 (4B), -10.4 (6B).

^{31}P{^{1}H} NMR, δ 75.76 (s, 1P).

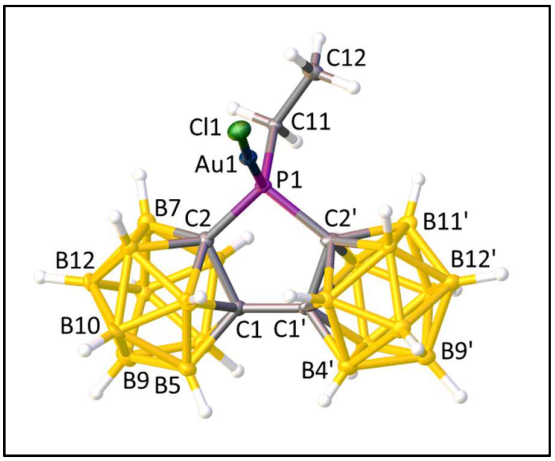

5.14 Synthesis of [μ-2,2′-PhPAuCl-{1-(1′-1′,2′-*closo*-$C_2B_{10}H_{10}$)-1,2-*closo*-$C_2B_{10}H_{10}$}] (12)

A DCM (5 mL) solution of [μ-2,2′-PPh-{1-(1′-1′,2′-*closo*-$C_2B_{10}H_{10}$)-1,2-*closo*-$C_2B_{10}H_{10}$}] (**2**) (0.100 g, 0.255 mmol) was transferred *via* cannula to a DCM (10 mL) solution of (tht)AuCl (0.082 g, 0.255 mmol) at 0 °C. The colourless solution was stirred at 0 °C for 30 mins, then reduced to ~3 mL *in vacuo.* Petroleum ether (10 mL) was added which caused precipitation a white powder. This was collected by filtration and washed with petroleum ether (10 mL) to give a white solid subsequently identified as [μ-2,2′-P(Ph)AuCl-{1-(1′-1′,2′-*closo*-$C_2B_{10}H_{10}$)-1,2-*closo*-$C_2B_{10}H_{10}$}] (**12**) (0.129 g, 81%).

EIMS: *m/z* 624.1 (M^+).

NMR: **^{1}H NMR,** δ 8.15-8.09 (m, 2H, C_6H_5), 7.86-7.81 (m, 1H, C_6H_5), 7.75-7.70 (m, 2H, C_6H_5).

^{11}B{^{1}H} NMR, δ -1.9 (2B), -0.7 to -13.9 (overlapping resonances with maxima at -3.6, -5.6, -7.6, -9.2, -10.9, 18B).

^{31}P{^{1}H} NMR, δ 68.96 (s, 1P).

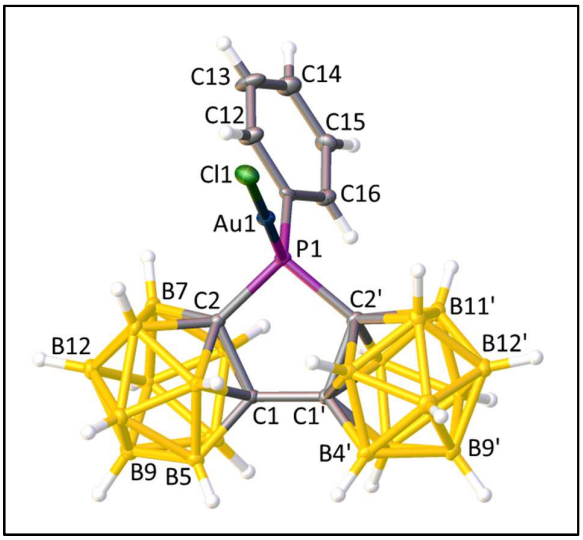

5.15 Synthesis of [μ-2,2′-P(Et)Se-{1-(1′-1′,2′-*closo*-$C_2B_{10}H_{10}$)-1,2-*closo*-$C_2B_{10}H_{10}$}] (13)

Elemental selenium (0.241 g, 3.052 mmol) was added to a toluene (10 mL) solution of [μ-2,2′-PEt-{1-(1′-1′,2′-*closo*-$C_2B_{10}H_{10}$)-1,2-*closo*-$C_2B_{10}H_{10}$}] (**1**) (0.100 g, 0.305 mmol) which was heated to reflux for 72 h. Excess selenium was removed by filtration and $^{31}P\{^1H\}$ NMR spectroscopy revealed an 71% conversion. Preparative TLC (DCM:petrol, 1:9) yielded the product as a colourless band at R_f = 0.73, [μ-2,2′-P(Et)Se-{1-(1′-1′,2′-*closo*-$C_2B_{10}H_{10}$)-1,2-*closo*-$C_2B_{10}H_{10}$}] (**13**) to afford a pale pink solid (0.049 g, 0.116 mmol, 38%).

EIMS: *m/z* 423.4 (M^+).

NMR: **^{1}H NMR,** δ 2.72 (dq, 2H, CH_2CH$_3$, $^{3}J_{HH}$ = 7.6 Hz, $^{2}J_{PH}$ = 11.6 Hz), 1.52 (dt, 3H, CH$_2$CH_3, $^{3}J_{HH}$ = 7.6 Hz, $^{3}J_{PH}$ = 25.9 Hz).

^{11}B{^{1}H} NMR, δ 0.9 (2B), -3.7 (2B), -4.8 to -12.3 (overlapping resonances with maxima at –6.2, -7.6, -8.7, -9.2, -10.6, 16B).

^{31}P{^{1}H} NMR, δ 58.05 (s, 1P, w/Se satellites at δ 60.80 and 55.28, $^{1}J_{PSe}$ = 894.2 Hz).

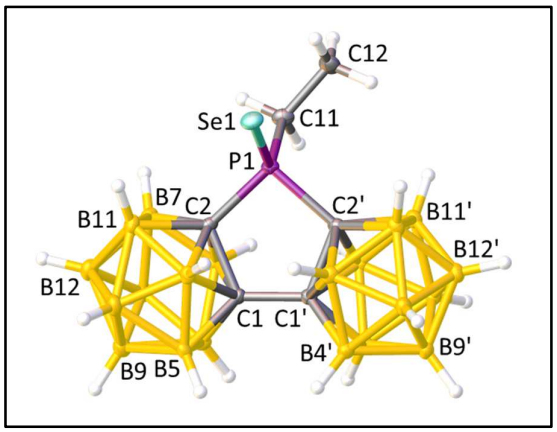

5.16 Synthesis of [μ-2,2′-P(Ph)Se-{1-(1′-1′,2′-*closo*-$C_2B_{10}H_{10}$)-1,2-*closo*-$C_2B_{10}H_{10}$}] (14)

Elemental selenium (0.201 g, 2.546 mmol) was added to a toluene (10 mL) solution of [μ-2,2′-PPh-{1-(1′-1′,2′-*closo*-$C_2B_{10}H_{10}$)-1,2-*closo*-$C_2B_{10}H_{10}$}] (**I**) (0.100 g, 0.255 mmol) which was then heated to reflux for 72 h. Excess selenium was removed by filtration and $^{31}P\{^1H\}$ NMR spectroscopy revealed an 74% conversion. Preparative TLC (DCM:petrol, 1:9) yielded the product as a colourless band at R_f = 0.59, [μ-2,2′-P(Ph)Se-{1-(1′-1′,2′-*closo*-$C_2B_{10}H_{10}$)-1,2-*closo*-$C_2B_{10}H_{10}$}] (**14**) to afford a pale pink solid (0.057 g, 0.120 mmol, 47%).

EIMS: *m/z* 471.3 (M^+).

NMR: **^{1}H NMR,** δ 8.31-8.25 (m, 2H, C_6H_5), 7.73-7.68 (m, 1H, C_6H_5), 7.63-7.57 (m. 2H, C_6H_5).

^{11}B{^{1}H} NMR, δ 1.2 (2B), -2.7 to -13.2 (overlapping resonances with maxima at -4.1, -6.0, -6.4, -8.5, -9.9, -11.2, 18B).

^{31}P{^{1}H} NMR, δ 50.52 (s, 1P, w/Se satellites at 53.27 and 47.77, $^{1}J_{PSe}$ = 891 Hz).

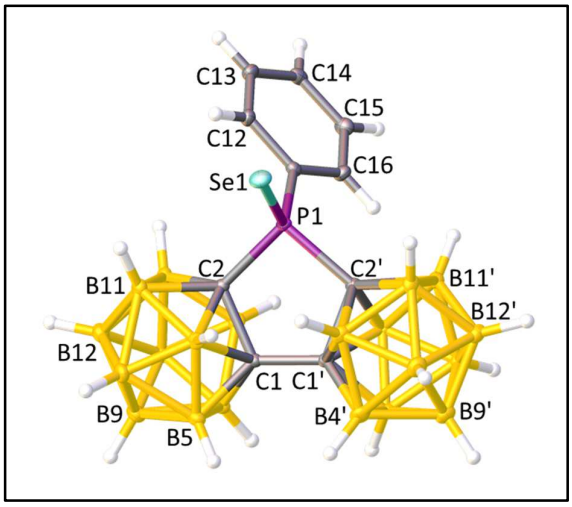

5.17 Synthesis of [μ-2,2′-C_6H_4-{1-(1′-1′,2′-*closo*-$C_2B_{10}H_{10}$)-1,2-*closo*-$C_2B_{10}H_{10}$}] (15)

n-BuLi (1.16 mL of 2.5 M solution 2.793 mmol) was added dropwise to a cooled (0°C) solution of 1,1'-bis(*o*-carborane) (0.400 g, 1.396 mmol) in THF (15 mL) and the products stirred for 1 hr. Copper(I) chloride (0.360 g, 3.637 mmol) was added in one portion to the pale yellow solution and the mixture stirred for 15 mins, then pyridine (0.84 mL) was added to afford an orange/brown solution. 1,2-Diiodobenzene (0.19 ml, 1.454 mmol) was added in one portion and the mixture was heated under reflux for 60 hrs to give a red/brown colour. The cooled mixture was diluted with diethyl ether (50 mL) and allowed to stand for 2 hrs. The copper complex was filtered off and washed with ether. The filtrate was washed with dil. HCl (3 M; 10 mL) and then distilled water (3 x 10 mL) and the organic layer was dried over $MgSO_4$, filtered and concentrated to give a yellow/green solid. Column chromatography (DCM:petroleum ether, 30:70) afforded a white solid which was washed with cold petrol to remove remaining 1,2-diiodobenzene. Preparative TLC (DCM/petroleum ether, 40:60) afforded a white solid (R_f = 0.93) which was identified as [μ-2,2′-C_6H_4-{1-(1′-1′,2′-*closo*-$C_2B_{10}H_{10}$)-1,2-*closo*-$C_2B_{10}H_{10}$}] (**15**) (0.050 g, 0.138 mmol, 10%).

EIMS: *m/z* 360.4 (M^+).

NMR: **^{1}H NMR,** δ 7.90-7.89 (m, 2H, C_6H_4), 7.06-7.02 (m, 2H, C_6H_4).

^{11}B{^{1}H} NMR, δ -2.5 (4B), -5.1 to -11.8 (overlapping resonances with maxima at -7.0, -8.2, -9.0, 16B).

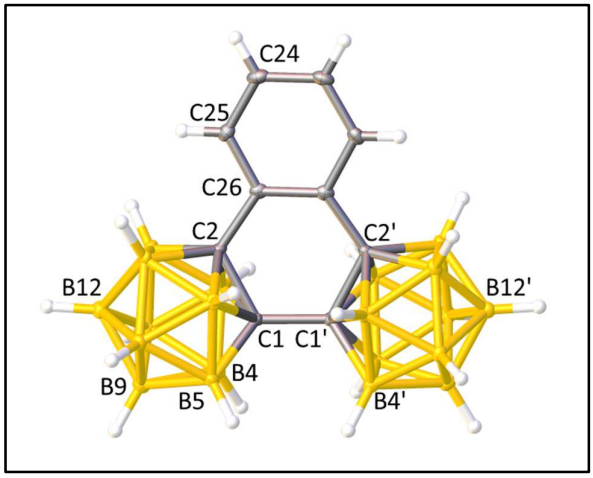

5.18 Synthesis of [HNMe$_3$][μ-2,2′-CH$_2$CH$_2$-{7-(1′-1′,2′-*closo*-C$_2$B$_{10}$H$_{10}$)-7,8-*nido*-C$_2$B$_9$H$_{10}$}] (16)

An ethanol solution (20 mL) of [μ-2,2′-CH$_2$CH$_2$-{1-(1′-1′,2′-*closo*-C$_2$B$_{10}$H$_{10}$)-1,2-*closo*-C$_2$B$_{10}$H$_{10}$}] (0.527 g, 1.764 mmol) and KOH (0.099 g, 1.764 mmol) was heated to reflux overnight. The solvent was removed *in vacuo* and the white solids dissolved in water (10 mL) and filtered to remove unreacted 1,1′-bis(*o*-carborane). An aqueous solution (10 mL) of [HNMe$_3$]Cl (0.185 g, 1.934 mmol) was added to the filtrate and the resultant white solid was filtered, washed with water (10 mL) and dried. The white solid was subsequently identified as a mixture of [HNMe$_3$][7-(1′-1′,2′-*closo*-C$_2$B$_{10}$H$_{10}$)-7,8-*nido*-C$_2$B$_9$H$_{11}$] and [HNMe$_3$][μ-2,2′-CH$_2$CH$_2$-{7-(1′-1′,2′-*closo*-C$_2$B$_{10}$H$_{10}$)-7,8-*nido*-C$_2$B$_9$H$_{10}$}] (**16**) (0.270 g total, ~0.746 mmol, ~42%).

Note: [μ-2,2′-CH$_2$CH$_2$-{1-(1′-1′,2′-*closo*-C$_2$B$_{10}$H$_{10}$)-1,2-*closo*-C$_2$B$_{10}$H$_{10}$}] was very difficult to separate from the starting material 1,1′-bis(*o*-carborane) during preparation and therefore a 50:50 ratio (ratio taken from NMR spectra) was used to calculate the moles of reactant and reagents used. The mixture of starting materials led to the formation of a mixture of decapitated products [HNMe$_3$][7-(1′-1′,2′-*closo*-C$_2$B$_{10}$H$_{10}$)-7,8-*nido*-C$_2$B$_9$H$_{11}$] and [HNMe$_3$][μ-2,2′-CH$_2$CH$_2$-{7-(1′-1′,2′-*closo*-C$_2$B$_{10}$H$_{10}$)-7,8-*nido*-C$_2$B$_9$H$_{10}$}] (**16**) which in turn gave very complicated NMR spectra and meant that crystallisation was impossible.

NMR: **^{1}H NMR,** δ 8.47 (br. s, 1H, *H*N(CH$_3$)$_3$), 4.38 (br. s, 0.6H, C$_{cage}$*H*) 3.25 (s, 9H, HN(C*H*$_3$)$_3$), 2.49-2.38 (m, 2H, C*H*$_2$CH$_2$), 2.21-2.15 (m, 2H, CH$_2$C*H*$_2$).

^{11}B{^{1}H} NMR, δ -3.8 (1B), -4.8 (1B), -5.9 (2B), -6.8 (3B), -8.7 (2B), -10.3 (7B), -11.0 (7B), -13.4 (3B), -14.3 (1B), -16.7 (2B), -18.0 (1B), -18.9 (1B), -20.0 (1B), -21.0 (1B), -22.3 (1B), -32.9 (2B), -35.2 (2B).

5.19 Synthesis of [2-(1′-1′,2′-*closo*-$C_2B_{10}H_{11}$)-4,5-(*p*-cymene)$_2$-7-Cl-4,5,2,3-*closo*-$Ru_2C_2B_9H_9$] (**17**) and [μ-2,2′-CH_2CH_2-{1-(1′-1′,2′-*closo*-$C_2B_{10}H_{10}$)-3-(*p*-cymene)-3,1,2-*closo*-$RuC_2B_9H_9$}] (**18**)

n-BuLi (0.36 mL of 2.5 M solution 0.912 mmol) was added dropwise to a cooled (0°C) solution of [$HNMe_3$][7-(1′-1′,2′-*closo*-$C_2B_{10}H_{10}$)-7,8-*nido*-$C_2B_9H_{11}$] and [$HNMe_3$][μ-2,2′-CH_2CH_2-{7-(1′-1′,2′-*closo*-$C_2B_{10}H_{10}$)-7,8-*nido*-$C_2B_9H_{10}$}] (**16**) (0.150 g, ~0.415 mmol) in THF (15 mL) and the products stirred for 1 hr. The pale yellow solution was cooled to -196 °C and [$RuCl_2$(*p*-cymene)]$_2$ (0.254 g, 0.415 mmol) added and stirred overnight to yield a brown solution. The solvent was removed *in vacuo* and the products purified by column chromatography (DCM:petroleum ether, 40:60) and preparative TLC (DCM:petroleum ether, 40:60) to give:

R_f = 0.48, colourless, [1-(1′-1′,2′-*closo*-$C_2B_{10}H_{11}$)-2-(*p*-cymene)-2,1,8-*closo*-$RuC_2B_9H_{10}$] (0.048 g, 0.094 mmol, 22%),

R_f = 0.37, pale yellow, [1-(1′-1′,2′-*closo*-$C_2B_{10}H_{11}$)-3-(*p*-cymene)-3,1,2-*closo*-$RuC_2B_9H_{10}$] (0.014 g, 0.028 mmol, 7%),

R_f = 0.30, bright yellow, [μ-2,2′-CH_2CH_2-{1-(1′-1′,2′-*closo*-$C_2B_{10}H_{10}$)-3-(*p*-cymene)-3,1,2-*closo*-$RuC_2B_9H_9$}] (**18**) (0.036 g, 0.067 mmol, 16%),

Baseline, red, [2-(1′-1′,2′-*closo*-$C_2B_{10}H_{11}$)-4,5-(*p*-cymene)$_2$-7-Cl-4,5,2,3-*closo*-$Ru_2C_2B_9H_9$] (**17**) (0.010 g, 0.013 mmol, 3%).

[2-(1′-1′,2′-*closo*-$C_2B_{10}H_{11}$)-4,5-(*p*-cymene)$_2$-7-Cl-4,5,2,3-*closo*-$Ru_2C_2B_9H_9$] (17)

CHN: $C_{24}H_{48}B_{19}ClRu_2 \cdot C_4H_8O$ requires C 39.48, H 6.63. Found for **17**: C 40.17, H 6.84%.

EIMS: *m/z* 780.4.

NMR: **^{1}H NMR,** δ 6.28-5.73 [m, 8H, $CH_3C_6H_4CH(CH_3)_2$], 3.75 (br. s, 3.75, $C_{cage}H$), 3.47 (br. s, $C_{cage}H$), 2.92-2.85 [m, 1H, $CH_3C_6H_4CH(CH_3)_2$], 2.82-2.75 [m, 1H, $CH_3C_6H_4CH(CH_3)_2$], 2.28 [s, 3H, $CH_3C_6H_4CH(CH_3)_2$], 2.24 [s, 3H, $CH_3C_6H_4CH(CH_3)_2$], 1.36-1.31 [m, 6H, $CH_3C_6H_4CH(CH_3)_2$], 1.25-1.23 [m, 6H, $CH_3C_6H_4CH(CH_3)_2$].

^{11}B{^{1}H} NMR, δ 20.8 (2B), 13.7 (1B), 10.6 (1B), 6.8 to -17.2 (overlapping resonances with maxima at 3.9, 2.4, -2.9, -5.6, -9.0, -10.4, -13.2, 15B).

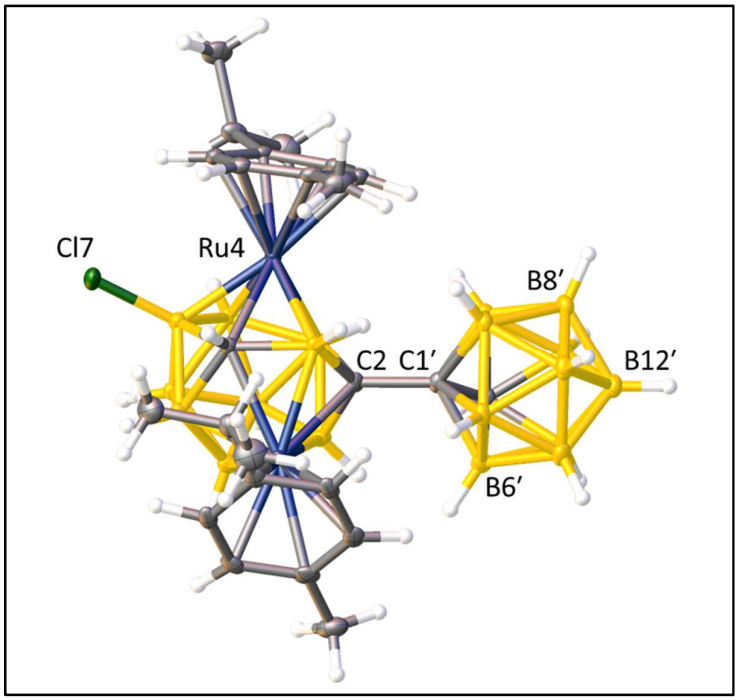

[μ-2,2′-CH_2CH_2-{1-(1′-1′,2′-*closo*-$C_2B_{10}H_{10}$)-3-(*p*-cymene)-3,1,2-*closo*-$RuC_2B_9H_9$}] (18)

CHN: $C_{16}H_{37}B_{19}Ru$ requires C 35.86, H 6.96. Found for **18**: C 35.95, H 6.99%.

EIMS: *m/z* 535.4.

NMR: **^{1}H NMR,** δ 6.05 [dd, $^3J_{HH}$ = 6.0 Hz, $^4J_{HH}$ = 1.4 Hz, 1H, $CH_3C_6H_4CH(CH_3)_2$], 6.01 [dd, $^3J_{HH}$ = 6.0 Hz, $^4J_{HH}$ = 1.4 Hz, 1H, $CH_3C_6H_4CH(CH_3)_2$], 5.93 [dd, $^3J_{HH}$ = 6.0 Hz, $^4J_{HH}$ = 1.4 Hz, 1H, $CH_3C_6H_4CH(CH_3)_2$], 5.87 [dd, $^3J_{HH}$ = 6.0 Hz, $^4J_{HH}$ = 1.4 Hz, 1H, $CH_3C_6H_4CH(CH_3)_2$], 3.24-3.11 (m, 2H, CH_2CH_2), 2.86-2.75 (m, 2H, CH_2CH_2) 2.52-2.47 [m, 1H, $CH_3C_6H_4CH(CH_3)_2$], 2.49 [s, 3H, $CH_3C_6H_4CH(CH_3)_2$], 1.40 [appt. t, 6H, $CH_3C_6H_4CH(CH_3)_2$].

^{11}B{^{1}H} NMR, δ 3.0 (1B), -0.6 (1B), -3.5 (2B), -4.8 (2B), -6.3 (3B), -8.1 (3B), -9.3 (3B), -11.2 (3B), -13.9 (1B).

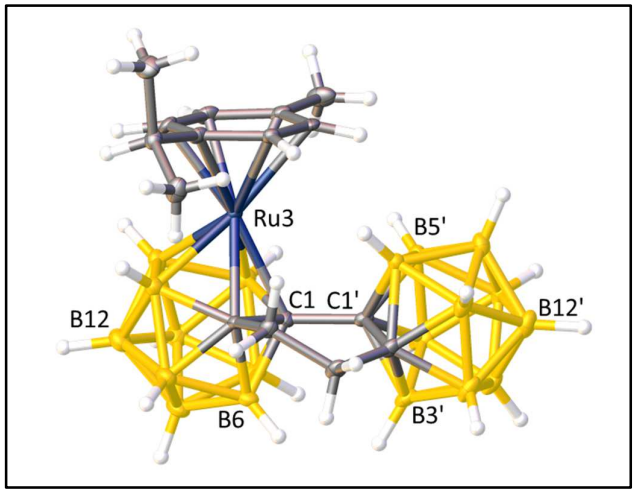

5.20 References

1. *Bruker AXS APEX2, version 2009-5*, Bruker AXS Inc., Madison, Wisconsin, USA, 2009.
2. G. M. Sheldrick, *Acta Crystallogr., Sect. A: Fundam. Crystallogr.*, 2008, **A64**, 112.
3. O. V. Dolomanov, L. J. Bourhis, R. J. Gildea, J. A. K. Howard and H. Puschmann, *J. Appl. Cryst.*, 2009, **42**, 339.
4. C. F. Macrae, P. R. Edgington, P. McCabe, E. Pidcock, G. P. Shields, R. Taylor, M. Towler and J. van de Streek, *J. Appl. Crystallogr.*, 2006, **39**, 453.
5. S. Ren and Z. Xie, *Organometallics*, 2008, **27**, 5167.
6. M. A. Bennett, T. N. Huang, T. W. Matheson and A. K. Smith, *Inorg. Synth.*, 1982, **21**, 74.
7. P. S. Hallman, T. A. Stephenson and G. Wilkinson, *Inorg. Synth.*, 1970, **12**, 237.
8. R. Uson, A. Laguna and M. Laguna, *Inorg. Synth.*, 1989, **26**, 85.
9. D. Zhao, J. J. Zhang, Z. Y. Lin and Z. W. Xie, *Chem. Commun.*, 2016, **52**, 9992.
10. J. W. Faller, B. J. Grimmond and D. G. D'Alliessi, *J. Am. Chem. Soc.*, 2001, **123**, 2525.
11. D. F. Schreiber, Y. Ortin, H. Mueller-Bunz and A. D. Phillips, *Organometallics*, 2011, **30**, 5381.

Appendix 1: Crystallographic Tables

Compound **1**	
[Ru(κ^3-2,2′,3′-{1-(1′-1′,2′-*closo*-$C_2B_{10}H_{10}$)-1,2-*closo*-$C_2B_{10}H_{10}$})(*p*-cymene)]	
Identification code	x85062
Empirical formula	$C_{14}H_{34}B_{20}Ru$
Formula weight	519.68 g mol^{-1}
Temperature	100.0 K
Wavelength	0.71073 Å
Crystal System	Triclinic
Space group	P-1
Unit cell dimensions	a = 9.9651(8) Å, α = 85.831(4)°
	b = 10.4007(8) Å, β = 70.460(4)°
	c = 13.6240(11) Å, γ = 72.262(4)°
Volume	1266.79(18) Å^3
Z	2
Density (calculated)	1.362 g cm^{-3}
Absorption coefficient	0.624 mm^{-1}
F(000)	524
Crystal size	0.36 x 0.32 x 0.10 mm
2-Theta range for data collection	5.3 to 54.6°
Index ranges	-9 ≤ h ≤ 12, -13 ≤ k ≤ 13,
	-17 ≤ l ≤ 17
Reflections collected	19182
Independent reflections	8854 [R(int) = 0.0320]
Completeness to theta = 27.28°	97.5%
Absorption correction	Semi-empirical from equivalents
Max. and min. transmission	0.746 and 0.678
Refinement method	Full-matrix least-squares on F^2
Data / restraints / parameters	5545 / 0 / 379
Goodness-of-fit on F^2	1.098
Final R indices [I>2sigma(I)]	R1 = 0.0338, wR2 = 0.0709
R indices (all data)	R1 = 0.0374, wR2 = 0.0724
Largest diff. peak and hole	1.77 and -0.82 e Å^{-3}

Compound **2**	
[Ru(κ^2-2,2′-{1-(1′-1′,2′-*closo*-$C_2B_{10}H_{10}$)-1,2-*closo*-$C_2B_{10}H_{10}$})(*p*-cymene)(CO)]	
Identification code	x85037
Empirical formula	$C_{15}H_{34}B_{20}ORu$
Formula weight	547.69 g mol^{-1}
Temperature	100.0 K
Wavelength	0.71073 Å
Crystal System	Orthorhombic
Space group	$Pna2_1$
Unit cell dimensions	a = 17.7285(10) Å, α = 90°
	b = 15.1002(8) Å, β = 90°
	c = 9.8309(5) Å, γ = 90°
Volume	2631.8(2) Å^3
Z	4
Density (calculated)	0.382 g cm^{-3}
Absorption coefficient	0.608 mm^{-1}
F(000)	1104
Crystal size	0.58 x 0.22 x 0.10 mm
2-Theta range for data collection	3.5 to 72.3°
Index ranges	-28 ≤ h ≤ 28, -22 ≤ k ≤ 24,
	-16 ≤ l ≤ 16
Reflections collected	70881
Independent reflections	11995 [R(int) = 0.0370]
Completeness to theta = 36.13°	95%
Absorption correction	Semi-empirical from equivalents
Max. and min. transmission	0.747 and 0.682
Refinement method	Full-matrix least-squares on F^2
Data / restraints / parameters	11995 / 1 / 397
Goodness-of-fit on F^2	1.123
Final R indices [I>2sigma(I)]	R1 = 0.0255, wR2 = 0.0581
R indices (all data)	R1 = 0.0340, wR2 = 0.0713
Largest diff. peak and hole	0.58 and -0.85 e Å^{-3}
Flack parameter	-0.032(9)

Compound **3**	
[Ru(κ^3-2,3′,3′-{1-(1′-1′,2′-*closo*-$C_2B_{10}H_{10}$)-1,2-*closo*-$C_2B_{10}H_{10}$})$(PPh_3)_2$]	
Identification code	x85186
Empirical formula	$C_{40}H_{50}B_{20}P_2Ru$
Formula weight	910.01 g mol^{-1}
Temperature	100.0 K
Wavelength	0.71073 Å
Crystal System	Triclinic
Space group	P-1
Unit cell dimensions	a = 11.2062(9) Å, α = 81.178(5)°
	b = 11.5418(10) Å, β = 90.736(5)°
	c = 17.9159(17) Å, γ = 85.546(5)°
Volume	2256.6(3) Å^3
Z	2
Density (calculated)	1.339 g cm^{-3}
Absorption coefficient	0.451 mm^{-1}
F(000)	928
Crystal size	0.38 x 0.20 x 0.06 mm
2-Theta range for data collection	2.3 to 55.6°
Index ranges	-14≤ h ≤ 14, -15 ≤ k ≤ 15,
	-23 ≤ l ≤ 23
Reflections collected	39229
Independent reflections	10416 [R(int) = 0.0753]
Completeness to theta = 27.77°	97.7%
Absorption correction	Semi-empirical from equivalents
Max. and min. transmission	0.990 and 0.893
Refinement method	Full-matrix least-squares on F^2
Data / restraints / parameters	10416 / 0 / 581
Goodness-of-fit on F^2	1.227
Final R indices [I>2sigma(I)]	R1 = 0.0944, wR2 = 0.1595
R indices (all data)	R1 = 0.1116, wR2 = 0.1664
Largest diff. peak and hole	1.76 and -1.35 e Å^{-3}

Compound **4**	
[Ru(κ^3-2,3′,3′-{1-(1′-1′,2′-*closo*-$C_2B_{10}H_{10}$)-1,2-*closo*-$C_2B_{10}H_{10}$})(dppe)]	
Identification code	x85326
Empirical formula	$C_{30}H_{44}B_{20}P_2Ru \cdot CH_2Cl_2$
Formula weight	868.79 g mol^{-1}
Temperature	100.0 K
Wavelength	0.71073 Å
Crystal System	Triclinic
Space group	P-1
Unit cell dimensions	a = 10.6782(14) Å, α = 79.065(7)°
	b = 12.1648(17) Å, β = 74.204(7)°
	c = 17.624(2) Å, γ = 71.267(7)°
Volume	2073.0(5) Å^3
Z	2
Density (calculated)	1.392 g cm^{-3}
Absorption coefficient	0.611 mm^{-1}
F(000)	880
Crystal size	0.34 x 0.20 x 0.18 mm
2-Theta range for data collection	4.6 to 61.9°
Index ranges	-15 ≤ h ≤ 15, -14 ≤ k ≤ 17,
	-25 ≤ l ≤ 25
Reflections collected	46792
Independent reflections	12793 [R(int) = 0.0564]
Completeness to theta = 30.93°	97.3%
Absorption correction	Semi-empirical from equivalents
Max. and min. transmission	0.746 and 0.695
Refinement method	Full-matrix least-squares on F^2
Data / restraints / parameters	12793 / 0 / 562
Goodness-of-fit on F^2	1.059
Final R indices [I>2sigma(I)]	R1 = 0.0382, wR2 = 0.0771
R indices (all data)	R1 = 0.0554, wR2 = 0.0835
Largest diff. peak and hole	0.62 and -0.68 e Å^{-3}

Compound **5**	
[Ru(κ^2-2,3′-{1-(1′-1′,2′-*closo*-$C_2B_{10}H_{10}$)-1,2-*closo*-$C_2B_{10}H_{10}$})(PPh_3)$(CO)_3$]	
Identification code	x85267
Empirical formula	$C_{25}H_{35}B_{20}O_3PRu \cdot CH_2Cl_2$
Formula weight	816.67 g mol^{-1}
Temperature	100.0 K
Wavelength	0.71073 Å
Crystal System	Triclinic
Space group	P-1
Unit cell dimensions	a = 10.774(2) Å, α = 63.017(11)°
	b = 14.223(3) Å, β = 79.932(10)°
	c = 14.245(3) Å, γ = 80.026(10)°
Volume	19.4.4(7) $Å^3$
Z	2
Density (calculated)	1.424 g cm^{-3}
Absorption coefficient	0.626 mm^{-1}
F(000)	820
Crystal size	0.40 x 0.22 x 0.06 mm
2-Theta range for data collection	4.8 to 62.7°
Index ranges	-11≤ h ≤ 15, -20 ≤ k ≤ 20,
	-20 ≤ l ≤ 20
Reflections collected	46419
Independent reflections	12119 [R(int) = 0.0609]
Completeness to theta = 31.36°	96.8%
Absorption correction	Semi-empirical from equivalents
Max. and min. transmission	0.746 and 0.703
Refinement method	Full-matrix least-squares on F^2
Data / restraints / parameters	12119 / 12 / 567
Goodness-of-fit on F^2	1.052
Final R indices [I>2sigma(I)]	R1 = 0.0427, wR2 = 0.0825
R indices (all data)	R1 = 0.0706, wR2 = 0.0920
Largest diff. peak and hole	0.71 and -0.71 e $Å^{-3}$

Compound **6**	
[Ru(κ^2-2,3′-{1-(1′-1′,2′-*closo*-$C_2B_{10}H_{10}$)-1,2-*closo*-$C_2B_{10}H_{10}$})(PPh_3)$(MeCN)_3$]	
Identification code	x85235
Empirical formula	$C_{28}H_{44}B_{20}N_3PRu$
Formula weight	770.90 g mol^{-1}
Temperature	100.0 K
Wavelength	0.71073 Å
Crystal System	Triclinic
Space group	P-1
Unit cell dimensions	a = 10.4838(14) Å, α = 87.152(8)°
	b = 10.6487(16) Å, β = 75.088(7)°
	c = 18.114(3) Å, γ = 82.148(7)°
Volume	1935.6(5)
Z	2
Density (calculated)	1.323 g cm^{-3}
Absorption coefficient	0.474 mm^{-1}
F(000)	784
Crystal size	0.45 x 0.40 x 0.20 mm
2-Theta range for data collection	2.3 to 68.4°
Index ranges	-16 ≤ h ≤ 16 -16 ≤ k ≤ 13,
	-28 ≤ l ≤ 28
Reflections collected	40052
Independent reflections	15554 [R(int) = 0.0399]
Completeness to theta = 34.18°	97.1%
Absorption correction	Semi-empirical from equivalents
Max. and min. transmission	0.747 and 0.712
Refinement method	Full-matrix least-squares on F^2
Data / restraints / parameters	15554 / 0 / 541
Goodness-of-fit on F^2	1.016
Final R indices [I>2sigma(I)]	R1 = 0.0368, wR2 = 0.0729
R indices (all data)	R1 = 0.0479, wR2 = 0.0781
Largest diff. peak and hole	0.57 and -0.69 e $Å^{-3}$

Compound **7**	
[Ru(κ^2-2,3′-{1-(1′-1′,2′-*closo*-$C_2B_{10}H_{10}$)-1,2-*closo*-$C_2B_{10}H_{10}$})(dppe)$(CO)_2$]	
Identification code	x85269
Empirical formula	$C_{32}H_{44}B_{20}O_2P_2Ru$
Formula weight	839.88 g mol^{-1}
Temperature	100.0 K
Wavelength	0.71073 Å
Crystal System	Triclinic
Space group	P-1
Unit cell dimensions	a = 11.704(3) Å, α = 104.475(7)°
	b = 12.184(3) Å, β = 106.328(6)°
	c = 16.339(4) Å, γ = 98.443(7)°
Volume	2105.1(9) $Å^3$
Z	2
Density (calculated)	1.325 g cm^{-3}
Absorption coefficient	0.480 mm^{-1}
F(000)	852
Crystal size	0.40 x 0.24 x 0.20 mm
2-Theta range for data collection	5.1 to 61.3°
Index ranges	-16 ≤ h ≤ 16, -17 ≤ k ≤ 17,
	-23 ≤ l ≤ 23
Reflections collected	47883
Independent reflections	12386 [R(int) = 0.0448]
Completeness to theta = 30.63°	95.3%
Absorption correction	Semi-empirical from equivalents
Max. and min. transmission	0.746 and 0.679
Refinement method	Full-matrix least-squares on F^2
Data / restraints / parameters	12386 / 0 / 574
Goodness-of-fit on F^2	1.031
Final R indices [I>2sigma(I)]	R1 = 0.0346, wR2 = 0.0770
R indices (all data)	R1 = 0.0492, wR2 = 0.0830
Largest diff. peak and hole	0.49 and -0.79 e $Å^{-3}$

Compound **8**	
[Ru(κ^2-2,3′-{1-(1′-1′,2′-*closo*-$C_2B_{10}H_{10}$)-1,2-*closo*-$C_2B_{10}H_{10}$})(dppe)$(MeCN)_2$]	
Identification code	x85259
Empirical formula	$C_{34}H_{50}B_{20}N_2P_2Ru \cdot 3CH_3CN$
Formula weight	989.13 g mol^{-1}
Temperature	100.0 K
Wavelength	0.71073 Å
Crystal System	Monoclinic
Space group	C2/c
Unit cell dimensions	a = 21.5530(9) Å, α = 90°
	b = 19.6096(8) Å, β = 94.465(2)°
	c = 23.5945(10) Å, γ = 90°
Volume	9941.8(7) $Å^3$
Z	8
Density (calculated)	1.322 g cm^{-1}
Absorption coefficient	0.417 mm^{-1}
F(000)	4064
Crystal size	0.56 x 0.34 x 0.28 mm
2-Theta range for data collection	4.5 to 60.2°
Index ranges	-30 ≤ h ≤ 30, -27 ≤ k ≤ 27,
	-33 ≤ l ≤ 33
Reflections collected	107310
Independent reflections	14492 [R(int) = 0.0429]
Completeness to theta = 30.10°	99.0%
Absorption correction	Semi-empirical from equivalents
Max. and min. transmission	0.746 and 0.712
Refinement method	Full-matrix least-squares on F^2
Data / restraints / parameters	14492 / 0 / 714
Goodness-of-fit on F^2	1.039
Final R indices [I>2sigma(I)]	R1 = 0.0353, wR2 = 0.0936
R indices (all data)	R1 = 0.0521, wR2 = 0.1044
Largest diff. peak and hole	0.54 and -1.00 e $Å^{-3}$

Compound **9**	
[μ-2,2′-EtP-{1-(1′-1′,2′-*closo*-$C_2B_{10}H_{10}$)-1,2-*closo*-$C_2B_{10}H_{10}$}]	
Identification code	x85428
Empirical formula	$C_6H_{25}B_{20}P$
Formula weight	344.43 g mol^{-1}
Temperature	100.0 K
Wavelength	0.71073 Å
Crystal System	Monoclinic
Space group	$P2_1/n$
Unit cell dimensions	a = 23.441(2) Å, α = 90°
	b = 7.2690(6) Å, β = 108.290(5)°
	c = 24.083(2) Å, γ = 90°
Volume	3896.2(6) $Å^3$
Z	8
Density (calculated)	1.174 g cm^{-1}
Absorption coefficient	0.129 mm^{-1}
F(000)	1408
Crystal size	0.42 x 0.08 x 0.04 mm
2-Theta range for data collection	2.1 to 47.5°
Index ranges	$-26 \le h \le 26$, $-6 \le k \le 8$,
	$-24 \le l \le 27$
Reflections collected	44057
Independent reflections	5928 [R(int) = 0.1415]
Completeness to theta = 23.77°	99.5%
Absorption correction	Semi-empirical from equivalents
Max. and min. transmission	0.601 and 0.745
Refinement method	Full-matrix least-squares on F^2
Data / restraints / parameters	5928 / 0 / 609
Goodness-of-fit on F^2	1.053
Final R indices [I>2sigma(I)]	R1 = 0.0795, wR2 = 0.1840
R indices (all data)	R1 = 0.1435, wR2 = 0.2132
Largest diff. peak and hole	0.48 and -0.41 e $Å^{-3}$

Compound **10**	
[μ-2,2′-PhP-{1-(1′-1′,2′-*closo*-$C_2B_{10}H_{10}$)-1,2-*closo*-$C_2B_{10}H_{10}$}]	
Identification code	x85075
Empirical formula	$C_{10}H_{25}B_{20}P$
Formula weight	392.47 g mol^{-1}
Temperature	100.0 K
Wavelength	0.71073 Å
Crystal System	Triclinic
Space group	P-1
Unit cell dimensions	a = 7.1139(10) Å, α = 81.884(5)°
	b = 11.4378(14) Å, β = 84.954(5)°
	c = 13.3912(15) Å, γ = 81.231(2)°
Volume	1063.6(2) $Å^3$
Z	2
Density (calculated)	1.225 g cm^{-1}
Absorption coefficient	0.127 mm^{-1}
F(000)	400
Crystal size	0.40 x 0.18 x 0.08 mm
2-Theta range for data collection	5.8 to 52.9°
Index ranges	$-8 \le h \le 8$, $-14 \le k \le 14$,
	$-16 \le l \le 16$
Reflections collected	15395
Independent reflections	4334 [R(int) = 0.0636]
Completeness to theta = 26.46°	98.7%
Absorption correction	Semi-empirical from equivalents
Max. and min. transmission	0.692 and 0.745
Refinement method	Full-matrix least-squares on F^2
Data / restraints / parameters	4334 / 0 / 340
Goodness-of-fit on F^2	1.133
Final R indices [I>2sigma(I)]	R1 = 0.0685, wR2 = 0.1256
R indices (all data)	R1 = 0.0871, wR2 = 0.1338
Largest diff. peak and hole	0.31 and -0.35 e $Å^{-3}$

Compound **11**	
[μ-2,2′-EtPAuCl-{1-(1′-1′,2′-*closo*-$C_2B_{10}H_{10}$)-1,2-*closo*-$C_2B_{10}H_{10}$}]	
Identification code	x85097
Empirical formula	$C_6H_{25}AuB_{20}P \cdot C_{2.5}H_{2.5}Cl_{3.5}$
Formula weight	683.00 g mol^{-1}
Temperature	100.0 K
Wavelength	0.71073 Å
Crystal System	Orthorhombic
Space group	Pbca
Unit cell dimensions	a = 10.4380(13) Å, α = 90°
	b = 17.711(2) Å, β = 90°
	c = 27.475(3) Å, γ = 90°
Volume	5079.3(10) $Å^3$
Z	8
Density (calculated)	1.786 g cm^{-1}
Absorption coefficient	6.224 mm^{-1}
F(000)	2596
Crystal size	0.36 x 0.28 x 0.12 mm
2-Theta range for data collection	4.6 to 54.5°
Index ranges	$-13 \le h \le 13$, $-22 \le k \le 19$,
	$-35 \le l \le 20$
Reflections collected	33633
Independent reflections	5651 [R(int) = 0.0526]
Completeness to theta = 27.24°	99.3%
Absorption correction	Semi-empirical from equivalents
Max. and min. transmission	0.510 and 0.746
Refinement method	Full-matrix least-squares on F^2
Data / restraints / parameters	5651 / 0 / 323
Goodness-of-fit on F^2	1.020
Final R indices [I>2sigma(I)]	R1 = 0.0297, wR2 = 0.0585
R indices (all data)	R1 = 0.0476, wR2 = 0.0622
Largest diff. peak and hole	0.69 and -0.65 e $Å^{-3}$

Compound **12**	
[μ-2,2′-PhPAuCl-{1-(1′-1′,2′-*closo*-$C_2B_{10}H_{10}$)-1,2-*closo*-$C_2B_{10}H_{10}$}]	
Identification code	x85429
Empirical formula	$C_{10}H_{25}AuB_{20}ClP$
Formula weight	624.89 g mol^{-1}
Temperature	100.0 K
Wavelength	0.71073 Å
Crystal System	Monoclinic
Space group	C2/c
Unit cell dimensions	a = 17.0588(8) Å, α = 90°
	b = 14.2499(7) Å, β = 102.497(3)°
	c = 20.0698(9) Å, γ = 90°
Volume	4763.1(4) $Å^3$
Z	8
Density (calculated)	1.743 g cm^{-1}
Absorption coefficient	6.357 mm^{-1}
F(000)	2368
Crystal size	0.32 x 0.18 x 0.15 mm
2-Theta range for data collection	4.5 to 64.0°
Index ranges	$-25 \le h \le 25$, $-20 \le k \le 21$,
	$-29 \le l \le 29$
Reflections collected	58934
Independent reflections	8266 [R(int) = 0.0796]
Completeness to theta = 30.01°	99.6%
Absorption correction	Semi-empirical from equivalents
Max. and min. transmission	0.522 and 0.746
Refinement method	Full-matrix least-squares on F^2
Data / restraints / parameters	8266 / 0 / 358
Goodness-of-fit on F^2	1.015
Final R indices [I>2sigma(I)]	R1 = 0.0342, wR2 = 0.0603
R indices (all data)	R1 = 0.0519, wR2 = 0.0648
Largest diff. peak and hole	0.93 and -1.81 e $Å^{-3}$

Compound **13**	
[μ-2,2′-EtPSe-{1-(1′-1′,2′-*closo*-$C_2B_{10}H_{10}$)-1,2-*closo*-$C_2B_{10}H_{10}$}]	
Identification code	x85450
Empirical formula	$C_6H_{25}B_{20}PSe$
Formula weight	423.39 g mol^{-1}
Temperature	100.0 K
Wavelength	0.71073 Å
Crystal System	Triclinic
Space group	P-1
Unit cell dimensions	a = 7.1663(7) Å, α = 111.478(9)°
	b = 11.0308(15) Å, β = 92.125(9)°
	c = 14.573(2) Å, γ = 104.679(6)°
Volume	1026.2(2) $Å^3$
Z	2
Density (calculated)	1.370 g cm^{-1}
Absorption coefficient	1.898 mm^{-1}
F(000)	420
Crystal size	0.50 x 0.28 x 0.18 mm
2-Theta range for data collection	5.9 to 60.3°
Index ranges	$-9 \le h \le 10$, $-15 \le k \le 14$,
	$-20 \le l \le 13$
Reflections collected	40192
Independent reflections	5691 [R(int) = 0.0622]
Completeness to theta = 30.14°	93.8%
Absorption correction	Semi-empirical from equivalents
Max. and min. transmission	0.504 and 0.746
Refinement method	Full-matrix least-squares on F^2
Data / restraints / parameters	5691 / 0 / 315
Goodness-of-fit on F^2	1.036
Final R indices [I>2sigma(I)]	R1 = 0.0410, wR2 = 0.0861
R indices (all data)	R1 = 0.0634, wR2 = 0.0939
Largest diff. peak and hole	0.61 and -0.58 e $Å^{-3}$

Compound **14**	
[μ-2,2′-PhPSe-{1-(1′-1′,2′-*closo*-$C_2B_{10}H_{10}$)-1,2-*closo*-$C_2B_{10}H_{10}$}]	
Identification code	x85454
Empirical formula	$C_{10}H_{25}B_{20}PSe$
Formula weight	471.43 g mol^{-1}
Temperature	100.0 K
Wavelength	0.71073 Å
Crystal System	Monoclinic
Space group	$P2_1/n$
Unit cell dimensions	a = 10.3457(12) Å, α = 90°
	b = 16.9431(17) Å, β = 105.612(6)°
	c = 13.6941(14) Å, γ = 90°
Volume	2311.9(4) $Å^3$
Z	4
Density (calculated)	1.354 g cm^{-1}
Absorption coefficient	1.639 mm^{-1}
F(000)	936
Crystal size	0.40 x 0.28 x 0.10 mm
2-Theta range for data collection	3.9 to 57.9°
Index ranges	$-14 \le h \le 14$, $-20 \le k \le 23$,
	$-18 \le l \le 17$
Reflections collected	43105
Independent reflections	6088 [R(int) = 0.0740]
Completeness to theta = 28.95°	99.6%
Absorption correction	Semi-empirical from equivalents
Max. and min. transmission	0.616 and 0.746
Refinement method	Full-matrix least-squares on F^2
Data / restraints / parameters	6088 / 0 / 349
Goodness-of-fit on F^2	1.034
Final R indices [I>2sigma(I)]	R1 = 0.0365, wR2 = 0.0767
R indices (all data)	R1 = 0.0554, wR2 = 0.0827
Largest diff. peak and hole	0.35 and -0.42 e $Å^{-3}$

Compound **15**	
[μ-2,2′-C_6H_4-{1-(1′-1′,2′-*closo*-$C_2B_{10}H_{10}$)-1,2-*closo*-$C_2B_{10}H_{10}$}]	
Identification code	x85003t7
Empirical formula	$C_{10}H_{24}B_{20}$
Formula weight	360.49 g mol^{-1}
Temperature	100.0 K
Wavelength	0.71073 Å
Crystal System	Orthorhombic
Space group	Pbcn
Unit cell dimensions	a = 18.2854(16) Å, α = 90°
	b = 10.1906(10) Å, β = 90°
	c = 10.3920(8) Å, γ = 90°
Volume	1936.4(3) $Å^3$
Z	4
Density (calculated)	1.237 g cm^{-1}
Absorption coefficient	0.054 mm^{-1}
F(000)	736
Crystal size	0.20 x 0.20 x 0.06 mm
2-Theta range for data collection	60.2 to 52.7°
Index ranges	$-22 \le h \le 22$, $-12 \le k \le 12$,
	$-12 \le l \le 12$
Reflections collected	20837
Independent reflections	1975 [R(int) = 0.1230]
Completeness to theta = 26.36°	99.8%
Absorption correction	Semi-empirical from equivalents
Max. and min. transmission	0.745 and 0.681
Refinement method	Full-matrix least-squares on F^2
Data / restraints / parameters	1975 / 0 / 136
Goodness-of-fit on F^2	1.247
Final R indices [I>2sigma(I)]	R1 = 0.0948, wR2 = 0.1751
R indices (all data)	R1 = 0.1161, wR2 = 0.1843
Largest diff. peak and hole	0.41 and -0.29 e $Å^{-3}$

Compound **17**	
[2-(1′-1′,2′-*closo*-$C_2B_{10}H_{10}$)-4,5-(*p*-cymene)-7-Cl-4,5,2,3-*closo*-$Ru_2C_2B_9H_9$]	
Identification code	EX17004
Empirical formula	$C_{24}H_{48}B_{19}ClRu_2 \cdot C_4H_8O$
Formula weight	779.65 g mol^{-1}
Temperature	120.0 K
Wavelength	0.71073 Å
Crystal System	Triclinic
Space group	P-1
Unit cell dimensions	a = 10.72705(18) Å, α = 96.8730(13)°
	b = 13.2012(2) Å, β = 95.1630(13)°
	c = 13.6564(2) Å, γ = 90.0750(13)°
Volume	1912.05(5) $Å^3$
Z	2
Density (calculated)	1.479 g cm^{-1}
Absorption coefficient	0.886 mm^{-1}
F(000)	864
Crystal size	0.21 x 0.11 x 0.05 mm
2-Theta range for data collection	5.7 to 59.5°
Index ranges	$-14 \le h \le 14$, $-18 \le k \le 18$,
	$-18 \le l \le 18$
Reflections collected	68695
Independent reflections	10166 [R(int) = 0.0472]
Completeness to theta = 29.75°	93.4%
Absorption correction	Semi-empirical from equivalents
Max. and min. transmission	0.564 and 1.000
Refinement method	Full-matrix least-squares on F^2
Data / restraints / parameters	10166 / 0 / 526
Goodness-of-fit on F^2	1.118
Final R indices [I>2sigma(I)]	R1 = 0.0382, wR2 = 0.0689
R indices (all data)	R1 = 0.0477, wR2 = 0.0717
Largest diff. peak and hole	1.48 and -0.72 e $Å^{-3}$

Compound **18**	
[μ-2,2′-CH_2CH_2-{1-(1′-1′,2′-*closo*-$C_2B_{10}H_{10}$)-3-(*p*-cymene)-3,1,2-*closo*-$RuC_2B_9H_9$}]	
Identification code	EX16061
Empirical formula	$C_{16}H_{37}B_{19}Ru$
Formula weight	535.91 g mol^{-1}
Temperature	120.0 K
Wavelength	0.71073 Å
Crystal System	Monoclinic
Space group	$P2_1$
Unit cell dimensions	a = 9.0245(2) Å, α = 90°
	b = 16.8629(3) Å, β = 112.339(3)°
	c = 9.1746(2) Å, γ = 90°
Volume	1291.40(6) $Å^3$
Z	2
Density (calculated)	1.378 g cm^{-1}
Absorption coefficient	0.615 mm^{-1}
F(000)	544
Crystal size	0.45 x 0.28 x 0.237 mm
2-Theta range for data collection	6.8 to 62.5°
Index ranges	$-13 \leq h \leq 12$, $-24 \leq k \leq 23$,
	$-12 \leq l \leq 12$
Reflections collected	27719
Independent reflections	7584 [R(int) = 0.0494]
Completeness to theta = 31.23°	90.0%
Absorption correction	Semi-empirical from equivalents
Max. and min. transmission	1.000 and 0.422
Refinement method	Full-matrix least-squares on F^2
Data / restraints / parameters	7584 / 1 / 385
Goodness-of-fit on F^2	1.039
Final R indices [I>2sigma(I)]	R1 = 0.0295, wR2 = 0.0600
R indices (all data)	R1 = 0.0320, wR2 = 0.0617
Largest diff. peak and hole	0.67 and -0.42 e $Å^{-3}$
Flack parameter	-0.083(16)